New High Temperature Transcritical CO_2 Heat Pump Concept for Spray Drying

A thesis

submitted in fulfilment

of the requirements for the degree

of

Doctor of Philosophy in Engineering

at

The University of Waikato

by

Lana Kong

THE UNIVERSITY OF
WAIKATO
Te Whare Wānanga o Waikato

2026

Abstract

The need to decarbonise the industrial sector requires new innovations in high temperature heating. The development of an industrial high temperature heat pump presents not only great emissions reduction potential but also cost saving potential for industrial process heat users. Compared to boilers with efficiencies ranging from 70 to 99%, heat pumps have the ability to leverage renewable electricity to supply heating as a standalone technology (air-source heat pumps), with one unit if electricity being able to supply multiple units of heat (Coefficient of Performance > 1) or integrate with existing boilers to reduce steam demand (air-source or waste heat recovery).

This thesis investigates a novel high temperature transcritical CO_2 heat pump concept using a case study in milk powder spray drying. A series of cycle architectures were modelled that incorporated internal heat exchangers and cascade arrangements to assess their effect on thermodynamic performance for not only large temperature lifts (>150 °C) but also large temperature glides (>150 °C). A transcritical-transcritical cascade configuration was found to achieve a sink temperature of 200 °C with a COP of 2.22 at moderate discharge pressures (150 bar) compared to what is currently available in the literature (>200 bar). Expansion work recovery, using ejectors and expanders, was further explored to reduce exergy losses, achieving incremental COP gains up to 2.35. However, it was determined that, at this stage, the marginal increases in COP did not overcome the challenges in complexity of integrating an expander or ejector within the system.

A comparison of integration options was undertaken that compared the high temperature heat pump integration with fuel switching to electrode or biomass boilers. Hybrid configurations of heat pump and boilers were also assessed at varying utility prices to determine whether an optimum sink temperature existed to minimise the operational cost. With this, a multi-temperature heat pump configuration was found to improve the COP of the heat pump to 2.55 for air heating to 200 °C, which emphasises the importance of temperature profile matching in heat pump design. Operating costs depended on the electricity-to-biomass price ratio and grid emissions intensity. In all cases, electrode boiler conversions had the highest operational cost. Price ratios below 2.75 were favourable for full electrification using a heat pump, while price ratios above 3.67 favoured a full biomass conversion. Between these two price ratios, the optimal hybrid configuration was to supply the air heating up to the temperature level for the fluidised bed (102 °C) using a heat pump and supply the remainder of the heating using a biomass boiler. In comparison to coal, the proposed solutions achieved emissions savings between 55 and 94 %.

The wider potential for the high temperature heat pump concept was then estimated, revealing a broader potential for CO_2 high temperature heat pumps to supply hundreds of petajoules per year of low-carbon heat across a diverse range

of industrial sectors. Due to being able to produce both large temperature glides and large temperature lifts, the CO_2 high temperature heat pump was particularly suited for a range of drying processes (further than milk powder spray drying). Potential source and sink streams for the heat pump were identified for each application to estimate possible COPs, which ranged between 2.0 and 3.05 for sink outlet temperatures ranging from 110 to 280 °C. Emissions reduction was shown to be viable for nearly all regions when displacing coal, but requires cleaner electricity grids or higher COPs when displacing natural gas.

This thesis contributes an in depth thermodynamic analysis of both a novel high temperature heat pump cycle architecture and a novel application of high temperature heat pumps into the milk powder spray drying process. Additionally, this thesis contributes a cross-sectoral analysis for implementation, collating potential source and sink streams across a variety of applications.

Acknowledgements

I would first like to thank my supervisors Associate Professor Tim Walmsley, Associate Professor James Carson, Dr Steffen Kloeppel, and Dr Qun Chen for their guidance, expertise and support. I would also like to express thanks to Dr Duy Hoang, who was part of my early supervisory panel, to Professor Don Cleland and Dr Florian Schlosser, who continually and generously contributed valuable insight and advice throughout the duration of my PhD.

I want to thank everyone at Ahuora for the experiences, friendships and resources that enabled me to complete my thesis. I also want express gratitude to Dr Panagiotis Stathopoulos and those at DLR for their kindness during my time with them in Germany and since then. I want to thank all of the visiting researchers that came and brought their knowledge to our research team. At the University of Waikato, I want to also thank the School of Engineering Office, particularly, Natalie, Janine, Levinia and Mary who I can recall on many occasions where their hard work behind the scenes helped me greatly.

To my friends, my partner's family, clients, bandmates and students that I had the opportunity to tutor throughout this thesis – there are too many to name individually, but thank you for the perspective, company, and distractions that kept me sane throughout this process.

Finally, my greatest thanks go to my husband and my family.

To Ben – thank you for your unwavering support, love and encouragement throughout this journey. It is hard to encompass everything you have done that I'm grateful for because there have just been too many things, but I'm excited for our future together and thank you for always supporting me.

To Mum, Dad and my sister Nicole – thank you for everything that you gave up to provide me with the opportunities I have today. I wouldn't have been where I am today without everything that you have taught me, and I hope I can repay you everything you have given me and more.

Contributing publications

The main content of this thesis comprises an amalgamation of journal articles and conference papers authored by the candidate. A greater part of Chapter 4 has been published in the journal *Applied Thermal Engineering* [1] and was also presented at the *PRES Conference, Bol, Croatia, 2022* [8]. Chapter 5 incorporates and extends the work from a conference paper that was presented at *International Congress of Refrigeration, Paris, France, 2023* [7]. Chapter 6 also incorporates and extends the work of a conference paper, which was presented at the *16th IIR-Gustav Lorentzen Conference on Natural Refrigerants, Maryland, USA, 2024* [9]. Half of Chapter 7 has been published in an engineering journal article [2]. Part of this article [2] also features in Chapter 2.

In addition, several co-authored publications led by other researchers have provided valuable context and foundational knowledge for this thesis. Chapter 2 builds upon the comprehensive literature review by Adamson et al. [4]. Further supporting context and preliminary findings are drawn from co-authored works, notably Schlosser et al. [3] and Lincoln et al. [5].

Journal Articles

[1] **L. Kong,** T. G. Walmsley, D. Hoang, F. Schlosser, Q. Chen, J. K. Carson, D. J. Cleland, "Transcritical-transcritical cascade CO2 heat pump cycles for high temperature heating: A numerical evaluation," Applied Thermal Engineering, vol. 238, p. 122005, Feb. 2024, doi: 10.1016/j.applthermaleng.2023.122005.

[2] **L. Kong,** S. Kloeppel, F. Schlosser, N. Kabat, J. K. Carson, and T. G. Walmsley, "Advances in high-temperature heat pump technologies for industrial process applications with large temperature glides: Assessing the potential for carbon dioxide as a refrigerant," Energy Conversion and Management, 2025, doi: 10.1016/j.enconman.2025.114578.

[3] F. Schlosser, S. Zysk, T. Walmsley, **L. Kong**, B. Zühlsdorf, and H. Meschede, "Break-even of High temperature Heat Pump Integration for Milk Spray Drying," *Energy Conversion and Management*, 2023, doi: 10.1016/j.enconman.2023.117304.

[4] K.-M. Adamson, T. G. Walmsley, J. K. Carson, Q. Chen, F. Schlosser, **L. Kong**, D. J. Cleland, "High temperature and transcritical heat pump cycles and advancements: a review," *Renewable and Sustainable Energy Reviews*, 2022.

[5] B. J. Lincoln, **L. Kong**, A. M. Pineda, and T. G. Walmsley, "Process integration and electrification for efficient milk evaporation systems," Energy, vol. 258, p. 124885, Nov. 2022, doi: 10.1016/j.energy.2022.124885.

[6] B. J. Lincoln, **L. Kong**, F. Schlosser, and T. G. Walmsley, "Process integration and electrification for retrofit: Case studies of milk evaporator systems,"

Case Studies in Thermal Engineering, vol. 60, p. 104601, Aug. 2024, doi: 10.1016/j.csite.2024.104601.

Conference Papers

[7] **L. Kong,** T. G. Walmsley, O. Abu Khass, F. Schlosser, D. J. Cleland, J. K. Carson, Q. Chen, D. Hoang, "Energy and exergy analysis of high temperature transcritical CO_2 heat pump cycles with ejectors," Proceedings of the International Congress of Refrigeration, Paris France, 2023.

[8] **L. Kong,** T. G. Walmsley, D. Hoang, F. Schlosser, Q. Chen, J. K. Carson, D. J. Cleland, "Thermodynamic Modelling of High temperature Cascaded Transcritical CO2 Heat Pump Cycle Structures with Internal Heat Exchange," Proceedings of the 25th Conference on Process Integration, Modelling and Optimisation for Energy Saving and Pollution Reduction, Split and Bol, Croatia, 2022.

[9] **L. Kong**, T. G. Walmsley, J. K. Carson, S. Klöppel, F. Schlosser, and D. J. Cleland, "High-temperature CO_2 heat pump integration for milk powder spray drying," in Proceedings of the 16th IIR–Gustav Lorentzen Conference on Natural Refrigerants, College Park, MD, USA, Aug. 11–14, 2024. doi: 10.18462/iir.gl2024.1205.

[10] B. J. Lincoln, **L. Kong**, T. G. Walmsley, "Process Retrofit and Electrification of Milk Evaporator Systems," Proceedings of the 25th Conference on Process Integration, Modelling and Optimisation for Energy Saving and Pollution Reduction, Split and Bol, Croatia, 2022.

[11] T. G. Walmsley, B. J. Lincoln, **L. Kong**, "Process Integration and Electrification through Exergy Pinch Analysis," Proceedings of the 25th Conference on Process Integration, Modelling and Optimisation for Energy Saving and Pollution Reduction, Split and Bol, Croatia, 2022.

Table of Contents

List of figures

List of tables

Nomenclature

Abbreviations

B	Alternative Fuel Group (Boiler Only)
CC	Composite Curve
CGC	Cascade Gas Cooler
CO_2	Carbon dioxide
COP	Coefficient of Performance
COW	Condensate of Whey
GCC	Grand Composite Curve
GWP	Global Warming Potential
HEN	Heat Exchanger Network
HP	Heat pump (only)
HP+B	Heat pump integrated with biomass boiler
HPS	High-pressure steam
HTHP	High temperature heat pump
HTGC	High temperature gas cooler
HTTHP	High temperature transcritical heat pump
HVAC	Heating, Ventilation & Air Conditioning
IHX	Internal heat exchanger
LPS	Low-pressure steam
MTGC	Mid-temperature gas cooler
MVR	Mechanical vapour recompression
ODP	Ozone-depleting potential
OPEX	Operational expenditure/cost
PLR	Pressure Lift Ratio
PTA	Problem Table Algorithm
sCO_2	Supercritical CO_2
SFB	Static fluidised bed
TVR	Thermal vapour recompression
VFB	Vibrating fluidised bed

Symbols

∂	Partial derivative
Δ	Change in a property
ΔT_{min}	Minimum approach temperature (°C or K)
μ	Entrainment ratio
η	Efficiency (%)
ω	Absolute humidity (kgH_2O/kg of dry air)
c	Calorific value (kWh/kg) or cost (NZD)
C	Concentration (wt% solids)
c_p	Specific heat capacity (kJ/kgK)
cv	Calorific value (kWh/kg)
e	Emissions ($kgCO_2$-e/unit)
h	Specific enthalpy (kJ/kg)

m	Mass (kg)
$\dot{m}$	Mass flowrate (kg/s)
P	Pressure (MPa or bar)
Q	Heat accumulated (kJ)
$\dot{Q}$	Heat flow (kW)
p	Price
R	Relative humidity
r	Ratio
s	Specific entropy (kJ/kg·K)
T	Temperature (°C)
t	Time
v	Velocity (m/s)
w	Specific work consumption (kJ/kg)
$\dot{W}$	Work (kW)
x	Specific exergy (kJ/kg) or vapour quality
$\dot{X}$	Exergy flow (kW)

Subscripts

0	Dead-state condition
A	Hot stream in a heat exchanger
a	Actual
air	Air
amb	Ambient
$annual$	Annual
atm	Atmospheric
ave	Average
B	Cold stream in a heat exchanger
BE	Breakeven
$boiler$	Boiler
bot	Bottom cycle
cap	Capital
$cold$	Cold stream
$comp$	Compressor
$conc.$	Concentrate
$cond$	Condensing
d	Diffuser
des	Destruction
dis	Compressor discharge
dp	Dew point
$distribution$	Distribution
$eject$	Ejector
$elec$	Electricity
$evap$	Evaporator
$evaporated$	Evaporated
ex	Exergetic
$exhaust$	Exhaust air stream
exp	Expander
f	Factor
$fuel$	Fuel
GC	Gas cooler

$grid$	Electrical grid
$Heating$	Heating
hot	Hot stream
HP	Heat pump
HPS	High pressure steam
$HVAC$	Heating, Ventilation & Air Conditioning
$HTGC$	High temperature gas cooler
I	Ejector primary flow
II	Ejector secondary flow
$ideal$	Ideal (isentropic)
in	Inlet
IHX	Internal heat exchanger
l	Lifetime
LM	Log mean
LPS	Low-pressure steam
$Lorenz$	Lorenz
max	Maximum
$mech$	Mechanical
$milk$	Milk
min	Minimum
mix	Ejector mixed flow
$MTGC$	Mid-temperature gas cooler
n	Number of iterations or nozzle
out	Outlet
p	Price
$pinch$	At the Pinch
$product$	Product (e.g. milk powder)
r	Ratio
ref	Refrigerant or reference
$required$	Required
s	Isentropic
$savings$	Savings
SC	Sensible cooling
SH	Superheater
$sink$	Heat pump sink stream
$source$	Heat pump source stream
SFB	Static fluidised bed
$steam$	Steam
$supply$	Supply
$target$	Target
top	Top cycle
$total$	Total
VFB	Vibrating fluidised bed

Units

$°C$	Degrees Celsius
$\%$	Percentage
bar	Bar (absolute)
h	Hour
K	Kelvin
kg	Kilogram

$kgCO_2 - e$	Kilogram CO_2 equivalent
kJ	Kilojoule
GJ	Gigajoule
kW	Kilowatt
kWh	Kilowatt hour
MJ	Megajoule
MPa	Megapascal
NZD	New Zealand dollar
PJ	Petajoule
s	Second
t	Metric tonnes
$wt\%$	Weight Percentage

Heat pump component symbols

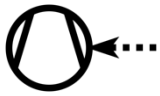	Compressor		Subcooler
	Expansion valve		Closed economiser
	Internal heat exchanger		Flash separator
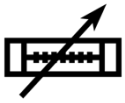	Gas Cooler		Cascade condenser
	Condenser		Expander
	Evaporator		Pump
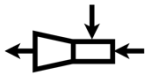	Ejector		

Chapter 1
Introduction

1.1 Background

Climate change is driving an increasing concern for the future of industrial process heat. Legislative measures have been introduced with the objective to pressure large energy users to rapidly reduce their carbon emissions. Of particular relevance is the Climate Change Response Amendment Act 2019 which sets out the goal to achieve net-zero emissions in New Zealand by 2050 [1]. Uncoincidentally, New Zealand's largest energy users are also generally the largest economic contributors, and therefore, a successful and economically viable transition to renewable energy sources is imperative. In New Zealand, dairy is the biggest export product and contributes approximately 17 billion dollars to the economy per year which includes the manufacture of dairy food products such as milk, milk powder, cheese and butter [2]. In 2016, 92% of the process heat used in the dairy industry to manufacture dairy food products was supplied using fossil fuels (Figure 1). Most of this process heat is used for the dewatering processes in milk powder production, namely evaporation and spray drying, which results in approximately 2.1 million tCO_2-e of emissions per year [3]. However, from 2037, these processes will no longer be able to rely on coal boilers to supply process heat, with the eventual phase out of natural gas boilers also inevitable under current legislation [4] and given the shortage of gas supply.

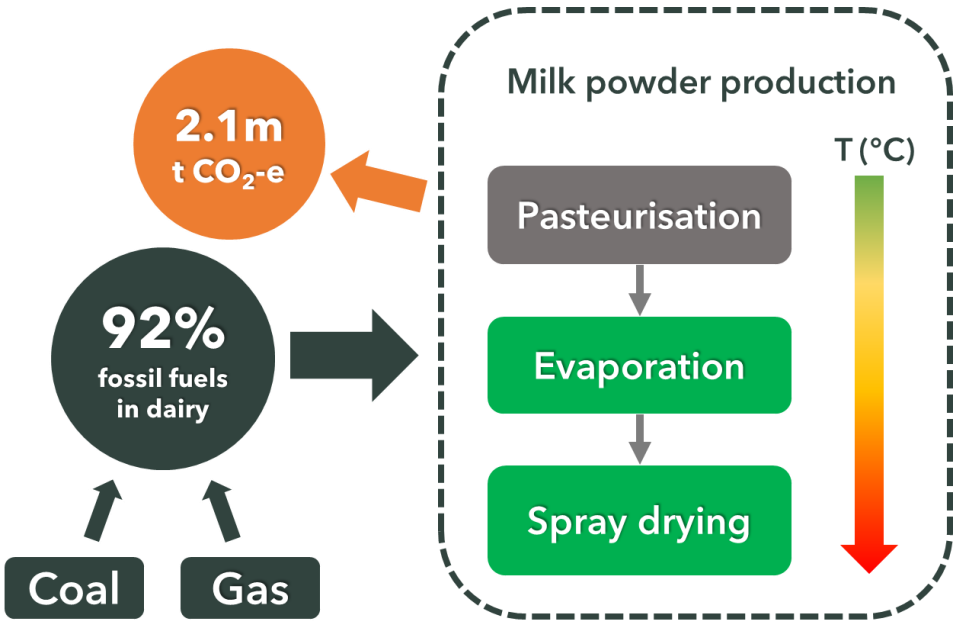

Figure 1. Emissions in the NZ dairy processing sector, 2016.

The transition away from traditional technologies is slowed by the lack of economically viable alternatives, particularly for higher temperature applications like spray drying (~200 °C). Conversion to biomass boilers is gaining popularity due to the relative similarity of biomass to conventional coal boilers [5], but the supply of biomass is constrained by the rate at which it can be produced and, as the demand increases, so will the cost. Alternatively, New Zealand holds a unique advantage, with more than 80 % of electricity being generated from renewable sources [6]. Paired with the high efficiencies that can be achieved by electrode boilers (~99 %), electrification is a promising option in terms of emissions reduction, however, even so, a similar challenge is faced in the relative cost of electricity to fossil fuels (per unit of heat) [7].

There are two general approaches to reduce cost in these necessary transitionary measures: 1) reduce demand, and 2) improve energy conversion efficiency or Coefficient of Performance (COP). In both respects, heat pumps are an attractive technology as waste heat from a process can be both utilised and "upgraded" to higher-temperature useful heat, using electricity. The heat produced from the heat pump is often multiple times greater than the required work input (COP>1), theoretically lowering the heating demand required from the boiler for the overall process. This ratio of heat output to electrical work input is referred to as the Coefficient of Performance (COP). Heat pumps are already well-established as a low-emissions technology for industrial process heat applications that operate at temperatures less than 100 °C, but heat pumps for generating higher temperatures are still in relative infancy, with the amount of existing research dwindling as process sink temperatures increase [8].

Since 2016, several large decarbonisation projects have been undertaken in the New Zealand dairy industry [5], [9] (Figure 2). Most conversions have involved either biomass or electrode boilers, with only a small number of large-scale heat pump installations. The heat pump projects to date have primarily targeted hot water generation [5], [10], accounting for less than 3 % of the total estimated emissions reduction. Among the identified projects, electrode boilers contributed approximately 58 % of the estimated emissions reduction, while biomass boilers contributed 37 %. Despite these efforts, the New Zealand dairy industry still emits an estimated 1.6 to 1.8 million tCO_2-e per year, not accounting for potential increases in production capacity. This highlights that substantial opportunities for further emissions reduction remain, reinforcing the need for high-performance technologies, such as industrial heat pumps (COP > 1), capable of providing process heat at temperatures currently achievable only with electrode and biomass boilers ($\eta < 100$ %).

Due to the varying heat profiles and process requirements across existing industries, the integration of high temperature heat pumps (HTHPs) requires a multi-faceted approach that is unique to the individual case [11] and is yet to be implemented at a large scale for milk powder spray drying. In the spray drying process, air is heated to approximately 200 °C using boiler steam heating, supplemented by hot water

waste heat recovery. The development of a HTHP that could displace the boiler steam heating in this process presents significant emissions reduction potential for New Zealand, as spray drying is the most energy intensive processes within the dairy industry. Spray drying is part of a class of applications that can be characterised by the large temperature glides experienced by the process sink stream (i.e., air heating), dominating the dryer energy demand.

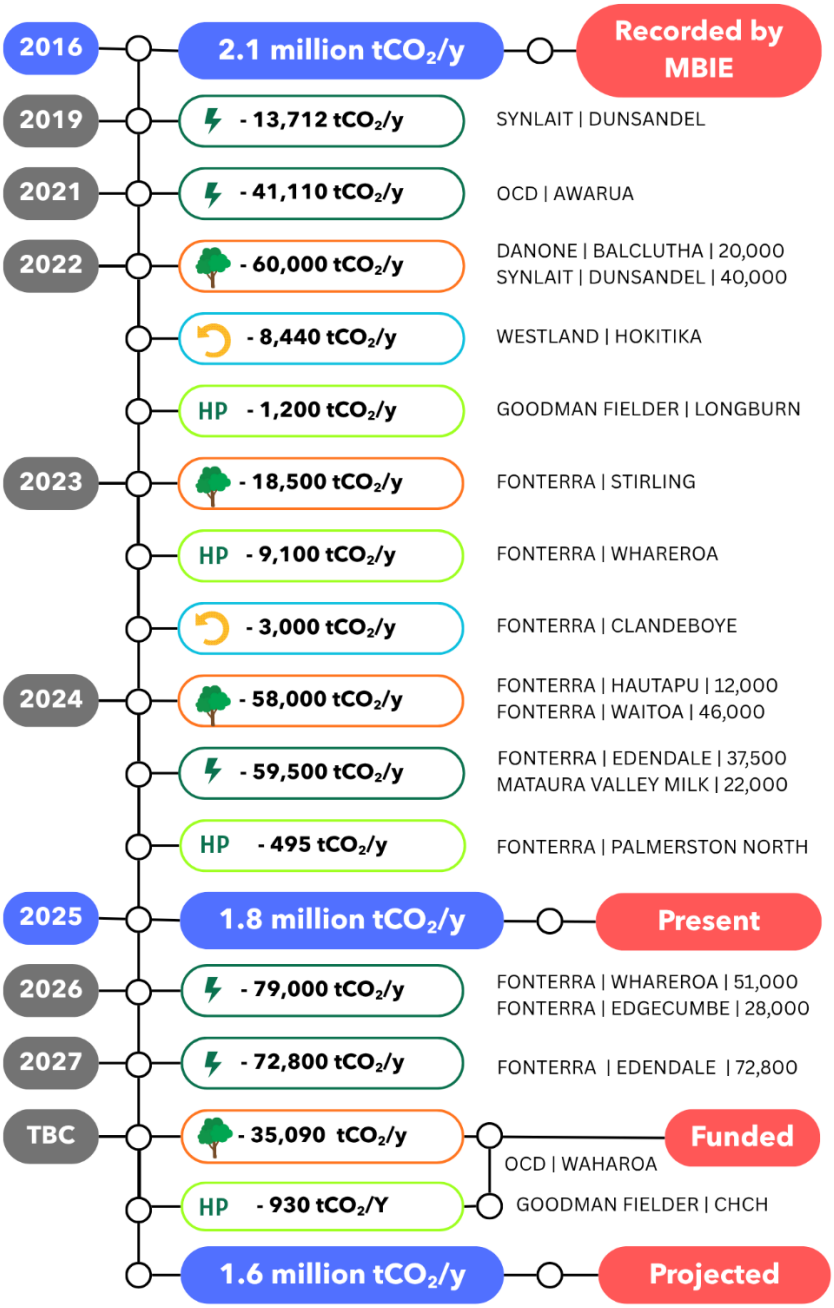

Figure 2. Recent decarbonisation efforts in the New Zealand dairy (processing) industry – since 2016.

In this context, a temperature glide refers to the temperature change of a process stream as it is heated or cooled, usually sensibly, rather than undergoing phase change at an approximately constant temperature. In spray drying, ambient air is heated continuously from near-ambient conditions to high temperatures, typically

in the range of 150 – 220 °C, before entering the drying chamber. This large temperature increase is required to provide sufficient driving force for moisture evaporation while maintaining product quality and throughput. As air is not an efficient heat carrier, a large energy demand is required to provide the target temperatures. For the development of a heat pump that can meet this energy demand, considerations around the optimal cycle configuration and components, the placement of the heat pump within the process and the refrigerant selection are necessary. Within this, detailed modelling is required to inform the design of a future prototype.

The refrigerant selection in the development of new heat pump technology is particularly constrained. The phase-out of ozone-depleting (high ODP) and high-emitting (high GWP) refrigerants restricts the choice of selection in new heat pump systems [12]. Ammonia is a popular refrigerant due to its high heating efficiency, zero ODP and zero GWP, however, the high toxicity of ammonia makes it less attractive, particularly at the scale required for New Zealand milk powder spray dryers (>MW). Although hydrocarbon refrigerants have low toxicity and high heating efficiencies, the high risk for fire and explosion are a significant barrier to uptake [13].

Refrigerants that are non-toxic and non-flammable with low ODP and GWP include air, water, and carbon dioxide (CO_2). While air would be a cheap and abundant refrigerant with no adverse effects due to leakage, relatively low COPs can be achieved. Additionally, the low specific heat capacity of air would require the heat pumps systems to be very large, which is unfavourable for retrofit into existing plants where space is constrained. Similarly, water would also be a cheap and abundant refrigerant, and has the highest specific heat capacity relative to other fluids, however, the vacuum pressures that would be required to evaporate water using low-temperature waste heat or ambient air would consume significant amounts of energy, such that the efficiency of the overall heat pump system would be severely decreased [14].

CO_2 is already a well-established refrigerant for commercial heat pump systems [14]. The low critical temperature and pressure of CO_2 lend itself well for use in transcritical heat pump cycles, rather than the more conventional subcritical cycles that use ammonia and hydrocarbons. The high volumetric heat capacity of CO_2 also minimises the size of the required components, and therefore the overall system [15]. Transcritical CO_2 heat pumps do not come without challenges, such as the high discharge pressures required from the compressor. However, for instances where upgrading the heat using a heat pump would require a large temperature increase, or temperature glide, such as is required for spray drying (~15 °C to 200 °C), more optimal temperature profile matching between the refrigerant and the heat sink (process stream) can be achieved, resulting in the potential for better performance when compared to conventional subcritical heat pumps and the ability to leverage the entire cooling profile of supercritical CO_2 [14].

1.2 Thesis aim

The aim of the thesis is to develop a new high temperature heat pump (HTHP) concept for heating large-temperature glide process applications. As a primary motivation, this thesis focuses on a milk powder spray drying process as the common case study of a large-temperature glide process. The scope of the research is focused on transcritical CO_2 cycles because of their low toxicity, flammability and good temperature-matching between the gas cooler and sinks with large-temperature glides (such as dryer air heating).

The research questions of this thesis are:

1. **Feasibility:** Can a closed cycle HTHP supply the full air-heating demand of the milk powder spray drying process?
2. **Cycle design:** What heat pump cycles and configurations offer high performance while remaining practical for industrial implementation?
3. **Process integration:** How should a HTHP be integrated in the milk powder spray drying process? Furthermore, can integration with other low-emissions technologies provide additional practical or economic advantages compared with a stand-alone heat pump system?
4. **Decarbonisation potential:** What is the potential emissions reduction achievable with a heat pump optimised for high temperature lifts and large temperature glides?

The objectives of this research are to evaluate and compare HTHP cycle configurations suitable for applications involving large temperature glides, and to examine the influence of expansion work recovery on cycle performance in this context. Additionally, the study aims to investigate practical strategies for integrating high temperature heat pumps into industrial processes under varying site constraints. Finally, the research seeks to explore the broader potential of high temperature heat pumps beyond the milk powder spray drying process, identifying opportunities for wider application across the food and process industries.

1.3 Thesis outline

This thesis has been structured to reflect the development stages of the research, from understanding the current state of HTHP technology to proposing and evaluating new cycle and integration concepts for industrial decarbonisation.

The body of the thesis begins with Chapter 2, which reviews the literature that has informed and guided this work. The chapter covers the key advances in high temperature and transcritical heat pump cycles, compressor technologies and their suitability for such applications, and the use of ejectors and expanders as potential cycle-enhancing components. Methods for modelling and comparing heat pump performance are also discussed, along with approaches to process integration and the experimental challenges associated with high-temperature componentry. This

review establishes the foundation for the research direction and highlights the technological gaps that motivate the subsequent chapters.

Chapter 3 introduces the case study that underpins this research and outlines the key design and boundary decisions that frame the investigation. This chapter provides the industrial and process context for evaluating the performance and integration of HTHP systems and defines the assumptions used consistently throughout the thesis.

The next stage of the research, presented in Chapter 4, focuses on the thermodynamic modelling of high temperature transcritical heat pump (HTTHP) cycle architectures using CO_2 as the working fluid. This chapter develops and compares several candidate cycle configurations and identifies a reference cycle that offers high performance under the process conditions of interest.

Building on these findings, Chapter 5 investigates the effect of expansion work recovery on the performance of the recommended CO_2 cycles. Different expander and ejector configurations are explored to assess their potential to improve efficiency and reduce exergy losses in high-temperature operation.

Chapter 6 explores the integration of the HTTHP results for a milk powder spray drying case study. It compares the performance and decarbonisation potential of the selected HTTHP with alternative fuel-switching options, such as electrode and biomass boilers. The chapter also explores the influence of site-specific constraints on integration feasibility and performance.

Chapter 7 broadens the discussion to consider potential applications of the technology beyond the milk powder spray drying process, highlighting opportunities for wider industrial decarbonisation.

Finally, Chapter 8 concludes the thesis by summarising the major findings and contributions of the research. The chapter also identifies areas where further research and development could accelerate the deployment of HTTHPs and support the broader transition to low-emission process heat.

Chapter 2
Literature review

2.1 Introduction

There has been extensive research into HTHPs in recent years, and a wide range of literature is available that pertains to different aspects in their advancement and development. For this thesis, the key areas of interest will be around heat pump performance and identifying the challenges related to developing a HTHP that can supply temperatures above 100 °C. Within this, the heat pump cycle design and process integration of heat pumps are of particular interest, with the objective to design a heat pump that is optimised for large-temperature glide applications, such as milk spray drying in New Zealand.

The aim of the literature review is to investigate HTHP cycles to identify suitable components for the development of a HTHP that can supply air heating for the spray drying process. As part of this, an investigation on appropriate performance metrics was undertaken to inform the method for comparing heat pump cycle performance and gain insights on the optimal heat pump cycle configurations. The scope will focus mainly on transcritical CO_2 heat pumps, as the source temperatures available for spray drying are generally at lower temperatures (<60 °). However, where the information is scarce, the scope may be widened to HTHPs using other refrigerants. The main parts of the literature review will examine existing refrigerants, transcritical heat pump cycle architectures, compressor technologies and process integration of HTHPs. The review is concluded by discussing a practical and economic pathway to investigate for the development of a HTHP for a milk powder spray drying case study.

2.1.1 Heat pump working principle

A standard industrial heat pump usually operates on the subcritical vapour compression cycle (Figure 3). A lower temperature heat source, such as waste heat or ambient air, is used to evaporate a refrigerant with a lower saturation temperature than the heat source. Once evaporated, the refrigerant is compressed to a higher temperature and pressure (P2) using electrical work input. The heat from the refrigerant is then rejected to a heat sink, which is usually a process heating stream that needs to be "upgraded" to a higher temperature, through condensing refrigerant vapour. Once condensed, the refrigerant is expanded to the evaporation pressure (P1) to restart the cycle.

A transcritical cycle differs slightly from a subcritical cycle in that the heat rejection stage occurs above the critical point of the refrigerant, and therefore, it does not condense. Hence, instead of having a condenser in the cycle, the heat rejection occurs in a gas cooler. Cooling of the refrigerant in a gaseous phase allows for the leveraging of the temperature profile, i.e., the temperature glide, exhibited by

sensible cooling, rather than condensation, at near constant temperature to reduce exergy destruction. A comparison of the heat rejection process for a subcritical heat pump (a) and a transcritical heat pump (b) is shown in Figure 4.

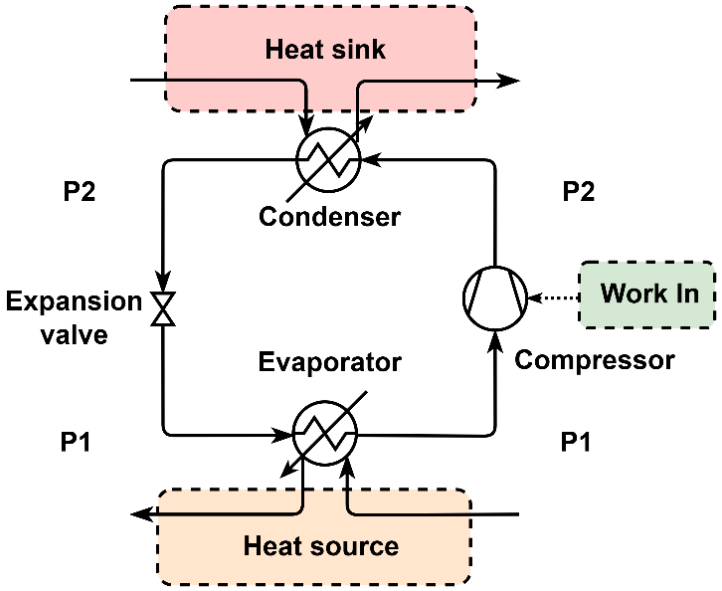

Figure 3. Subcritical vapour compression cycle.

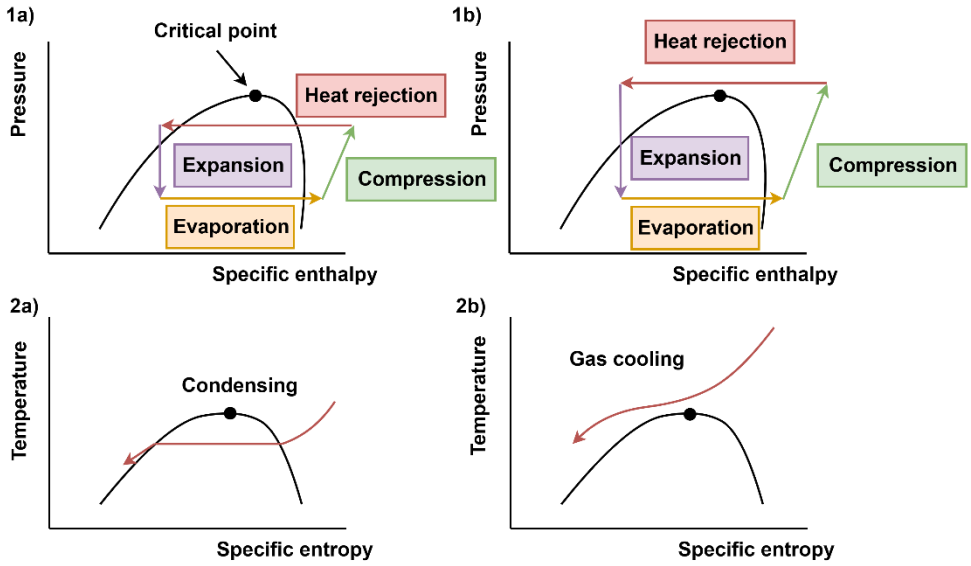

Figure 4. Comparison of 1) Pressure-enthalpy and 2) Temperature-entropy diagrams between a) subcritical and b) transcritical heat pumps – adapted from Austin and Sumathy [16].

2.1.2 Configurations

There are two main aspects for the arrangement of components for a heat pump system – one is the configuration of the heat pump, and the other is the components within the heat pump itself, i.e., the cycle architecture – particularly in the case of a closed cycle heat pump. In this work, the configuration of a heat pump refers to whether the heat pump, as a system, is open cycle or closed cycle and/or

whether it has any additional components outside of the heat pump itself that is integral to the intended operation of the heat pump system.

Arpagaus [17] identified five main configurations that are employed in the field of HTHPs. The first and most common configuration of heat pump for all temperature levels (not just HTHPs) is the closed cycle configuration (Figure 5). All closed cycle heat pumps will include some form of heat absorption (onto a refrigerant), compression, heat rejection (from the refrigerant), and expansion, where the refrigerant is in a closed cycle and there is indirect heat exchange between the sink stream and the refrigerant stream.

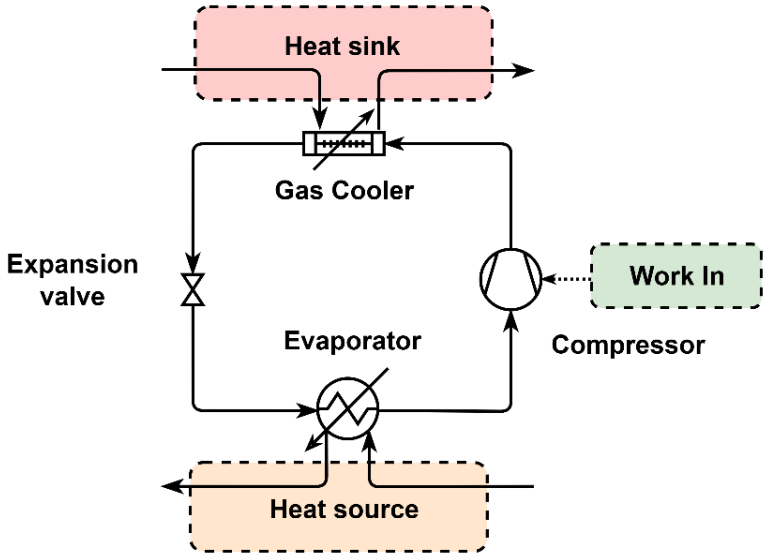

Figure 5. Closed cycle heat pump (transcritical).

The second heat pump configuration is an open cycle heat pump (Figure 6a). Open cycle heat pumps will generally use a process heating stream, such as steam, as the working fluid. In an open cycle configuration, the exhausted process heat vapour is recompressed to the set point temperature, where the process itself acts as the heat rejection, expansion, and heat absorption stages – if equated to a closed cycle heat pump. The most common employment of the open cycle heat pump is Mechanical Vapour Recompression (MVR) which recompresses steam to a higher saturation pressure and temperature.

The third heat pump configuration is an open cycle with a flash tank (Figure 6b). Similarly to the open cycle configuration (Figure 6a), the open cycle with a flash tank can also be used when the process heating fluid is used as the working fluid. However, the open cycle with a flash tank is most appropriate for when the process heating fluid is exhausted from the process as a liquid rather than a vapour. Dropping the pressure of the exhausted liquid allows a portion of the waste heat stream to be vapourised, which can then be compressed through an MVR. This can be done directly on the process stream or indirectly using a separate feedwater stream, annotated by the blue dotted line in Figure 6b. The third configuration (Figure 6b) is most suitable for when the waste heat temperatures are relatively

high, i.e. the temperature lift across the MVR is relatively small, as a single MVR unit can only increase the saturation temperature by up to 15 K [18].

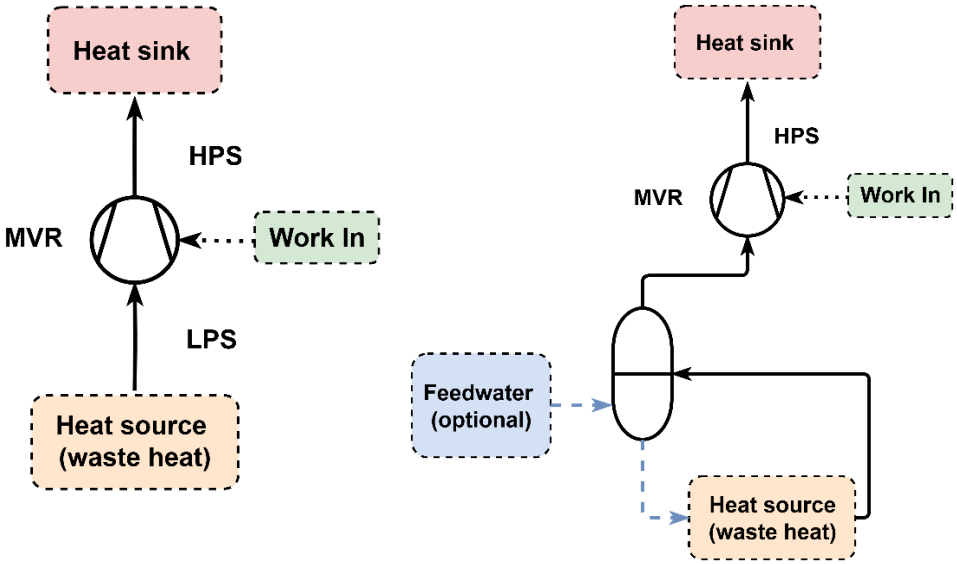

a) Open cycle heat pump

b) Open cycle heat pump with a flash tank

Figure 6. a) Open cycle heat pump and b) open cycle heat pump with a flash tank.

If the waste heat temperature was too low, it would require multiple MVR units integrated in series to achieve the required temperature lift. As a result, the capital cost would increase significantly, particularly if more than one additional MVR unit is needed. Instead, a fourth configuration could be employed to achieve the higher temperature lift requirement (Figure 7a). The fourth configuration is similar to the third configuration; however, the lower temperature waste heat is first upgraded using a closed cycle heat pump. The available heat now exists at a higher temperature as a liquid and is then flashed to produce vapour that is compressed to a higher pressure. This exploits the higher COP that can be achieved by an MVR for increasing the temperature of the steam but reduces the need for staging the MVR units. At the same time, moderately high COPs can be achieved from a heat pump over the larger temperature increase.

The fifth configuration takes a similar process to the fourth configuration but instead uses a closed cycle to heat a pressurised hot water loop, and which is then used to produce steam in a steam generator (Figure 7b). The heat transfer between to produce steam is done indirectly through a pressurised water loop, whereas in the fourth configuration, the heat sink of the closed cycle heat pump is the fluid which is flashed and upgraded in the MVR.

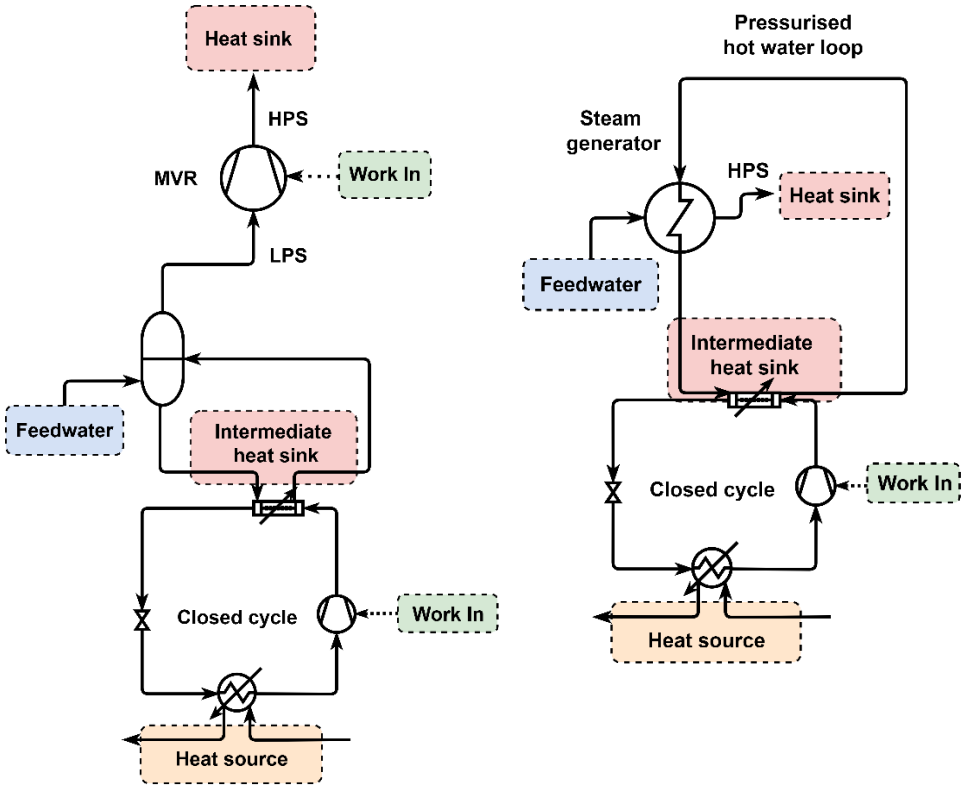

a) Closed cycle + flash tank + MVR (open cycle)

b) Closed cycle + pressurised hot water loop + steam generator

Figure 7. a) Closed cycle + flash tank + MVR (open cycle) heat pump configuration and b) closed cycle + pressurised hot water + steam generator heat pump configuration.

2.1.3 Refrigerant selection

Refrigerant selection is a critical decision in the development and integration of a HTHP within an application. The selection process is inherently complex, as the choice of refrigerant must be driven by the process requirements, yet it also directly influences the cycle architecture, performance, and design of the heat pump. These process requirements include safety (toxicity, flammability, and operating pressures), environmental impact (GWP and ODP) and thermodynamic suitability for achieving the required temperature lift and capacity per unit size. Additionally, the cost and long-term availability of a refrigerant should be considered to ensure the viability and sustainability of the heat pump system. Crucially, no single refrigerant excels in all these aspects, and the optimal choice will be a balance of trade-offs specific to each application.

Refrigerants for HTHPs are typically classified as synthetic (HCFOs, HFOs, HFCs) or natural refrigerants [8]. While halogenated synthetic refrigerants (HCFOs, HFOs and HFCs) often deliver higher performance, the use of these refrigerants is being banned in many regions, such as the EU, with the potential for other countries to follow in this direction [12]. Despite trade-offs in performance, safety, and environmental impact, opting for low-GWP and low-ODP refrigerants generally

ensures better alignment with climate targets and evolving regulations. As a result, research to improve the performance of natural refrigerants will be required.

Table 1 lists natural refrigerants that are suitable for HTHPs, which include CO_2, air, water, and hydrocarbons. The corresponding advantages and disadvantages of the refrigerants are also listed with the corresponding 20 year- (GWP20) and 100 year-Global Warming Potentials (GWP100) relative to CO_2. Ammonia is the most commonly used natural refrigerant. While traditionally used for refrigeration, recent demonstrations show the potential for higher temperature applications [19]. Simulation studies of ammonia HTHPs have shown that the COPs achieved can be relatively high [13], but its high toxicity can be a prohibitive barrier. Hydrocarbons have also been demonstrated to achieve high COPs for HTHPs, though their widespread adoption is limited by concerns over flammability [13].

Air is an abundant and low-cost refrigerant, but its low specific heat capacity leads to poor COPs and requires oversized components. Air can be suitable for Brayton heat pumps as some of the exergy can be recovered using an expander to compensate for the generally low performance [20]. Like air, water is also an abundant and inexpensive refrigerant with the added benefit of having a very high specific heat capacity, enabling high COPs. However, the boiling point of water at near atmospheric conditions is relatively high, which necessitates high source temperatures – making it unsuitable for processes with low-grade waste heat.

CO_2 has low toxicity and low flammability. Although the COPs of CO_2 heat pumps for large temperature glides is lower than the COPs that can be achieved hydrocarbon heat pumps, CO_2 has a very high volumetric heat capacity [21]. This enables compact heat pump designs which is a large advantage for the retrofit of existing plants. For large scale applications, CO_2 can be advantageous over the higher performing natural refrigerants at the temperature lift and glide required, namely ammonia and hydrocarbons [13].

Other natural refrigerants can also be used for Brayton heat pumps such as helium, argon and nitrogen. While inert and non-toxic, helium would be a costly option for an industrial-scale HTHP due to the sheer amount of helium required and its rarity relative to other refrigerants. At present, some helium HTHPs (reversed Stirling cycle) have been developed, however, the COPs are generally closer to 1 at the required temperatures [22], [23]. Limited research exists for argon and nitrogen in the use of high temperature heat pumps. Argon and nitrogen have comparable specific heat capacities to CO_2 but much lower volumetric heat capacities. A comparison of these natural refrigerants in Brayton and Stirling heat pumps has been given in the Appendix (Section 8.5).

Table 1. Natural refrigerants for high temperature heat pumps [24], [25]

Refrigerant	ASHRAE		P_{crit} (bar)	T_{crit} (°C)	GWP20/ GWP100	Advantages	Disadvantages
	No.	Class.					
Ammonia	R717	B2	113	132.3	0/0	Already well established in refrigeration	Toxic Flammable
CO_2	R744	A1	74	31.0	1/1	High volumetric heating capacity Suitable for large temperature glides Transcritical operation is common	High pressures required Lower COPs
Butane	R600	A3	38	152.0	0.022/ 0.006	High COPs	Flammable Low volumetric heating capacity
Isobutane	R600a	A3	36	134.7	-/3	High COPs	Flammable Low volumetric heating capacity
Pentane	R601	A3	34	196.6	-/4	High COPs	Flammable High source temperature required Low volumetric heating capacity
Isopentane	R601a	A3	34	187.8	-/4	High COPs	Flammable Low volumetric heating capacity
Water	R718	A1	221	373.9	-/0.2	High COPs Abundant refrigerant	High source temperatures required Low volumetric heating capacity
Air	R729	-	38	-140.6	-/<0.001	Abundant refrigerant Suitable for high temperature lifts Possible for large temperature glides	Low COPs Low volumetric heating capacity
Helium	R704	A1	2.27	-268.0	0/0	Inert and non-toxic	Limited production and growing demand Low volumetric heating capacity

The toxicity of ammonia is generally considered a well mitigated risk in the refrigeration industry and therefore the adoption risk for ammonia can be perceived to be lower. However, the refrigerant charge in a high temperature ammonia heat pump for spray drying would be significantly larger than a typical ammonia refrigeration unit, as the minimum heating demand would be much greater than the minimum cooling demand [26]. In addition, ammonia is flammable at concentrations between 15 and 28% by volume in air and when mixed with lubricating oils, the flammable concentration range increases [27]. The risks of using hydrocarbons are also amplified in large scale applications as a result of the charge and high flammability of hydrocarbons. The volumetric heat capacity of hydrocarbons is lower than CO_2, necessitating much larger heat pump systems. The use of CO_2 in HTHPs does not come without challenges. While CO_2 has low toxicity, it presents an asphyxiation risk. Additionally, extreme pressures (>100 bar) are required for CO_2 systems, which leads to higher cost componentry to maintain safety requirements. Developments in CO_2 HTTHPs need to address the challenges to lower the adoption risk [8].

2.1.4 Challenges for heat pumps

Adoption of heat pump technology is rapidly growing, however, the penetration level of heat pumps in large-scale industrial processes is still relatively low [28]. There are various challenges, including geographical, technological, economic and regulatory challenges, that are continuing to limit the uptake of heat pumps for industrial processes.

2.1.4.1 Technological

Adamson et al. [8] reviewed high temperature and transcritical heat pump developments, identifying six key technological challenges for HTTHP development with possible solutions, summarised in Table 2. The challenges are mainly related to the high pressures required for CO_2 heat pumps, which creates difficulty in the identification of a suitable compressor for a CO_2 HTTHP. Additionally, the limitations of the electrical network are also an important technical barrier. Voltage drops in the grid were identified by Aguilera et al. [29] as a significant potential cause for unexpected shutdowns of large-scale heat pump systems and the resulting compressor damage.

2.1.4.2 Lack of expertise, policy, and regulation

As new HTHP innovations are developed, COP is no longer a sufficient performance metric to compare heat pump systems due to an increase in the number of factors to consider, which makes it difficult to categorise the heat pumps into accessible information for the potential adopter. A lack of information and expertise around process integration and installation of large-scale HTHPs reinforces the reluctance for users to adopt heat pump technology with uncertainty further inflated by lack of clear policies for heat decarbonisation pathways and lack of regulation and standards around the installation of HTHPs [28]. User-friendly, informative tools related to the technical and economic considerations for installing heat pumps have

the potential to reduce the risk for the potential adopter, however, are currently not readily available [30].

Table 2. Technological challenges for high temperature transcritical heat pumps identified by Adamson et al. [8]

	Challenge	Possible solution
1	Extreme discharge pressures required (>150 bar for CO_2) which surpass the performance of existing compressor technologies.	Select cycle structures that limit the discharge pressure through: • Superheating prior to compression • Using refrigerants with lower critical pressures.
2	Requires compression ratios greater than 8 also surpassing the current specifications of commercially available compressor technologies.	Use multiple compression stages.
3	Identifying efficient refrigerants.	Optimise temperature profile match between the refrigerant and the source/sink.
4	Large heat transfer surfaces required.	Investigate trade-offs between fluid velocity, pressure drop, required pumping power, and cycle temperature lift.
5	Requires lubricants that is suitable across the full temperature range.	Use oil-free compressors.
6	High expansion losses due to high compression ratios.	Cool the refrigerant prior to expansion. Use expansion work recovery devices, such as ejectors.

2.1.4.3 Economic

While the use of heat pumps has been demonstrated to yield reduced operating costs, considerable capital investment is required [31]. The capital investment not only encompasses the high upfront cost of the heat pump but also the required costs for structural changes to retrofit existing industrial systems. Government initiatives can help to ease the financial risk for the potential user; however, expertise and technological readiness is still required. An example of such an initiative is the Government Investment in Decarbonising Industry Fund (GIDI) in New Zealand, where the New Zealand Government pledged 650 million dollars of funding for the subsidisation of process heat decarbonisation [32].

2.1.4.4 Geographical location

The efficacy of heat pumps in the context of decarbonisation is reliant on the way electricity is generated at the location where the heat pump is installed. For example, the emissions reduction of displacing natural gas consumption in a process by installing a heat pump would result in marginal, if any, reduction in

emissions if the electricity in the region is generated using coal. Additionally, the climate of the location can influence the efficiency of the heat pump. Yokoyama et al. [33] found that the COP of a transcritical CO_2 heat pump decreases with ambient temperature, and thus temperature control of the space where the heat pump being installed is an additional factor to consider in the installation of transcritical CO_2 heat pumps.

2.2 State-of-the-art for high temperature heat pumps

Heat pump performance varies significantly depending on the refrigerant, cycle configuration and placement of the heat pump within the process [8]. In general, as the temperature lift between the source and sink increases, the performance of a heat pump decreases, which is a challenge that must be mitigated in the development of a HTHP. Inherently, this is true as a result of the thermodynamic limits, i.e., the Carnot COP decreases. However, as the temperatures increase, there is also greater thermodynamic strain on the system components, which can decrease the performance of the overall heat pump system. While some developments have produced high temperature heat pumps that can achieve large temperature lifts, they do not necessarily produce large temperature glides, and vice versa, which would be required to substitute the function of a traditional boiler.

2.2.1 Developments in high temperature heat pump technologies

HTHPs are being continually developed to increase the sink temperatures that they can supply [34]. HTTHPs are gaining interest due to the ability to exploit the temperature profile or "temperature glide" in the gas cooler to increase the efficiency of high temperature heating. The IEA Annex 58 Task 1 – Technologies [35] provides an overview of HTHP demonstration cases above 100 °C. In the 150 – 200 °C temperature range, many of the heat pumps that have been developed are focussed on steam generation. A Stirling heat pump with R704 (helium) as the refrigerant has achieved temperatures up to 183 °C for steam generation and has been demonstrated for a pharmaceutical application. The heat pump system has a reported capacity of 1.5 MW and a technological readiness level (TRL) of 7 to 9 with a COP of 1.7 when using a 36 °C source [36]. In this system, a very large temperature lift (approximately 150 °C on average) can be achieved but the temperature glide at steady state operation is only 5 °C. Another demonstration steam generating heat pump, using R600a (isobutane) as the refrigerant, is under construction at a pulp and paper plant. At a source temperature of 15 °C and sink heating from 104 °C to 170 °C (66 °C temperature glide), the system expects to achieve a COP of 2 [37]. The 12 MW heat pump is intended to supply steam at 170 °C for thermal power production. The manufacturers claim that the systems can achieve a maximum heat sink temperature of up to 250 °C with a maximum temperature lift exceeding 100 °C. Table 3 lists further demonstration cases of heat pumps supplying temperatures above 150 °C.

Table 3. High temperature heat pump demonstrations reported in the Annex 58 that can produce temperatures above 150 °C [35, p. 1].

No	Manufacturer	Refrigerant	$T_{sink\ in}/T_{sink\ out}$ (°C)	ΔT_{glide} (°C)	$T_{source\ in}$ (°C)	ΔT_{lift} (°C)	Capacity (MW)	COP
1	KOBELCO [38]	R245fa +R134a (HP)/ R718 (comp.)	20/115 (HP), 165 (comp.)	95 (HP)	70	95	0.624	2.5
					50	115		2.2
2	AtmosZero [39]	Synthetic (unspecified)	90/150	60	-10	160	0.65	1.4 – 1.6
					15	135		1.7 – 1.9
					40	110		1.9 – 2.1
			90/165	75	15	150		1.6 – 1.7
3	ecop Technologies GmbH [40]	R704 +Argon +Krypton	120/150	30	120	30	0.7	5.8
4	Rank [41]	R245fa, R1336mzz(Z), R1233zd(E)	-/160	-	100	60	0.12 – 2.0	3.0
			-/160	-	116	44		2.8
5	Svenska Rotor Maskiner International AB [42]	R718	159/160	1	91	69	1.0	1.9

No	Manufacturer	Refrigerant	$T_{sink\ in}/T_{sink\ out}$ (°C)	ΔT_{glide} (°C)	$T_{source\ in}$ (°C)	ΔT_{lift} (°C)	Capacity (MW)	COP
					101	59	1.31	2.6
					111	49	2.13	3.8
6	SPH Sustainable Process Heat GmbH [43]	R1234ze, R1233zd, R1224yd, R1336mzz-E, R1336mzz-Z	-/159	-	95	64	0.3 – 5.0	3.0
7	Olvondo Technology AS [23]	R704	178/183	5	36	148	0.5	1.7
					60	123		1.9
			154/159		60	99		2.1
8	Heaten [44]	HCs, HFOs (unspecified)	155/165	10	120	45	1.0 – 8.0	4.6
9	Enerin [45]	R704, R728	206/212	6	85	117	0.3 – 10.0	2.0 – 2.15
					16	196		1.6 – 1.7
			154/160		135	25		3.3 – 3.7

No	Manufacturer	Refrigerant	$T_{sink\ in}/T_{sink\ out}$ (°C)	ΔT_{glide} (°C)	$T_{source\ in}$ (°C)	ΔT_{lift} (°C)	Capacity (MW)	COP
					80	80		2.2 – 2.45
					16	144		1.75 – 1.9
10	Turboden S.p.A [37]	R600a (HP), R718 (comp.)	104/170	66	15	155	5.0 – 40.0	2
11	MAN Energy Solutions [46]	R744	50/150	100	20	130	10.0 – 50.0	2.85
12	Siemens Energy [47]	R1233zd(E), R1234ze(E)	105/150	45	115	35	8.0 – 70.0	4.1
			20/190 (incl. comp.)	-	80	-		2.9

Some manufacturers have explored the use of heat pumps to supply pressurised water at temperatures above 100 °C, which is expanded and flashed to produce steam and then compressed to a higher temperature and pressure. An example of such a system was commercialised in 2011, which can produce approximately 600 kW of steam at 165 °C [38]. The system can achieve a COP of 1.9 with a source temperature of 50 °C and a sink inlet temperature of 20 °C. The refrigerant used was a R245fa/R134a mixture. Another option is to use an open cycle system, where the heat is rejected to the process. One open cycle system [48] is able to produce superheated steam at 240 °C (201 °C saturation temperature) with a high COP of 4.7 for a pulp drying application (approximately 11 MW heating capacity). However, the system requires a very high source temperature of 133 °C, which makes it less suitable for many process heating applications.

2.2.2 Transcritical heat pump cycle concepts

For the development of a CO_2 HTTHP, it is important to consider cycle configurations that can achieve the high sink temperatures required while maximising the COP of the system. Transcritical CO_2 heat pump systems in the literature that have sink temperatures greater than 80 °C were the focus of the review with some unique cycle configurations identified with sink temperatures less than 80 °C also included to identify potential cycle-enhancing components or configurations.

HTHP and transcritical heat pump cycles were reviewed by Adamson et al. [7]; the article introduced a coding system to classify the 49 unique cycles found in the literature. The following review will use the same coding convention, summarised in the Appendix: Table 34 to classify the cycles and also for additional cycles found from other review papers (review articles in Table 35 and individual research articles in Table 40). For individual articles, both simulation/thermodynamic analysis and experimental research articles were considered that included the key terms: “transcritical R744 cycles”, “transcritical heat pumps”, “transcritical CO2 cycles” and “high temperature transcritical heat pumps”. The operating conditions for the heat pump and the type of research conducted (simulation or experiment) for each individual article is also identified in Table 34. A review of market available heat pumps was also conducted to understand the current climate of transcritical heat pumps in industry (Table 41).

2.2.2.1 Internal heat exchangers

The simplest transcritical heat pump cycle (T1-1) is shown in Figure 8, featuring an evaporator, compressor, gas cooler and an expansion valve. In transcritical CO_2 heat pumps, the large pressure differences across the compressor and expansion valve can result in significant exergy destruction and therefore limits the performance of the heat pump. The most common modification to improve the cycle performance would be the addition of an internal heat exchanger (IHX). The simplest IHX cycle (T1-2) is also shown in Figure 8. IHXs are commonly used to preheat the refrigerant at the compressor suction inlet by cooling the refrigerant at the gas cooler

(condenser for a subcritical cycle) outlet [8]. This simultaneously minimises the compressor work and reduces exergy destruction during expansion.

T1-1 – Single-stage cycle T1-2 – Single-stage cycle with IHX

Figure 8. Cycle diagrams for T1-1 and T1-2.

Cao et al. [49] performed an experimental comparison between the T1-1 and T1-2 cycle, i.e. without IHX and with IHX respectively, for heating water to 70 – 90 °C, finding COP improvements ranging between 1 and 7 % from the addition of an IHX. In another study, Cao et al. [50] also simulated the T1-2 system with discharge temperatures up to 140 °C, finding COP improvements of up to 13% in comparison to T1-1. The results of both studies suggested that the IHX becomes more beneficial for the overall system performance when the gas cooler outlet temperature of the refrigerant is higher, which can be attributed to greater heat recovery within the cycle.

2.2.2.2 Economisers

Economisers are similar to IHXs in that they are primarily used to subcool the refrigerant prior to expansion, however, instead of transferring heat to the suction inlet of the compressor, the refrigerant at the gas cooler outlet is expanded to an intermediate pressure and temperature for compression intercooling. Economisers can be in an open or closed configuration (Figure 9). In an open economiser (sometimes referred to as a flash economiser), the expanded fluid enters a separator where the vapour is separated and injected into the compressor between the first and second stages. The separated liquid is further expanded prior to evaporation. In a closed economiser, a portion of the refrigerant from the gas cooler outlet is diverted and expanded to an intermediate pressure and temperature. The intermediate pressure fluid exchanges heat with the remaining refrigerant from the gas cooler outlet before injection [51].

The use of economisers was more commonly found in refrigeration applications. Cecchinato et al. [52] studied the performance of four transcritical CO_2 cycles (TI-3, TE-2, TE-4, TP-1) for a refrigeration application. The study found that two-stage compression with double throttling and closed economisers (TE-2 and TE-4) gave efficiency improvements of up to 70 % compared to single-stage compression with single throttling (TI-3), however, the cycles were much more complex, increasing the required installation costs. For heating applications, Agrawal et al. [53] investigated cycles TI-1, TI-3 and TE-3 (Figure 9). TE-3 exhibited the highest COP of

the cycles; the COP of TI-1 was limited due to the additional mass in the second stage compressor and gas bypass enabled by the TE-3 configuration increased the effectiveness of the evaporator in comparison to TI-3. However, the highest discharge temperature of 240 °C was able to be reached by TI-3 with COPs that were comparable to TE-3 for a discharge temperature of 160 °C, suggesting that TI-3 is more suitable for high-temperature applications.

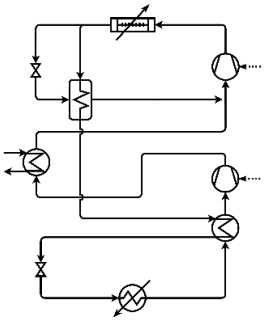

TE-2 – Two compression stages with closed economiser, IHX and external intercooling

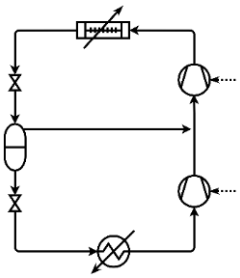

TE-3 – Two compression stages with open economiser

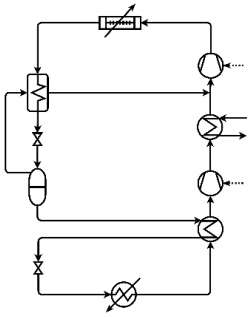

TE-4 – Two compression stages with closed and flash economisers and external intercooling

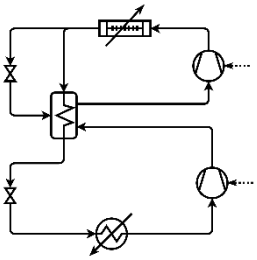

TE-5 – Two compression stages with closed economiser

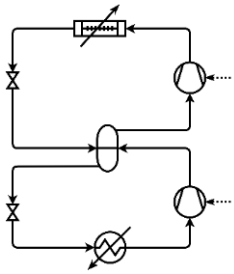

TI-1 – Two compression stages with open economiser/ intercooler

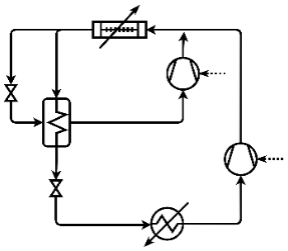

TP-1 – Single-stage with closed economiser and parallel compression

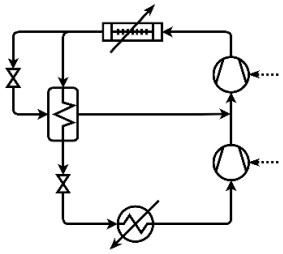

TP-2 – Two compression stages with closed economiser

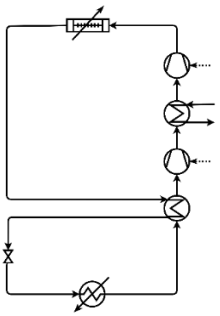

TI-3 – Two compression stages with IHX and external intercooling

Figure 9. Cycle diagrams for open and closed economiser heat pumps, two-stage compression heat pumps and parallel compression heat pumps.

2.2.2.3 Cascade cycles

Limited research exists for transcritical CO_2 heat pump cycles that produce sink temperatures at 200 °C. A study by Sarkar et al. [13], conducted in 2007, modelled

T1-2 (and the subcritical equivalent) for various natural refrigerants, heating water from 30 °C to 200 °C. For the CO_2 cycle, a COP of only 1.67 could be achieved, markedly lower than the COPs of the ammonia, propane and isobutane cycles.

Coupled with lower efficiencies for standard heat pump cycle configurations, CO_2 heat pumps are generally regarded as unsuitable for industrial processes due to the low critical temperature of CO_2 compared to the temperatures of industrial waste heat [54]. Transcritical CO_2 heat pumps are commonly air-sourced at temperatures less than 30 °C, making high temperature lifts, such as what is required for industrial HTHPs, less intuitive. Temperature lifts in heat pumps are a prevalent limitation to HTHP development. Increasing the temperature lift in a heat pump requires the refrigerant to be compressed to a higher pressure and may require more than one compression stage. Generally, the efficiency loss due to increasing the temperature lift is mitigated through intercooling (in multi-stage compression cycles), for example, by using economisers or external intercooling, and/or cascade arrangements.

Cascade cycles are used to combine two heat pump cycles, generally the bottom cycle condenser or gas cooler also acts as the evaporator or superheater for the top cycle (Figure 10). One advantage of cascade cycles is that different refrigerants can be used for each cycle, allowing for better refrigerant matching. Both Wu et al. [55] and Yang et al. [56] analysed cascade systems with a subcritical top cycle, using R1234ze(z) and R152a respectively, and transcritical bottom cycle (TS-1), both using CO_2, that produced sink temperatures ranging between 90 and 102 °C. Although the operating conditions were generally similar, the COPs for the R152a cycle were much higher for sink temperatures of approximately 100 °C, highlighting the importance of refrigerant selection in high temperature heat pumps.

A more standard cascade configuration (TS-2) with IHX on both the top and bottom cycles was analysed by Yao et al. [57], achieving a COP of 2.2 for a discharge temperature of 130 °C. Adamson et al. [8] proposed a unique transcritical-transcritical cascade cycle concept (TT-1), where a single-stage transcritical cycle is used to superheat the suction inlet of another single-stage cycle to increase the possible temperature lift.

Cascade systems can also be advantageous due their ability to better exploit multiple sources and produce multiple sinks. In the cycle analysed by Wu et al. [55] and Yang et al. [56] (TS-1), the two cycles have individual sinks and sources, cascaded by a superheater for the bottom cycle and subcooler for the top cycle. For an industrial heat pump, there is the potential for such a cycle to supply cooling and heating for multiple process streams and thus, displace more utility demand. Further, multi-temperature heat pumps can also exist as a non-cascade system. While the COPs are generally lower for these systems, single-stage multi-temperature heat pumps can be advantageous to improve temperature matching in the gas cooler or evaporator [58].

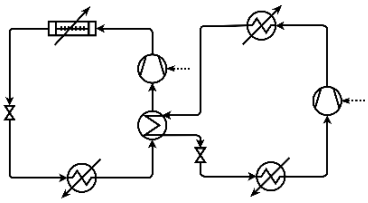

TS-1 – Cascade with transcritical, single-stage (left cycle/bottom) and subcritical, single-stage (right cycle/top) with subcooler

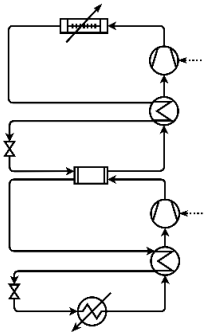

TS-2 – Cascade with transcritical, single-stage with IHX (top) and subcritical, single-stage with IHX (bottom)

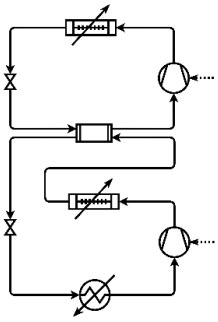

TT-5 – Cascade with transcritical, single-stage (top) and transcritical, single-stage (bottom) with gas cooler and cascade in series

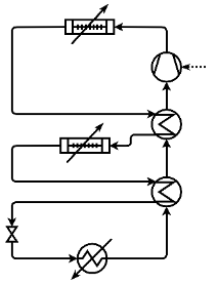

TI-3 – Single-stage with mid-gas cooler IHX and normal IHX

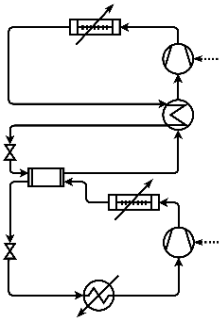

TM-6 – Cascade with transcritical, single-stage with IHX (top) and transcritical, single-stage (bottom) with gas cooler and cascade exchanger in series

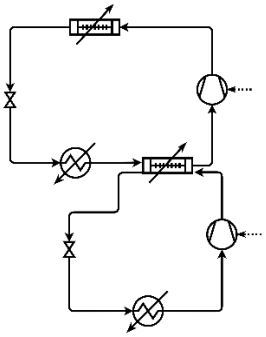

TT-1 – Cascade with transcritical, single-stage (top) and transcritical, single-stage (bottom)

Figure 10. Cycle diagrams for cascade and multi-temperature heat pumps.

2.2.2.4 Temperature profile matching

While the COP increase between T1-1 and T1-2 was the main focus of the study by Cao et al. [49], the most significant effect on the overall system COP was found to be related to the temperature profiles of the exchanging fluids in the gas cooler. For heating water to 70 °C, a COP of 3.81 was achieved for a sink inlet temperature of 10 °C, however, the COP was only 2.92 for a sink inlet temperature of 40 °C for T1-2. Similarly, Jiang [59] found in an experimental study that the COP of T1-1 increased by 15 % when heating water from 15 °C to 65 °C compared to heating the water from 25 °C to 65 °C and Sarkar et al. [13] showed that the COP decreased from 1.67 to 1.52 for T1-1 when the sink was heated from 100 °C to 200 °C compared to 30 °C to 200 °C heating. Another study by Sarkar et al. [60] concluded

that 90 % of losses in the gas cooler are due to the temperature difference between the exchanging fluids.

Closely matching the temperature profiles, i.e. minimising the approach temperatures, of the CO_2 and sink improves heat exchanger effectiveness and minimise losses in the gas cooler, therefore improving the system performance. Ye et al. [61] used a pinch point analysis approach to achieve closer temperature profile matching in the gas cooler by varying the discharge pressure, achieving a COP improvement of 26.3 %. The extent which the temperature profile matches can be optimised for a single gas cooler is limited, however, due to the nonlinear dependence of the specific heat of CO_2 on temperature. As a result, high expansion losses can still occur.

2.2.2.5 Expander and ejector cycles

With such high expansion losses in CO_2 cycles, expansion work recovery becomes a viable modification for CO_2 HTTHPs, using either an expander or an ejector (Figure 11). Expanders operate inversely to compressors and thus have similarities in type, e.g. piston, screw, screw and turbo [62]. When the refrigerant is expanded, work can be recovered which minimises the total work required by the heat pump system. Ejectors recover the expansion work of the high pressure refrigerant by converting expansion work into to kinetic energy. In doing this, a vacuum is created (as a result of the high velocity), which entrains the lower pressure refrigerant out of the evaporator. An intermediate pressure fluid results which simultaneously decreases the compression work required by the compressor and reduces the expansion losses.

Ma et al. [63] performed a comparative analysis of expander CO_2 cycles (TX-1, TX-3, TX-4, TX-5) where the expander was used to power the compressor or one of the compressors for two stage compression. The study found that the use of an expander for two-stage compression without intercooling held little benefit compared to a single-stage expander system. However, the COP of the two-stage system could be significantly improved with the addition of intercooling. Powering the high (TX-5) or low (TX-4) stage compressor using the expander did not differ significantly for the heating COP, however, the cooling COP for TX-5 was higher. For cases where the objective is simultaneous heating and cooling, using an expander to power a high-stage compressor with intercooling would be advantageous.

While expanders tend to have higher efficiencies than ejectors, the complexity and the capital cost of an expander heat pump is far greater than an ejector heat pump. However, in situations where the heat pump could have fluctuating loads, an ejector system would cause challenges due to its fixed geometry. The operation of a spray dryer is generally fixed, which makes it possible to use ejectors for expansion work recovery. Zhang et al. [64] performed an extensive review of ejector heat pump systems, concluding that the performance of heat pump cycles in general can be improved by more than 30 % through the use of ejectors. Many experimental transcritical CO_2 ejector heat pump systems have also demonstrated

the performance improvement resulting from ejector cycles, T1e-1 and T1e-2, compared to basic transcritical cycles, T1-1 and T1-2 [65], [66], [67]. With the substantial COP improvements and very low capital cost, ejectors have significant potential in future heat pump development, therefore, ejector developments will be investigated further in this review (Section 2.2.3.2).

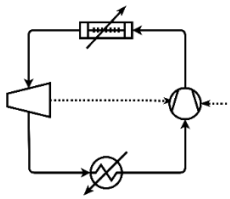

TX-1 – Single-stage with expander

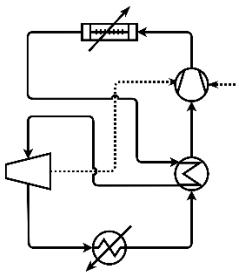

TX-2 – Single-stage with expander and IHX

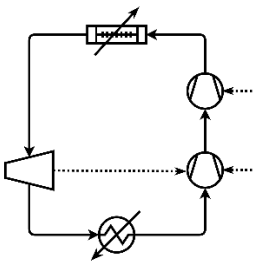

TX-3 – Two compression stages with expander on the low stage

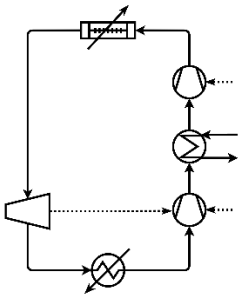

TX-4 – Two cimpression stages with expander on the low stage and external intercooling

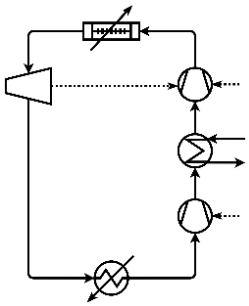

TX-5 – Two compression stages with expander on the high stage and external intercooling

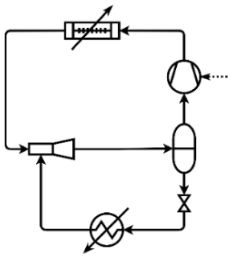

T1e-1 – Single-stage with ejector and separator

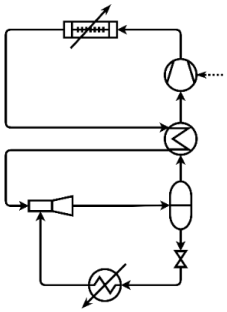

T1e-2 – Single-stage with IHX, ejector and separator

Figure 11. Cycle diagrams of expander and ejector heat pumps.

2.2.2.6 Conclusions

The primary objective in HTHP development is to increase the temperatures which it is possible for heat pumps to operate at economically. At present, high-temperature lifts in transcritical heat pumps result in restrictively low COPs with little research cascade and single-stage cycle configurations that can produce sink temperatures above 200 °C, utilising expansion work recovery, internal heat

exchange and optimising the temperature profile matches in the gas cooler to minimise the discharge pressure requirements and increase the cycle performance.

2.2.3 Components

2.2.3.1 Compressors

One of the key challenges in HTHP development is that some technologies operate at conditions which surpass current compressor performance parameters. The objective of this section of the review is to provide an overview of the current state-of-the-art for market available compressors and identify which compressor types are the most suitable for a CO_2 HTTHP. It should be noted that compressors in HTHPs are largely bespoke due to the generally bespoke nature of high temperature heat pumps and therefore the technical information is not readily available.

Compressors are used to increase the pressure and, consequently, the temperature of a gaseous fluid. There are two main types of compressors: positive displacement and dynamic. All compressors are generally powered by electric motors which consume work to power the shaft (shaft work). A positive displacement compressor works by decreasing the volume of the fluid. The method by which the volume is decreased is different depending on the type of positive displacement compressor. For example, in a reciprocating compressor, the volume of the fluid is decreased using a piston and cylinder whereas for a scroll compressor the volume of the fluid is decreased using two spirals, one which is stationary and one which orbits. The different types of positive displacement compressor and their respective working principles are given in Table 4. A dynamic compressor compresses a fluid by accelerating the fluid to high velocity and then converts the kinetic energy into static pressure. Dynamic compressors are categorised by the direction of fluid flow, given in Table 5.

The pressures required for CO_2 are often multiple times greater than that of other refrigerants, resulting in large pressure differences across the compressor and high expansion losses. In 2004, Hays and Brasz [68] developed a turbine-compressor (expander-compressor) to integrate expansion work recovery for vapour compression cycles. Although this design was shown to increase the efficiency of the cycle, it was not until recently that centrifugal compressors were starting to be seen on the transcritical CO_2 compressor market at the scale that could be used for a heat pump. The reason for this delayed uptake is likely due to complexity and cost. In 2021, MAN Energy Solutions (now Everllence) introduced a high-temperature CO_2 heat pump which uses a centrifugal compressor with an integrated expander (HOFIM^{TM}), achieving sink temperatures of 150 °C. The HOFIM^{TM} compressor is designed for pressures of up to 30 MPa. It was stated that the maximum sink temperatures that could be produced by the heat pump could not be increased due to the limitations of using CO_2 as a refrigerant. Thermodynamically, this has been proven to be untrue [13]. However, it is unclear whether this statement was related to the performance capabilities of the compressor or the chosen cycle (TX-2).

Table 4. Positive displacement compressors.

Type of compressor	Subcategory	Working principle
Reciprocating	Reciprocating	The fluid is drawn into the cylinder and compressed using the piston. The fluid is then discharged from the cylinder.
Scroll	Orbital	The fluid is compressed between two spirals (scrolls). One spiral is orbiting while the other is static, resulting in a reduction of the volume of the fluid as the pockets of fluid between the scrolls are slowly pushed towards the centre.
Screw	Rotary	The fluid is compressed between two adjacent, interlocking helical rotors (screws) that turn in opposing directions within the housing. The fluid is trapped between the two screws, and the volume is gradually decreased throughout the rotation as the fluid moves from the inlet to the outlet.
Vane	Rotary	The fluid enters a chamber containing an eccentric rotating shaft with vanes that slide in and out of the housing to meet the outer wall of the chamber. As the shaft is off-centre from the chamber, the vanes shorten as they rotate, causing the volume that the fluid occupies to decrease.
Swing	Rotary	The fluid is drawn into the chamber by the orbiting motion of a piston which is eccentrically connected to a shaft, vane and spring. The “swinging” orbital motion of the piston draws fluid into the chamber, reduces the volume and discharges the fluid.

Table 5. Dynamic compressor types.

Type of compressor	Working principle
Radial (Centrifugal)	The fluid is drawn into the compressor tangentially to the axis of rotation. The radial motion and radial design of the blades in the impeller cause the fluid velocity to increase and the static pressure to rise as a result of the centrifugal force. The static pressure is then further increased by passing the high-velocity fluid into a diffuser.
Axial	The flow of the fluid in an axial compressor is parallel to the axis of rotation. The fluid velocity is increased by multiple rotating blades and then diffused (resulting in increased static pressure) by multiple stationary blades.
Mixed-flow (Diagonal)	Aspects of axial and radial compressors are combined to produce a diagonal fluid flow to the axis of rotation.

The majority of compressors found as part of the review were reciprocating compressors. A summary of the standardised market available compressors for CO_2 HTTHPs that were found is given in Table 6. A Bock semi-hermetic piston compressor (HGX34/130-4 S CO2 TGEA) was used in a lab-scale experimental prototype developed by Zhang et al. [69] for producing water up to 86 °C. The GEA AddCool CO_2 HTHP also uses a Bock semi-hermetic piston compressor to heat water up to 120 °C [70]. Dürr thermea thermeco2 [71] uses reciprocating compressors manufactured by either Dorin or Bitzer for supply temperatures up to 120 °C. The Mayekawa Eco Sirocco [72]and Eco Cute Unimo [73] heat pumps both used rotary screw compressors for sink temperatures up to 120 °C, however, the technical information for the compressor could not be found.

The Mistubishi Q-ton heat pump was the only one found to use a rotary scroll compressor [74]. With the exception of the Bitzer and MAN Energy Solutions compressors, which can achieve discharge pressures up to 16 and 30 MPa respectively, all the compressors that were identified in the review would be unable to achieve the pressures required for a HTHP (>13 MPa). The implementation of HTHPs is very limited in this respect, however, with the growing popularity of Carbon Capture and Storage (CCS), which requires CO_2 compression to pressures far greater than 15 MPa, there is the possibility that borrowing innovations from large-scale CCS compressors to create compressors for HTHPs are not far in the future. Although, it is uncertain when the scale and cost of these technologies will become accessible for HTHP implementation [75]. Initially, it would be beneficial to investigate ways in which the discharge pressure requirements for the HTHP could be reduced until compressor technologies advance in their design.

The modelling of heat pumps is generally done through the analysis of individual control volumes around each component, with varying levels of detail that exist in heat pump compressor modelling. Sarkar et al. [13] used the simplest form of compressor modelling for a high temperature transcritical CO_2 heat pump where the compression process is assumed to be steady-state and adiabatic but non-isentropic, using an assumed isentropic efficiency. The assumption for isentropic efficiency has a significant effect on the calculated sink temperatures and COP. The isentropic efficiency used by Sarkar et al. was 70 % for compression from 5.7 MPa to 20 MPa. Neksa et al. [76] developed a series of semi-hermetic reciprocating CO_2 compressors, measuring an isentropic efficiency (including the motor efficiency) and volumetric efficiency of 0.69 and 0.77 for a single stage, compressing from 2.7 MPa to 6.9 MPa, suggesting that an isentropic efficiency assumption of 70 % is too high for compression up to 20 MPa as the isentropic efficiency is expected to decrease due to increased entropy generation at higher temperatures. Modelling of compressors using manufacturer data is generally more accurate, however, the same problem is faced when investigating compressors at more extreme operating conditions [77]. For detailed modelling, CFD can be used, however this would not only require the design of a compressor but is often computationally intensive.

Table 6. Review of standardised market-available CO_2 compressors for heat pumps.

Manufacturer	Compressor type	Inlet pressure (MPa)	Outlet pressure (MPa)	Frequency (Hz)	Displacement (m^3/h)	Power consumption (kW)	Lubricant/ Lubricant charge (L)	Other notes	Reference
Atlas Copco*	Centrifugal	0.01	20.5	50 – 60	-	-	-	Eight-stages with intercooling. Large-scale (for carbon capture and power cycles)	[75]
GEA Bock	Piston	1 -5	4 – 13	20 – 70	6 – 45	10 – 58.7	BOCKlubE85/2.3 -2.6	Semi-hermetic	[78]
Emerson	Piston	4 - 9	4 – 12	-	-	-	-	-	[79]
Bitzer	Reciprocating	4 – 10	4 – 16	50 – 60	17.5 – 21.1	< 33.7	BSE85K/-	-	[80]
Mehrer	-	0.01	1.9 – 10	-	-	22	Oil-free/-	-	[81]
Dorin	Piston	2 – 8.5	5.5 – 13	30 – 70	13.8 – 16.6	-	-/2.5	Maximum temperature is 160 °C. Semi-hermetic.	[82]
MAN Energy Solutions	Centrifugal	-	< 30	-	-	In the MW range.	Oil-free/-	Hermetic with integrated expander	[83]

2.2.3.2 Ejectors

In conventional heat pump cycles, such as in Figure 3, losses can occur during expansion which results from friction. The magnitude of these losses is dependent on multiple factors, including the thermodynamic properties of the refrigerant. However, large compression ratios generally result in greater expansion losses which is particularly relevant for HTHPs. One way which expansion losses can be minimised in heat pumps is by using ejectors. An example of how an ejector can be placed in a heat pump is shown in Figure 12. Compared to the conventional heat pump system, given in Figure 3, the ejector introduces a third, intermediate pressure (P3 as shown in Figure 12 where P1<P3<P2) which reduces the compression ratio across the expansion valve and thus reduces the expansion losses. Additionally, the pressure of the refrigerant leaving the evaporator is increased through the ejector, lowering the compression ratio across the compressor. Theoretically, this lowers the compression work required and increases the COP of the heat pump.

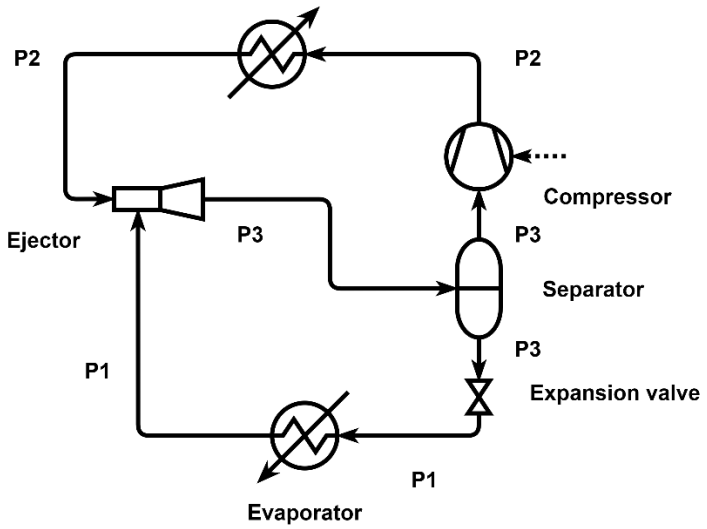

Figure 12. Ejector heat pump cycle example.

The working principle for an ejector involves two fluids, generally, a high-pressure liquid or gas and a low-pressure vapour that mix to produce an intermediate pressure vapour (Figure 13). The high-pressure stream is referred to as the motive fluid [84]. The motive fluid enters a nozzle that causes the fluid to accelerate and generate a vacuum pressure or pressure which is lower than the pressure of the low-pressure stream. This draws the low-pressure stream into the ejector from a secondary inlet, mixing with the motive stream in the mixing section. Once combined, the stream enters a diffuser section within the ejector where the velocity of the stream decreases and pressure is regained. The resulting pressure at the outlet of the ejector will be between the high and low inlet pressures.

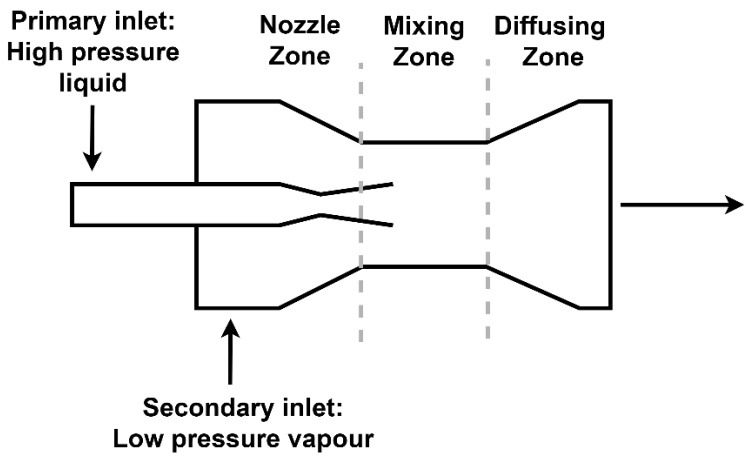

Figure 13. Ejector working principle – image adapted from Adamson et al. [8].

Ejectors are a low cost, simple in structure (compared to an expander), and low maintenance modification that can be made to recover expansion work that would normally be lost during throttling in heat pump systems. Ejectors also enhance the cycle performance by increasing the suction pressure or decreasing the discharge pressure, thus reducing the compression work and can function as a flash gas bypass, reducing the required evaporator size [64]. The objective of the review was to identify ways to optimise ejector design and placement in transcritical heat pump cycles. The secondary objective of the review was to determine the level of depth required for an ejector model that is sufficient to develop a prototype system. Review papers related to ejector technologies were included in the review (Table 36), which discussed the application of ejectors in vapour compression cycles. Individual research articles related to high temperature transcritical CO_2 ejector heat pumps and their associated challenges were also considered (Table 37). Some unique ejector cycles that were identified with sink temperatures lower than 80 °C were included in Table 34.

The function of ejectors in vapor compression cycles can be categorised into three applications related to the placement of the ejector in the cycle: 1) Ejector in heat-driven refrigeration, 2) ejector for expansion work recovery and 3) ejector after compression (Figure 14). The concept of ejectors used in heat-driven refrigeration is not applicable to high temperature heat pumps as the temperature of the heat source for the generator must be greater than the sink temperature being generated. Ejectors for expansion work recovery, e.g. cycles T1e-1 and T1e-2, are the most common application of ejectors in transcritical CO_2 cycles due to the large amounts of exergy destruction that result from the pressure lift required [85].

The majority of publications found related to ejectors used for expansion work recovery focussed on refrigeration applications rather than heating, with limited studies that could be found for the use of ejectors in CO_2 HTTHPs [86]. Sarkar [87] proposed to modify the conventional ejector expansion cycle (T1e-1) to include double expansion from the separator for evaporator quality control (T1e-1a). The analysis considered sink temperatures up to 103 °C with the maximum sink

temperature increasing by 10 °C with the proposed modification. However, the COPs of T1e-1a were found to be lower than T1e-1 due to a lower optimum discharge pressure.

Zhu et al. [65] found that T1e-2 increased the COP by up to 10.3 % compared to the equivalent non-ejector cycle (T1-2) for sink temperatures ranging between 50 and 90 °C. The optimal benefit from using an ejector occurred at approximately 70 °C sink temperature (10.3% COP increase), however, the benefit of using an ejector was still significant at 90 °C sink temperatures with a COP increase of 8.5 %. A unique ejector expansion cycle with two evaporators (T1e-3) was modelled by Qin et al. [88] for sink temperatures up to 110 °C, resulting in similar heating COPs as T1e-2 (COP of approximately 4) for the same conditions, however, it could achieve a much higher total COP (COP heating and COP cooling), nearly double the total COP of T1e-2.

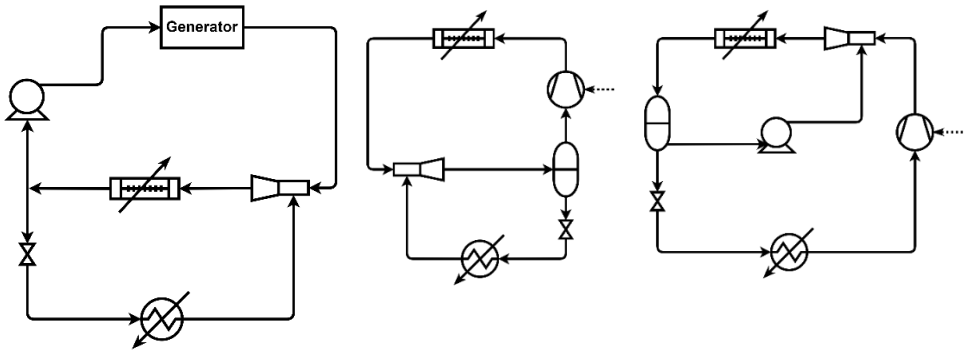

a) Heat-driven ejector refrigeration

b) Ejector for expansion work recovery

c) Ejector after compression with pump

Figure 14. Application of ejectors in vapor compression cycles – figure adapted from Sumeru, Nasution and Ani [89].

The use of an ejector after compression aims to reduce the overall work required by the system as less work is required to compress a liquid compared to a vapour. Although the liquid pressure out of the pump must be lower than the vapour pressure out of the compressor, the volume of vapour that would need to be compressed to that higher pressure would be significantly smaller than a conventional heat pump system. Theoretically, this results in a large increase in the system efficiency and a much more compact system, provided that the compressor can supply the high temperature requirements. Bergander [90] modelled the cycle (Figure 14c) for a refrigeration application, finding that the cooling COP could theoretically be increased by up to 38 %, with an energy saving of 16% shown under the experimental conditions.

Chen et al. [91] also investigated a subcritical ejector refrigeration cycle with the ejector after the compressor, however, instead of a pump after the gas cooler, a closed economiser was used. The analysis showed that the volumetric heating capacity could be improved by up to 7 % and the COP improved by 15 to 37 % compared to a conventional heat pump system. There were no studies that could

be found that investigated the performance of this configuration in a transcritical cycle. The application of this concept in a transcritical cycle would likely require a combination of the concepts proposed by Bergander [90] and Chen et al. [91], with a pressure reducer (e.g. closed economiser) after the gas cooler, prior to the separator, to condense the fluid for pumping.

The use of ejectors in CO_2 HTTHPs shows very promising efficiency gains, however, ejectors can introduce significant challenges for heat pump design. The behaviour of ejectors, particularly transcritical ejectors, can be difficult to predict, with multiple parameters that can affect the ejector efficiency such as discharge pressure, ejector geometry and load characteristics [92]. The performance of an ejector is most often characterised by the ejector efficiency (η_{eject}, Equation 2.1), mass entrainment ratio (μ, Equation 2.2) and pressure lift ratio (PLR, Equation 2.3) [93].

$$\eta_{eject} = \frac{\dot{W}_{rec}}{\dot{W}_{rec,max}} \quad 2.1$$

$$\mu = \frac{\dot{m}_I}{\dot{m}_{II}} \quad 2.2$$

$$PLR = \frac{P_e}{P_{i,II}} \quad 2.3$$

The simulation methods for CO_2 ejectors are generally either a 1D or 3D approach [94]. In the 1D approach, the ejector is divided into four control volumes: 1) primary nozzle, secondary nozzle, mixing section and the diffuser and analysed using thermodynamic analysis. For the 3D approach, Computational Fluid Dynamics (CFD) is used. From the perspective of heat pump modelling, 1D approaches are more commonly used as they are less computationally intensive, however, are far less accurate. Another challenge associated with ejectors is the inability to operate at part load. For spray drying, this is less significant as the conditions are generally steady, however, issues could arise during start-up and shut-down.

2.3 Process integration of heat pumps

The performance, selection, and, therefore, the design of a heat pump is heavily influenced by how the heat pump is integrated in the process. Process integration methods can be used to identify the optimal source (and sink) to supply the heat pump and also to target the addition of components within the heat pump cycle, for example, external subcoolers and superheaters. Presently, a lack of knowledge exists around the integration of HTHP for industrial processes and is a key barrier to uptake [95]. The review will focus on papers that discuss HTHP for industrial processes but also includes some more general integration studies to help illustrate heat pump integration methodologies. The objective of the review is to identify

practical, accessible and efficient methods of HTHP integration that can be used to integrate a new HTHP into the spray drying process.

2.3.1 Waste heat recovery using heat pumps

When a process stream exists at a lower temperature than what is "useful" in an industrial process, it is referred to as waste heat. This generally occurs following a heat transfer process. Waste heat is often discarded; however, in many cases, there is the potential for the waste heat to be recovered and further utilised within the process to improve the overall efficiency of the system. In milk powder production, there is hot water, generally Condensate of Whey (COW water), that can be considered a waste heat stream from the evaporation process and exhaust air can be considered a waste heat stream from the spray drying process. Waste heat recovery is increasing in popularity as a way to reduce energy consumption and is already implemented in various forms within the dairy industry. In evaporation, mechanical vapour recompression (MVR) and thermal vapour recompression (TVR) are used to recover the water vapour from the milk (tube side) which is then used for heating on the shell side. Additionally, using the COW water from the evaporation process to partially heat the air for spray drying is also a method of waste heat recovery.

Waste heat recovery can be achieved heuristically, however, process integration methods to achieve more efficient waste heat recovery are being continually researched and developed. At the basis of many process integration methods is Pinch Analysis, originally proposed by Linnhoff et al. [96]. Pinch Analysis is a graphical method to help determine areas of heat surpluses and heat deficits within a process to help establish the theoretical minimum amount of utility, or utility targets, that needs to be supplied to the process and to maximise waste heat recovery. The undertaking of a Pinch Analysis involves the construction of a Problem Table Algorithm (PTA), hot and cold composite curves (CCs) and the Grand Composite Curve (GCC) for the process. The CCs and GCC, as shown in Figure 15, are a representation of the hot and cold streams within the process. The pinch temperature, commonly referred to as "the Pinch", is a key feature in Pinch Analysis, indicating where the hot and cold CCs converge to the minimum approach temperature (ΔT_{min}) [97].

The GCC and principles of Pinch Analysis are most used for the design of heat exchanger networks but can also be used for the integration of heat pumps. Conventionally, the objective of Pinch Analysis is to utilise as much of the heat recovery potential within the process as practically possible (Figure 15b). Where there is no potential for heat recovery, heating or cooling utility needs to be supplied. The way in which a heat pump operates is to supply heating to a stream using heat that is acquired by cooling a lower temperature stream and compressed to a higher temperature and pressure. By Pinch principles, heating should only be supplied above the Pinch and cooling should only be supplied below the Pinch as heating below the Pinch and cooling above the Pinch should theoretically be fully realisable through heat recovery, for example, using heat exchanger networks

(HENs). As a result, to supply simultaneous heating and cooling with a heat pump, the appropriate placement of the heat pump to reduce energy consumption and maximise economic benefit is across the Pinch (Figure 16).

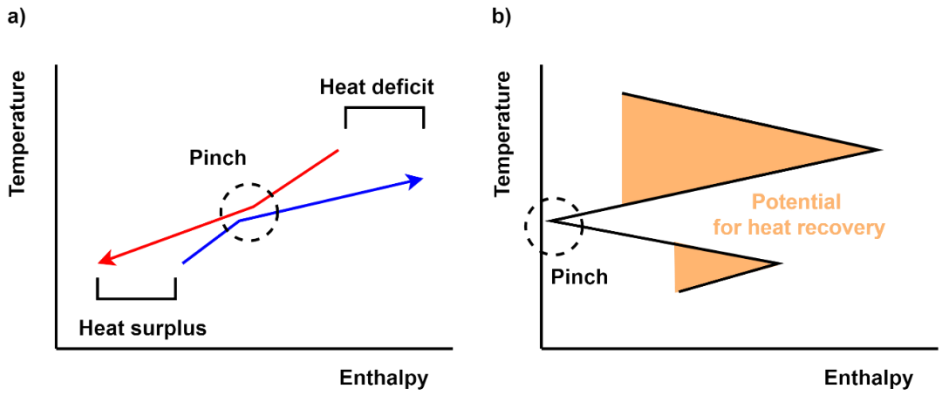

Figure 15. a) Example of a Combined (hot and cold) Composite Curve and b) example of a Grand Composite Curve.

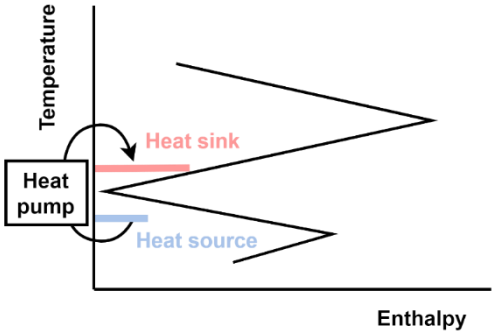

Figure 16. Example of heat pump integration using the GCC.

The integration of HTHPs requires a multi-faceted approach that considers many factors, such as system efficiency, sizing, capital cost, complexity and scheduling. Many have studied methods to integrate heat pumps in industrial processes to optimise the system efficiency, however, practical considerations are more complex as they are unique to the individual application, with few studies investigating the integration of HTHPs with sink temperatures greater than 90 °C. The results of the review found that heat pump integration methods could be classified into four general categories:

1. Pinch Analysis or insight based
2. Mathematical optimisation based
3. Process simulation based
4. Hybrid of 1 – 3.

Pinch Analysis based methods were found to be the most accessible heat pump integration methods. Graphical visualisation through the GCC is used to obtain the

appropriate placement of a heat pump within the process [98]. Schlosser et al. [99] extended Pinch Analysis principles for targeting heat pump integration for retrofit applications, proposing a heat pump bridge analysis method using modified energy transfer diagrams.

Mathematical optimisation based heat pump integration can ensure the identification of optimal results for the selected objectives and constraints. Additionally, mathematical optimisation based heat pump integration methods provide the advantage of reducing the manual input, however, for the same reason, there is less flexibility in considering the practical limitations for the application [100]. A hybrid approach that combined Pinch Analysis and mathematical optimisation for heat pump and storage integration for non-continuous processes was proposed by Stampfli et al. [101]. Wallerand et al. [102] proposed an interesting method which also combined Pinch Analysis and mathematical optimisation for the integration of industrial heat pumps. The method involved targeted the design of heat pump superstructures with optimal COPs and lowest total annualised costs.

Yang et al. [100] noted that these existing methods of heat pump integration rely on the accuracy of the heat pump models to determine the heat pump performance. Additionally, conventional heat pump integration cases are more widely established for subcritical heat pumps, where the 2nd law efficiency of the cycle is estimated based on the ratio of the irreversible process to the Carnot equivalent process [101]. Schlosser et al. [30] recommended that for transcritical heat pumps, it would be more appropriate to use the Lorenz efficiency. Jensen et al. [103] developed a generalised method for the estimation of heat pump COP using the Lorentz cycle, finding that Lorenz efficiencies between 45 and 50 % could be used as a reasonable assumption. It is unclear whether the assumptions are reliable for transcritical heat pump cycles with greater cycle complexity.

Yang et al. [100] proposed a heat pump integration method which combined Pinch Analysis and rigorous simulation. The proposed method aimed to improve the potential reliability of conventional process integration methods which rely on accurate heat pump models. Process simulation based heat pump integration methods have the benefit of providing insight to the interactions within a process, however, they can possibly lead to missed opportunities for efficiency gains related to the process structure and can be computationally intensive [104]. Although the contributions of Yang et al. [100] proved to be effective, the method relies on Aspen HYSYS and MATLAB which are not only computationally intensive process simulators but also can be inaccessibly expensive for energy users needing to decarbonise.

Schlosser et al. [30] found that heat pumps with COPs between 3 and 6 were favourable for heat pump implementation in industrial applications. However, a heat pump is generally considered economically feasible if the COP is greater than the ratio of electricity cost to fuel cost multiplied by the efficiency of the alternative

heat generation [105]. With the rapidly increasing prices of fuel, resulting from supply constraints or taxation, the COP required for the heat pump to be economically feasible will decrease, which is favourable for high temperature heat pump integration.

From the review, it is clear that there is a lack of integration methods for integrating HTHPs in the spray drying process, resulting in potential missed opportunities for efficiency gains and heat recovery that is integrated with the heat pump. Incorporating Pinch Analysis principles in the design of the heat pump, e.g. temperature profile matching or the appropriate placement of expansion and compression operations, could also be a promising avenue for research.

2.3.2 Quantifying economic heat pumping

There is a wide range of metrics and associated "rules of thumb" used to define the performance of a heat pump and are subsequently used for the integration of the heat pump. The review aims to provide more in-depth analysis to the applicability of the metrics for the comparison of HTHP performance and integration.

COP is the most common metric used to characterise heat pump performance; however, many types of COPs exist that benefit different applications. At the simplest level, the Carnot COP (COP_{Carnot}) describes the theoretical maximum COP that can be achieved by the heat pump for the given temperatures (Equations 2.4 and 2.5), where T_H is the temperature of the high-temperature sink reservoir and T_L is the temperature of the low-temperature source reservoir and is often taken as the temperature of the sink outlet and the temperature of the source outlet respectively (Figure 17a).

$$COP_{Carnot,H} = \frac{T_H}{T_H - T_L} \qquad 2.4$$

$$COP_{Carnot,L} = \frac{T_L}{T_H - T_L} \qquad 2.5$$

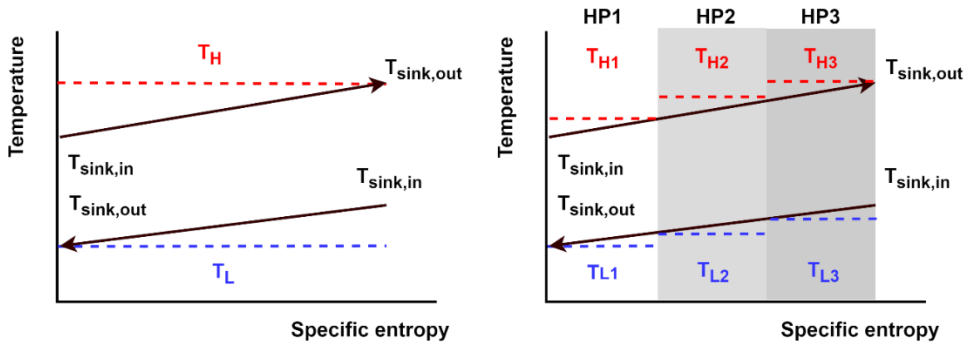

a) Single heat pump b) Three heat pumps

Figure 17. Comparison of Carnot using a single heat pump and multiple heat pumps to calculate COP.

The Carnot COP is commonly used to provide a benchmark for the performance of the heat pump as a measure of the theoretical maximum efficiency. However, for applications where there is a large temperature glide in either the heat source or heat sink, such as in HTHPs, the Carnot COP could provide misleading results. Reinholdt et al. [106] showed that by discretising the source and sink temperatures, such that a mean COP can be calculated through the approximation of multiple heat pumps and applying the Carnot relations, the COP will approach the actual theoretical maximum, i.e. ideal COP. Figure 17b shows this concept for the case of three heat pumps.

The Lorenz COP uses the same concept proposed by Reinholdt et al. but for an infinite number of heat pumps, increasing the accuracy of the approximation. The Lorenz COP is calculated using the logarithmic mean temperatures for the source and sink rather than the sink and source outlet temperatures that are used to calculate Carnot COP (Equation 2.6) [106]. Reinholdt et al. considered the discretisation of the source and sink temperatures both finitely and infinitely, using Lorenz COP, finding that the results differed significantly from the conventional Carnot COP by 37% and 51% respectively ($T_{source,in}$ / $T_{source,out}$ =40/15 °C, $T_{sink,in}$/$T_{sink,out}$=60/90 °C), shown in Table 7. Additionally, the same calculations were included for a smaller sink temperature glide ($T_{sink,in}$/$T_{sink,out}$=80/90 °C) where the percentage difference was shown to be less significant.

$$COP_{Lorenz} = \frac{T_{LM,H}}{T_{LM,H} - T_{LM,L}} \quad 2.6$$

$$T_{LM,L} = \frac{T_{L,out} - T_{L,in}}{\ln(T_{L,out}) - \ln(T_{L,in})} \quad 2.7$$

$$T_{LM,H} = \frac{T_{H,out} - T_{H,in}}{\ln(T_{H,out}) - \ln(T_{H,in})} \quad 2.8$$

For real life, i.e., irreversible heat pumps, the COP is usually defined as the ratio between the useful heating or cooling and the required compressor work, referred to in this review as the actual COP. It is a useful metric as it is directly related to the operating cost of the heat pump. For heating, cooling and simultaneous heating and cooling, the COPs are given by Equations 2.9, 2.10 and 2.11 respectively.

$$COP_H = \frac{\dot{Q}_H}{\dot{W}_{total}} \quad 2.9$$

$$COP_C = \frac{\dot{Q}_C}{\dot{W}_{total}} \quad 2.10$$

$$COP_{combined} = \frac{\dot{Q}_H + \dot{Q}_C}{\dot{W}_{total}} \quad 2.11$$

Table 7. Comparison using Carnot COP (conventional), discretised as 3 HP and discretised as n heat pumps (Lorenz COP) for the source and sink temperatures used in Reinholdt et al. [106] and for sink inlet temperature of 80 °C.

Operating conditions	$T_{source,in}/T_{source,out}$ = 40/15 °C $T_{sink,in}/T_{sink,out}$ =60/90 °C		$T_{source,in}/T_{source,out}$ = 40/15 °C $T_{sink,in}/T_{sink,out}$ =80/90 °C	
Method	**COP**	**% difference**	**COP**	**% difference**
Carnot 1HP	4.84	0	4.84	0
Carnot 3HP	6.68	38	5.04	4
Lorenz	7.33	51	6.21	28

The accuracy of these COPs relies on the accuracy of the values used for heating/cooling capacity and work input, which either requires modelling or experimentation on physical systems to develop correlations. This can involve complex modelling using first principles and requires knowledge of factors such as the working fluid and compressor technology. Many studies have proposed COP correlations that simplify the estimation of COP based on the required operating parameters. Schlosser et al. [30] developed correlations to calculate the COP using regression analysis for different temperature ranges for industrial heat pumps, including transcritical CO_2 heat pumps, and the logarithmic mean source and sink temperatures. However, the validity of the correlations only holds up to the sink temperatures (~90 ° C) which existing heat pumps operate at. It was also noted by Pieper et al. [107] that heat pump COP correlations are usually derived from single-stage heat pumps and are unreliable for two-stage heat pumps. The same would be true for newer cycle innovations and therefore it is necessary to develop either a robust and detailed thermodynamic model or develop a representative prototype in order to calculate the COP.

The second law efficiency combines the concept of the actual COP and ideal COP to determine the effectiveness of the heat pump relative to its maximum possible performance. Generally, the Carnot COP is used as the ideal COP to calculate the second law efficiency (Equation 2.12). The Lorenz efficiency is the equivalent of the second law efficiency but using the Lorenz COP in place of the Carnot COP (Equation 2.13). Another common method to calculate the second law efficiency is by using exergy (Equation 2.14), using the ratio of exergy transferred to the ratio of exergy input. The Carnot and exergy second law efficiencies can vary significantly while the Lorenz efficiency and exergy efficiency tend to be more in agreement [108]. Exergetic efficiency requires more calculation than the other methods, however, it provides the benefit of easily identifying areas within the cycle where component

irreversibilities can be minimised [60]. The second law efficiency, in its various forms, is a useful metric as it can be used as an optimisation variable in the design of heat pumps.

$$\eta_{II} = \frac{COP_{actual}}{COP_{Carnot}} \tag{2.12}$$

$$\eta_{Lorenz} = \frac{COP_{actual}}{COP_{Lorenz}} \tag{2.13}$$

$$\eta_{ex} = \frac{\dot{X}_{sink,out} - \dot{X}_{sink,in}}{\dot{X}_{source,in} - \dot{X}_{source,out} + \dot{W}_{total}} \tag{2.14}$$

The performance metrics discussed so far are relatively well-established but the number of differing metrics and methods to calculate them can make it difficult to make design decisions for heat pump implementation. There are two decisions that need to be made from which insight can be lost depending on which performance metrics are used:

1. What temperatures should the heat pump operate at?
2. What is the best cycle design?

The temperatures that the heat pump operates at are usually quantified in heat pump literature by the temperature lift [30]. The temperature lift is defined as the difference between the source inlet temperature and the sink outlet temperature. Generally, the smaller the temperature lift, the greater the COP for the heat pump. However, Bellemo and Bergamini [109] showed that the optimal heat pump COP does not necessarily result in the optimal efficiency for the overall system. While the operating temperatures of heat pumps tend to be dictated by the process requirements, opportunities for flexibility should be investigated. Further, these metrics do not take into consideration cycle complexity and capital cost. Some studies have used total annualised cost as a separate metric to account for the capital costs [110].

In general, heat pump configurations with an increased number of components are intended to achieve higher efficiencies, but the resulting capital expenditure also increases, and the efficiency of a heat pump must compensate for the often-unfavourable electricity-to-reference energy carrier price ratio. Thus, there is a trade-off between capital costs influenced by the number of cycle components and operating costs affected by this price ratio and heat pump efficiency [30]. Depending on the available energy sources as well as political and legal framework conditions, different competing reference energy carriers and price ratios exist.

In Scandinavian countries, electricity-to-natural gas price ratios of less than 2 are already being achieved [111]. In other European countries such as Germany, the ratio was on average around 4 in 2021 [112]. The price dynamics caused by global

crisis situations, such as the COVID-19 pandemic, make a long-term forecast difficult. Nonetheless, a decreasing emissions factor in the electricity mix [113] and increasing fossil fuel prices [114] can be assumed in order to achieve the climate protection goals within the framework of the energy transition. Studies therefore assume an electricity-natural gas price ratio in Germany and the rest of Europe of 1.7 and 1.3 respectively by the year 2045 [115]. To promote renewable energy, recent government regulations in New Zealand have required all coal-fired boilers for applications below 300 °C to be shut down by 2037. New Zealand is rich in renewable energy sources, including hydropower, geothermal, wind power and old plantation forests. As a result, the price ratio between electricity and reference fuel (formerly coal, now biomass) has fallen dramatically to between 1.5 and 2.0. [116]

2.3.3 Heat recovery in spray drying

The exhaust air from a spray dryer, which combines exhaust air from the main dryer chamber and fluidised beds, typically exits between 60 °C and 93 °C [117]. Manufacturers have claimed that the energy consumption of a dryer can be reduced by up to 25 % by recovering the heat from the exhaust air [117]. A study by Atkins, Walmsley and Neale [118] modelled a potential 12 to 20 % reduction in hot utility required through the use of exhaust heat recovery for milk powder spray drying. Exhaust heat recovery systems can exist as air-to-air configurations or air-liquid-air configurations where the exhaust air is used to preheat the inlet drying air. Air-liquid-air configurations can be beneficial for retrofit as the ducting required from the exhaust air to the inlet air streams are smaller than what is required for air-to-air configurations. Uptake of exhaust heat recovery within the dairy industry has been slowed by three main factors: 1) economics, 2) particle loading and fouling, and 3) relatively low exhaust temperatures [118]. Atkins, Walmsley, and Neale recommend the consideration of the entire production process to enact effective heat recovery. Particulate loading and fouling causes increased resistance to heat transfer within the recovery heat exchangers. As a result, heat recovery becomes less cost effective. The main factors which affect heat exchanger particulate fouling are particle surface stickiness, air velocity, impact angle, particle size and wall properties [119]. Milk powder stickiness is largely related to the glass transition temperature and viscosity, with the major amorphous component in milk powder being lactose. The average glass transition temperature for lactose is around 103 °C [119].

Some studies have shown success in the integration of HTHPs in the milk powder production process. Bellemo and Bergamini [109] used process simulation based integration to investigate six case studies for the integration of a CO_2 HTTHP into the milk spray drying process. The heat pump (T1-2) was used to supply air heating from ambient to 120 °C and the remaining heating was supplied by a natural gas boiler. The results showed that the overall COP of air heating could be increased by using a boiler economiser to recuperate heat from the combined steam heating condensate and heat pump condensate, achieving a COP of 2.4 for the heat pump and overall heating COP of 1.3.

Zuhlsdorf et al. [120] also integrated a HTHP into the spray drying process that used zeotropic working fluids. Only one configuration was suggested where the incoming air was heated to 70 °C with heat recovery, then a heat pump was used to heat the air further to 120 °C, achieving a COP of 3.08. The remaining heating to 210 °C was supplied using a natural gas boiler. The process integration method was not described. Lincoln et al. [31] integrated medium temperature transcritical CO_2 heat pumps in for the design of an electrified milk evaporation system. The study proposed a process integration method which combined Pinch Analysis, process simulation and Exergy Pinch Analysis that differed from conventional integration in that the target was minimised work rather than minimised heating and cooling utility. The method proposed by Lincoln et al. [31] is more suitable for the integration of HTHPs as conventional heat pump methods generally integrate heat pumps after heat recovery using the remaining low-temperature surplus heat to supply the heat pump. By targeting minimised work, it unlocks the potential for higher temperature waste heat to be utilised first, resulting in potential performance gains for the system [121].

2.4 Conclusions

This chapter has reviewed the state of knowledge on high temperature heat pumps (HTHPs) for industrial decarbonisation, with a focus on their potential application to large temperature glide processes such as spray drying. Several key insights emerge from the literature related to the lack of technology for large temperature glide processes, refrigerant limitations, potential opportunities to improve performance through cycle architecture and integration challenges. A research gap also exists in HTHPs for spray drying applications. While HTHPs have been successfully demonstrated in medium-temperature applications, there is a lack of proven technologies that can efficiently decarbonise processes with large temperature glides. Spray drying in the food industry is one such example, where no commercially available heat pump system has yet been shown to fully replace fossil-fuelled heating. This gap highlights the importance of developing tailored solutions for industrial processes that cannot be addressed by standard heat pump designs.

No single refrigerant satisfies all the requirements for high-temperature operation. Halogenated refrigerants are being phased out due to environmental regulations, making natural refrigerants the primary long-term candidates. However, each option carries limitations: ammonia and hydrocarbons offer high efficiency but raise toxicity and flammability concerns, while air and water are restricted to niche applications. CO_2 stands out for food applications due to its high volumetric heating capacity, non-flammability, and low toxicity. These characteristics make it particularly attractive for processes such as spray drying, where safety and plant integration are critical. Nevertheless, CO_2 systems require extreme operating pressures, and their efficiency decreases over large temperature glides. More research is needed to improve cycle performance and address the engineering challenges of safe, cost-effective high-pressure operation.

Integrating HTHPs into industrial sites is not straightforward. Conventional integration approaches, developed for low-temperature systems, are underdeveloped for high-temperature applications. Identifying suitable source and sink streams is complex, and conventional metrics such as COP are insufficient to effectively compare and select the optimal heat pump for the application. Instead, integration must be assessed in terms of process feasibility, system interactions, and overall plant performance.

Research has shown that the performance of CO_2 HTHPs can be improved by exploiting cycle architecture. Relatively simple modifications, such as the use of internal heat exchangers or cascade configurations, have demonstrated efficiency gains, though applications at high temperatures remain limited. Expansion work recovery is another promising avenue, as the large pressure differences that are inherent in CO_2 cycles offer significant potential for efficiency improvements. Despite the potential advantages of CO_2, there is a lack of studies which have explored its use to supply all of the heating required for spray drying. This represents a critical research gap, given the importance of spray drying in food manufacturing and the large carbon footprint that is currently associated.

Chapter 3
Overview of the process requirements and research approach

3.1 Introduction

HTHPs are expected to play a significant role in the industrial transition to net zero emissions. However, further research is required to determine the most efficient solutions for implementing heat pumps into a wide variety of industrial processes – each with unique challenges and requirements. As the performance of a heat pump depends on many factors, no single heat pump solution can be universally applied. This makes it difficult for large energy users to identify and compare the heat pump cycles that are best suited for their processes. The effective integration of a heat pump requires careful consideration of several key factors identified from the literature, including:

- Process requirements and constraints
- Refrigerant selection
- Heat pump configurations
- Appropriate placement within the process
- Safety considerations

3.1.1 Process requirements and constraints

The most important factor for the successful integration of a heat pump is a clear understanding of the process requirements and constraints under which the heat pump will operate. This informs the availability of surplus heat which is available to supply the heat source to the heat pump and will also determine the optimal refrigerant and heat pump configuration. Operational characteristics such as whether the process is continuous or non-continuous (batch), as well as the scheduling and variability in operating conditions, can significantly affect performance and feasibility for a heat pump installation. In many cases, heat pumps will be retrofitted into existing industrial processes, rather than new industrial sites, which will constrain the optimal placement of the heat pump within the process. These constraints are often driven by capital cost, retrofit feasibility and system complexity.

3.1.2 Refrigerant selection

The refrigerant, or working fluid, of a heat pump has a major influence on the heat pump performance as its thermodynamic properties directly impact the effectiveness of heat transfer. In HTHPs, this choice becomes even more critical due

to the more demanding operating conditions and the limited number of refrigerants that can perform efficiently and reliably at extreme temperatures. Selecting a suitable refrigerant is further complicated by the ongoing phase out of high GWP and high ODP refrigerants. Concurrently, growing safety regulations and industry concerns for the installation and use of certain refrigerants in heat pumps – particularly those which are flammable and toxic – are still evolving, leading to uncertainty and reduced industrial confidence. As a result, choosing the right refrigerant involves navigating a complex, changing landscape of technical, environmental, safety, and regulatory considerations.

3.1.3 Heat pump configuration and cycles

In general, refrigerants that have low environmental impact have significant barriers to overcome, which can include lower performance in many cases. One way in which these performance challenges can be overcome is through customising the heat pump configuration or cycle architecture. In HTHPs, selecting the optimal cycle architecture is crucial, as high temperature applications impose greater thermal demands on the performance of the components; the choice of cycle directly influences the achievable temperature lift and the amount of exergy destruction within the system. It should also be considered whether the heat pump, as a system which supplies process heat, can be stand-alone or if it needs to be integrated in conjunction with other components such as steam generators and flash vessels to achieve the process heating requirements. As with refrigerant selection, identifying the optimal cycle and configuration involves assessing the complex trade-off between performance, cost, reliability and design constraints.

3.1.4 Appropriate placement of heat pumps within the process

In addition to understanding the requirements and constraints of a process, the method by which a heat pump is integrated into that process can have a significant effect on overall system efficiency. Established process integration techniques, such as Pinch Analysis, are not always well-suited for HTHP applications (compared to low and medium temperature heat pumps). For instance, conventional Pinch Analysis recommends maximising direct heat recovery between process streams first through heat recovery heat exchangers. After which, a heat pump is integrated to upgrade any remaining low-grade heat. While this approach generally enhances the system efficiency, it may not be optimal for a HTHP, as it is possible to unnecessarily increase the temperature lift across the heat pump compressors, penalising the heat pump performance. Conventional integration techniques can still be useful in the integration of HTHPs, but it is important to evaluate the trade-off between the heat pump performance and the overall system efficiency.

3.1.5 Objectives

With the multitude of factors that need to be considered for heat pump integration, it is impossible to consider all the combinations of refrigerants, cycles and integrations of HTHPs for industrial processes. Thus, the purpose of this chapter is to outline the motivations for key design decisions that are carried throughout the research chapters of the thesis, and these aspects are used to define the scope of

the research. This chapter also aims to provide an overview for the research approach to design and integrate a heat pump into the spray drying process.

3.2 Overview of milk powder spray drying

Milk powder spray drying is a particularly energy intensive process in the food industry and contributes significantly to industrial emissions in New Zealand. As New Zealand's electricity grid has a high percentage of renewable generation, integrating a HTHP into the spray drying process has the potential to make a substantial reduction in industrial emissions compared to traditional fossil fuel heating. As a caveat, current heat pump solutions struggle to meet the requirements. Presently, HTHPs that can achieve temperatures above 150 °C are generally designed to operate for a high temperature lift and smaller temperature glide or for a large temperature glide and a lower temperature lift. Milk powder spray drying presents a unique challenge for the research field of HTHPs as both high temperature lifts and large temperature glides are required.

3.2.1 Process description

In spray drying, the high temperature heating requirement is the dryer air that needs to be heated to 200 °C (Figure 18). The 200 °C dryer air is used to heat and remove moisture from the milk concentrate as it is atomised in the dryer. Depending on the equipment and the type of milk (whole, skim, goat, infant formula, etc.), this design temperature can vary between 160 and 220 °C. To heat the dryer air, a common configuration uses steam heaters, possibly with some heat recovery for the lower temperature portion of the heating. The heat recovery portion is generally waste hot water from the milk evaporation process. Alternatively, the dryer air can be heated using natural gas heaters where the combustion heat is used to heat the air directly. In the dryer, as the milk concentrate is dried, most of the water content of the milk is evaporated into the air, causing the absolute humidity of the air to increase. At the bottom of the dryer, the milk powder enters a static fluidised bed (SFB), that is heated with hot air at approximately 100 °C to further remove moisture from the powder and improve moisture content uniformity. The total mass flow of this dryer and SFB air is then blown into a baghouse to remove particulates and/or exhausted directly into the atmosphere at approximately 60 °C. Some configurations of dryer systems will also have vibrating fluidised beds (VFB) after the SFBs which operate at approximately 80 °C for a higher temperature stage and at room temperature for a lower temperature stage. The humidified air from the fluidised beds in these configurations also contributes to the exhaust air.

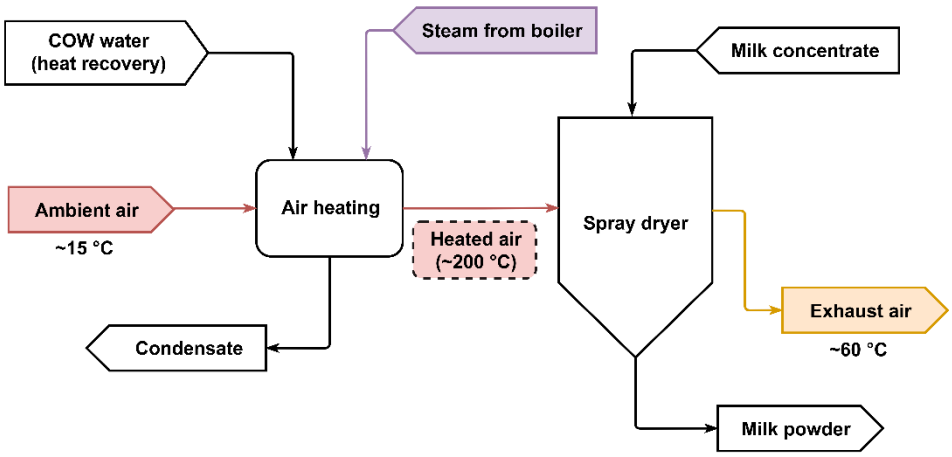

Figure 18. Simplified diagram of the milk powder spray drying process.

The exhaust air is the main source of waste heat from the milk powder spray drying process. A significant amount of waste heat recovery potential exists in the exhaust air due to the large amount of energy stored in the water vapour that had evaporated into the air during the drying process. Newer plants will generally employ exhaust heat recovery systems that utilises the heat available, either through latent or sensible cooling of the exhaust air, to preheat the inlet air to the dryer. However, for many older plants, including many in New Zealand, exhaust heat recovery systems are currently not in use due to the high cost of retrofit. Where plants do employ exhaust heat recovery systems, the greatest heat recovery occurs when the humid air is cooled past the dew point, as the latent heat of the water vapour in the air is released when the water vapour condenses.

3.2.2 Centralised vs. decentralised heat pump integration for spray drying

Heating of the process air is largely achieved using fossil fuel boilers, to produce steam, or natural gas heaters, that heat the air directly. To displace the use of fossil fuel systems by integrating a HTHP, a key design decision involves choosing between a centralised utility heat pump – that can supply heat to multiple processes – or having decentralised heat pumps that are optimised for a specific process or set of processes. At the simplest level, the HTHP can be used to replace the steam heaters or gas heaters that heat the main dryer air at 200 °C (Figure 19). This would represent a version of decentralised heat pump integration. As the largest source of waste heat in the process is exhaust air, it is logical in the first stage to consider using the exhaust heat to supply the source side of the heat pump. Another potential source for the heat pump could include ambient air source. These will be the integration strategies that are first considered in this thesis.

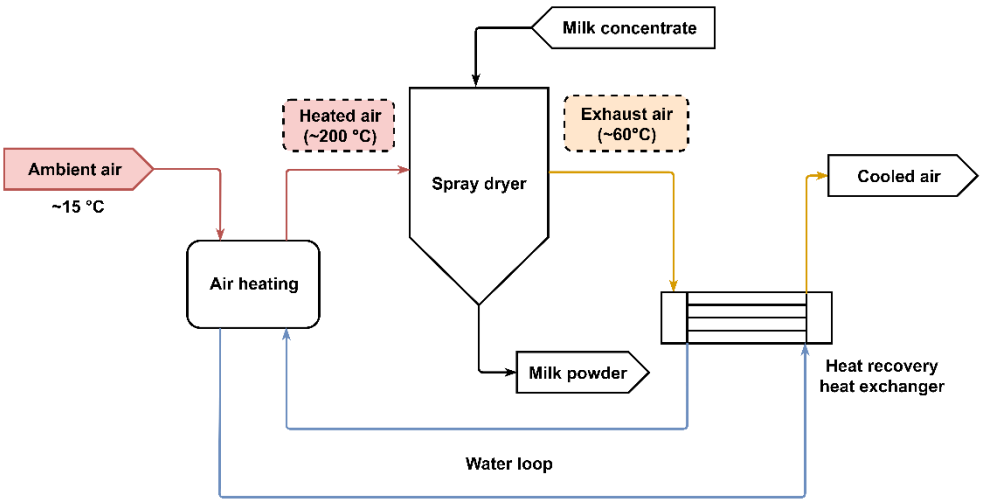

Figure 19. Simplified process flow diagram for HTHP pump integration into the milk powder spray drying process.

As an alternative integration strategy, the heat pump can be used to supply steam to the entire site. This would involve using the heat pump to generate steam and, most likely, compressing it to a higher temperature using a steam compressor or MVR. Traditionally, process heating is often supplied using large, centralised fossil fuel boilers and a steam distribution system which naturally makes a large, centralised steam generating heat pump an attractive option. However, the lower efficiency and lack of flexibility can limit their effectiveness since the performance of a heat pump can be dramatically reduced when operating at part load. Decentralised heat pump integration presents a compelling advantage: by being localised to the process, the heat pump systems can be optimised to match the individual temperature profiles, leading to higher operational efficiency and energy savings. This approach also enhances the system flexibility, resilience and control, as each heat pump operates independently, without being affected by the needs or changes in other parts of the plant. Although decentralised heat pump integration is likely to involve greater initial complexity and investment, the long-term benefits in performance, adaptability and energy efficiency have the potential to outweigh these upfront challenges.

3.2.3 Process requirements, constraints and assumptions for the thesis research

A base case design, as described below, will be used as a basis for comparison for the heat pump integration options to be considered in the thesis (Figure 20). The base case design represents a common configuration for steam heating of the dryer air. As shown in Figure 20, the primary dryer air is heated to 200 °C using two steam heating sections, high pressure steam (HPS) and low pressure steam (LPS), and a condensate heating section. In the HPS section, it is common for 40 bar steam to be used despite the temperature level being higher than what is required to heat the air to 200 °C as this also allows some of the steam generated to be used for cogeneration of power on site. The HPS section generally heats the air from 160 °C to 200 °C. The expended HPS is then flashed down to a lower pressure, approximately 10 bar, and combined with supplementary LPS to heat the air up to

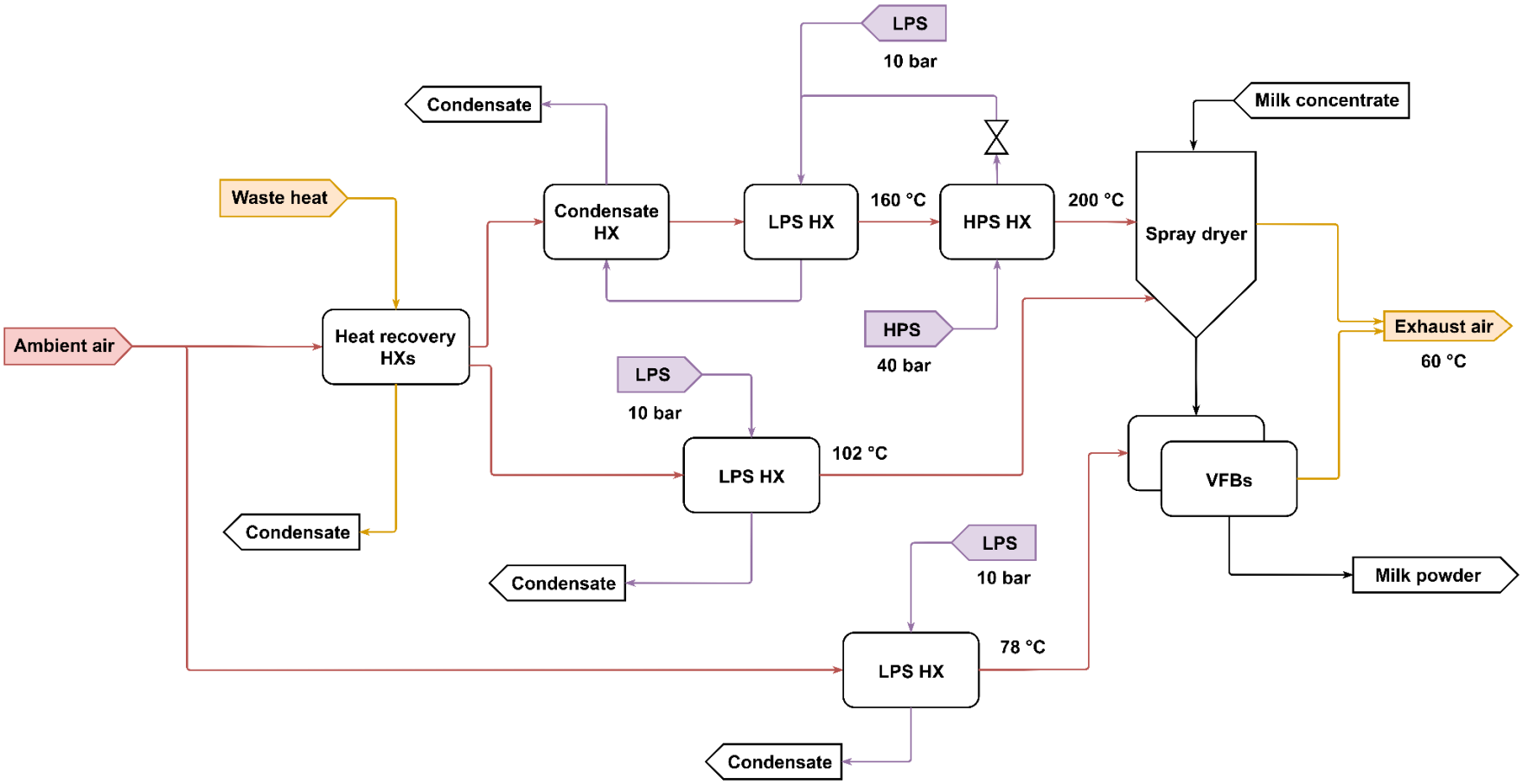

Figure 20. Base case design for a milk powder spray dryer.

160 °C. The condensate heating section uses the condensed LPS and HPS from the two steam heating sections combined with wastewater recovered from the evaporation process to do the lower temperature portion of the air heating. The temperature that can be reached in the condensate heating section varies depending on the amount of heat recovery that is available.

It was assumed that the spray dryer exhaust air exits the dryer at approximately 60 °C, which could be used to supply the source side of the heat pump. In the cases where exhaust heat recovery was considered, a water loop was used between the spray dryer exhaust and the heat pump due to the physical distance between the exhaust and the air heating section ($T_{source,in}$= 40 °C). Similarly, a water loop could be used on the sink side of the heat pump to heat the spray dryer air from 15 °C to 200 °C for hygiene reasons. This was accounted for by using a ΔT_{min} of 20 °C between the refrigerant and the air which enables the possibility for exchanging heat from the refrigerant to the water loop with a ΔT_{min} of 5 °C and from the water loop to the air with a ΔT_{min} of 15 °C.

The primary heating requirement for the dryer is heating the air to 200 °C which occupies approximately two thirds of the total air heating by mass. In addition to this, the fluidised bed air makes up the remaining third of the air heating requirement. The process requirements for the fluidised bed air were 102 °C inlet air temperature for the static fluid bed at the bottom of the dryer and 78 °C for the higher temperature stage of the vibrating fluidised beds. These streams were heated with LPS, respectively.

3.3 Refrigerant selection

CO_2 was chosen as the refrigerant focus for this thesis and the spray drying case study due to its high volumetric heating capacity, low toxicity and low flammability. In New Zealand in particular, CO_2 is commonly regarded as a more practical option for industrial high temperature heat pumps than ammonia or hydrocarbon refrigerants, particularly in food and dairy processing environments, due to the safety requirements associated with ammonia and hydrocarbons. Its typical transcritical operation is well suited to the low source temperatures such as the exhaust heat in spray drying or ambient air.

The use of CO_2, however, does not come without significant challenges. At high temperatures, CO_2 operates at extreme pressures (>15 MPa/150 bar), which surpass the operating conditions of most compressors that are readily available in the HTHP market. Although increasing pressure generally increases the specific heat capacity and improves COP (Figure 21), this effect diminishes for CO_2 at 200 °C. Consequently, a maximum discharge pressure of 15 MPa/150 bar was chosen for the initial analysis which is also approximately the maximum pressure at which market available compressors for CO_2 compressors can operate [122].

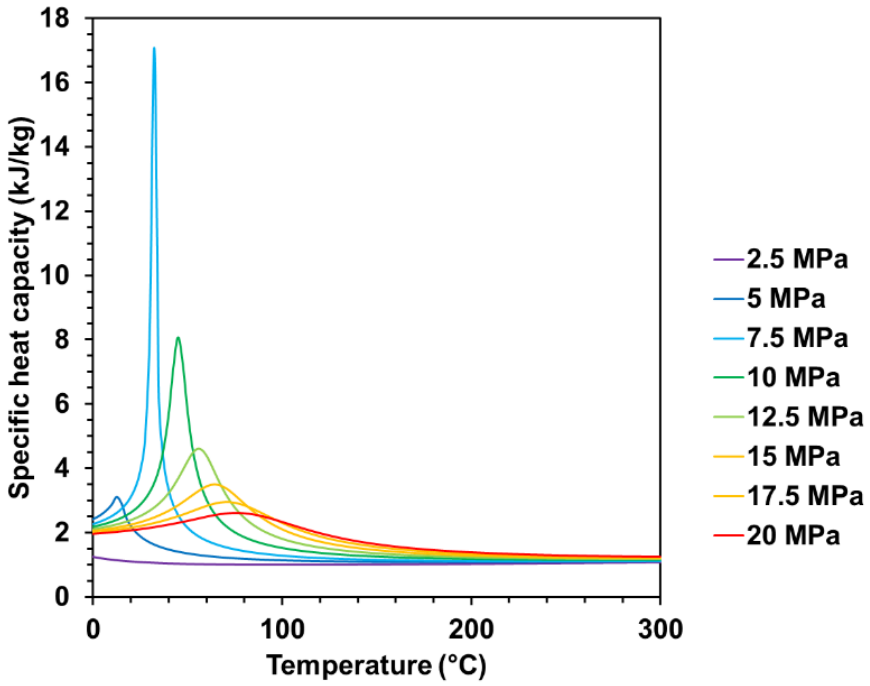

Figure 21. Isobaric specific heat of CO_2 at different temperatures and pressures [123].

3.4 Heat pump configuration and cycle

A decentralised heat pump for heating the spray drying air will be first considered in the research, therefore the selected heat pump configuration was a closed cycle heat pump. The closed cycle heat pump was selected because the heat rejection of supercritical CO_2 has a similar temperature profile to the heating requirements of the spray dryer air to be heated to 200 °C. Although the remaining four types of configurations (Section 2.1.2) were not focussed on for this research, they would be beneficial for the case of a centralised heat pump system that uses steam as the heat sink medium.

The cycle architecture of the closed cycle heat pump will be a key focus for the thesis research. The motivation for exploring different cycle configurations lies in improving the overall system performance – specifically, increasing the COP, achieving higher temperature lifts and minimising exergy destruction. Various components can be integrated into the cycle to help meet these goals. From the literature review, promising cycle advancements for HTHPs were internal heat exchangers (IHX), cascade cycles, ejectors and expanders.

The maximum sink temperature for a heat pump cycle is dependent on the compressor suction inlet temperature and the discharge pressure of the refrigerant. In transcritical heat pump cycles, the CO_2 is compressed above its critical point, therefore, the discharge temperature out of the compressor is less dependent on the pressure in comparison to a subcritical cycle, where the condensing temperature is directly correlated to the discharge pressure. Since the objective of the research is to increase the achievable temperature lift and glide, i.e. increase

the sink outlet temperature, while limiting the maximum discharge pressure, the research will focus on increasing the suction superheat prior to compression.

The amount of superheat that can be supplied to the refrigerant at the compressor inlet is usually provided from the heat source or through the use of an IHX. Adamson et al. [8] proposed a novel cycle structure where the compressor inlet was superheated for a transcritical heat pump was superheated by another transcritical heat pump. The cycle looks similar to a conventional cascade heat pump cycle, however, instead of using the cascade heat exchanger as the gas cooler/condenser for the bottom cycle and the evaporator for the top cycle, the cascade heat exchanger is used as a superheater after the evaporator which is supplied separately by an external source (Figure 22). Theoretically, this improves the temperature profile match between the superheating of the top-cycle refrigerant and the cooling of the bottom-cycle refrigerant and reduces the amount of compression required to reach the same discharge temperature.

IHXs are the most common modification to the simple transcritical CO_2 heat pump cycle where heat is exchanged from the refrigerant at the gas cooler outlet to the suction inlet of the compressor. An IHX can sometimes be referred to as a suction line heat exchanger. The effect of using an IHX is that the refrigerant is superheated prior to compression and subcooled prior to expansion. As a result, the compression energy required is reduced as the discharge pressure required is decreased and the throttling loss is reduced. The heat pump cycle architectures that will be evaluated in this chapter will combine IHX and cascade configurations.

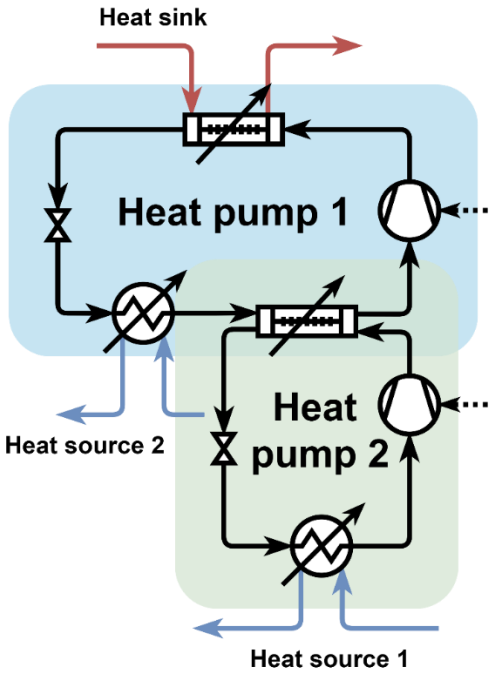

Figure 22. High temperature transcritical heat pump cycle concept proposed by Adamson et al. [8].

3.5 Heat pump integrated with boiler systems

It is recognised that a heat pump solution may not always be the most cost-effective or practical option for supplying all of the process heating requirement – particularly in retrofit scenarios or where the high temperature lift significantly reduces the COP. As a result, the potential benefits of hybrid configurations, where the heat pump supplies the lower-temperature portion of the thermal load and a boiler is used to provide the final temperature lift, were investigated. This approach allows the heat pump to operate with a more favourable temperature range, improving its efficiency and reducing operational costs, while still enabling high temperature air delivery to the process. The hybrid configuration also offers flexibility in system design and can lower the capital cost barrier for early adoption of HTHPs in industry.

Two boiler types were considered for the integration: biomass boilers and electrode boilers. Biomass boilers can provide renewable high temperature heat, but they often have slower ramp up times and higher maintenance requirements. Electrode boilers, on the other hand, offer rapid response and ease of integration but may result in higher operational costs depending on electricity pricing and carbon intensity. As part of the thesis research, different design temperatures for the heat pump design and how the hybrid systems perform from an operational cost perspective at varying electricity and biomass prices will be evaluated. Additionally, this stage of research considers how the secondary air heating requirements for the SFBs and VFBs should be integrated.

3.6 Wider application potential for high temperature transcritical CO_2 heat pumps

While the focus of this research is on the application of CO_2 HTTHPs for milk powder spray drying, there is significant potential to apply this technology across a broader range of industrial processes. The potential decarbonisation impact of deploying CO_2 HTTHPs in other sectors will be explored. By identifying typical heat demand profiles, identifying compatible heat sources, and estimating the global thermal energy demand of these applications, an overall emissions reduction potential can be estimated. The findings aim to support the case for broader investment and development of this technology beyond a single-use case, contributing to industrial decarbonisation at scale.

3.7 Summary and research approach

Milk powder spray drying presents a unique challenge for the research field of HTHPs as both high temperature lifts and large temperature glides are required. The research for this thesis will focus on the design of a heat pump system that is localised to the spray drying process, i.e., decentralised, as this has the highest theoretical performance for the heat pump and therefore the lowest operational cost. The approach to research will be to first consider the simplest system that can achieve the requirements. The reason for this is that simpler systems generally

correlate to a lower retrofit capital expenditure which is a large motivation for many industrial sites looking to decarbonise. The results of this preliminary analysis will then inform what further modifications should be made to the heat pump design or the integration of the heat pump to increase the performance of the overall system.

As the exhaust heat from the spray dryer is the largest source of waste heat, this will be considered first to supply heat source for the heat pump. Exhaust heat recovery is a preferable waste source for many reasons, such as that the exhaust air will always exist when the spray dryer is running. However, for some factories, exhaust heat recovery may not be viable due to the capital investment required, therefore, ambient air source will also be considered as a potential heat source for the heat pump. As the waste heat available in the spray drying process is at relatively low temperatures, CO_2 is a suitable refrigerant due to its low critical temperature, particularly when operated within a transcritical heat pump cycle. Additionally, CO_2 has the benefit of having a high volumetric heating capacity, thus, smaller systems can be theoretically achieved for the same heating requirements – a major advantage for retrofit of existing systems.

In a closed cycle, there are many cycle architectures that have varying components. In general, the objective of including more components in the cycle further than the conventional evaporator, compressor, expansion valve and condenser is to decrease the amount of work required during compression and/or decrease the amount of work lost through expansion. This becomes particularly applicable for CO_2 HTTHPs due to the large pressure differences within the cycle. The core of the research focusses on optimising the cycle architecture for a transcritical CO_2 heat pump to supply 200 °C sink temperatures. To achieve this, well-established cycle components/arrangements, such as IHX and cascade, in novel arrangements will be explored to identify innovative ways of improving performance while maintaining technical simplicity. These configurations will also serve as a foundation for deeper insights into system behaviour, exergetic efficiency and temperature lift capabilities.

Based on the findings from the analysis of these cycle architectures, the research will then explore more complex enhancements – ejectors and expanders – to identify ways to further increase performances. While these advanced components have the potential to offer significant performance gains, they also introduce complexity, integration challenges and cost. Thus, the performance gain in the context of high temperature heating needs to be quantified to assess whether their integration is worthwhile.

An additional approach will be explored that considers the integration of a CO_2 HTTHP with boiler systems, evaluating whether this hybrid configuration can offer more practical or cost-effective pathways to decarbonisation. This analysis will consider the optimum heat pump sink temperature for a range of biomass and electricity price scenarios.

Finally, the broader application potential of CO_2 HTTHP will be assessed by identifying other industrial sectors where this technology could displace fossil fuel heating. As part of this, compatible heat sources and temperature demands will be identified and the heat potential that could be decarbonised globally will be estimated.

The common process requirements and constraints applied to the research in this thesis are summarised in Table 8.

Table 8. Process requirements and constraints.

Component/Stream	**Constraint**
Heat sink (air)	Primary heating requirement: $T_{sink,out} = 200\ °C$ Secondary heating requirements: $T_{sink,SFB} = 102\ °C$ $T_{sink,VFB} = 78\ °C$
Exhaust air	$T_{exhaust} = 60\ °C$
Heat source (water)	$T_{source,in} = 40\ °C$
Ambient conditions	$P_{amb} = 1.01325\ bar$ $T_{amb} = 15\ °C = T_{sink\ in}$
Heat exchangers	CO_2 to air: $\Delta T_{min} = 20\ °C$ CO_2 to CO_2: $\Delta T_{min} = 5\ °C$ Water to CO_2: $\Delta T_{\min evap} = 5\ °C$
Steam	$P_{HPS} = 40\ bar$ $P_{LPS} = 10\ bar$

Chapter 4
Thermodynamic modelling for the proposed cycle

4.1 Introduction

The design of a heat pump cycle architecture is generally motivated by two objectives: 1) to minimise the required work input to the compressor, and 2) to minimise the exergy destruction in the components, particularly during expansion. An additional challenge is introduced by using CO_2 as a refrigerant due to the high pressures required, and therefore, a third key objective would be to increase the achievable sink temperature while limiting the maximum discharge pressure in the cycle. Traditionally, heat pump design and placement focused on maximising COP by minimising the temperature lift of the heat pump. However, with HTHPs, the objective shifts – particularly in the context of industrial decarbonisation, where cost is no longer the sole biggest consideration in retrofit projects. As a result, the impact of different cycle architectures, and the role of specific components within those cycles, is less well understood for HTHP applications.

The aim of this chapter is to optimise cycle architectures, specifically the effect of IHX and cascade cycle arrangements on the performance of a CO_2 high temperature transcritical heat pump (HTTHP), to increase the achievable temperature lift and temperature glide, while simultaneously limiting the maximum discharge pressure. Six heat pump cycle architectures are analysed, including a novel cascade transcritical heat pump cycle proposed by Adamson et al. [8] that was yet to be modelled in the literature. This chapter will also provide an in depth description of the modelling method for the heat pumps for the entire thesis. The analysis will help to provide an understanding of where more complex components can be best utilised.

4.2 Cycle concepts

Six configurations were considered, as shown in Figure 23. The symbols for each of the components are given in the Nomenclature. Model T1-1 is a single-stage transcritical heat pump cycle. Model T1-2 is a single-stage cycle with an IHX from the gas cooler outlet to the compressor inlet. Model TT-1 is a transcritical-transcritical cascade cycle based on the concept proposed by Adamson et al. [8] where the bottom cycle is used to superheat the compressor inlet for the top cycle.

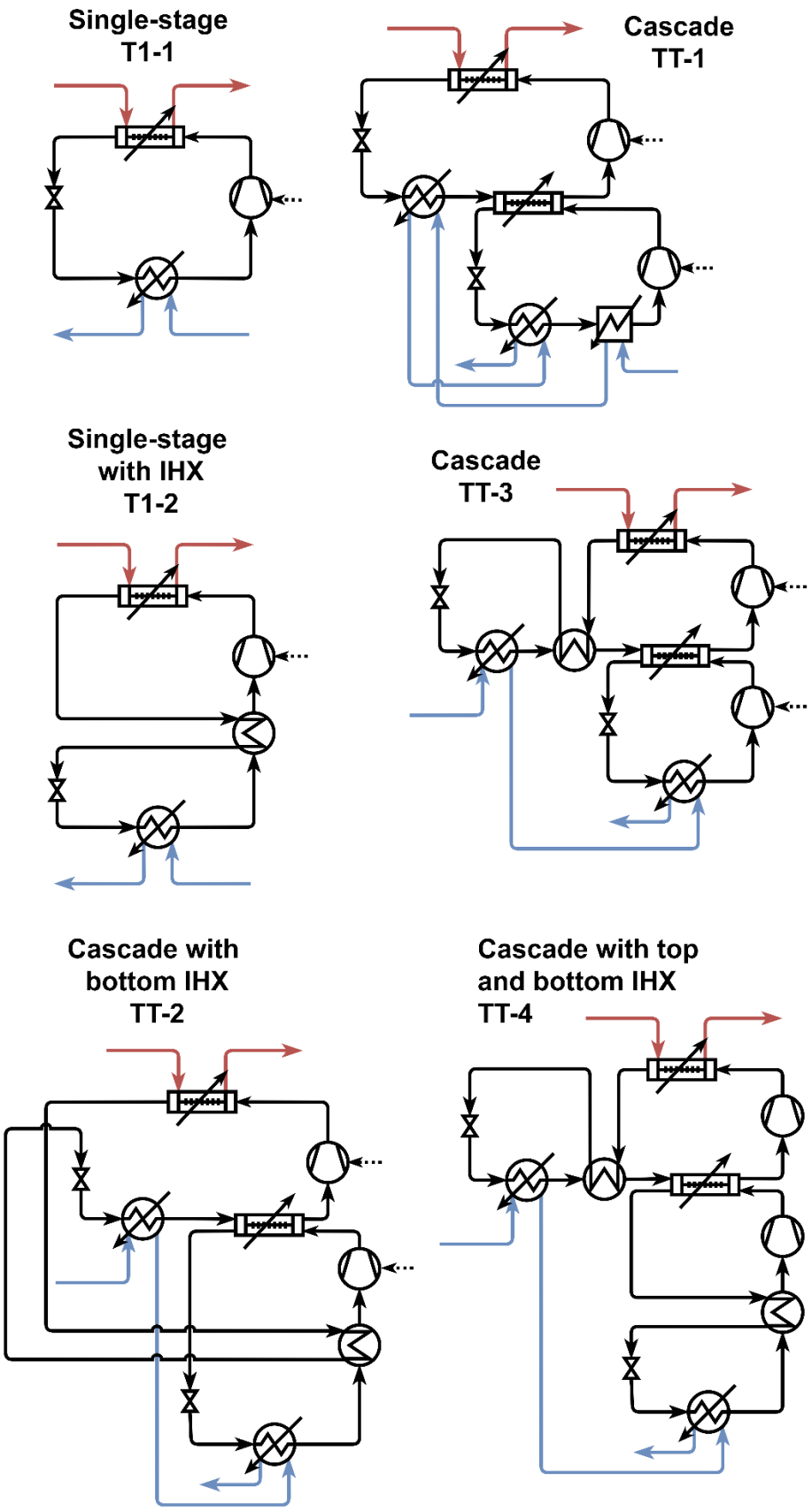

Figure 23. Internal heat exchanger and cascade heat pump cycles evaluated.

The source for the heat pump is supplied by exhaust air heat recovery from a dryer. The exhaust air is a large heat source due to the high moisture content. It is assumed that a water loop is used to transport the heat from the spray dryer exhaust to the heat pump due to the physical distance; the exhaust tends to be on the roof, and the heat pump would likely be on the ground or on a lower floor. The evaporation temperature for the top cycle of the heat pump ($T_{evap,top}$) is higher than the evaporation temperature for the bottom cycle ($T_{evap,bot}$), however, it is still significantly lower than the inlet temperature for the heat source ($T_{source,in}$) when using exhaust heat recovery. Therefore, a separate superheater was also included in the bottom cycle to use the heat source more efficiently (Figure 24).

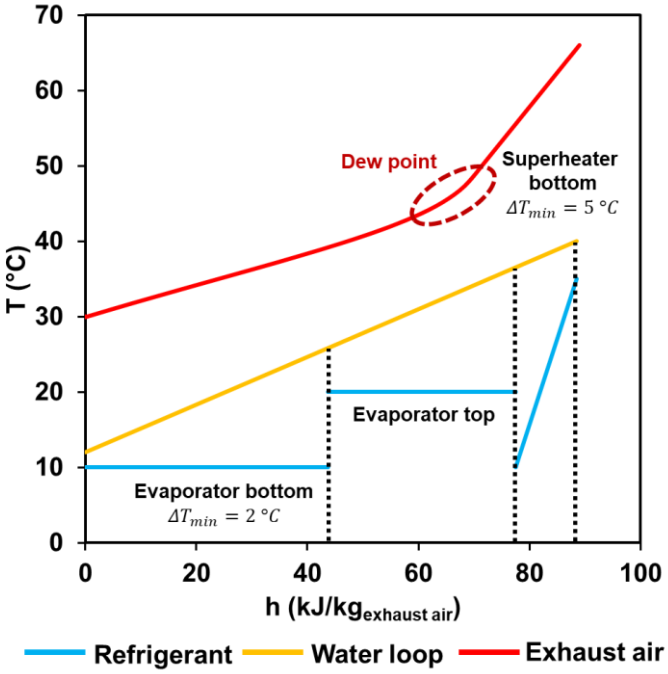

Figure 24. Exhaust air water loop to supply to the heat pump.

Models TT-2, TT-3, and TT-4 are variations on Model TT-3 with differing IHX placements within the cycle. Model TT-2 has an IHX which exchanges heat from the top-cycle gas cooler outlet to the compressor inlet of the bottom cycle or a bottom-cycle only IHX. Model TT-3 has an IHX which exchanges heat from the top-cycle gas cooler outlet to the top-cycle compressor inlet or top-cycle only IHX. Model TT-4 has IHXs in both the top and bottom cycles, exchanging heat from their respective gas cooler outlets to their respective compressor inlets.

4.3 Methods

This section outlines the method for modelling the performance of the six CO_2 HTTHP cycles. It describes the model constraints, assumptions and software used for the analysis. The thermodynamic correlations applied in the cycle simulations are presented, including the iterative approach used to determine the optimal mass flow rates of heat exchanger sink streams to maintain the minimum approach temperature. The evaluation of cycle performance is then described, focusing on

the COP and the exergy destruction as key metrics. The method described in this section has also since been published in a journal article [123].

4.3.1 Modelling software

The models were developed using Microsoft Excel VBA. The thermodynamic properties for the fluids were obtained using CoolProp [124]. For cycle selection, the graphical nature of Excel, being able to view state points and cycle components simultaneously, made it advantageous in comparison to other modelling environments, such as Python or Aspen Plus. The number of data points to collect was also relatively small, and thus, Excel was suitable for modelling. In the case that a large number of data points needed to be collected, Python would be more suitable.

4.3.2 Model constraints and assumptions

The following assumptions were used to simplify the analysis of the heat pump models:

- Steady-state operation
- Isobaric heat exchange
- Isenthalpic expansion
- Non-isentropic compression
- Negligible piping pressure-drop, heat losses or heat gain

The common parameters and inputs applied to the models are summarised in Table 9. For cycles T1-1 and T1-2, the parameters for the bottom cycle of TT-1 were applied. At this stage of analysis, the system boundary is drawn around the cycle only. The spray dryer conditions will be applied in later chapters, with the exception of the exhaust air, which was used to establish the source temperature that supplied the heat pump ($T_{source,in} = 40$ °C) and the ambient conditions which were used to establish the sink inlet conditions ($T_{sink,in} = 15$ °C, $P_{sink,in} = 1.01325$ bar). The evaporators were modelled initially with saturation temperatures (T_{evap}) of 10 °C for the bottom cycle and 20 °C for the top cycle, consistent with those of Sarkar et al. [13] (for the top cycle).

It was assumed that the refrigerant could be superheated from the source to a minimum approach temperature ($\Delta T_{min,SH}$) of 5 °C, therefore the temperature exiting the superheater of the bottom cycle in cycle TT-1 was 35 °C. The compressor isentropic efficiency (η_s) was assumed to be 70 % and an additional efficiency (η_{mech}) of 96% was assumed to account for any mechanical losses. As established in Section 3.2.3, the maximum discharge pressure ($P_{dis\ max}$) of the compressor was limited to 150 bar. The minimum temperature differences in the gas coolers and internal heat exchangers were set at 5 °C for CO_2 to CO_2 heat exchange and 20 °C for CO_2 to air heat exchange (see Section 3.2.3 for justification).

Table 9. Model parameters and inputs [122], [125], [126], [127].

Component/Stream	**Constraint**
Heat source (water)	$T_{source,in} = 40\ °C$ $\Delta T_{min,SH} = 5\ °C$
Heat sink (air)	$T_{sink,in} = 15\ °C$ $P_{sink,in} = 1.01325\ bar$
Evaporator	$T_{evap\ bottom} = 10\ °C$ (saturation) $T_{evap\ top} = 20\ °C$ (saturation)
Compressor	$\eta_s = 70\%$ $\eta_{mech} = 96\%$ $P_{dis\ max} = 150\ bar$
Gas cooler/internal heat exchanger	CO_2 to air: $\Delta T_{min} = 20\ °C$ CO_2 to CO_2: $\Delta T_{min} = 5\ °C$

4.3.3 Thermodynamic modelling

The model was developed starting with the source conditions and defined evaporation temperatures. It was assumed that the CO_2 left the evaporator as a saturated vapour ($x = 1$) to obtain the evaporation pressure using CoolProp (Equation 4.1).

$$P_{evap} = f(T_{evap}, x) \tag{4.1}$$

In the cycles where the refrigerant was superheated coming out of the evaporator, the refrigerant properties at the exit of the evaporator were obtained from the temperature at the exit and the evaporation pressure, where the temperature at the exit of the evaporator is defined by Equation 4.2. For cycle TT-1, this was the calculation for the temperature of the refrigerant coming out of the superheater.

$$T_{SH,out} = T_{evap,out} = T_{source,in} - \Delta T_{min} \tag{4.2}$$

The gas cooler outlet temperature ($T_{GC,out}$) for the CO_2 to air heat exchange was set as an optimisation variable with the constraint that the value of the temperature could not be less than the sink inlet temperature plus the minimum approach temperature (Equation 4.3).

$$T_{GC,out} \geq T_{sink.in} + \Delta T_{min} \quad 4.3$$

The refrigerant at the outlet of the gas cooler is used as a heating stream in the internal heat exchangers. This stream heats the cold refrigerant to a minimum temperature difference of 5 °C (Equation 4.4). From there, the properties of the cold refrigerant at the outlet of the IHX, which is at the suction inlet of the compressor, can be determined from the evaporation pressure (P_{evap}) and the cold refrigerant outlet temperature from the IHX ($T_{IHX\ cold,out}$).

$$T_{IHX\ cold,out} = T_{comp,in} = T_{IHX\ hot,in} - \Delta T_{min} \quad 4.4$$

The pressure ratios across the compressors (P_r) were also set as optimisation variables with the constraint that the outlet pressure of the compressors ($P_{comp,out}$) is less than the maximum discharge pressure ($P_{dis\ max}$) of 150 bar. The pressure ratio is defined as the ratio between the discharge pressure ($P_{comp,out}$) and the suction pressure ($P_{comp,in}$), as shown in Equation 4.5.

$$P_r = \frac{P_{comp,out}}{P_{comp,in}} \quad 4.5$$

The specific enthalpy at the outlet of the compressor ($h_{comp,out\ (a)}$) is determined using the isentropic compressor relation (Equation 4.6) where $h_{comp,out\ (s)}$ is determined from the entropy of the refrigerant at the compressor inlet ($s_{comp,out} = s_{comp,in}$) and the compressor outlet pressure ($P_{comp,out}$).

$$\eta_s = \frac{h_{comp,out\ (s)} - h_{comp,in}}{h_{comp,out\ (a)} - h_{comp,in}} \quad 4.6$$

Determining the compressor outlet pressure also fully defines the properties of the refrigerant at the gas cooler outlet. As the pressure of the refrigerant doesn't change in the IHX, the pressure of the refrigerant on the hot side of the IHX is also same as the compressor outlet pressure ($P_{GC,out} = P_{IHX\ hot,out} = P_{comp,out}$). The enthalpy at the outlet of the hot stream of the IHX ($h_{IHX\ hot,out}$) can then be calculated from an energy balance (Equation 4.7). In general, the flowrate of the hot refrigerant stream ($\dot{m}_{ref\ hot}$) is the same as the flowrate of the cold refrigerant ($\dot{m}_{ref\ cold}$), except for cycle TT-2 as the hot stream and cold stream are from different stages.

$$h_{IHX\ hot,out} = h_{IHX\ hot,in} - \frac{\dot{m}_{ref\ cold} \cdot \left(h_{IHX\ cold,in} - h_{IHX\ cold,out}\right)}{\dot{m}_{ref\ hot}} \quad 4.7$$

There are three regions in which the minimum approach or "pinch" during the heat rejection from the refrigerant to the sink can occur: 1) at the lowest temperatures (cold stream inlet, hot stream outlet), 2) at the highest temperatures (cold stream outlet, hot stream inlet), or 3) in the middle of the heat exchange (counterflow).

For a subcritical cycle, if the pinch is in the middle of the heat exchange, this occurs at the saturated vapour point of the refrigerant, which is a predictable and numerically calculable location. However, with supercritical CO_2, the sensible cooling profile is nonlinear and also varies with pressure. An example of this is shown Figure 25, where CO_2 with the same inlet conditions was compressed to a) 150 bar and b) 100 bar. When compressed to 150 bar, the pinch occurred when the refrigerant had cooled to 81.8 °C and the sink had heated to 61.8 °C ($\Delta T_{min} = 20$ °C) [129]. When compressed to 100 bar, the pinch occurred when the refrigerant had cooled to 50.4 °C and the sink had heated to 30.4 °C. During the optimisation of the pressure ratios, the location of the pinch in the gas coolers need to be determined. One could fix the pinch points at the lowest temperature (1) or the highest temperature (2); however, this could result in a large amount of exergy destruction.

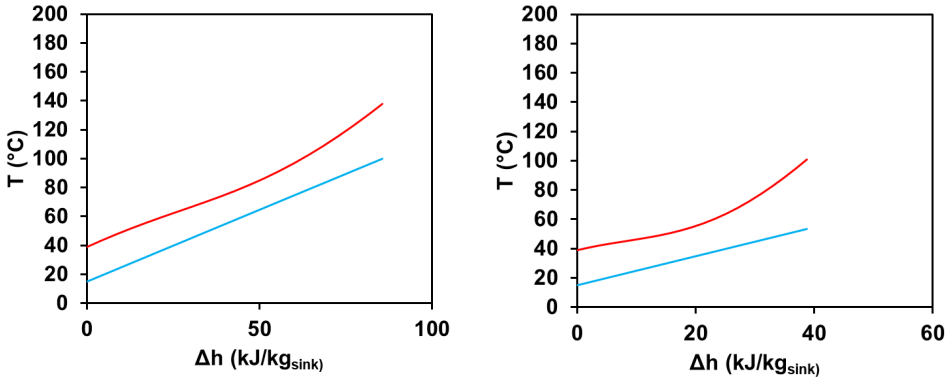

a) $P_{dis} = 150$ bar b) $P_{dis} = 100$ bar

Figure 25. Comparison of sensible cooling of CO_2 at a) 150 bar and b) 100 bar.

To determine the location of the pinch and also prevent temperature cross in the gas coolers (infeasible heat transfer), an iterative calculation was used. The objective of the iterative calculation was to determine the cold stream mass flowrate ($\dot{m}_B$) which achieves the desired minimum temperature difference (ΔT_{min}). The calculation uses the principle that the products of the mass flowrate ($\dot{m}$) and specific heat capacity (c_p) of the hot stream (stream A) and cold stream (B) are equal at the pinch (Equations 4.8 to 4.10). Equation 4.8 describes that the gradients, i.e., the inverse of the capacity rate, of both the hot and cold stream at the pinch are equal, as noted by Linnhoff et al. [128].

$$\frac{\delta T_A}{\delta Q_A} = \frac{\delta T_B}{\delta Q_B} \tag{4.8}$$

$$\dot{m}_A \frac{\delta h_A}{\delta T_A} = \dot{m}_B \frac{\delta h_B}{\delta T_B} \tag{4.9}$$

$$\left(\dot{m} c_p\right)_A = \left(\dot{m} c_p\right)_B \tag{4.10}$$

The process for the iterative calculation is summarised in Figure 26. At the beginning of the calculation, the hot stream outlet and inlet conditions are known. The cold stream intensive properties (pressure, temperature) at the inlet are also known. In addition to iterating for the mass flowrate of the cold stream ($\dot{m}_B$), the quantity of heat that is transferred at the pinch for the hot stream ($\Delta\dot{Q}_A$) and the specific heat capacity of the cold stream ($c_{p,ave\ B}$) are also variables in the iteration. Initial values are set for the variables for the first variation n. A depiction of the variables $\Delta\dot{Q}$ and ΔT for the respective streams are shown in Figure 27. These inputs are used to first calculate the change in specific enthalpy for the hot stream (Δh_A) from the inlet to the pinch (Equation 4.11) which can then be used to calculate the specific enthalpy of the hot stream at the pinch ($h_{pinch,A}$), as shown in Equation 4.12.

$$\Delta h_A = \frac{\Delta\dot{Q}_A}{\dot{m}_A} \tag{4.11}$$

$$h_{pinch,A} = h_{in,A} + \Delta h_{pinch,A} \tag{4.12}$$

Once the specific enthalpy of the hot stream at the pinch is determined, the temperature ($T_{pinch,A}$) and specific heat capacity ($c_{p,A}$) of the hot stream at the pinch can be obtained and the temperature of the cold stream ($T_{pinch,B}$) at the pinch can be calculated using 4.13. This value can then be used to obtain the specific enthalpy ($h_{pinch,B}$) and specific heat capacity of the cold stream at the pinch ($c_{p,B}$).

The mass flow rate of the cold stream is calculated using the $\dot{m}c_p$ relation (Equation 4.10).

$$T_{pinch,B} = T_{pinch,A} - \Delta T_{min} \tag{4.13}$$

The heat transferred at the pinch for the cold stream can be calculated as shown in Equation 4.14 where $\Delta h_{pinch,B}$ is the value of $h_{pinch,B}$ minus the value of the inlet enthalpy ($h_{in,B}$).

$$\Delta\dot{Q}_B = \dot{m}_B \cdot \Delta h_{pinch,B} \tag{4.14}$$

The calculation will iterate until $\Delta\dot{Q}_A$ and $\Delta\dot{Q}_B$ converge to the same value, i.e. $\Delta\dot{Q}$ in Figure 27. Once converged, the mass flowrate of the cold stream is returned. Finally, the outlet temperature can be obtained through calculating the enthalpy of the sink outlet from the heat transferred in the gas cooler (Equation 4.15).

$$h_{out,B} = \frac{\dot{Q}_{GC}}{\dot{m}_B} \tag{4.15}$$

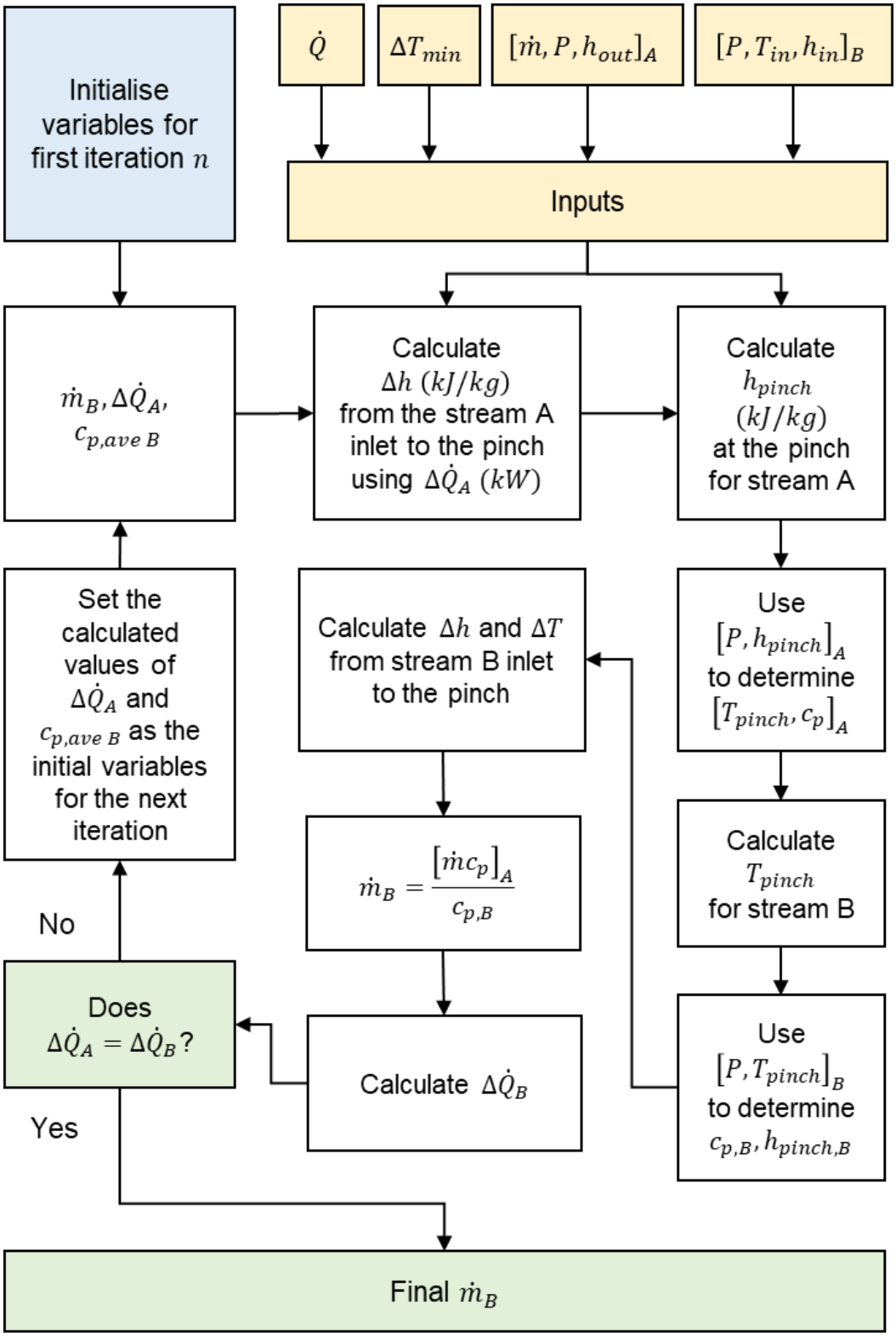

Figure 26. Process for calculating the mass flowrate for the cold stream (B) to prevent temperature cross with the hot stream (A) in the gas coolers.

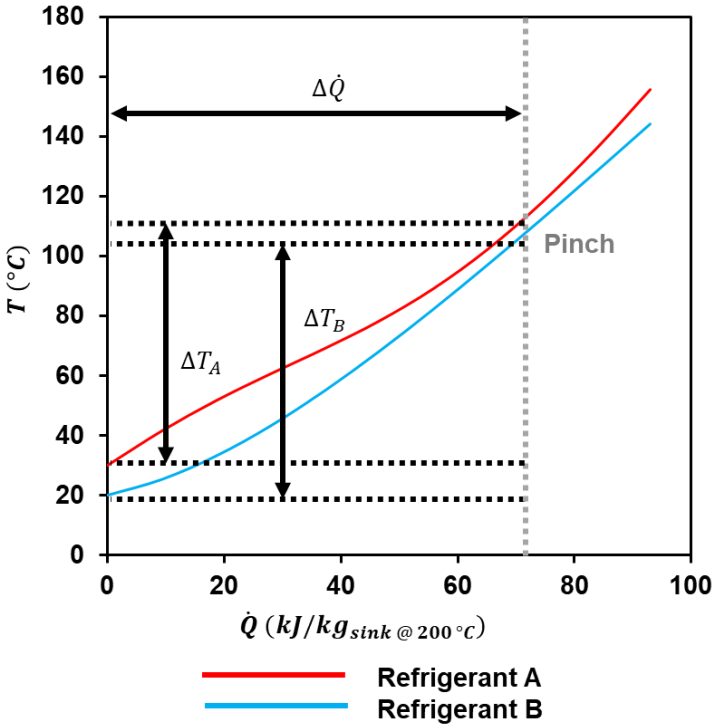

Figure 27. Temperature-heat diagram for the top-cycle mass flowrate calculations for a sink outlet temperature 200 °C.

4.3.4 Thermodynamic performance evaluation

Heating COP was the main performance evaluation metric used to compare the different cycles (Equation 4.16) as the source and sink conditions for each heat pump were the same. The models were optimised using Excel Solver (GRG nonlinear) to maximise the COP at different sink temperatures. The refrigerant outlet temperature and pressure ratios across the compressors were the manipulated variables.

$$COP_{Heating} = \frac{\dot{Q}_{GC\ top}}{\dot{W}_{total}} \qquad 4.16$$

With HTHPs, the COPs are lower than what would be conventionally seen for low temperature (<80 °C) heat pumps due to the large temperature lifts required. To benchmark, the COPs are compared to the theoretical maximum COPs for the temperature lift. The Lorenz COP was used to determine the maximum theoretical COP rather than Carnot due to the large temperature glides that exist within the system. The Lorenz COP (Equation 4.17) is calculated using the logarithmic mean temperatures for the source and sink (Equations 4.18 and 4.19).

$$COP_{Lorenz} = \frac{T_{LM,sink}}{T_{LM,sink} - T_{LM,source}} \qquad 4.17$$

$$T_{LM,source} = \frac{T_{source,out} - T_{source,in}}{\ln(T_{source,out}) - \ln(T_{source,in})} \quad 4.18$$

$$T_{LM,sink} = \frac{T_{sink,out} - T_{sink,in}}{\ln(T_{sink,out}) - \ln(T_{snk,in})} \quad 4.19$$

The exergy destruction $\dot{X}_{des}$ (kW) across the cycle components was also calculated to determine where the inefficiencies occur within the cycle. In the heat exchangers, the exergy destruction was the difference between the exergy transferred for each of the streams (Equation 4.20).

$$\dot{X}_{des,component} = \sum \dot{X}_{out,component} - \sum \dot{X}_{in,component} \quad 4.20$$

Where the thermo-mechanical exergy for the stream $\dot{X}$ (kW) is defined by the specific enthalpy and the specific entropy of the stream referenced to a dead state condition of $T_0 = 15\ °C$ and $P_0 = 101.325\ kPa$ (Equation 4.21).

$$\dot{X} = \dot{m}\big((h - h_0) - T_0(s - s_0)\big) \quad 4.21$$

Finally, the exergetic efficiency η_{ex} was calculated from the change in the exergies of the sink and source, and the total work consumption (Equation 4.22).

$$\eta_{ex} = \frac{\dot{X}_{sink,out} - \dot{X}_{sink,in}}{\dot{X}_{source,in} - \dot{X}_{source,out} + \dot{W}_{total}} \quad 4.22$$

4.3.5 Determining the maximum sink temperature

For data collection, the cycles were modelled over a range of sink temperatures that were thermodynamically valid within the specified parameters for source temperature ($T_{source} = 40$ °C) and also the selected parameters for maximum discharge pressure ($P_{dis,max} = 150$ bar) and minimum approach temperatures in the heat exchangers (ΔT_{min}). In each simulation, a target sink temperature was set, and the model was optimised to achieve the maximum COP by varying gas cooler outlet temperature and the pressure ratios. The target sink temperatures in each optimisation were varied by 1 °C increments.

4.3.6 Verification

As the cascade cycles have not been developed physically, experimental validation of the models is currently not possible. The models for T1-1 and T1-2 were compared to the results of Cao et al. [129], which includes experimental validation of transcritical cycle modelling, to verify the modelling method. The models were tested for two conditions. The maximum error between the models were 1.0 % for the COP and 6.9 % for the discharge pressures which may be attributed to differing isentropic efficiencies (Table 10).

Table 10. Model verification for T1-1 and T1-2.

$T_{sink,in}/T_{sink,out}$ (°C)	10/70		10/90	
	COP	P_{dis} (MPa)	COP	P_{dis} (MPa)
Model T1-1	3.77	10.9	2.73	11.6
Cao et al.	3.76	10.2	2.75	11.9
Error (%)	0.5	6.9	0.6	2.7
Model T1-2	3.78	10.2	2.88	11.7
Cao et al.	3.81	9.9	2.91	11.3
Error (%)	0.8	3.0	1.0	3.5

4.4 Results

4.4.1 Maximum sink temperatures

At the specified conditions outlined in Section 4.3, each model exhibited different maximum sink temperatures (Table 11). Models T1-1 and T1-2 exhibited a maximum sink temperature of 130 °C and 190 °C, respectively. The IHX in Model T1-2 allowed for the gas cooler outlet temperature to be higher than Model T1-1 in addition to increasing the suction inlet temperature to the compressor which both resulted in an increase in the sink outlet temperature for the same compressor outlet pressure.

Table 11. Maximum sink temperatures for six high temperature transcritical heat pump cycles with cycle features.

Model	Maximum $T_{sink,out}$ (°C)	Cycle features
T1-1	130	Single stage
T1-2	190	Single stage with IHX
TT-1	240	Cascade
TT-2	290	Cascade with bottom cycle IHX
TT-3	230	Cascade with top cycle IHX
TT-4	290	Cascade with both top and bottom cycle IHX

By utilising a cascade configuration (TT-1, TT-2, TT-3, and TT-4), the maximum sink temperature could be further increased in comparison to a single stage cycle (T1-1 and T1-2). Models TT-1 and TT-3 had maximum sink temperatures of approximately 240 °C whereas Models TT-2 and TT-4 had maximum sink temperatures of approximately 290 °C for the given conditions. Unlike Models TT-1 and TT-3, there was a commonality between Models TT-2 and TT-4 in that they both had an IHX in the bottom cycles of the cascade. For Model TT-2, the IHX used heat from the top cycle gas cooler to heat the suction inlet of the bottom cycle compressor. Model TT-4 had IHXs in both the top cycle and the bottom cycle that transferred heat from the gas cooler to the suction inlet of the respective stages.

The results suggest that the IHX in the bottom cycle has a larger influence on the maximum sink temperature of the cycle. This is further supported by the observation that Model TT-3 has a similar maximum sink temperature to TT-1 and Model TT-4 has a similar maximum sink temperature as TT-2, where TT-3 and TT-4 have IHX in the top cycle, as without the top cycle IHX, TT-3 and TT-4 become thermodynamically equivalent to TT-1 and TT-4, respectively.

4.4.2 Cycle COPs

With HTTHPs, there is a trade-off between COP and the sink outlet temperature. In general, the COP of the system is higher when the gas cooler outlet temperature for the refrigerant is lower because more heat is transferred from the supercritical CO_2 to the heat sink. However, higher gas cooler outlet temperatures allow the sink temperature to increase. An example of this is shown in Figure 28. In T1-1 (Figure 28a and b), where there is no IHX, the compressor discharge temperature stays the same but the pinch point shifts upwards which causes the COP to decrease as the amount of heat transferred for the same amount of work decreases. For TT-4 (Figure 28c and d), where there is an IHX, an additional effect is observed as the compressor outlet temperature also increases due to the increased temperature provided to the compressor suction inlet.

The COPs of the six HTTHP cycles at sink temperatures between 50 and 300 °C are shown in Figure 29. At the lowest temperatures, Models TT-3 and TT-4 had the highest COPs, followed by Models T1-1 and T1-2, then TT-1 and TT-2. For the single stage cycles, T1-1 and T1-2, sink temperatures between 50 °C and 110 °C were achievable at the lowest gas cooler outlet temperature (35 °C) and therefore the IHX in T1-2 is not effective as the evaporator outlet is also at 35 °C (15 °C superheat). In the case that there was no superheat provided to the evaporator from the source, the IHX would increase the COP. Similarly, the single stage cycles (Models T1-1 and T1-2) performed better than the generic cascade model (TT-1) at temperatures below 100 °C as the additional superheat provided from cascading is unnecessary to achieve these lower sink temperatures. However, TT-3 and TT-4, which both have an IHX in the top cycle, were able to achieve higher COPs (up to 4.88) at sink temperatures below 80 °C.

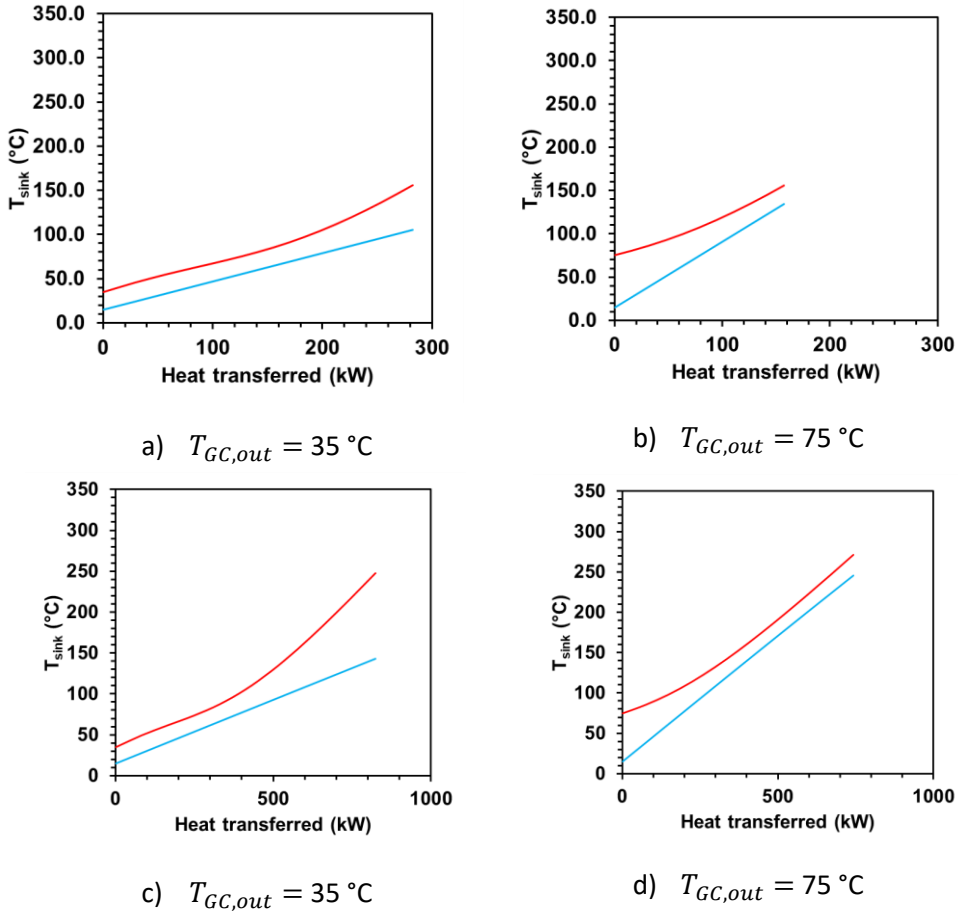

Figure 28. Comparison of gas cooler heat transferred at different refrigerant outlet temperatures for TT-4.

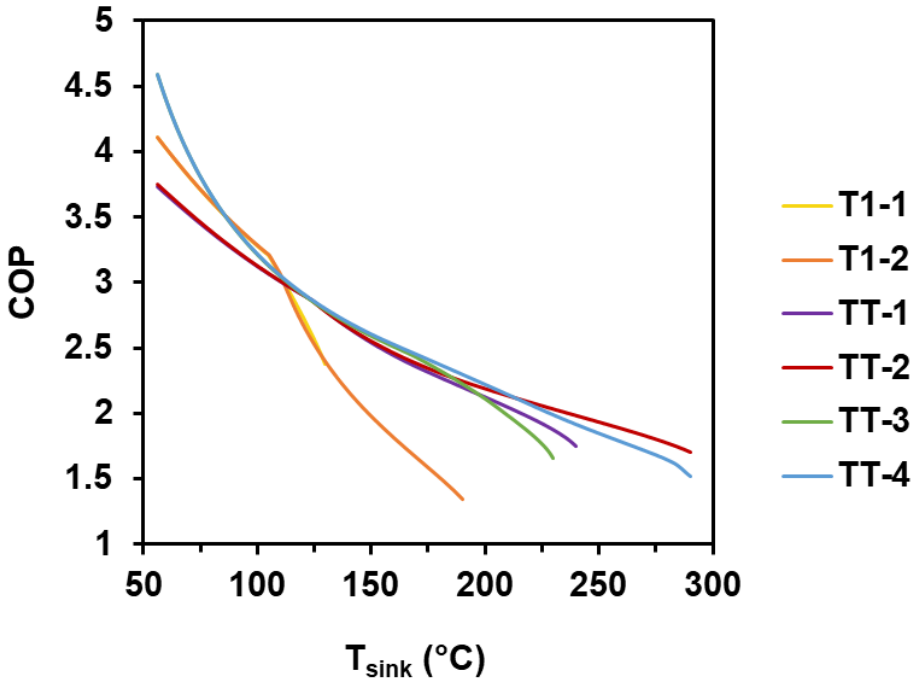

Figure 29. COPs at different sink temperatures for six high temperature transcritical heat pump cycles.

The positive effect of the IHX on the COP in the top cycle resulted from the ability to relax the ΔT_{min} constraint in the gas cooler, which prevents the single stage cycles from achieving higher COPs at these temperatures. This effect can be seen in Figure 29, where there is an abrupt change in the slope of the curve for T1-1 and T1-2, which is where the gas cooler outlet temperature for the refrigerant cannot decrease any further without breaking the ΔT_{min} constraint of 20 °C. Contrastingly, the IHXs in the top cycles of TT-3 and TT-4 achieve higher COPs by providing subcooling to the refrigerant and recovering the heat within the cycle. TT-2 and TT-4 were the only models able to achieve the highest sink temperatures ($T_{sink} =$ 290 °C). TT-2 had the highest COP of the two models at 1.70 whereas the COP of TT-4 was only 1.52. However, up to 220 °C, TT-4 exhibited higher COPs.

4.4.3 Spray drying case study

The results of the analysis showed that the optimal performance of the heat pump cycles was dependant on the operating temperature range. The thermodynamically optimal cycles for a range of sink temperatures are given in Table 12. For each thermodynamically optimal cycle, the corresponding COP, exergetic efficiency and efficiency limits have been provided. The efficiency limits given are expressed in terms of Lorenz COP (COP_{Lorenz}) and the calculated COP for ideal operation of the components (COP_{ideal}). Ideal operation of the compressor (100% isentropic efficiency) at a maximum discharge pressure of 150 bar cannot achieve sink temperatures of 250 °C and 290 °C for Model TT-2. Because of this, the COP_{ideal} values for these two sink temperatures were calculated for a maximum discharge pressure of 200 bar. The results of this chapter have also since been published in Kong et al. [123] where the break-even electricity to reference price ratios (r_p) were also calculated (not by the candidate), and have also been provided in Table 12. The break-even price ratio can give insight into where the heat pump is still competitive in cost. For example, at a sink temperature of 100 °C, electricity can be 3.19 times more expensive than natural gas for the heat pump still to be competitive. The pressure-enthalpy and temperature-entropy plots for TT-1, TT-2, TT-3 and TT-4 are shown in Figure 30.

Table 12. Thermodynamically optimal cycles at different sink temperatures.

T_{sink} (°C)	Optimal cycle	Break-even r_p [123]	COP	COP_{Lorenz}	COP_{ideal}	η_{ex} (%)
100	T1-1/T1-2	3.19	3.28	11.00	3.99/3.84	41
150	TT-3/TT-4	2.44/2.42	2.60	6.70	3.26/3.28	43
200	TT-4	2.06	2.22	5.03	2.52	50
250	TT-2	1.81	1.93	4.14	2.38*	50
290	TT-2	1.59	1.70	3.68	2.17*	49

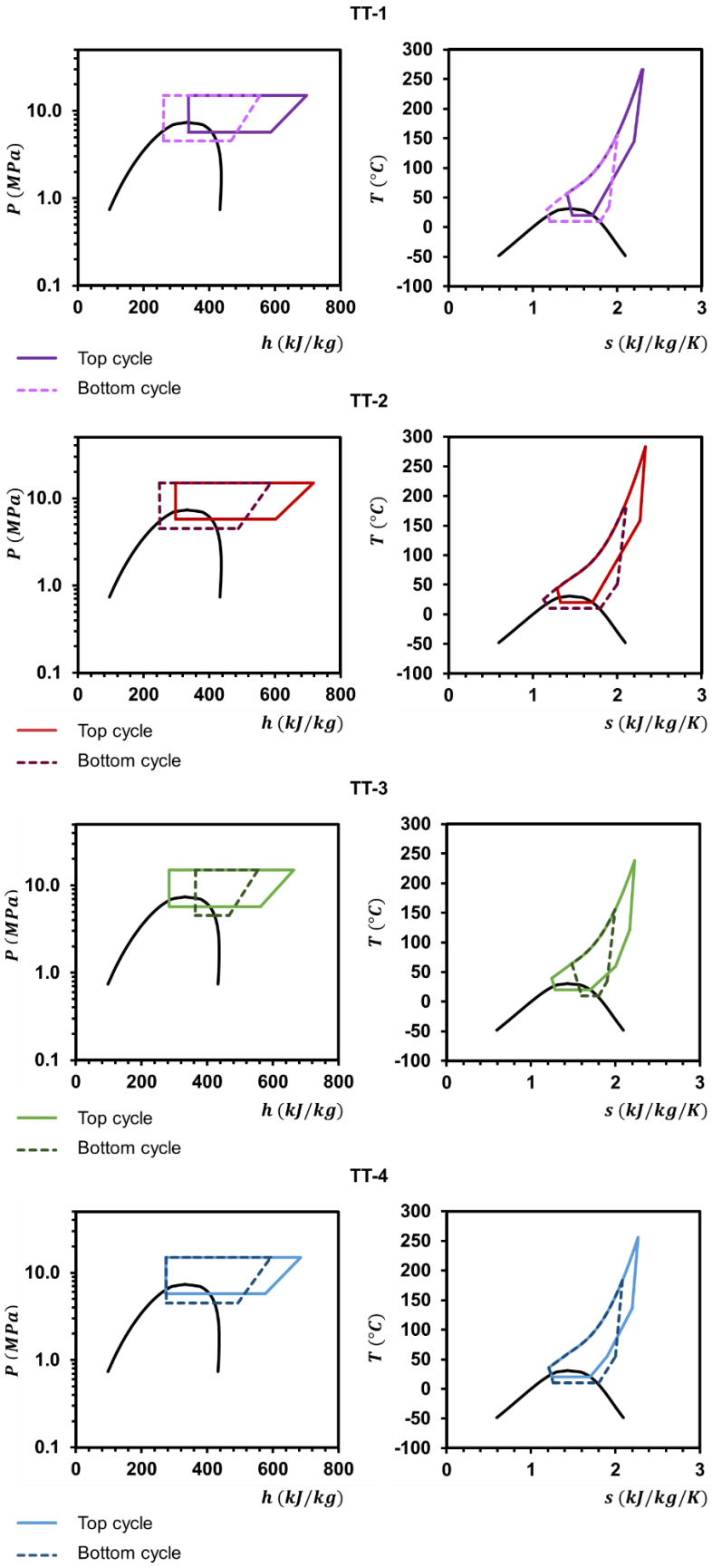

Figure 30. Pressure-enthalpy and temperature entropy diagrams - Models TT-1, TT-2, TT-3 and TT-4.

For spray drying, a sink (air) temperature of 200 °C is required. The maximum sink temperatures for the single stage models (T1-1 and T1-2) were both below 200 °C due to the maximum pressure constraint of 150 bar. The transcritical cascade cycle (TT-1) was able to achieve a COP of 2.13. By including an additional IHX in the bottom cycle (TT-2), the COP increased slightly to 2.19. However, including an additional IHX in the top cycle only (TT-3) resulted in a slight decrease in COP to 2.11 due to an increase in the outlet temperature from the cascade gas cooler for the refrigerant in the bottom cycle. The increased temperature caused more exergy destruction in the bottom cycle during expansion. Not only this, but the amount of superheating that can be achieved prior to compression in the top cycle is decreased, therefore a higher discharge pressure, and subsequently more work, is required to reach the required discharge temperature. By including IHX in both the top and bottom cycles of the cascade, the COP of the system increased to 2.22.

The optimum discharge pressures for both the top and bottom cycles for all models was 150 bar (at the maximum limit). It is possible to achieve a 200 °C sink temperature at lower pressures for the bottom cycle (which would increase the COP of the bottom cycle only). However, the COP of the overall heat pump system would be penalised because less superheat would be provided to the top cycle, increasing the amount of compression require in the top cycle disproportionately. As the top cycle has a significantly larger mass flow, penalties in the top cycle COP affect the overall cycle COP more than penalties in the bottom cycle COP.

4.4.4 Exergy destruction

The exergy destruction across the cycle components for the cascade models were calculated, as shown in Table 13. For all cycles, the highest exergy destruction occurred in the top cycle compressor. Significant exergy destruction also occurred in the top cycle gas coolers as the nonlinearity of the cooling profile of the supercritical CO_2 resulted in areas where the heat exchange experienced large temperature differences.

TT-1 was the initial cycle concept proposed by Adamson et al. [8] The results showed that by adding an IHX in the bottom cycle only (TT-2), the total exergy destruction in the cycle decreased by 2.6 kJ/kg_{sink}, whereas adding an additional IHX in the top cycle (TT-3) increased the exergy destruction of the cycle by 0.3 kJ/kg_{sink}, consistent with the COPs achieved by the respective cycles. By having IHX in both the top and bottom cycles (TT-4), the exergy destruction decreased further, by 5.7 kJ/kg_{sink} compared to TT-1.

Significant exergy destruction also occurred during expansion for Model TT-1, particularly in the top cycle. By having an IHX in one of the cycles, the exergy destruction in the expansion valve decreased slightly, however, for Model TT-3, the exergy destruction during expansion increased significantly as the gas cooler outlet temperature was increased. TT-4 had the lowest exergy destruction during expansion, which was the most significant difference in exergy across the different components between the four models. Although Model TT-4 had the highest COP

at 200 °C sink outlet temperatures, the COPs of Model TT-1 and TT-3 were similar while having significantly more exergy destruction during expansion. This suggests that Models TT-1 and TT-3 could be good candidates to integrate expansion work recovery.

Table 13. Exergy destruction (kJ/kg$_{sink}$) in all components for Models TT-1, TT-2, TT-3, and TT-4 for a sink temperature of 200 °C.

	Model			
Component	TT-1	TT-2	TT-3	TT-4
Compressor (top/bottom)	12.0/6.6	11.2/6.4	13.7/5.3	12.4/5.2
Gas cooler (top/bottom)	11.8/2.4	12.3/2.4	10.7/1.2	11.2/1.6
IHX (top/bottom)	-/-	-/1.1	2.3/-	1.6/0.9
Expansion valve (top/bottom)	9.0/3.8	6.1/3.5	7.6/6.3	2.6/3.2
Evaporator (top/bottom)	1.3/1.7	2.3/1.4	1.6/0.2	2.0/2.9
Superheater (top/bottom)	/0.7	-/-	-/0.6	-/-
Total	49.3	46.7	49.6	43.6

4.5 Sensitivity analysis

In a study by Qin et al. [130], it was shown that the evaporation temperatures, isentropic efficiency and gas cooler outlet temperature have significant effects on the system COP. The evaporation temperatures and compressor isentropic efficiencies were varied to determine the effects on the COP, exergetic efficiency and the optimal gas cooler outlet temperature. In addition to these parameters, the sink inlet temperature, pressure drop in the gas cooler, and heat exchanger minimum approach temperatures were also varied for the sensitivity analysis. For the analysis, the sink outlet temperature was kept constant at 200 °C.

The effect of the bottom cycle evaporator temperature is shown in Figure 31. There was little effect of varying evaporation temperature on the COP for Model TT-1. For Models TT-2 and TT-4, the COP increased by up to 3% by increasing the evaporation temperature to 15 °C which resulted from a reduction in the required compressor work. For Model TT-3, the COP and exergetic efficiency both decreased with increasing bottom cycle evaporation temperature. Model TT-4 consistently showed the highest COP for all bottom cycle evaporation temperatures. For all cycles, increasing the bottom cycle evaporation caused the gas cooler outlet temperature to increase.

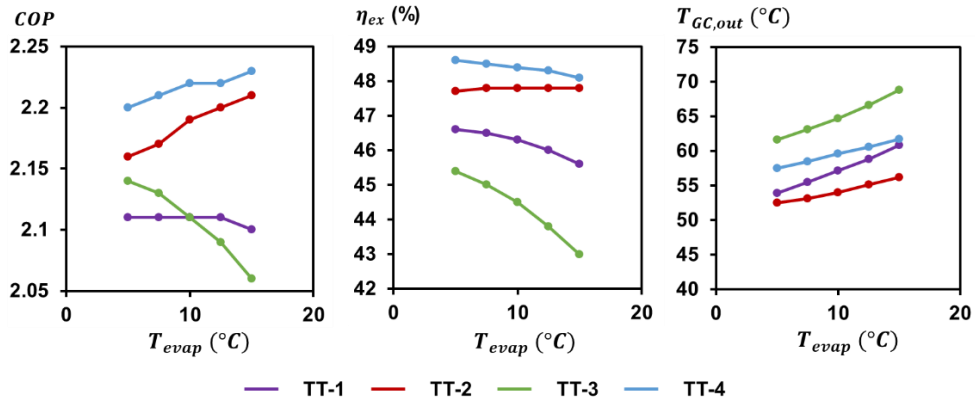

Figure 31. Sensitivity analysis - bottom cycle evaporation temperature.

The effect of varying the top cycle evaporator temperature from 15 °C to 25 °C was also investigated (Figure 32). The COP and exergetic efficiency of TT-3 also decreased with increasing top cycle evaporation temperature due to greater exergy destruction in the bottom cycle compressor and expansion valve. TT-4 consistently exhibited the highest COP for all top cycle evaporation temperatures, although little effect was observed on TT-1, TT-2 and TT-4 with varying evaporation temperatures. The gas cooler outlet for all models also increased with increasing top cycle evaporation temperature.

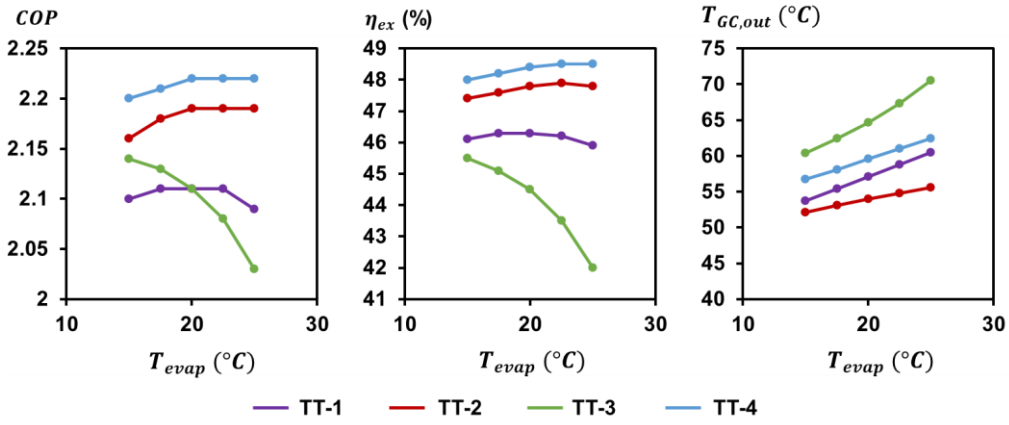

Figure 32. Sensitivity analysis – top cycle evaporation temperature.

The sink inlet temperature was varied between 10 and 20 °C (Figure 33). For all models, increasing the sink temperature resulted in a decrease in COP and exergetic efficiency due to an increase in exergy destruction in the gas coolers. This was an unexpected result as increasing the temperature lift generally decreases the COP for subcritical cycles. However, for this transcritical cycle, increasing the sink inlet temperature resulted in a degradation of the temperature profile match in the gas cooler, decreasing the COP.

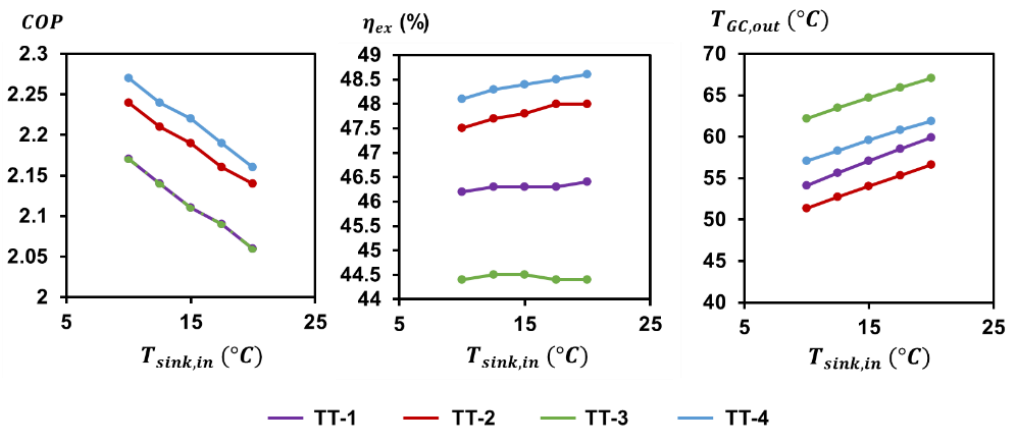

Figure 33. Sensitivity analysis - sink inlet temperature.

At present, the isentropic efficiency value for a suitable compressor is not readily available. The initial study is performed with an assumption for isentropic efficiency of 70%, as used by Sarkar et al. [122]. For both the top (Figure 34) and bottom cycles (Figure 35), the compressor isentropic efficiencies were varied between 50% and 80%. Model TT-3 showed the least sensitivity to changes in isentropic efficiencies with Model TT-4 consistently achieving the highest COP for all isentropic efficiencies. Changes in the top cycle compressor isentropic efficiency had a greater effect on the cycle COP in comparison to the bottom cycle compressor isentropic efficiency.

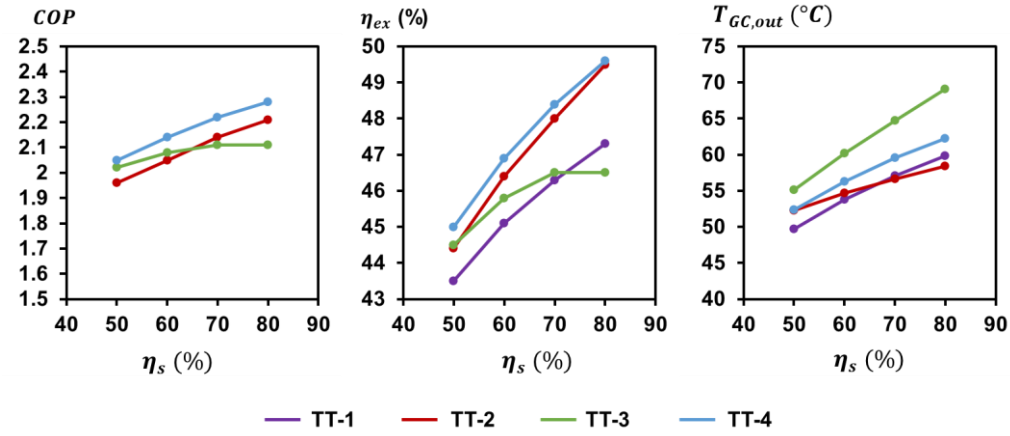

Figure 34. Sensitivity analysis – top cycle compressor isentropic efficiency.

Increasing the minimum approach temperature in the IHXs and gas coolers caused the COP to decrease for all models (Figure 36), which was an expected result as less heat is transferred during the heat exchange. Thermodynamically, it's more beneficial to minimise the approach temperature in the heat exchangers, but this requires a greater heat exchange area and therefore the heat exchanger would need to be larger in size.

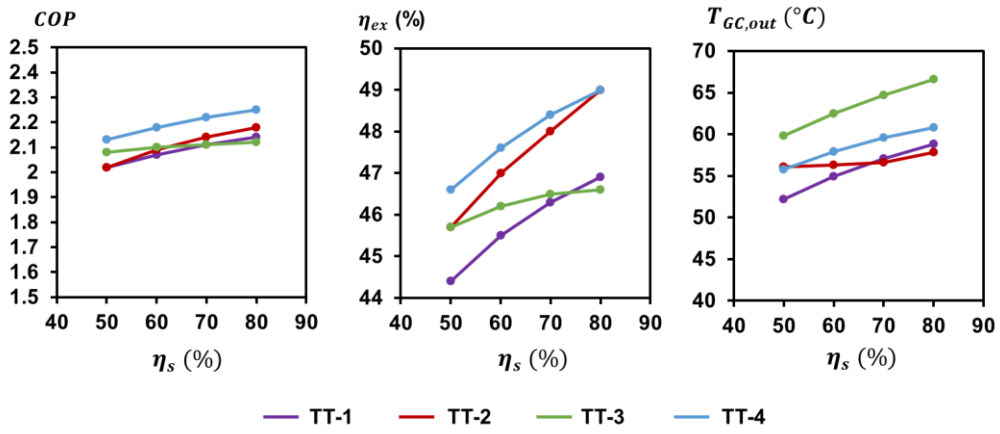

Figure 35. Sensitivity analysis – bottom cycle compressor isentropic efficiency.

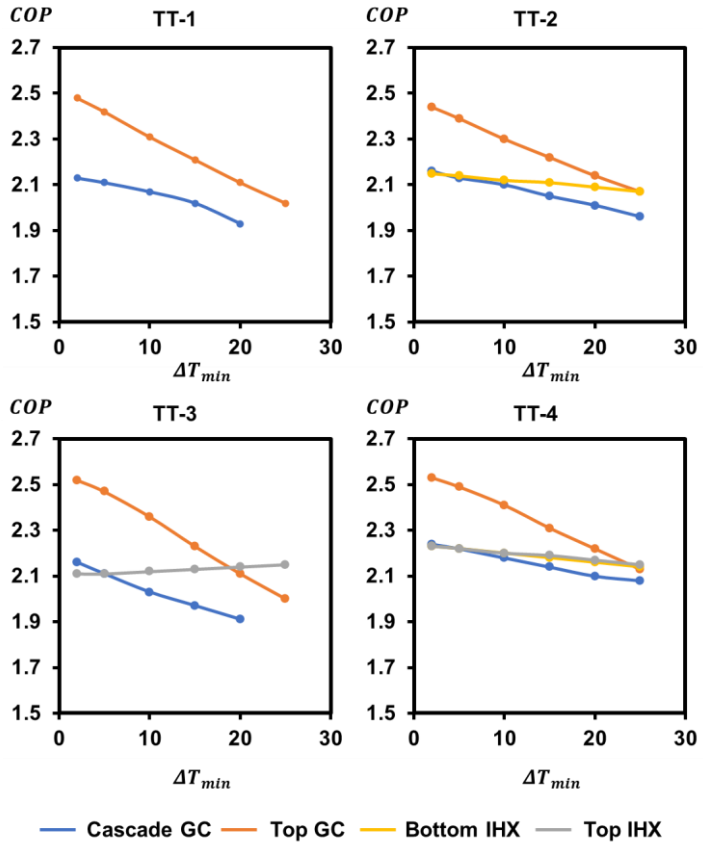

Figure 36. Sensitivity analysis - minimum approach temperature in the IHXs and gas coolers.

The IHX approach temperatures had very little effect on the overall COP, and therefore, having larger minimum approach temperatures in the IHXs could be beneficial to reduce the footprint of the heat pump system. The greatest effect on COP occurred when the minimum approach temperature of the top cycle gas cooler was increased. The COPs of all models at varying minimum approach temperatures in the top cycle gas cooler are shown in Figure 37. At lower minimum approach temperatures (10 °C), the COPs of all models converge to approximately 2.5, with particular similarity between Model TT-2 and TT-4. At the selected minimum

approach temperature of 20 °C, Model TT-4 clearly had the highest COP at 2.2. At a minimum approach temperature 40 °C, Model TT-2 had the lowest COP of approximately 1.6, whereas Model TT-3 showed a similar COP to TT-4 at approximately 1.9.

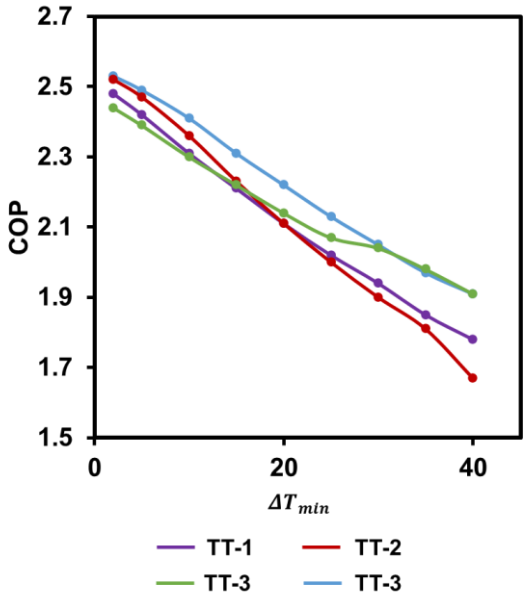

Figure 37. Sensitivity analysis – cascade gas cooler minimum approach temperature for TT-1, TT-2, TT-3 and TT-4.

Pressure drop in the high temperature gas cooler is likely to be significant in the design of a prototype. Pressure drop was varied as a percentage of the inlet pressure (150 bar) to determine the effect on the cycle COP (Table 14). There was a COP reduction of up to 11.04 % for a pressure drop of 20 %. Without the detailed design of the heat exchanger, it is difficult to determine the magnitude of the expected pressure drop. However, Sarkar et al. [131] reported that for a supercritical CO_2 system operating at 100 bar, the pressure drop was up to 1.4 bar (1.4 %) which would correlate to less than 2 % COP reduction in Table 14.

Table 14. Sensitivity analysis – COP with varying pressure drop for TT-4.

Gas cooler outlet pressure (bar)	Pressure drop (%)	COP	COP reduction (%)
150.0	0	2.22	0.00
142.5	5	2.16	2.63
135.0	10	2.10	5.35
127.5	15	2.04	8.16
120.0	20	1.97	11.04

4.6 Practical implications for implementation

COP is not the only metric for determining whether a HTTHP should be implemented. A multi-dimensional approach that considers the process integration, capital and complexity must also be considered. Although Model TT-4 consistently showed the highest COP for the spray drying application, there may be cases where it is favourable to minimise the capital cost and complexity and implement one of the cycles with fewer components. For example, at a sink temperature of 200 °C, the COP of Model TT-4 was only marginally higher than the COP of Model TT-2, therefore, to reduce the amount of space and cost, it may be more favourable to implement TT-2 to reduce the capital cost.

A spray drying application is also constrained by food hygiene standards, safety and footprint limitations. The sink air is used to directly heat the product in a spray dryer, which means that an intermediary water loop, heated by the heat pump, would likely need to be used to reduce the risk of contamination. In this study, the water loop was accounted for by using a larger minimum approach temperature ($\Delta T_{min} =$ 20 °C) for the top cycle gas cooler that could be equated to a minimum approach of 5 °C from refrigerant to water and 15 °C from water to air.

Although Model TT-3 did not have the best performance of the models considered, the COP for Model TT-3 at a minimum approach temperature of 40 °C was similar to the COP of Model TT-4. It is likely that a realised heat pump system would be retrofitted into existing plant, therefore the available space for the heat pump to occupy would be limited which may necessitate using smaller componentry (larger ΔT_{min}). In this case, implementing TT-3 may be advantageous over TT-4, as the COPs are fairly similar at larger minimum approach temperatures in the top cycle gas cooler in addition to TT-3 having one less heat exchanger than TT-4.

A significant challenge still exists in the construction of the proposed models due to the high pressures and temperatures required when using CO_2 as the refrigerant. The discharge pressure and temperature required out of the compressor stretches the boundaries of existing compressor technologies currently used in heat pumps. As a result, the uncertainty around the isentropic efficiencies could call into question the validity of the results in this chapter. One way in which these challenges could be overcome is to look to other industries that currently have technology to compress supercritical CO_2, such as the oil and gas sector, and adapt them for use in HTHPs. Another method that could also be employed is to explore the use of expansion work recovery, in the form of ejectors, to lower the required temperature and pressure lift of the compressor.

4.7 Conclusions

The performance of six models was evaluated under a range of operating conditions that resulted in sink outlet temperatures ranging between 50 °C and 290 °C. The six models represented multiple configurations that highlighted the effect of the transcritical-transcritical cascade cycle arrangement, and the effect of

internal heat exchange, with three of the models being novel cycle architectures. A key constraint in the analysis was to limit the maximum discharge pressure to 150 bar. Single stage cycles were modelled for performance comparison. It was found that the single stage cycles were unable to reach a temperature of 200 °C with the maximum pressure constraint (150 bar) and the defined minimum approach temperatures (ΔT_{min}) as not enough superheat was available at the suction inlet to the compressor.

In addition to outlining the method for modelling HTTHPs for this thesis, the key findings that resulted from the analysis in this chapter were:

- The use of an internal heat exchanger increases the maximum sink temperature for a single stage heat pump cycle.
- The transcritical-transcritical cascade cycle arrangement increases the maximum sink temperature in comparison to a single stage heat pump cycle and a single stage heat pump cycle with an internal heat exchanger.
- The inclusion of an internal heat exchanger in the bottom cycle of a transcritical-transcritical cascade heat pump cycle increases the maximum sink temperature.
- The inclusion of internal heat exchangers in the top and bottom cycles of the transcritical-transcritical cascade heat pump cycle had the highest COP of the models evaluated, achieving a COP of 2.22 for a sink temperature of 200 °C.
- Models TT-1 (transcritical-transcritical cascade) and TT-3 (top cycle internal heat exchanger) had significantly greater exergy destruction during expansion despite having similar COPs to TT-4 (top and bottom cycle internal heat exchangers), making them good candidates for expansion work recovery.

These findings demonstrate the potential of transcritical cascade cycle configurations with internal heat exchangers to achieve high sink temperatures while maintaining acceptable discharge pressures for process conditions that are applicable for milk powder spray drying. However, the analysis also uncovered an opportunity to utilise expansion work recovery to potentially increase the COPs of the lower performing cycles. The next chapter will explore the integration of expansion work recovery as a means to improve the cycle performance and reduce exergy losses within the cycle.

Chapter 5
Expansion work recovery

5.1 Introduction

In Chapter 4, the modelling method for evaluating the performance of high temperature transcritical heat pumps (HTTHPs) in this thesis was demonstrated. From the analysis of six HTTHPs, one transcritical-transcritical cascade heat pump cycle configuration showed the highest COP of 2.22 for the specified conditions. The specified conditions were based on the requirements for milk powder spray drying. However, the analysis also showed that two additional heat pump cycles, while exhibiting slightly lower COPs, involved fewer components and delivered performance comparable to the highest performing cycle at the specified conditions. A key finding was that these two simpler heat pumps had approximately double the exergy destruction during expansion in comparison to the model with the highest COP. This suggests that the two heat pump cycles may be strong candidates for the integration of expansion work recovery to increase the overall system COP for the given application.

In heat pumps, expansion work recovery generally comes in the form of ejectors or expanders. Ejectors are a relatively low cost, simple in structure (compared to an expander), and low maintenance modification that can be made to recover expansion work that would normally be lost during throttling in heat pump systems. Ejectors can enhance the cycle performance by increasing the suction pressure or decreasing the discharge pressure in and out of the compressor respectively, thus reducing the compression work [64]. Additionally, the pressure ratio of the compressor is also reduced, which is favourable due to the mechanical limits of the compressor. The working principle of an ejector involves two fluids, generally a high-pressure liquid or gas and a low-pressure vapour, which mix to produce an intermediate pressure vapour. It is usually placed after the gas cooler in a transcritical cycle or condenser in a subcritical cycle. Alternatively, work can be recovered through the use of an expander. Expanders produce work through the expansion of the refrigerant, decreasing the net work required by the system. Expanders generally recover more work than ejectors, however, expanders are expensive and have multiple moving parts, thus requiring more maintenance, which can be a prohibitive disadvantage [8]. One large scale heat pump has demonstrated the use of expanders in high temperature CO_2 for sink heating up to 150 °C [46]. The cycle is a single stage cycle with an expander and expansion valve (TX-2).

The objective of this chapter is to investigate the integration of expansion work recovery into HTTHP cycles for milk powder spray drying. Building on the six base cycle configurations from Chapter 4, ejectors and expanders will be incorporated into selected configurations to evaluate their impact on the thermodynamic

performance. Although expanders have been demonstrated for high temperature applications, ejectors are largely used for refrigeration systems. Thus, assessing the influence of ejectors on the thermodynamic behaviour of a HTTHP cycles operating at sink temperatures up to 200 °C is the novel contribution of this chapter.

5.2 Methods

The analysis will use the HTTHP modelling method as described in Section 4.3.3. In addition to this, ejector and expander modelling will be included.

5.2.1 Ejector modelling

An ejector works by utilising a high pressure vapour to "compress" a low pressure vapour, resulting in an intermediate pressure mixture (Figure 38). In a heat pump cycle, the high pressure vapour, referred to as the primary flow (I), is typically the refrigerant vapour exiting the gas cooler or further subcooled by an IHX (hot side). The low pressure vapour or secondary flow (II) is the low pressure refrigerant vapour that exits the evaporator. As the primary flow enters the ejector, the fluid undergoes isentropic expansion, converting the pressure energy into kinetic energy. The high velocity, low pressure flow characteristic of the primary flow causes a low pressure zone that draws the secondary flow into the ejector. The two flows mix turbulently in the mixing zone, and the resulting mixture enters the diffusing zone, where the velocity decreases and the pressure increases. An intermediate pressure flow exits the ejector, which has a lower pressure than the primary flow but a higher pressure than the secondary flow. The intermediate pressure outlet flow is often two phase, which is then separated into vapour and liquid streams. The vapour is compressed, either directly or after further heating using an IHX (cold side). The increased pressure at the suction inlet (in comparison to at the evaporator outlet) to the compressor decreases the amount of compression work required. The liquid portion from the ejector, which does not go to the compressor, is expanded and then evaporated.

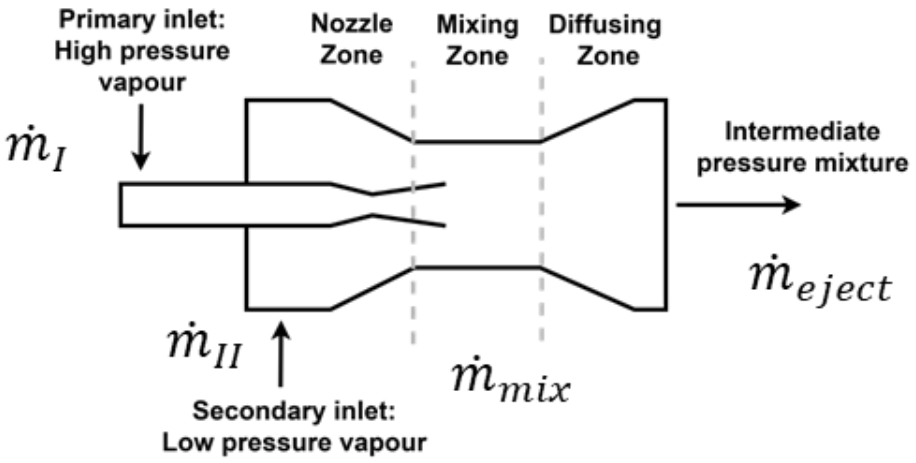

Figure 38. Ejector structure with three different flow regimes – adapted from Adamson et al. [8].

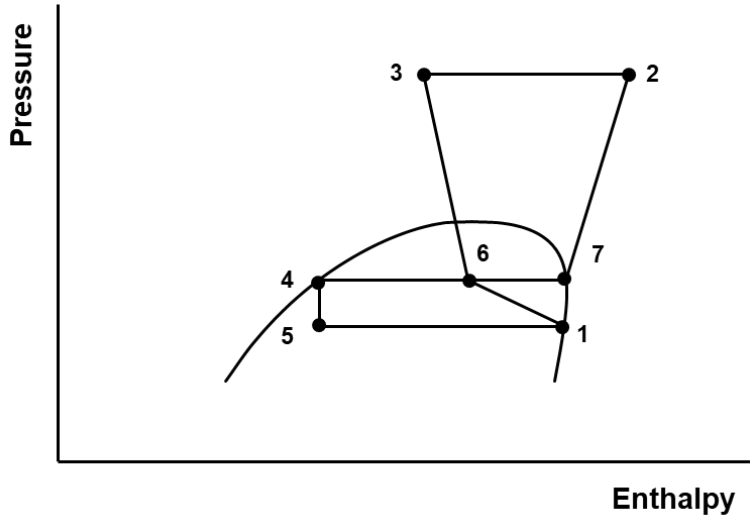

Figure 39. P-h diagram of a simple ejector cycle T1e-1 with state points: 1) evaporator out, 2) compressor out, 3) gas cooler out, 4) ejector out, liquid portion/expansion valve in, 5) expansion valve out, 6) ejector outlet and 7) ejector out, vapour portion/compressor in.

The method for modelling the ejector in this thesis follows the constant pressure mixing model, which was validated for transcritical CO_2 ejectors by You et al. [84]. A nozzle isentropic efficiency (η_n) of 80% was assumed to calculate the enthalpies ($h_{n,out}$) and the velocities ($v_{n,out}$) of the primary and secondary flows, respectively [132], at the outlet of the nozzle zone using Equations 5.1 and 5.2. Between the inlet and the outlet, a pressure drop will occur as a result of frictional losses. The magnitude of the pressure drop varies depending on the operational parameters. As the cycles proposed have yet to be physically developed, it was assumed that the pressure drop was 0.03 MPa, based on the work of Li and Groll [133].

$$h_{n,out} = h_{n,in} - \eta_n \cdot (h_{n,in} - h_{n,out\,(s)}) \quad 5.1$$

$$v_{n,out} = \sqrt{2 \cdot \left(h_{n,in} - h_{n,out}\right)} \quad 5.2$$

The entrainment ratio (μ) is defined as the ratio between the mass flows of the secondary and primary flows (Equation 5.3), which can be used to calculate the velocity of the combined flow (v_{mix}) in the mixing zone (Equation 5.4).

$$\mu = \frac{\dot{m}_{II}}{\dot{m}_{I}} \quad 5.3$$

$$v_{mix} = \frac{v_{n,out\,I}}{1 + \mu} \quad 5.4$$

Using the velocity of the mixture and the conservation of energy principle, the specific enthalpy of the mixture (h_{mix}) can be calculated using Equation 5.5.

$$h_{mix} = \frac{\frac{1}{\mu}\left(h_{n,out\ I} + \frac{v_{n,out\ I}^2 - v_{mix}^2}{2}\right) + h_{n,out\ II} - \frac{v_{mix}^2 - v_{n,out\ II}^2}{2}}{\frac{1}{\mu} + 1} \quad 5.5$$

The enthalpy at the ejector outlet ($h_{eject\ (a)}$), i.e. the actual specific enthalpy of the mixed fluid out of the diffusing zone, is obtained using an energy balance between the primary and secondary flow inlets (Equation 5.6). Where it was not possible to provide an enthalpy for the primary inlet ($h_{n,in\ I}$), the quality of the mixed flow at the exit of the ejector (x_{eject}) was calculated using Equation 5.7 with an estimated initial value for entrainment ratio (μ). A solver was used to minimise the difference between the quality of the intermediate pressure flow (x_{eject}) from Equation 5.7 and the value for quality ($x_{eject\ (a)}$) calculated from Equation 5.8.

$$h_{eject\ (a)} = \frac{1}{1+\mu} \cdot h_{n,in\ I} + \frac{\mu}{1+\mu} \cdot h_{n,in\ II} \quad 5.6$$

$$x_{eject} = \frac{1}{1+\mu} \quad 5.7$$

$$x_{eject\ (a)} = f(h_{eject\ (a)}, P_{eject}) \quad 5.8$$

To determine the value of the intermediate pressure flow exiting the ejector (P_{eject}) for Equation 5.8, the isentropic enthalpy at the outlet of the ejector ($h_{eject\ (s)}$) is calculated using an assumed isentropic efficiency value of 80% for the diffuser section (η_d), as shown in Equation 5.9. Then the ejector outlet pressure is a function of the ideal outlet enthalpy and the entropy of the mixture (s_{mix}), as shown in Equation 5.10.

$$h_{eject\ (s)} = \eta_d \cdot h_{eject\ (a)} + (1 - \eta_d) \cdot h_{mix} \quad 5.9$$

$$P_{eject} = f(h_{eject\ (s)}, s_{mix}) \quad 5.10$$

Finally, the Pressure Lift Ratio (PLR) for the ejector is given by Equation 5.11.

$$PLR = \frac{P_{eject}}{P_{n,in\ II}} \quad 5.11$$

5.2.2 Expander modelling

Expanders work by converting pressure energy into shaft work, either through a turbine or volumetric expander, such as a piston expander. In heat pump cycles, expanders often act in place of or in conjunction with an expansion valve and the shaft work generated is used to provide power to the compressor shaft, reducing

the overall work input for the heat pump. To model the expander, the isentropic relations, and an assumed isentropic efficiency of 70% were used, as shown in Equation 5.12.

$$\eta_{exp} = \frac{h_{in} - h_{out\,(a)}}{h_{in} - h_{out\,(s)}} \qquad 5.12$$

Some expanders can handle two phase flow but it's preferable to operate away from the two phase region due to mechanical limitations. Therefore, to determine the outlet pressure from the expander, the pressure ratio is set as an optimisation variable, such that the fluid exited the expander as a liquid or supercritical phase, to determine the actual enthalpy at the outlet of the expander ($h_{out\,(a)}$) as consistent with the method of Wolscht et al. [134]. The calculated value of isentropic efficiency was constrained to be equal to the assumed value. In some cases where the optimum pressure approached the critical point, a constraint was set to keep the fluid in the supercritical region. The remaining expansion required to reach the evaporation pressure is completed with an isenthalpic expansion valve.

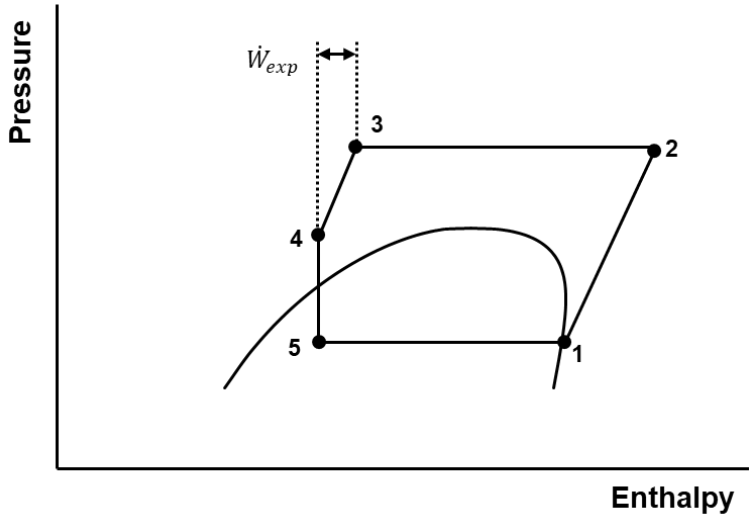

Figure 40. P-h diagram of a simple expander cycle TX-1 with state points: 1) evaporator out, 2) compressor out, 3) gas cooler out, 4) expander out, and 5) expansion valve out.

Expanders are capital intensive devices and cost estimations are not readily available in the open literature at the operating conditions that are required for HTHPs. However, the breakeven cost of an expander ($c_{cap,BE}$) can be estimated in comparison to the equivalent original cycle concept (ref). To determine this cost, the electricity savings per kW of delivered heat ($w_{savings}$) is first calculated from the cycle COPs (5.13).

$$w_{savings} = \frac{1}{COP_{expand}} - \frac{1}{COP_{ref}} \qquad 5.13$$

The annual electricity savings ($w_{savings,annual}$) can then be calculated using Equation 5.14. The annual operating hours (t) was assumed to be 6000 hours per year at an electricity price (p_{elec}) of 40 NZD/GJ.

$$w_{savings,annual} = w_{savings} \cdot t \cdot p_{elec} \quad 5.14$$

Over an assumed lifetime (t_l) of 15 years for the heat pump system, the break-even cost ($c_{cap,BE}$), in which the expander must cost less than, can be calculated. The calculation assumes the same maintenance cost.

$$c_{cap,BE} = w_{savings,annual} \cdot t_l \quad 5.15$$

5.2.3 Cycle concepts

The ejector (e) and expander cycles (X) modelled in this chapter are shown in Figure 41. All cycles are variations of the models analysed in the previous chapter but with expansion work recovery integrated. The single stage ejector and expander cycles (T1e-1, T1e-2, TX-1a and TX-2a) are modelled for comparative purposes, however the main focus of the modelling will be on the cascade cycles that had high exergy destruction during expansion to determine whether integrating an ejector or an expander can increase the performance significantly in comparison to the highest performant cycle from Chapter 4 (TT-4).

Model TT-1 had the highest exergy destruction during expansion in the top cycle, with 9.0 kJ/kg_{sink}. Models TTe-1 and TTX-1 are variations of TT-1 with expansion work recovery integrated in place of the expansion valve in the top cycle. Model TT-2 had the most comparable COP to TT-4 for the spray dryer air heating conditions, despite having more than double the exergy destruction in the top cycle expansion valve (6.1 kJ/kg_{sink}). Models TTe-2 and TTX-2 have expansion work recovery integrated in the top cycle after the IHX which exchanges heat from the top cycle gas cooler outlet to the bottom cycle compressor inlet.

In these cycles, the exergy destruction during expansion for the bottom cycle was comparable to the highest performing cycle (TT-4), therefore, expansion work recovery was only integrated in the top cycles. However, Model TT-3 exhibited large amounts of exergy destruction in both the top and bottom cycles. As a result, the variations of TT-3 (TTe-3 and TTX-3), have expansion work recovery integrated in both the top and bottom cycles.

5.2.4 Thermodynamic performance evaluation

The cycles were modelled for the spray drying case study ($T_{source,in}$ = 40 °C, $T_{sink,in/out}$ = 15/200 °C). The main metrics used to evaluate the performance of the ejector and expander cycles will be COP and exergy destruction as described in Section 4.3.4.

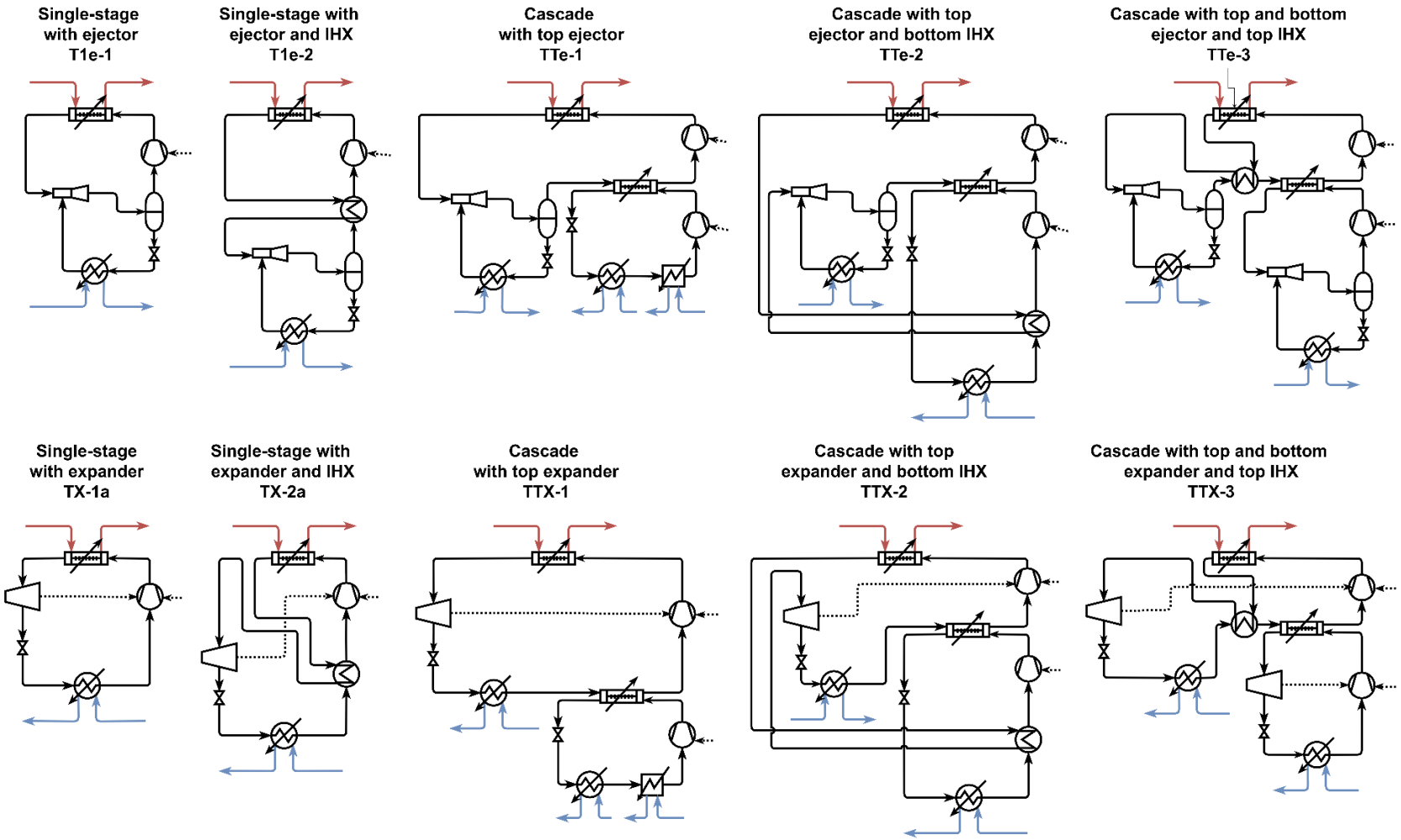

Figure 41. Ejector and expander cycle concepts.

5.3 Results

The objective of the analysis was to investigate ways to increase the COP in comparison to the original cycle concepts. As ejectors and expanders recover expansion work, the compression work required for the heat pump is theoretically decreased. However, each expansion device has its own challenges. Ejectors are relatively low cost; however, part-load operation can be challenging. This is less of an issue for the case study of milk powder spray drying, as the set point conditions tend to be steady, but it would have significant impact for other applications. Expanders generally recover more work; however, expanders are much more costly, both in capital and maintenance cost, and increase the system complexity. Therefore, a significant increase in COP compared to the original cycle concepts would be required to proceed with the integration of an expansion work recovery device.

5.3.1 Maximum sink temperatures

In the initial modelling stages, it was found that the specified evaporation temperatures for the transcritical cascade cycles were not suitable for the target conditions. For cycle TTe-3, the selected top cycle evaporation temperature of 20 °C, resulted in an ejector outlet pressure in the supercritical region. While it is possible to use a supercritical CO_2 (sCO_2) ejector, additional complexity is introduced as sCO_2 ejectors are far less established in comparison to two phase ejectors and analytical frameworks for modelling sCO_2 ejectors are limited in open literature [135]. To avoid this, a simpler approach was adopted by lowering the evaporation temperature to increase the maximum sink temperature. However, this is a trade-off, as lowering the evaporation temperature can result in a greater pressure ratio across the compressor, increasing the work input and also the thermodynamic strain on the system. Furthermore, many cycles were unable to reach the target sink temperature of 200 °C under the maximum pressure constraint at the specified evaporation temperatures. Consequently, the evaporation temperature was varied to determine the maximum sink temperature for the ejector (Figure 42) and expander cycles (Figure 43).

The equivalent ejector and expander cycles to the single-stage cycle T1-1 were T1e-1 and TX-1a, respectively. The inclusion of ejector (T1e-1) was found to reduce the maximum sink temperature for the same evaporation temperature of 10 °C whereas the inclusion of expander (TX-1a) had little effect on the maximum sink temperature in comparison to T1-1. A similar trend was followed for T1e-2 and TX-2a which are the equivalent cycles to the single-stage cycle with an IHX T1-2. T1e-2 was able to achieve the target sink temperature at an evaporation temperature of -5 °C and TX-2a was able to achieve the target sink temperature at evaporation temperatures below 10 °C. For all of the cascade cycles, the top cycle evaporation temperature had a greater influence on the maximum sink temperature than the bottom cycle evaporation temperature. The equivalent cycles for TT-2 achieved the highest maximum sink temperatures for both the ejector (TTe-2) and expander

(TTX-2) equivalent cycles. The maximum sink temperature was severely limited by the addition of an ejector (TTe-3) in comparison to TT-3 and TTX-3. The maximum sink temperatures for TTX-1 and TTe-1 were similar for the range of evaporation temperatures.

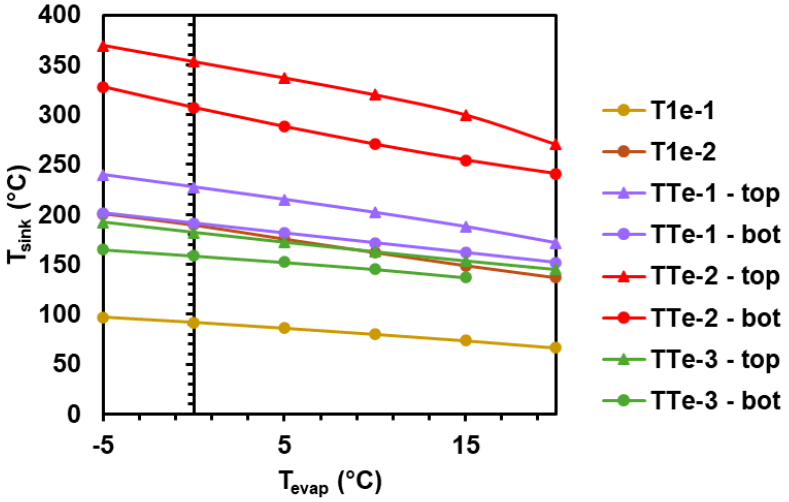

Figure 42. Maximum sink temperature at varying evaporation temperatures - ejector cycles.

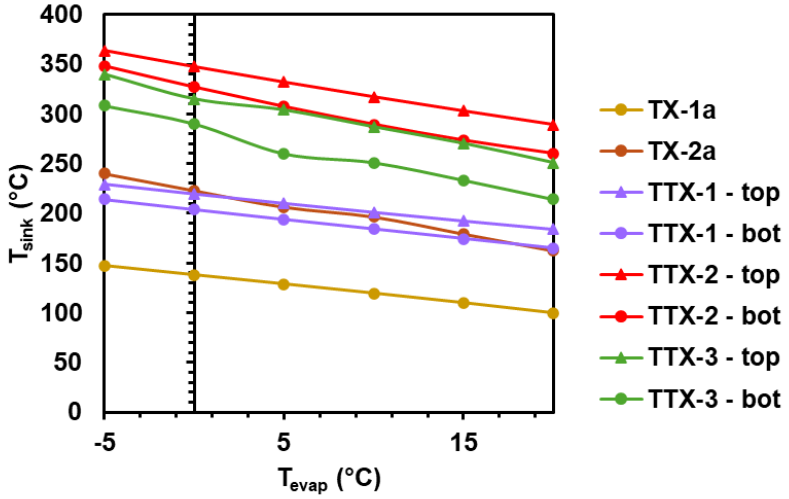

Figure 43. Maximum sink temperature at varying evaporation temperatures - expander cycles.

An example of the effect of the ejector on the maximum sink temperature can be seen in a comparison between cycles TT-1 an TTe-1, shown in Figure 44. In the diagrams, the evaporation temperatures are held constant at 10 °C for the bottom cycle and 20 °C for the top cycle. For the specified conditions, TT-1 is able to achieve the target sink temperature of 200 °C, however, TTe-1 can only achieve a maximum sink temperature of 171.52 °C as result of the lower pressure ratio across the compressor. It's possible to increase the sink temperature, however, this would

require increasing the pressure ratio or reducing the minimum approach temperature in the gas cooler.

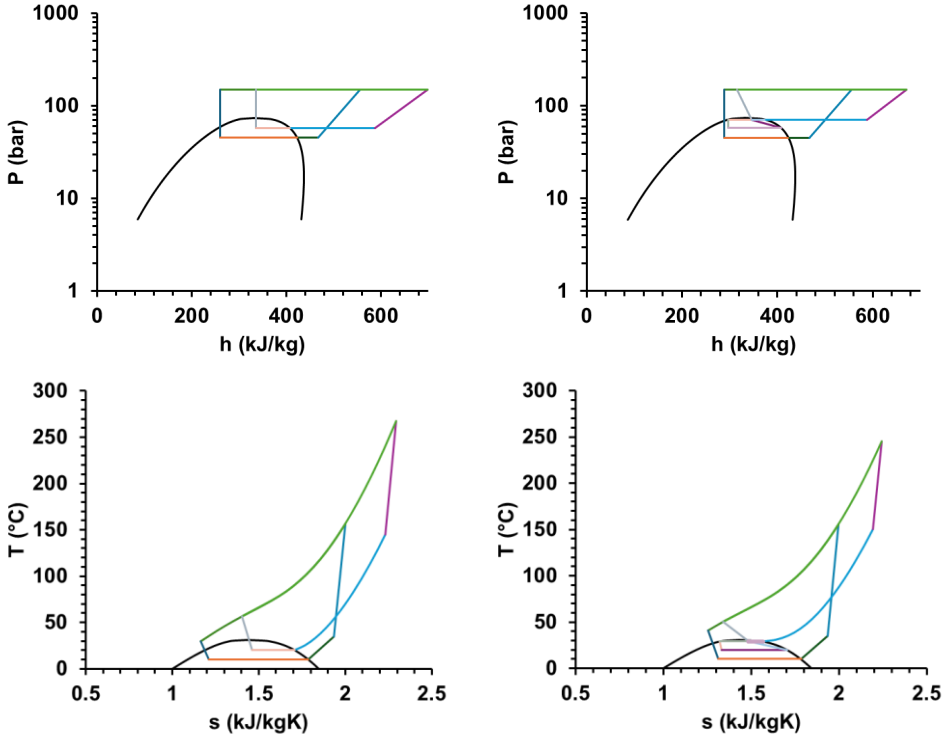

a) TT-1 at T_{sink} = 200 °C b) TTe-1 at $T_{sink,max}$ = 171.5 °C

Figure 44. P-h and T-s diagrams for a) TT-1 and b) TTe-1 for $T_{evap,bot}$ = 10 °C and $T_{evap,top}$ = 20 °C.

5.3.2 Cycle COPs and spray drying case study

At the same sink temperature (171.52 °C), TT-1 still performed better than TTe-1. One of the reasons for this was a significant decrease in performance of the bottom cycle (without the ejector), despite the ejector increasing performance of the top cycle. In the top cycle, the compressor work requirements decreased significantly from 45.88 to 38.92 kJ/kg_{sink} which increased the COP of the top cycle from 3.45 to 4.06 (Table 15). However, the COP of the bottom cycle decreased from 3.21 to 2.90 as less heat was transferred in the cascade gas cooler. Additionally, the CO_2 exited the gas coolers of both the top and bottom cycles at higher temperatures, which reduces the ability to leverage the higher heat capacities of CO_2 at temperatures closer to the critical point (~31 °C). This compounds with higher exergy destruction during expansion from the higher temperatures in the bottom cycle. A similar effect on the COPs between the original cycle concepts and the ejector cycles was also observed in the TT-2 and TT-3 variants.

Table 15. COPs of TT-1 and TTe-1 at a sink temperature of 171.5 °C.

	TT-1	**TTe-1**
COP_{top}	3.45	4.06
COP_{bot}	3.21	2.90
COP_{HP}	2.32	2.21

The evaporation temperatures were set as additional optimisation variables for the spray drying case study, and the discharge pressure was fixed at 150 bar. The optimisation maximised the cycle COP for a target air temperature of 200 °C. In the ejector cycles, the entrainment ratio(s) was also an optimisation variable, with the constraint that the estimated vapour fraction at the exit of the ejector was equal to the calculated vapour fraction. The estimated vapour fraction was initialised using the entrainment ratio (μ) as shown in Equations 5.7 and 5.8 (Section 5.2.1). The resultant entrainment ratios and also the pressure lift ratios for the ejectors are given in Table 16. Cycle T1e-1 was excluded as the cycle was unable to achieve the target sink temperature at the specified conditions despite lowering the evaporation temperature. For all of the remaining ejector cycles, the entrainment ratios varied between 0.38 and 0.71. Palacz et al. [136] noted that the entrainment ratio of two phase CO_2 ejectors for refrigeration cycles tended not to exceed 0.5. However, data from You et al. [84] showed that a higher motive pressure of up to 120 bar increased the entrainment ratio to approximately 0.7. The pressure lift ratios (PLR) varied between 1.18 and 1.51, which resulted in pressure lifts of approximately 10 to 15 bar. This was within the typical 2- 16 bar lift that was noted by Palacz et al. [136].

Table 16. Entrainment and pressure lift ratios for the ejector cycles.

	T1e-2	**TTe-1**	**TTe-2**	**TTe-3**
μ_{top}	-	0.43	0.63	0.71
μ_{bot}	0.60	-	-	0.38
PLR_{top}	-	1.36	1.20	1.18
PLR_{bot}	1.27	-	-	1.51

A comparison of the COPs that could be achieved by the ejector and expander cycles with the equivalent original cycle concepts from Chapter 4 are given in Figure 45. It should be noted that the COP of the original cycle concepts may vary slightly compared to the resulted presented in Section 4.4 as the evaporation temperatures were no longer fixed as they were in the previous chapter. The COP of highest performant cycle from Chapter 4, TT-4, was also given for comparison, but the cycle did not have an ejector or expander equivalent cycle that was analysed as the

ejector and expander cycles aimed to achieve higher COPs while maintaining, ideally, fewer or the same number of cycle components.

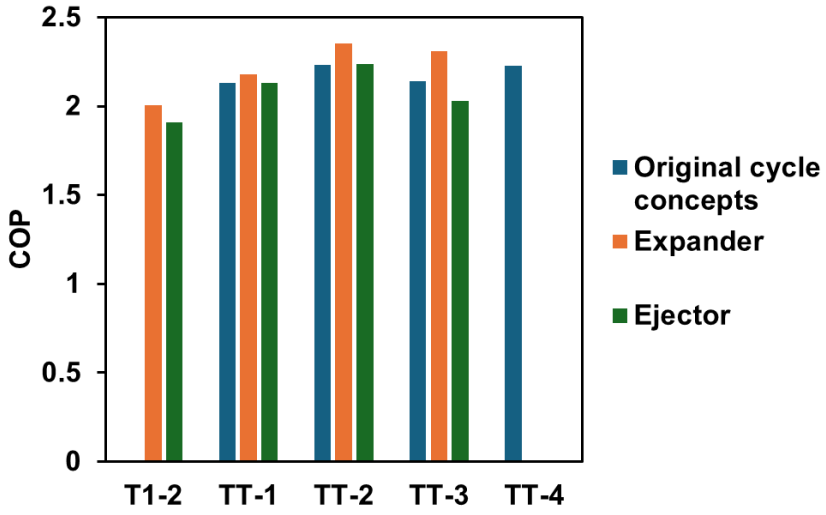

Figure 45. Comparison of the COPs achieved by the expansion work recovery cycles.

With the optimised evaporation temperatures, TT-4 achieved a COP of 2.23. An interesting result also occurred where the COP of TT-2 was the same as TT-4 once the evaporation temperatures had been optimised. This presents a case to use TT-2 over TT-4 as the performance at the target temperature is the same despite having one less heat exchanger. However, the results of Section 4.5 should also be considered where TT-4 consistently outperformed TT-2 at varying conditions. From the analysis presented in Kong et al. [123], the capital cost estimations between TT-2 and TT-4 were relatively similar at 124,295 EUR and 125,489 EUR, respectively.

In all of the expander cycles, the COP was increased through the use of an expander. The most notable effect was between TT-3 and TTX-3, however, this is likely due to TTX-3 having two expanders whereas the rest of the cycles only have one. For expander cycles with one expander, the most notable increase was in TTX-2 which also had the highest COP of all the cycles at 2.35. Capital cost estimations for CO_2 expanders in a similar operating range were not readily available in the open literature; therefore, it is difficult to determine whether the increased COP for TTX-2 at 2.35 is significant enough to warrant integrating into the system over TT-2/TT-4 with a COP of 2.23. However, a break-even cost for the expander can be estimated (Table 17).

At this stage, TT-4 still remains the preferable cycle over TT-2, but the break-even cost is most accurately calculated between TTX-2 and TT-2 as the main difference between the two cycles is the addition of an expander. This then can be used as a relative cost comparison for TT-4 because, as mentioned previously, it had been shown in Kong et al. [123] that TT-2 and TT-4 have similar capital cost estimations. The amount of electricity used per kW of delivered heat can be taken as the inverse of the COP, resulting in 0.43 kW_{elec}/kW_{th} for TTX-2 and 0.45 kW_{elec}/kW_{th} for TT-2 –

an electricity savings of 0.02 kW_{elec}/kW_{th}. For an annual operating time of 6000 hours per year and a lifetime for the heat pump of 15 years, the break-even capital cost for the expander is 297 NZD per kW of delivered heat (for the heat pump). Although, it is likely that the breakeven cost needs to be even less as the maintenance cost over the lifetime of the heat pump is likely to be greater for TTX-2 than TT-2.

Table 17. Expander break-even cost calculation breakdown.

	TT-2	**TTX-2**
COP	2.23	2.35
$w_{savings}$	0.02 kW_{elec}/kW_{th}	
$w_{savings,annual}$	19.78 NZD/(kW_{th}· year)	
$c_{cap,BE}$	298.6 NZD/kW_{th}	

Another challenge that needs to be considered for the expander cycles is that, in many cases, the optimal expander outlet pressures were very close to the critical point (Table 18). Near the critical point, small changes in temperature/pressure can cause very large changes in density, compressibility, and heat capacity. This makes the mechanical design of the expander very difficult as the flow conditions are varying rapidly. It is unclear exactly how this would affect the mechanical and operational limitations. Alternatively, expanding to a smaller pressure ratio, to stay away from the critical point could be an option, however, this would decrease the break-even cost of the expander (the expander would need to be much cheaper) for it to be economically viable as the COP increase between TT-2/TT-4 and TTX-2 would be less.

Table 18. Expander outlet pressures for cycles TX-2a, TTX-1, TTX-2 and TTX-3.

Cycle	$P_{expand\ out}$ **(bar)**
TX-2a	73.8
TTX-1	72.0
TTX-2	77.6
TTX-3 (top | bottom)	61.5 | 74.3

The CO_2 expander in this study was modelled using an assumed isentropic efficiency of 70 % to represent a more realistic, non-ideal expansion. Nevertheless, the approach still simplifies the analysis and lumps all of the irreversibilities present in

actual devices like mechanical losses, leakage, friction, and turbulence. These limitations are particularly prevalent in supercritical CO_2, where the properties vary sharply near the critical point. Additional factors, including heat transfer between the working fluid and the expander walls, potential condensation, and mechanical constraints due to the high fluid density are also not considered. As a result, the model may overestimate system performance gains. Future work should incorporate CFD modelling and experimental validation to improve confidence in the predicted expander performance.

5.3.3 Exergy destruction

The ejector cycles were unable to achieve higher COPs than the original cycle concepts. T1-2 was unable to achieve the target sink temperature of 200 °C and was therefore excluded. T1e-2 achieved a COP of 1.91 which was lower than could be achieved by TX-2a at 2.01. Despite T1e-2 having lower exergy destruction during expansion (10.2 kJ/kg_{sink}) in comparison to TX-2a (13.7 kJ/kg_{sink}), the lower COP resulted from a greater pressure ratio required across the compressor to achieve the target sink temperature. The pressure ratio required to achieve the 200 °C sink outlet temperature was 4.7 in T1e-2 whereas TX-2a only required a pressure ratio of 3.7. The COPs of TTe-1 (2.13) and TTe-2 (2.23) were identical to those of their respective original cycle configurations but remained below those achieved by the expander cycles (2.18 and 2.35, respectively). Conversely, TTe-3 demonstrated a lower COP (2.03) compared with both TT-3 (2.14) and TTX-3 (2.31).

The exergy destruction in the components for the TT-1, TT-2 and TT-3 cycle variants are shown in Figure 46, Figure 47 and Figure 48. The “EXPANS” category in these figures includes the total exergy destruction related to expansion of the refrigerant from a valve, ejector, expander, or a combination of expansion devices. In the case of TTe-3, the bottom cycle pressure ratio (3.6) was decreased in comparison to TT-3 (3.6). However, the top cycle pressure ratio, which has most of the refrigerant mass flow, was increased from 2.9 to 3.7, resulting in greater exergy destruction in the compressor (Figure 48).

The changes in exergy destruction in TTe-1 and TTe-2 compared to TT-1 and TT-2 were more moderate, which was to be expected from the resulting COPs. The exergy destruction during expansion for TTe-1 was decreased for both the top (8.6 to 7.0 kJ/kg_{sink}) and bottom cycles (4.2 to 3.8 kJ/kg_{sink}) but was increased in the both the top and bottom cycle evaporators from 1.5 to 2.2 kJ/kg_{sink} in the top cycle and 2.0 to 4.3 kJ/kg_{sink} in the bottom cycle (Figure 46). The exergy destruction during compression was reduced slightly from 2.7 to 2.6 kJ/kg_{sink} in the bottom cycle for TTe-1 but this was negated by the slight increase in exergy destruction from 11.2 to 12.5 kJ/kg_{sink} in the top cycle compressor. Likewise, the exergy destruction was reduced slightly between TTe-2 (5.6 kJ/kg_{sink}) and TT-2 (6.2 kJ/kg_{sink}) but the compressor exergy destruction in the top cycle compressor (11.6 to 12.3 kJ/kg_{sink}) and bottom cycle evaporator was increased (1.5 to 1.8 kJ/kg_{sink}), as shown in Figure 47.

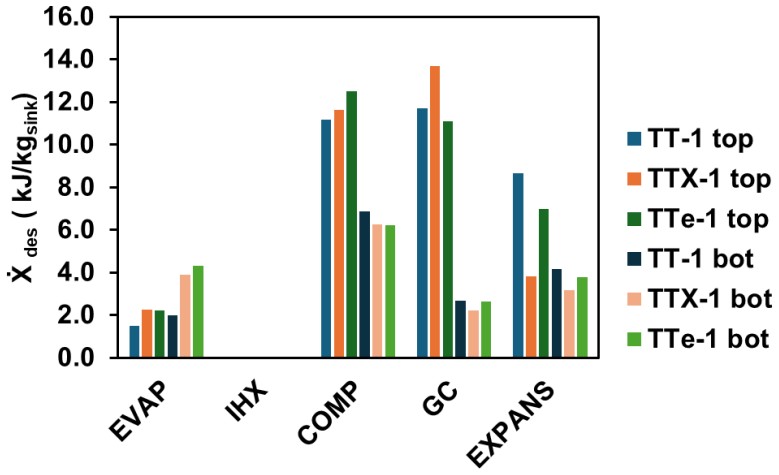

Figure 46. Exergy destruction in the cycle components for TT-1 variants.

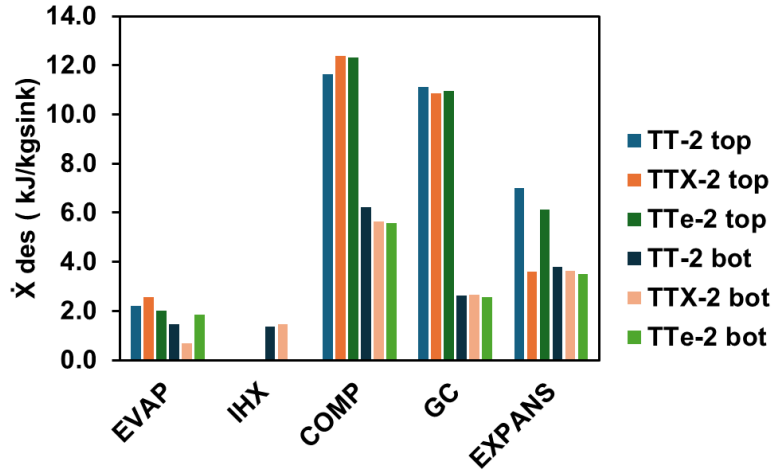

Figure 47. Exergy destruction in the cycle components for TT-2 variants.

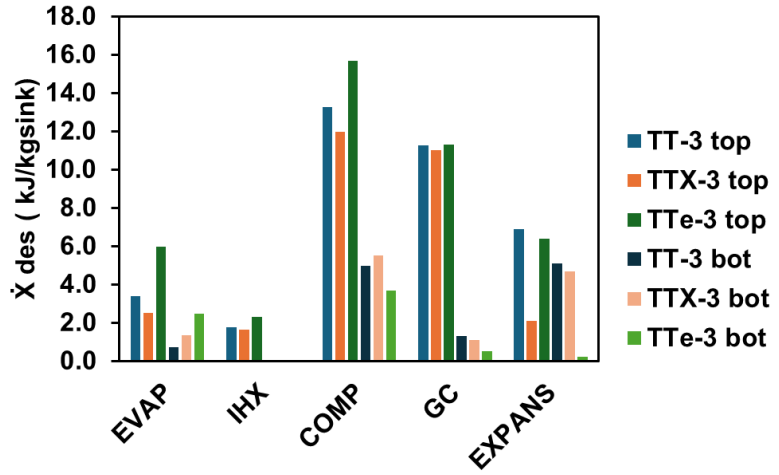

Figure 48. Exergy destruction in the cycle components for TT-3 variants.

Compared to TT-1, the inclusion of an expander caused small increases in exergy destruction across most of the components (Figure 46). However, TTX-1 had significantly lower exergy destruction during expansion (7.0 kJ/kg_{sink} total) compared to TT-1 (12.8 kJ/kg_{sink} total). Decreases in exergy destruction were also observed in the bottom cycle compressor by 0.6 kJ/kg_{sink} and gas cooler by 0.5 kJ/kg_{sink}. In TTX-2 (Figure 47), increases in exergy destruction (compared to TT-2) were observed in the evaporator (0.4 kJ/kg_{sink}) and compressor (0.8 kJ/kg_{sink}) of the top cycle, and the IHX (0.1 kJ/kg_{sink}) and gas cooler (0.1 kJ/kg_{sink}) of the bottom cycle. However, the exergy destruction for the rest of the components was decreased. Like the TT-1 variants, the most notable decrease in exergy destruction was during expansion from 11.8 kJ/kg_{sink} total for TT-2 to 7.2 kJ/kg_{sink} total for TTX-2.

The difference between the expander and original cycle concept COPs were the most notable for the TT-3 variants (Figure 48), with TT-3 having a COP of 2.14 and TTX-3 having a COP of 2.31 (Figure 45). Although the exergy destruction increased slightly for some of the bottom cycle components, the exergy destruction across all of the top cycle components were decreased. The most significant decrease in exergy destruction during expansion from 12.0 kJ/kg_{sink} total in TT-3 to 6.8 kJ/kg_{sink} total in TTX-3.

5.3.4 Compressor discharge pressures

To simplify the optimisation, the top pressures of both cycles in Sections 5.3.1 to 5.3.3 were kept constant at 150 bar for both the top and bottom cycles. The effect of varying the discharge pressures on the COP was analysed for the ejector cycles to determine whether the ejector had a greater effect on the cycle at lower discharge pressures. Figure 49 shows the effect of varying the discharge pressure for TT-1 and TTe-1 with TT-4 also given for comparison. Figure 50 presents the results for TT-2 and TTe-2, and Figure 51 presents the results for TT-3 and TTe-3. For all three figures, the discharge pressures were only varied for either the top or bottom cycle. In the top/bottom cycle when the pressure was not varied, the discharge pressure was kept constant at 150 bar. The discharge pressures were varied between 120 and 150 bar.

Cycles TT-1 and TTe-1 (Figure 49) had nearly identical COPs for all discharge pressures investigated. Varying the pressure of the bottom cycles for had a lesser effect on the COP than the top cycles. For all pressures, the TT-1 and TTe-1 had lower COPs than TT-4, except for an overlap between the TT-1 and TTe-1 bottom cycles and TT-4 top cycles at 120 bar. Similarly, the top cycle discharge pressures also had the largest effect on COP for TT-2 and TTe-2 (Figure 47) compared to the bottom cycles but the negative effect on COP with decreasing discharge pressure was much more prominent for TT-2 than TTe-2. Additionally, TTe-2 was able to achieve slightly higher COPs than TT-4 at the varying pressures, with the COPs of the three cycles converging at 150 bar. TT-3 and TTe-3 (Figure 51) was the cycle group that was the most sensitive to changes in discharge pressure but consistently had lower performance than TT-4.

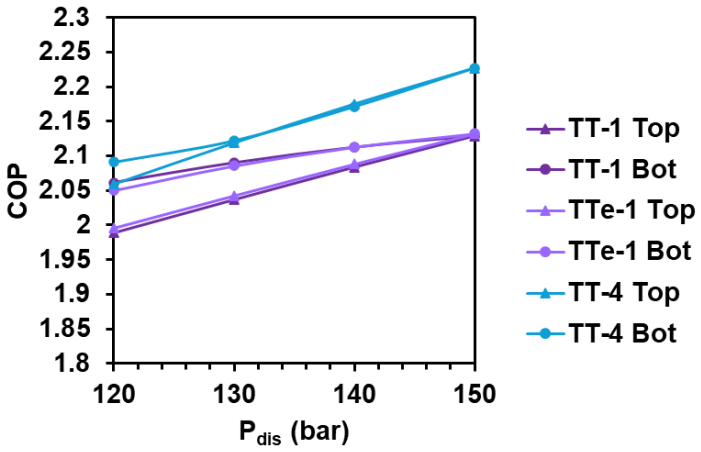

Figure 49. COPs of TT-1, TTe-1 and TT-4 at varying maximum pressures for one cycle/150 bar for the other cycle.

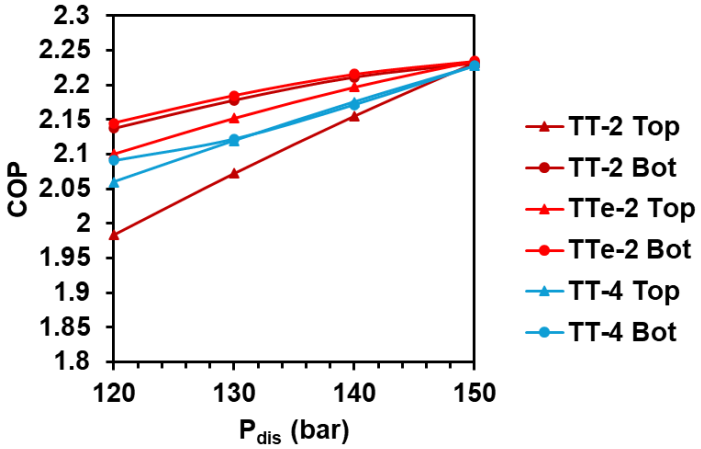

Figure 50. COPs of TT-2, TTe-2 and TT-4 at varying maximum pressures for one cycle/150 bar for the other cycle.

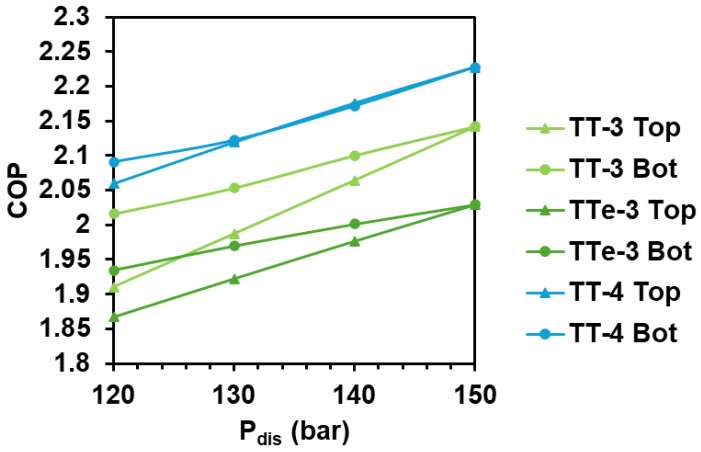

Figure 51. COPs of TT-3, TTe-3 and TT-4 at varying maximum pressures for one cycle/150 bar for the other cycle.

The same maximum discharge pressure for both the top and bottom cycles was also investigated. TT-1 and TTe-1 (Figure 52) had similar COPs but were both lower than TT-4. Interestingly, TT-2 had higher COPs at lower pressures in comparison to TT-4 but the cycles converged to the same COP at 150 bar (Figure 53). The maximum pressure range was extended up to 200 bar, which showed that the COP of TT-4 was higher than TT-2 at pressures between 150 and 200 bar. Depending on compressor limitations, this supports the selection of cycle TT-2. However, as compressor technology improves, TT-4 is likely to be the better cycle. TT-3 had better performance than TT-e3 but not TT-4 for the discharge pressures investigated (Figure 54).

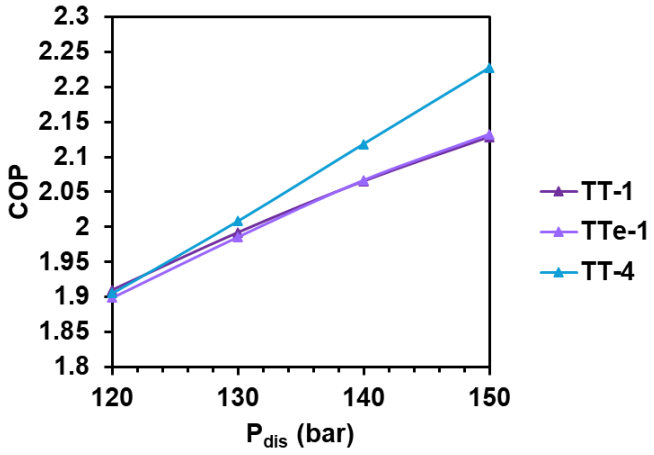

Figure 52. COPs of TT-1, TTe-1 and TT-4 at varying maximum pressures for both cycles.

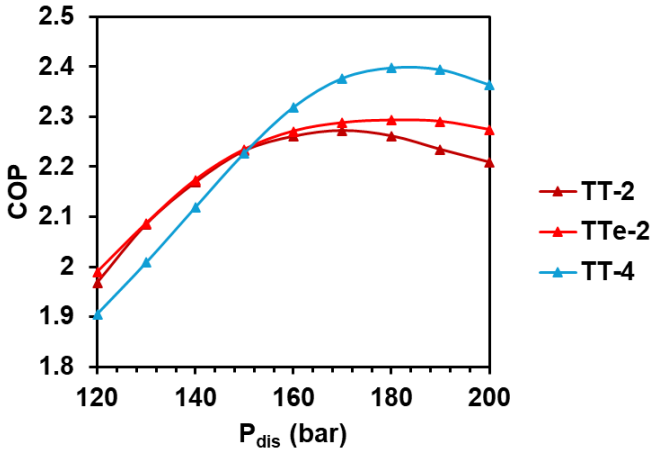

Figure 53. COPs of TT-2, TTe-2 and TT-4 at varying maximum pressures for both cycles.

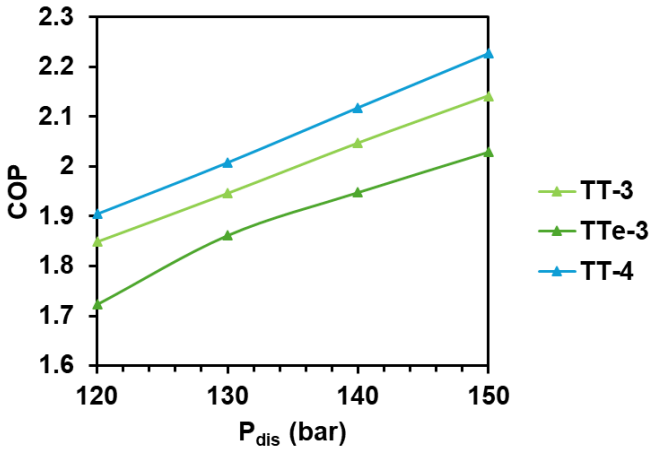

Figure 54. COPs of TT-3, TTe-3 and TT-4 at varying maximum pressures for both cycles.

5.4 Conclusions

The objective of this chapter was to evaluate the integration of expanders and ejectors to reduce the exergy destruction in the CO_2 HTTHP cycles proposed in Chapter 4. Five ejector cycles and five expander cycles were analysed and compared to the equivalent original cycle concepts. The placement of the ejectors and expanders within the cycle were informed by the exergy destruction results from the previous chapter.

The key findings from this chapter were:

- Many of the ejector cycles required higher pressure ratios and higher gas cooler outlet temperatures to achieve the target sink temperature, but this caused penalties in the COP as the performance of the cascade heat exchanger is degraded.
- In general, the expander cycles had the highest COPs, with the highest expander cycle COP being 0.12 greater than the highest performant cycle from the previous chapter, TT-4.
- Although the COPs of the expander cycles were slightly higher than the original cycle concepts, the magnitude of improvement did not outrightly suggest that an expander should be integrated in the heat pump cycle. As capital cost estimations for an appropriate CO_2 expander were not readily available in the open literature, a break-even capital cost for the expander of 297 NZD/kW of delivered heat was calculated.
- Cycles TT-2 and TT-4 exhibited similar COPs once the evaporation temperatures had been optimised (discharge pressure of 150 bar). At discharge pressures below 150 bar, TT-2 was able to achieve slightly higher COPs than TT-4, despite having one less heat exchanger. However, at discharge pressures above 150 bar, TT-4 had better performance.

Limitations in this study exist related to the modelling assumptions, including fixed isentropic efficiencies, steady-state operation, and neglect of mechanical

implications. Future work should incorporate CFD modelling and experimental validation to improve confidence in the predicted expander performance.

Overall, the results did not find a clear improvement from the integration of expansion work recovery devices. Although the COPs of the expander cycles were slightly higher, it was not enough to proceed with integrating an expander cycle, unless the expander can achieve the break-even cost. To conclude, Cycle TT-4 is still regarded as the highest performant cycle due to the consistently higher performance of cycle TT-4 over TT-2 in Section 4.5, but one could make the decision to use TT-2 to save spatial footprint and capital cost for the spray drying case study, particularly in the case where the maximum discharge pressure needs to be lower than 150 bar. The insight from this chapter provides the basis for selection of a heat pump to integrate into the spray drying process to be discussed in the next chapter, where TT-2 and TT-4 will both be investigated.

Chapter 6
Integration case study for milk powder spray drying

6.1 Introduction

In New Zealand, air heating for spray drying is typically supplied using steam heaters, which in turn are supplied by fossil fuel boilers. As shown in Figure 55, spray drying facilities are widespread across both the North and South Island, and all will eventually need to transition away from fossil fuel use. In the North Island, natural gas is the predominantly used fuel, whereas in the South Island, coal is more prevalent due to a lack of natural gas infrastructure. Current legislation in New Zealand dictates the phase-out of coal boilers by 2037, with other fossil fuels, such as natural gas, likely to follow [137]. Despite this, the decarbonisation of spray drying remains challenging, as there is not one clear solution for decarbonisation and a lack of economically viable alternatives slows the transition away from fossil fuel boilers.

Figure 55. Milk powder drying facilities in New Zealand - non-exhaustive, coloured by company (undisclosed) [138], [139].

The options which dairy factories in New Zealand have to consider include biomass, electrode boilers, geothermal steam, and a future potential for hydrogen and heat pumps. Biomass boiler transitions are popular due to the relative simplicity of retrofitting a coal boiler to burn biomass, however, the supply of biomass is constrained by the rate at which short rotation forestry can be planted and harvested. In any case, it would be advantageous to reduce the biomass demand. The use of geothermal steam has successfully been implemented by the dairy company Miraka [140], and while attractive in terms of cost and renewability, is not

suitable for many dairy companies due to geographic location. The price of electricity has historically been the largest barrier for the implementation of electrode boilers. Additionally, high capital investment is required, particularly when the need to upgrade electrical grid exit points exists. This is a similar problem faced by using heat pumps for large-scale utility supply, however, the relatively high efficiencies resulting from heat pumps makes it an attractive option when considering electrification.

Conventional heat pump integration methods have primarily been developed for low to medium temperature applications. A common heat pump integration method is to use Pinch Analysis, which is useful for identifying where there are opportunities to recover heat within a process. However, Pinch Analysis has limitations when it comes to integrating HTHPs as it is generally recommended to fully utilise the available heat recovery through heat exchangers and then the leftover heat should be "upgraded" using a heat pump. However, with HTHPs, the temperature lift and the temperature glide have a major impact on the overall system performance. By fully utilising the heat recovery through heat exchangers before heat pumping, the temperature lift and temperature glide can be unnecessarily degraded, either by increasing the lift, or changing the temperature glide in a way that penalises the temperature profile match between the refrigerant and the sink stream. Therefore, economically optimal HTHP integration opportunities may be missed using conventional heat pump integration methods.

While conversion to biomass or electrode boilers is simpler in terms of retrofit, the relative price of electricity and biomass, compared to the fossil fuel systems they replace, has the potential to be cost prohibitive in the long term. Heat pumps, either as a standalone technology or integrated with a biomass/electrode boiler, have the potential to reduce the cost of supplying utility due to the high COPs that can be achieved. Previous chapters in this thesis investigated the technological potential for a simulative high temperature transcritical CO_2 heat pump to supply all of the primary air heating requirement for milk powder spray drying. In those chapters, the heat pump was heating from 15 °C to 200 °C, and a COP of 2.22 was achieved. Despite this promising result, a prototype HTHP that is suitable for large temperature glides and lifts is still a while away from being realised. Additionally, the heating of air from 15 °C to 200 °C is a simplified representation of the air heating requirements in spray drying and doesn't account for the fluidised bed air heating.

This chapter analyses the possible integration opportunities for the HTHP into the milk powder spray drying process and how this compares to other current fuel-switching options. Cost and emissions reduction potential are considered as important metrics in this comparison. The hypotheses which this chapter will investigate are:

- An optimal sink temperature exists where integrating a heat pump with an electrode or biomass boiler can lower the operating cost compared to using each technology individually.
- The nonlinearity of sensible cooling of supercritical CO_2 can be leveraged at different temperature levels.

6.2 Methods

6.2.1 Overview of the proposed integration options

Three design groups were investigated to supply the spray dryer air heating requirements:

1. Boiler heating only (B)
2. Full electrification using a heat pump only (HP)
3. Electrification using a heat pump integrated with a boiler (HP+B)

The boiler heating group considers switching to other fuel sources excluding heat pumps, for example, biomass and electrode boilers from fossil fuels, which encompasses the base design for a spray dryer air heating system supplied by coal or natural gas. The full electrification group presents a case where all of the heating required for the spray dryer air heating section is supplied by heat pump(s). A partial electrification group considers the integration of a heat pump to supply the lower temperature requirements of the air heating and a biomass boiler to supply the high temperature heat required.

6.2.2 Model assumptions

The following common assumptions, in addition to those described in Section 4.3.2, are applied to the models.

- Ambient air conditions: $T_{amb} = 15\ °C, R = 70\%, P_{amb} = 1.01325\ bar$
- Compressor efficiency: $\eta_s = 70\ \%$, $\eta_{mech} = 96\ \%$
- Target air temperature: $200\ °C$
- Source temperature: $40\ °C$

The moisture content of air was assumed to remain constant during indirect heat exchange (through the heat exchangers). The steam requirements for the biomass boiler were calculated from modelling of the air heater system. Boiler efficiencies of 80 % and 99 % were assumed for biomass and electrode boilers, respectively [78]. A steam distribution efficiency of 90 % was also assumed [79]. The amount of air and steam required was calculated for drying milk concentrate at 70 °C for an inlet concentration of 52 wt% milk solids to an outlet concentration of 97 wt% milk solids [74].

6.2.3 Air heater modelling for the boiler calculations

The base case design (Figure 20) for the spray dryer air heating system consists of a hot water (COW water) recovery section followed by 10 bar low-pressure steam (LPS) and 40 bar high-pressure steam (HPS) heating sections. The HPS and LPS are

considered as utility streams supplied by a boiler system, as shown in Figure 20. In the drying process, the milk powder concentrate is dried to 94 wt% milk solids in the dryer with an in-built static fluidised bed and then further dried to 97 wt% solids in a high temperature vibrating fluidised bed at 78 °C and a low temperature vibrating fluidised bed with cool air [141]. The primary air stream is used to heat the dryer at 200 °C and the secondary air stream is used for the static fluidised bed at the bottom of the dryer at 102 °C. CoolProp (i.e., HAPropsSI function) [142] was used to determine the humid air properties and water properties. The mass flowrate of concentrated milk ($\dot{m}_{milk\ conc.}$) entering the spray dryer was calculated from the desired mass of milk powder product ($\dot{m}_{milk\ product}$) and the mass fraction solids concentrations of the respective streams (C), as shown in Equation 6.1.

$$\dot{m}_{milk\ conc.} = \dot{m}_{milk\ product} \cdot \frac{C_{milk\ product}}{C_{milk\ conc.}} \tag{6.1}$$

The amount of water in the milk ($\dot{m}_{water}$) was calculated using Equation 6.2.

$$\dot{m}_{water} = \dot{m}_{milk\ conc.} \cdot (1 - C_{milk\ conc.}) \tag{6.2}$$

Within the COW water heat recovery section, the air is first heated to a set point of 21 °C by an HVAC system. The air is then heated by the COW water recovery exchangers, with the residual heat in the COW water used to supply the source to the HVAC system. The temperature at which the air can be heated to by the COW water is dictated by the amount of mass and the temperature of the COW water, therefore a range of temperatures between 35 and 65 °C was investigated. To calculate the work consumption of the HVAC system ($\dot{W}_{HVAC}$), a COP of 3 was assumed (Equation 6.3).

$$\dot{W}_{HVAC} = \frac{\dot{Q}}{COP} \tag{6.3}$$

The heating supplied by utility is divided into three sections: condensate, LPS (10 bar) and HPS (40 bar). HPS does the highest temperature section of the heating and is used to heat the air to 200 °C. The HPS is condensed and then throttled to the pressure of the LPS. Supplementary LPS is also used which, combined, supplies the LPS section that heats the air to 160 °C. It was assumed that the steam fully condensed from a saturated vapour to a saturated liquid in the HPS and LPS heating sections. The combined condensate heats the air from the air temperature after heat recovery to an intermediate temperature. The intermediate temperature is dependent on the amount of heat recovery that can be achieved from waste heat for heating the air from ambient conditions. Additionally, low-pressure steam is

used to heat the secondary air for the dryer to 102 °C and the air for the vibrating fluidised beds (VFBs) to 78 °C separately [74].

The mass flowrate of boiler steam required ($\dot{m}_{steam}$) can be determined by the sum of the steam inputs required for each air heating section based on the mass flowrate of air required ($\dot{m}_{air}$), as shown in Equation 6.4. The mass flow of the air for the dryer was determined from the amount of water evaporated in the dryer ($\dot{m}_{water,evaporated}$) and the change in moisture content of the air streams from the inlet to the outlet ($\Delta\omega$), shown in Equation 6.5.

$$\dot{m}_{steam} = \sum \frac{\dot{Q}_{required}}{\Delta h_{steam}} = \sum \frac{\dot{m}_{air}\Delta h_{air}}{\Delta h_{steam}} \quad 6.4$$

$$\dot{m}_{air} = \frac{\dot{m}_{water,evaporated}}{\Delta\omega} = \frac{\dot{m}_{water,in} - \dot{m}_{water,out}}{\omega_{air,out} - \omega_{air,in}} \quad 6.5$$

6.2.4 Heat pump modelling

Significant exergy destruction occurs from the heat exchange in the gas coolers. Zuhlsdorf et al. [143] showed that optimising the temperature profile match between the refrigerant and the sink can contribute to increased performance for the heat pump cycle. In spray drying, there are two temperature levels which require heating: 1) fluidised bed air at approximately 100 °C and 2) dryer air at approximately 200 °C. For transcritical CO_2 heat pumps, this is possibly advantageous as the sensible cooling profile for CO_2 above the critical point has two distinct regions with differing gradients (Figure 56).

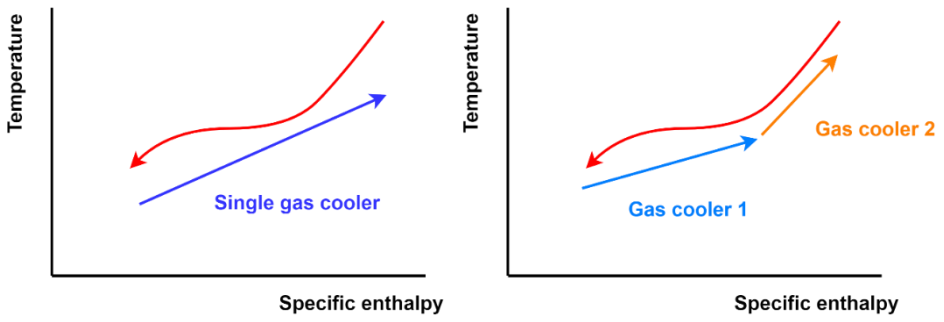

Figure 56. Temperature profile matching comparison in a single gas cooler cycle (left) and a double gas cooler cycle (right).

As a result, the HTHP cycles recommended in Chapter 4 and Chapter 5, TT-2 and TT-4, have been modified to include two gas coolers in the top cycle. The high temperature gas cooler (HTGC) following compression is used to heat the dryer air from 102 °C to 200 °C and the mid-temperature gas cooler (MTGC) is used to heat all of the air, including the fluidised bed air, from ambient conditions to 102 °C. Between the two top-cycle gas coolers, approximately one third of the total mass

of the air is diverted for use in the fluidised beds. The modified TT-2 and TT-4 cycles are shown in Figure 57 and Figure 58.

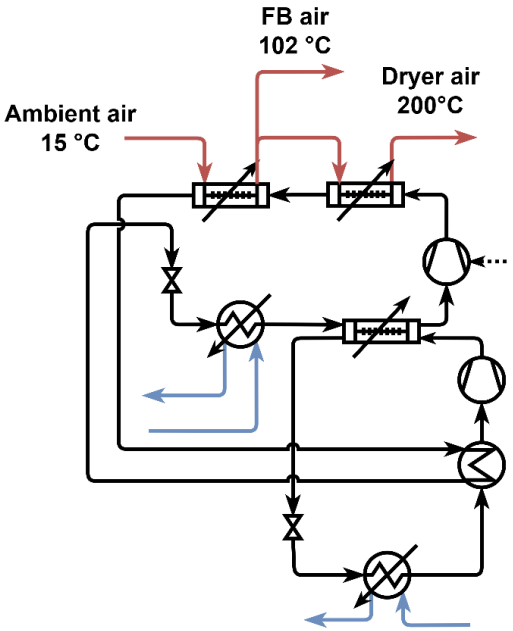

Figure 57. Cycle TT-2 with additional gas cooler.

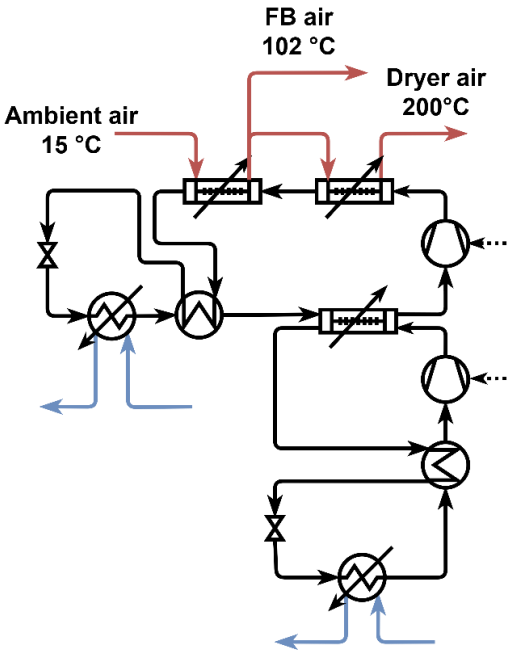

Figure 58. Cycle TT-4 with additional gas cooler.

The modelling method for the heat pump follows the methods described in Section 4.3. The heating COP for the system was calculated from the total heat supplied from the heat pump ($\dot{Q}$) divided by the work consumption of both compressors ($\dot{W}$), as shown in Equation 6.6.

$$COP = \frac{\sum \dot{Q}}{\sum \dot{W}} = \frac{\dot{Q}_{HTGC} + \dot{Q}_{MTGC}}{\dot{W}_{comp,top} + \dot{W}_{comp,bot}} \quad 6.6$$

The specific work consumption (w) per kg of air heated using the heat pump ($\dot{m}_{air,HP}$) was calculated for determining the annual operating cost, as per Equation 6.7.

$$w = \frac{\sum \dot{W}}{\dot{m}_{air,HP}} \quad 6.7$$

6.2.5 Operating and breakeven cost calculations

The operational cost per year excluding maintenance ($OPEX$) was calculated for an operational period (t) of 6000 hours per year and a production capacity of 20 t/h of milk powder. The steam cost for the boiler system was calculated from the total mass flowrate of steam required ($\dot{m}_{steam}$) multiplied by the respective inlet enthalpies for each steam heating section (h_{steam}) to determine the heating requirements for the process air stream. This value was then divided by the efficiencies of the boiler (η_{boiler}) and the steam distribution system ($\eta_{distribution}$) to determine the heat demand from the boiler. The heat demand of the boiler was multiplied by the operational hours and price per unit of fuel (p_{fuel}) to obtain the steam cost (Equation 6.8)

$$OPEX_{boiler} = \frac{\sum(\dot{m}_{steam} h_{steam})}{\eta_{boiler} \cdot \eta_{distribution}} \cdot t \cdot p_{fuel} \cdot 0.0036 \quad 6.8$$

The heat pump operating cost was calculated from the process air requirement for the specified powder production capacity ($\dot{m}_{air}$) and the specific work consumption per unit of air for the process conditions (w) multiplied by the electricity price (p_{elec}).

$$OPEX_{HP} = \dot{m}_{air} \cdot w \cdot t \cdot p_{elec} \cdot 0.0036 \quad 6.9$$

The utility prices considered for the analysis are given in Table 19.

Table 19. Utility prices for electricity and biomass.

Utility type	Range	Unit	Reference
Electricity (delivered)	40-70	NZD/GJ	[144]
Biomass price (delivered heat)	10-25	NZD/GJ	[145]

The price ratio (r_p, Equation 6.10) between biomass (p_{fuel}) and electricity (p_{elec}) can be used to determine what sink temperature is optimal for the heat pump to run. The breakeven price ratio will occur when the operational cost of the biomass boiler ($OPEX_{boiler}$) is equal to the operational cost of the heat pump ($OPEX_{HP}$), shown in Equation 6.11. Substituting Equations 6.8 and 6.9 into Equation 6.11 forms Equation 6.12. Rearranging for the price ratio (r_p) and simplifying the equation results in Equation 6.13.

$$r_p = \frac{p_{elec}}{p_{fuel}} \tag{6.10}$$

$$OPEX_{HP} = OPEX_{boiler} \tag{6.11}$$

$$\frac{\sum(\dot{m}_{steam} h_{steam})}{\eta_{boiler} \cdot \eta_{distribution}} \cdot t \cdot p_{fuel} \cdot 0.0036 = \dot{m}_{air} \cdot w \cdot t \cdot p_{elec} \cdot 0.0036 \tag{6.12}$$

$$r_p = \frac{p_{elec}}{p_{fuel}} = \frac{\sum(\dot{m}_{steam} h_{steam})}{\dot{m}_{air} \cdot w \cdot \eta_{boiler} \cdot \eta_{distribution}} \tag{6.13}$$

The breakeven price ratio between the hybrid scenarios (Scenarios 3.1 to 3.4) and biomass alone ($r_{p,HP+B}$) can be calculated in a similar fashion. However, the utility cost of the hybrid scenarios ($OPEX_{HP+B}$) will combine the heat pump and boiler equations, as shown in Equation 6.14. The amount of steam required in the hybrid scenarios is denoted by $\dot{m}^*_{steam}$ and the amount of steam required to heat the air from 15 °C to 200 °C is denoted by $\dot{m}_{steam}$. Combining Equations 6.8, 6.14 and 6.15 gives the breakeven price ratio between the hybrid scenarios and biomass only (Equation 6.16).

$$OPEX_{HP+B} = \left(\dot{m}_{air} \cdot w \cdot p_{elec} + \frac{\dot{m}^*_{steam} h_{steam}}{\eta_{boiler} \cdot \eta_{distribution}} \cdot p_{fuel}\right) \cdot t \cdot 0.0036 \tag{6.14}$$

$$OPEX_{HP+B} = OPEX_{boiler} \tag{6.15}$$

$$r_{p,HP+B} = \frac{p_{elec}}{p_{fuel}} = \frac{(\dot{m}_{steam} - \dot{m}^*_{steam}) \cdot h_{steam}}{\dot{m}_{air} \cdot w \cdot \eta_{boiler} \cdot \eta_{distribution}} \tag{6.16}$$

6.2.6 Emissions calculations

The CO_2 emissions (e) of each heating scenario is calculated to compare the emissions reduction potential in comparison to coal. The emissions factors of each source outlined in Table 20. The grid emissions for New Zealand and Germany were used to represent (respectively) a lower grid emissions and a higher grid emissions scenario. In 2022, the electricity generation in New Zealand was 87 % renewable [146] on average compared to Germany with a 39 % average [147]. For the boiler analysis, it was assumed that the biomass used was "sustainably sourced and efficiently used", and therefore, renewable, such as is the case currently in New Zealand [148]. The boiler emissions (e_{boiler}) were calculated from the sum of the annual steam consumption from the boiler divided by the calorific value of the fuel (cv_{fuel}), multiplied by the emissions factor. The calorific values of coal (lignite) and biomass were taken as 3.9 kWh/kg [149] and 4.85 kWh/kg [150], respectively. The emissions contributions (e) for the boiler scenarios (biomass or coal) and heat pump were calculated as shown in Equations 6.17 and 6.18. For the partial electrification scenarios, the emissions were taken as the sum of the emissions from the biomass boiler and the heat pump.

Table 20. Emissions factors for different heating scenarios.

Source	e_f	Unit	Reference
Low grid emissions scenario	0.0742	$kgCO_2$-e/kWh	[151]
High grid emissions scenario	0.450	$kgCO_2$-e/kWh	[152]
Biomass emissions	0.0146	tCO_2-e/t_{fuel}	[151]
Coal emissions (lignite)	1.55	$kgCO_2$-e/kg_{coal}	[151]

$$e_{boiler} = \frac{\sum \dot{m}_{steam} h_{steam}}{\eta_{boiler} \cdot \eta_{distribution} \cdot cv_{fuel}} \cdot t \cdot e_f \quad 6.17$$

$$e_{HP} = \dot{m}_{air} \cdot w \cdot t \cdot e_f \quad 6.18$$

6.3 Results

6.3.1 Simulation results

The simulation results for the heat pump and air heater modelling are given in Table 21 and have been verified through an Engineering Equation Solver (EES) model developed by Arpagaus et al. [153]. Across all scenarios, the sink inlet temperature to the heat pump was fixed at 15 °C. The T_{sink} values in Table 21 represent the outlet temperatures of the heat pumps, TT-2 and TT-4. Where the T_{sink} value was

less than 200 °C, the remainder of the air heating requirement (up to 200 °C) was met using boiler steam, quantified by $\dot{m}_{steam}$. Six scenarios for the three design groups were investigated:

- **Scenario 1 (base case):** air heating entirely supplied by boiler steam (coal, biomass or electrode) with heat recovery that can heat the air to 35 °C.
- **Scenario 2:** full electrification of the air heating requirements using a heat pump.
- **Scenarios 3.1 to 3.4:** hybrid configurations where the heat pump preheated the air and the boiler steam supplied the remaining heating requirements up to 200 °C. Scenario 3.1 preheats the air to 180 °C. NB: It is also possible to run the dryer at 180 °C, but it lowers the throughput. Scenario 3.2 preheats the air to 150 °C, which is the sink temperature that (as so far published) can currently be achieved with the MAN Heat Pump [46]. Scenario 3.3 uses the heat pump to supply air heating up to 120 °C, which is synonymous to the GEA AddCool [70]. Scenario 3.4 considers using the heat pump to heat the air to the temperature level of the static fluidised bed at 102 °C.

Table 21. Simulation results for the heat pumps and steam requirements from the boiler.

		w (kJ/kg$_{air}$)		COP		
	T_{sink} (°C)	TT-2	TT-4	TT-2	TT-4	$\dot{m}_{steam}$ (kg/s)
1	Boiler only	-	-	-	-	6.67
2	200	63.0	61.4	2.48	2.55	0.00
3.1	180	54.7	54.1	2.60	2.63	0.78
3.2	150	43.1	42.7	2.83	2.85	1.82
3.3	120	33.1	32.6	3.05	3.10	2.74
3.4	102	27.5	27.4	3.22	3.26	3.25

For the base case (Scenario 1), 6.67 kg/s of steam was required to supply the 20 t/h dryer. In Scenario 2, the steam use was eliminated in favour of a decentralised heat pump, with COPs of 2.48 (TT-2) and 2.55 (TT-4) achieved. This result also shows that the multi-temperature level heat pump configuration, which aimed to improve the temperature profile match between the refrigerant and the air, significantly increased the COP of the heat pumps, in comparison to heating the air from 15 °C to 200 °C in one gas cooler (COP of ~2.2). Partial heat pumping in combination with boiler heating (Scenarios 3.1 to 3.4) were modelled, which aimed to improve the

overall system efficiency by leveraging higher COPs (at lower sink temperatures) and lower steam demand. For example, heating to 180 °C with the heat pump (Scenario 3.1) achieved COPs of 2.60 (TT-2) and 2.63 (TT-4) while lowering steam demand to 0.78 kg/s. At 150 °C (Scenario 3.2), COPs of 2.83 and 2.85 could be achieved, but the steam demand was higher at 1.82 kg/s. At 120 °C (Scenario 3.3), COPs of 3.05 and 3.10 could be achieved with a steam demand of 2.74 kg/s. At 102 °C (Scenario 3.4), COPs of 3.22 and 3.26 could be achieved with 3.25 kg/s of boiler steam required.

6.3.2 Operating cost calculations

The operating (utility) costs for Scenarios 1 and 2 are shown in Figure 59.

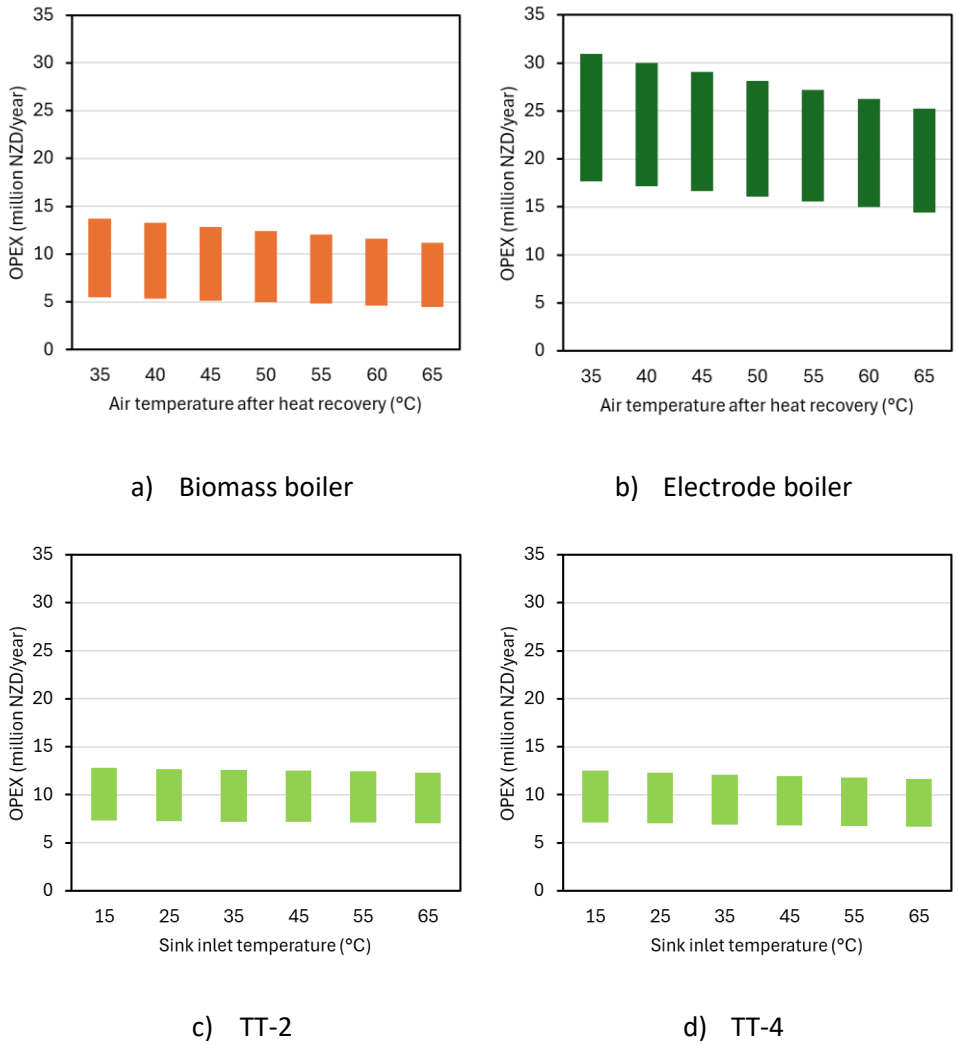

Figure 59. Comparison of operational cost at varying heat recovery temperatures for a) biomass boiler (Scenario 1), b) electrode boiler (Scenario 1)), c) TT-2 (Scenario 2) and d) TT-4 (Scenario 2).

The operating costs were calculated for a range of heat recovery scenarios: 35 – 65 °C for Scenario 1 (Figure 59a and b) and 15 – 65 °C for Scenario 2 (Figure 59c and d). The bottom of the bar represents the minimum operating cost, and the top of

the bar represents the maximum operating costs for the range of utility prices considered (Table 19). In Scenario 1, two boiler types are considered: biomass and electrode. In Scenario 2, the heat pumps modelled were TT-2 and TT-4 with the additional gas cooler for the static fluidised bed air.

For the scenarios considered in Figure 59, the costliest option was to use an electrode boiler (Figure 59b), with the minimum cost (14.4 million NZD/year) being more than the maximum cost of any other case (13.7 million NZD/year). In the case that biomass is cheap (10 NZD/GJ), biomass is the lowest cost option of the scenarios, particularly when greater heat recovery is available (Figure 59a). However, in the case that biomass is expensive (25 NZD/GJ), the heat pumps (Figure 59c and d) are more cost effective, operationally. Compared to the biomass and electrode boilers, TT-2 and TT-4 have relatively similar minimum and maximum costs. However, even so, TT-4 costs approximately $300,000 NZD/year less than TT-2.

A notable result is that the cost of the heat pump scenarios did not vary much with increased heat recovery (increased sink inlet temperature) due to a degradation in temperature profile match between the refrigerant and the air as the sink inlet temperature increases, penalising the COPs. This suggests that it would be more effective, in terms of cost reduction and energy savings, to use the existing heat recovery (COW water) in other parts of the plant, such as the evaporator hall [97].

An example of the temperature profile match for heat pumping to 200 °C is given in the temperature-entropy diagram of TT-4 where the red line shows the sink air streams for the two gas coolers (Figure 60). The pressure-enthalpy diagram is also given.

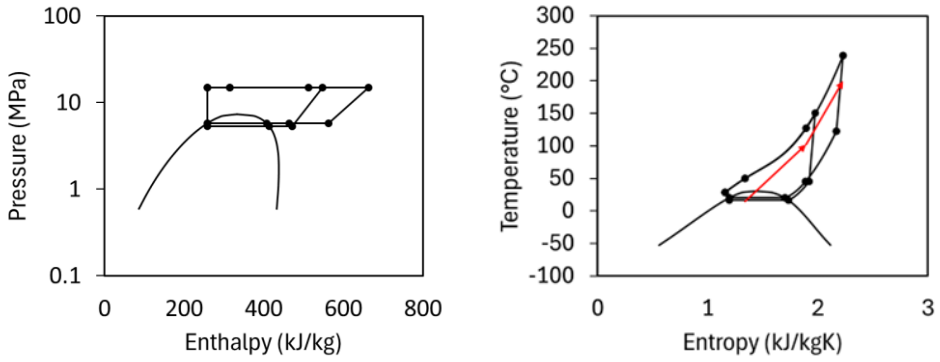

Figure 60. Pressure-enthalpy and temperature-entropy diagrams for TT-4 for a sink temperature of 200 °C.

As TT-4 was consistently the highest performing heat pump from the results of Table 21, further results for Scenarios 3.1 to 3.4 were run with TT-4. The operational expenditures for Scenarios 3.1 to 3.4 were calculated for hybrid configurations with both a biomass boiler (Figure 61) and an electrode boiler (Figure 62). The operational expenditure for Scenario 2 (green) is also given in Figure 61 and Figure

62 for comparison. As expected from the results in Figure 59, the hybrid biomass configurations had lower expenditure in comparison to the hybrid electrode boiler configurations.

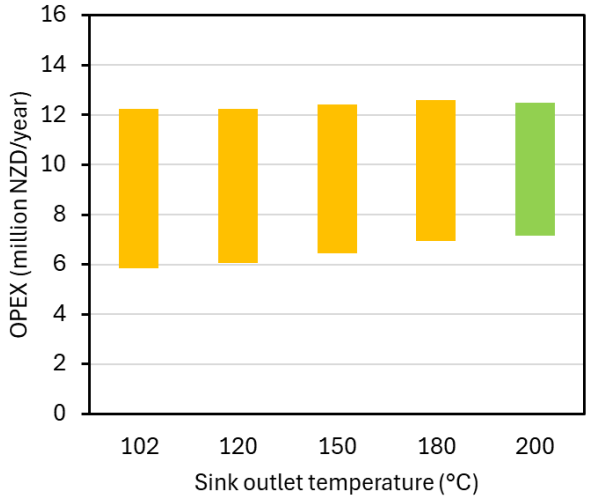

Figure 61. Maximum and minimum operational expenditure for a TT-4 + biomass boiler combined system.

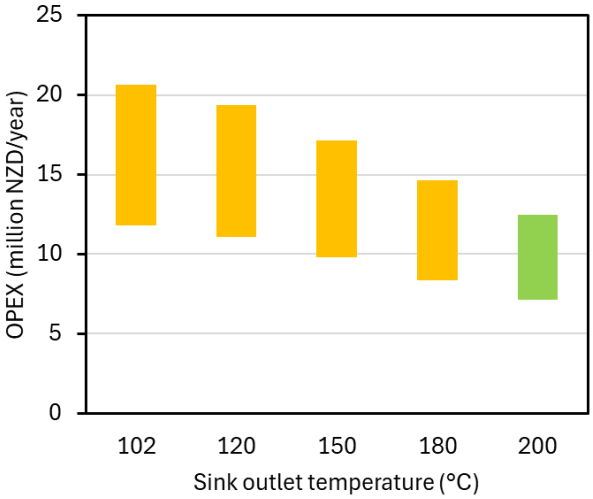

Figure 62. Maximum and minimum operational expenditure for TT-4 + electrode boiler combined system.

For the hybrid biomass configurations (Figure 61), all scenarios had similar maximum utility costs at approximately 12 million NZD/year, with a full heat pumping option (Scenario 2) also having a comparable maximum utility price. Scenario 3.1 had the lowest minimum utility cost at approximately 6 million NZD/year. The minimum utility cost increased with increasing sink outlet temperature, ranging between 6 million and 7.1 million NZD/year. Compared to Scenario 1, using biomass only, the hybrid configurations had lower maximum utility costs when the heat recovery temperature in Scenario 1 was 45 °C or below.

However, Scenario 1 had lower minimum utility costs for all heat recovery temperatures.

Figure 63 and Figure 64 break down Figure 61 and Figure 62 to show the contribution of the heat pump and boiler costs for different pricing scenarios. At a low biomass price scenario, full biomass conversion (Scenario 1) is the lowest cost option, particularly when there is greater heat recovery, followed by Scenario 3.1. For a high biomass price/low electricity price scenario, the heat pump is the lowest cost option, followed by Scenario 3.4. In a high electricity/high biomass price scenario, Scenario 2 is comparable in cost to Scenarios 3.1 to 3.4. These cases are lower in cost compared to Scenario 1 (biomass) if the heat recovery available can only preheat the air up to 45 °C. At 50 °C or greater, Scenario 1 has a lower cost. In all price scenarios for the hybrid electrode configurations, Scenario 3.4 has the lowest cost.

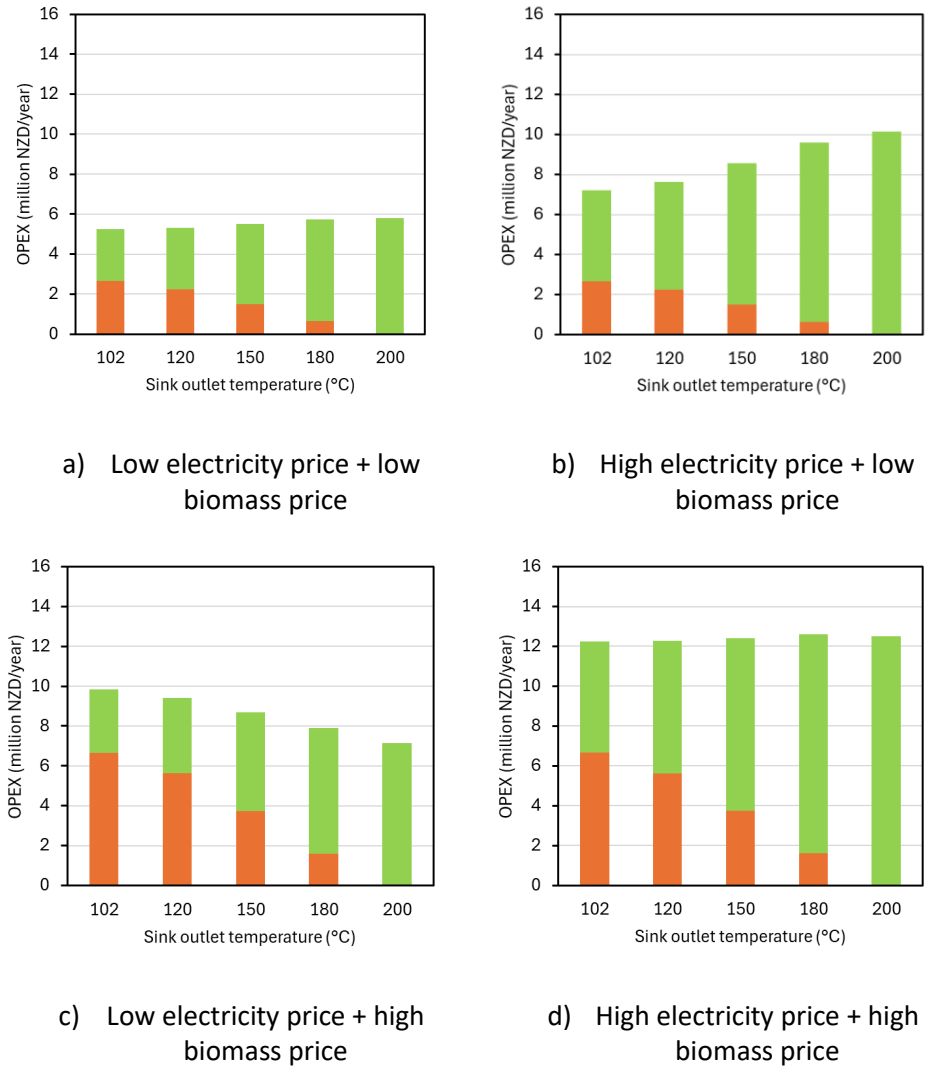

a) Low electricity price + low biomass price

b) High electricity price + low biomass price

c) Low electricity price + high biomass price

d) High electricity price + high biomass price

Figure 63. Operational cost breakdown of heat pump and biomass boiler at varying utility prices.

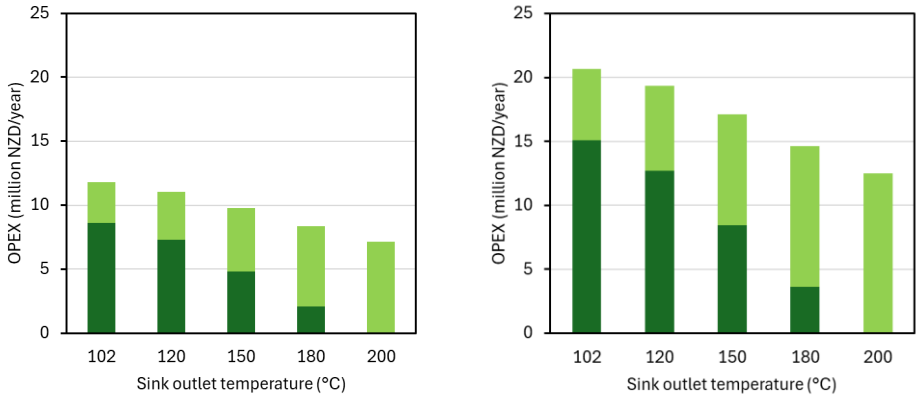

a) Low electricity price b) High electricity price

Figure 64. Operational cost breakdown of heat pump and electrode boiler at low electricity and high electricity prices.

6.3.3 Breakeven price ratios

The breakeven electricity-to-biomass price ratio for each solution was calculated for the various sink outlet temperatures which ranged between 3.05 and 3.5 (Figure 65). If the price ratio is lower than the values given in Figure 65, then utility costs for the heat pump scenario (Scenarios 2 or 3.1 to 3.4) will be more economically favourable than the biomass boiler (Scenario 1).

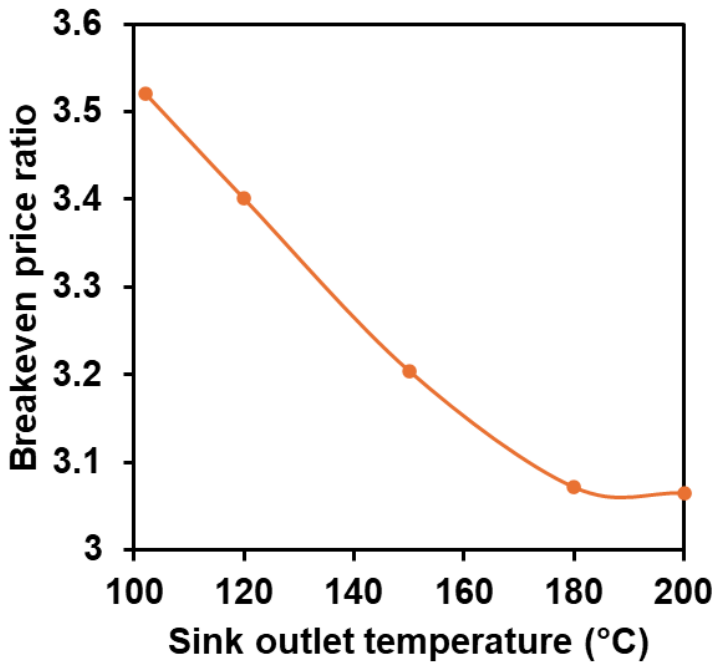

Figure 65. Breakeven price ratio for varying sink outlet temperatures.

The breakeven price ratio excludes the capital cost, however, EECA [154] has reported capital costs between 750,000 NZD per MW to 1.1 million NZD per MW for new biomass boiler installations, and 80,000 NZD per MW to 290,000 NZD per

MW for coal boiler conversions. From the estimations in Kong et al. [154], and accounting for the additional gas cooler, the cost of the heat pump (only) is estimated to be approximately 570,000 NZD per MW, however, it is likely that the estimated capital cost for the heat pump would be higher as there would be greater changes for the distribution of heat, e.g. piping or exhaust heat recovery, and the potential that network upgrades would be required to support the installation. Additionally, the carbon emissions factors for biomass are lower than the emissions factor for the electricity grid in New Zealand, therefore additional carbon costs may be associated with the heat pump in comparison to biomass.

Many scenarios have the potential to meet the breakeven price ratio simultaneously. To identify which scenario is most economically favourable at differing utility prices, i.e. differing price ratios, the OPEX equations for each scenario (Equations 6.8, 6.9 and 6.14) were minimised. The OPEX equations could not be directly optimised as the values for specific work consumption of the heat pump, and the steam mass flows were calculated from the heat pump and air heater models. For the optimisation, the specific work consumption (Figure 66a) and steam mass flows (Figure 66b) were approximated, using regression, against the sink outlet temperature from the results of the heat pump and air heat models for the optimisation. The scenario corresponding to the lowest OPEX value was then selected as the recommended option.

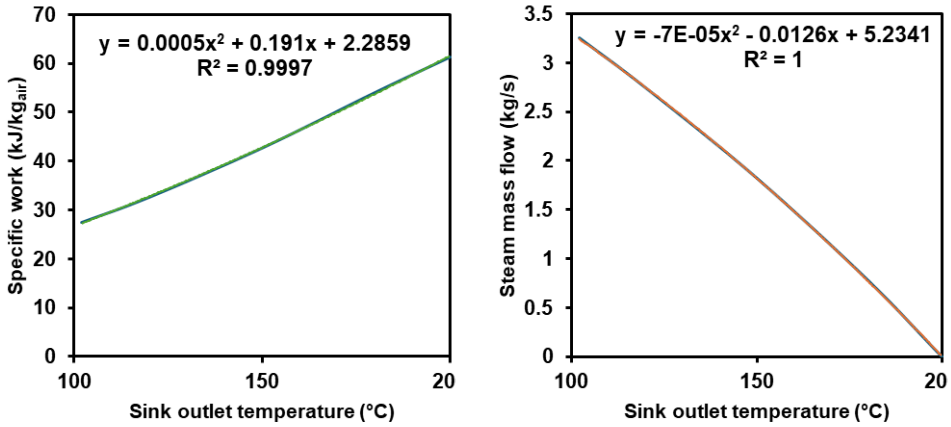

a) Specific work consumption of the heat pump

b) Steam mass flow

Figure 66. a) Specific work consumption of the heat pump and b) boiler steam mass flow rates at varying sink outlet temperatures with corresponding trendline equations.

The minimised cost option for each combination of electricity and biomass prices considered for this chapter are presented in Table 22, while the corresponding electricity-to-biomass price ratios for the range of prices considered are given in Table 23. The results show that Scenario 1 was the most economical in all cases when the biomass price was 10 NZD/GJ, and also for the case when the biomass price was 15 NZD/GJ and the electricity price was above 55 NZD/GJ (Table 22),

which corresponds to price ratios above 3.67 (Table 23). In nearly all cases where the biomass price was 25 NZD/GJ, full electrification to 200 °C was the lowest cost option (Table 22). Full electrification was also preferable when the biomass price was 20 NZD/GJ and the electricity price was 55 NZD/GJ or less (Table 22), corresponding to price ratios below 2.75 (Table 23). Between price ratios of 2.75 and 3.67, using the heat pump to supply the air heating up to 102 °C (Scenario 3.1) was the lowest cost option (Table 23).

Table 22. Minimised cost option at varying utility prices with a maximum sink outlet temperature of 200 °C.

	Electricity price (NZD/GJ)						
Biomass price (NZD/GJ)	40	45	50	55	60	65	70
10	B	B	B	B	B	B	B
15	200.0	102.0	102.0	B	B	B	B
20	200.0	200.0	200.0	200.0	102.0	102.0	102.0
25	200.0	200.0	200.0	200.0	200.0	200.0	102.0

Table 23. Electricity-to-biomass price ratios at varying utility prices.

	Electricity price (NZD/GJ)						
Biomass price (NZD/GJ)	40	45	50	55	60	65	70
10	4.00	4.50	5.00	5.50	6.00	6.50	7.00
15	2.67	3.00	3.33	3.67	4.00	4.33	4.67
20	2.00	2.25	2.50	2.75	3.00	3.25	3.50
25	1.60	1.80	2.00	2.20	2.40	2.60	2.80

The minimised cost options were also calculated for a maximum sink temperature of 150 °C (Scenario 3.3, Table 24), as this is the highest sink outlet temperature currently reported for a CO_2 HTHP in the Annex 58 [29]. The results showed that, even with the lower sink outlet temperature of 150 °C, the maximum amount of electrification is still favourable at price ratios below 2.60 and heat pumping up to 102 °C is favourable between price ratios of 2.60 and 3.67.

Table 24. Minimised cost option at varying utility prices with a maximum sink outlet temperature of 150 °C.

	Electricity price (NZD/GJ)						
Biomass price (NZD/GJ)	40	45	50	55	60	65	70
10	B	B	B	B	B	B	B
15	102	102	102	B	B	B	B
20	150	150	150	102	102	102	102
25	150	150	150	150	150	150	102

6.3.4 Emissions calculations

As many dairy plants in New Zealand use coal to supply process heat [3], the emissions reduction potential of the scenarios was compared to two coal heating scenarios: minimum heat recovery and maximum heat recovery. The minimum heat recovery takes the air temperature after heat recovery as 35 °C and the maximum heat recovery takes the air temperature after heat recovery as 65 °C. A complete fuel switch to a biomass boiler (Scenario 1) would give an emissions reduction potential of almost 100 %, with a small quantity (1 %) of emissions resulting from the diesel machinery used for harvest and transport. For electrification with an electrode boiler only (Scenario 1), the highest emissions reduction potential occurred when replacing a coal boiler and minimum heat recovery with an electrode boiler and maximum heat recovery in a low grid emissions location (87.7 %). However, even if only minimum heat recovery can be achieved, the emissions reduction potential was estimated at 84.9 % (Table 25).

Table 25. Emissions reduction potential of the B (electrode) scenario compared to coal.

Case	Minimum heat recovery (electrode)	Maximum heat recovery (electrode)
Minimum heat recovery - low grid emissions	84.9%	87.7%
Minimum heat recovery - high grid emissions	8.5%	25.3%
Maximum heat recovery - low grid emissions	81.5%	84.9%
Maximum heat recovery - high grid emissions	-12.0%	8.5%

For the high grid emissions case, electrification with an electrode boiler only achieved a maximum emissions reduction potential of 25.3 %, when a coal boiler with minimum heat recovery was replaced with an electrode boiler with maximum heat recovery. Although it is unlikely that a coal boiler with maximum heat recovery would be replaced with an electrode boiler with minimum heat recovery, in a high grid emissions location, this would cause an increase in emissions by 12 %. Of the remaining scenarios, the lowest emissions reduction potential resulted from when an electrode boiler replaces a coal boiler without increasing the amount of heat recovery in a high grid emissions location (8.5 %).

The emissions reduction potential of both the heat pump (Scenario 2) and the hybrid boiler/heat pump configurations (Scenarios 3.1 to 3.4) are given in Table 26 for biomass and Table 27 for electrode boilers.

Table 26. Emissions reduction potential of the HP and HP + B (biomass) scenarios compared to coal.

Case	**HP**	**HP + boiler (biomass)**			
$T_{sink,out}$ (°C)	200	180	150	120	102
Minimum heat recovery - low grid emissions	93.9%	94.6%	95.6%	96.5%	97.0%
Minimum heat recovery - high grid emissions	63.1%	67.4%	74.2%	80.2%	83.2%
Maximum heat recovery - low grid emissions	92.5%	93.3%	94.6%	95.8%	96.3%
Maximum heat recovery - high grid emissions	54.8%	60.1%	68.4%	75.7%	79.5%

Using a heat pump only (Scenario 2) resulted in emissions reduction potentials ranging from 54.8 % to 93.9 %. Additionally, supported by the results from Section 6.3.2, the benefit of Scenario 2 is that existing or opportunities for heat recovery could be used in other areas of the plant for further emissions reduction (and efficiency) improvements. For the biomass hybrid configurations, the emissions reduction potentials ranged from 60.1 % to 97 %, where a higher proportion of biomass boiler heating resulted in greater emissions reduction potential. The opposite occurred for the electrode hybrid configurations, which ranged from 31.2 % to 93.1 %, where a higher proportion of heat pumping had greater emissions reduction potential.

Table 27. Emissions reduction potential of the HP and HP + B (electrode) scenarios compared to coal.

Case	HP	HP + boiler (electrode)			
$T_{sink,out}$ (°C)	200	180	150	120	102
Minimum heat recovery - low grid emissions	93.9%	93.1%	92.1%	91.2%	90.7%
Minimum heat recovery - high grid emissions	63.1%	57.9%	52.1%	46.8%	43.8%
Maximum heat recovery - low grid emissions	92.5%	91.5%	90.3%	89.3%	88.7%
Maximum heat recovery - high grid emissions	54.8%	48.5%	41.3%	34.9%	31.2%

6.3.5 Further integration opportunities for future research

An opportunity exists to use two heat pumps optimised at different temperatures to supply the heating for the static fluid bed air and the spray dryer air separately. Although this option is undoubtedly capital-intensive, the benefits related to efficiency should be explored in future research. Alternatively, the heat pump could be run at the present temperature levels (102 °C and 200 °C), with the VFB air (~70 °C) supplied by a decentralised heat pump. Since CO_2 does not generally have the best performance at the temperature level of the VFBs, using a heat pump with a different refrigerant could provide significant performance gains. Additionally, the clean-in-place water could also be supplied as it is at a similar temperature level (~85 °C). Another avenue that could be explored is to run the dryer at a lower temperature. The primary air temperature for a milk powder dryer is able to be as low as 180 °C. The development of an integration method that incorporates these aspects and is designed specifically for HTHPs would be beneficial for future research.

6.4 Conclusions

Six air heating scenarios were investigated in this chapter as decarbonisation options: 1) boiler only using biomass or electrode boilers, 2) full electrification using a heat pump only, and 3.1 to 3.4) hybrid configurations with a heat pump and a boiler. The heat pump was based on the highest performing cycles of Chapter 4 and Chapter 5 but the cycles were modified to include a second temperature level for the fluidised bed air heating up to 102 °C. The utility cost and emissions reduction potential of the three scenarios were calculated and compared, and a range of utility prices were considered.

Two hypotheses were tested in this chapter: 1) an optimal sink temperature exists where integrating a heat pump with a boiler can lower the operating cost compared to using each technology individually, and 2) the nonlinearity of sensible cooling for supercritical CO_2 can be leveraged at different temperature levels, i.e., multi-temperature heat pumping.

6.4.1 Optimal sink temperature

A full conversion to an electrode boiler (Scenario 1) had the highest cost range of all the options of up to 30 million NZD/year for a 20 t/h (powder) dryer. A full conversion to biomass (Scenario 1) or heat pumping (Scenario 2) had similar costs, with biomass having the lower minimum cost at approximately 5 million NZD/year but the heat pump having a lower maximum cost at approximately 13 million NZD/year. For Scenario 2, the results showed that the costs were similar for all hot water heat recovery cases. Therefore, additional efficiency and cost savings could be potentially achieved by utilising existing hot water heat recovery elsewhere in the process, such as for the evaporation plant. The lowest minimum cost scenario occurred for Scenario 1 with a biomass boiler at 10 NZD/GJ unit biomass price. The hybrid configurations for a heat pump with a biomass boiler had lower maximum costs compared to a boiler alone. In all hybrid configurations with a heat pump and electrode boiler, the minimum and maximum costs were significantly lower (up to 10 million NZD/year) than using solely an electrode boiler.

At present, the lowest cost solution is to convert to biomass boilers if a unit price of approximately 10 NZD/GJ (hog fuel) can be secured. However, if the price of biomass is approximately 25 NZD/GJ (pellets), then heat pumping becomes the lowest cost solution, even if the electricity price is higher (70 NZD/GJ). In any case that an electrode boiler is considered, a hybrid configuration with heat pumping should also be considered to lower the cost. The breakeven electricity-to-biomass price ratios were calculated for Scenarios 2 and 3.1 to 3.4 which ranged from 3.05 to 3.5. Industrial sites with electricity-to-biomass price ratios lower than these values should consider electrification using a heat pump, whereas sites with electricity-to-biomass price ratios above the breakeven values are more suited towards full biomass conversion.

As many price ratios exist which can be suitable for Scenarios 2 and 3.1 to 3.4, the OPEX was minimised for varying utility prices. The lowest cost recommendations based on the electricity-to-biomass price ratios (r_p) are as follows:

- $\boldsymbol{r_p < 2.75}$ → Supply all heating using a heat pump (Scenario 2).
- $\boldsymbol{2.75 < r_p < 3.67}$ → Supply the fluidised bed air heating up to 102 °C with a heat pump and the rest of the heating with a biomass boiler (Scenario 3.1).
- $\boldsymbol{r_p > 3.67}$ → Supply all of the heating with a biomass boiler.

6.4.2 Multi-temperature heat pumping

This chapter also introduces a novel multi-temperature heat pump integration strategy for milk powder spray drying. The results demonstrated that splitting the dryer air and fluidised bed air heating streams within the same heat pump significantly improves the COP (COP of 2.55) in comparison to heating the air from 15 °C to 200 °C in one gas cooler (COP of 2.22). In the multi-temperature heat pump configuration, TT-4 performed slightly better than TT-2, particularly when the full air heating was supplied with a heat pump only.

6.4.3 Emissions reduction potential

The emissions reduction potential for the biomass boiler (Scenario 1) was the highest at almost 100 %. A low grid emissions and a high grid emissions scenario were both considered. Full heat pumping (Scenario 2) resulted in emissions reduction potentials ranging between 54.8 and 93.9 %. In the hybrid configurations of a heat pump integrated with a biomass boiler, the highest emissions reduction potential (97 %) occurred when the greater proportion of the heating was done with the boiler (Scenario 3.4). In contrast, the highest emissions reduction potential (93.1 %) for the hybrid configurations of a heat pump integrated with an electrode boiler occurred when the greater proportion of the heating was done with the heat pump (Scenario 3.1). In locations with high grid emissions, electrode boiler conversions will not provide significant emissions reduction, unless the amount of heat recovery in the process is increased. Future research should consider opportunities to decentralise the lower temperature fluidised bed air. Additionally, the trade-off between throughput and a lower setpoint temperature for the dryer, that would provide benefit in terms of technological readiness for HTHPs, should be explored.

Chapter 7
The wider potential for uptake globally

7.1 Introduction

This chapter discusses further design considerations related to the development of a CO_2 HTTHP to lay a foundation for future work in this area. Such considerations include the potential impact that such a system could have on industrial process heat consumption and mechanical design considerations. This thesis discusses the fact that not all HTHPs are suitable for all applications. As heat pump performance varies widely depending on the cycle configuration, boundary conditions and refrigerant used, it can be difficult for process heat users to identify suitable heat pumps for their systems. For example, although many HTHPs are being developed up to 200 °C, very few can produce temperature glides exceeding 100 °C [34]. Alternatively, the heat source temperature required may be very high (>50 °C) which would need to be available as waste heat from the process.

The previous chapters investigated how a CO_2 HTTHP can be designed and optimised for milk powder spray drying, however, the development of a CO_2 HTTHP system has the potential benefit many other industrial processes. Part of this chapter aims to identify suitable industrial process heat applications and to quantify the decarbonisation potential that could be realised from the development of the CO_2 HTTHP system. The other part of this chapter discusses some of the challenges around implementing the heat pump.

7.2 Methods

7.2.1 Scope for identifying suitable applications

Applications for a high temperature transcritical CO_2 heat pump will be identified for the following process criteria:

- **Sink** – Process heating requirements from ambient to 200 °C or similar,
- **Source** – Waste heat available at 50 °C or below,
- **Temperature glide –** Greater than 100 °C.

For this investigation, temperature glide is defined as the temperature difference between the sink inlet and the sink outlet, and temperature lift is defined as the difference in temperature between the source inlet temperature and the sink outlet temperature.

7.2.2 Estimation of heat potential

To estimate the amount of heat that could potentially be supplied using a CO_2 HTTHP with a large temperature glide ($Q_{potential}$), potential applications are first identified. For each application where the process results in a product, the heat potential is estimated by taking the total mass of product produced per year globally ($m_{product}$) and multiplying it by the specific energy consumption required to produce the product (h).

$$Q_{potential} = \sum m_{product} h$$

The accuracy with which the heat potential can be estimated is limited due to large variation in the way that individual types of products are produced, the age of technology used for the process and, therefore, the efficiency of production. For any given application, this results in large variations in the specific energy consumption required.

7.2.3 COP calculations

TT-4, as per the configuration in Chapter 3, will be modelled in the identified applications. The COP will be estimated for an ambient air source case and, where possible, using heat recovery, such as exhaust air, as the source to supply the heat pump. The temperature of the source varies depending on the application identified. Where the waste heat was exhaust air, it was assumed that a water loop was used to transport the waste heat from the exhaust to the heat pump. Heating of the water is modelled in two sections: 1) sensible cooling of the air and 2) condensing the water out of the air, to determine the final temperature of the heat source available (Figure 57).

The exhaust air temperature ($T_{exhaust}$) and dew point temperature (T_{dp}) are identified from the application. From these values, the absolute humidity of the air between the sensible cooling portion and the condensing portion can be identified ($\omega_{SC,out}$) using HAPropsSI (CoolProp) with the assumption that the air is fully saturated at this temperature, i.e. the relative humidity (R) is 100 %, as shown in Equation 7.1.

$$\omega_{SC,out} = f(P_{atm}, T_{dp}, R) \qquad 7.1$$

Then, the absolute humidity of the exhaust air ($\omega_{exhaust}$) is equal to the absolute humidity before the water condenses which can be used to determine the specific enthalpy ($h_{exhaust}$), as shown in Equation 7.2 and 7.3.

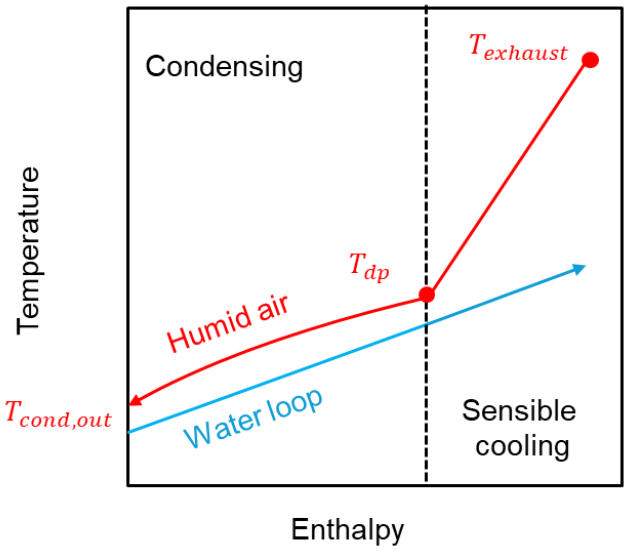

Figure 67. Humid air and water loop temperature profile.

$$\omega_{exhaust} = \omega_{SC,out} \quad 7.2$$

$$h_{exhaust} = f(P_{atm}, T_{exhaust}, \omega_{exhaust}) \quad 7.3$$

The air temperature after condensing ($T_{cond,out}$) is specified based on the application and the relative humidity remains at 100 % based on the dehumidification profile of the air (Figure 68). From there, the specific enthalpy of the air ($h_{cond,out}$) can be calculated (Equation 7.4).

$$h_{cond,out} = f(P_{atm}, T_{cond,out}, R) \quad 7.4$$

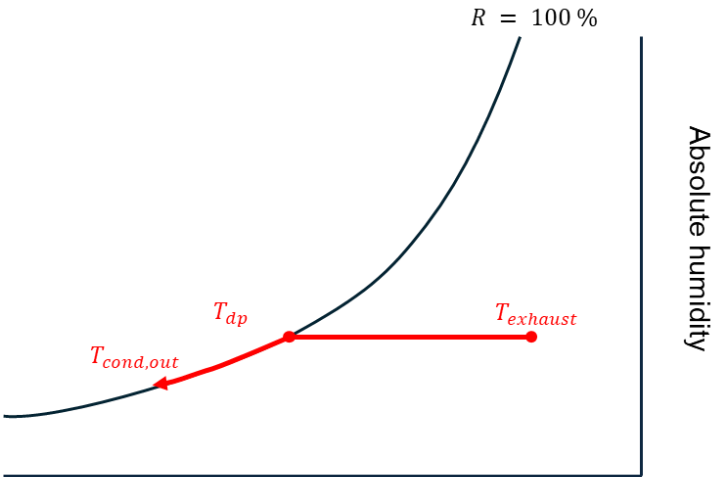

Figure 68. Dehumidification of exhaust air on a psychrometric chart - example.

The temperature of the water loop to supply the heat pump can then be calculated from an energy balance, where the minimum approach temperature was assumed to be 5 °C.

7.2.4 CO_2-abatement potential

The integration of a HTHP aims to reduce the emissions related to process heating, however, for a heat pump, the emissions are related to the grid emissions factor in the location which the heat pump is installed. The breakeven grid emissions factor ($e_{f,grid\ BE}$), i.e., the value that the grid emissions factor must be less than, occurs when the heat pump emissions per unit of heat ($e_{f,HP}$) is equal to the reference boiler emissions per unit of heat ($e_{f,boiler}$). The heat pump emissions can be calculated from the grid emissions factor ($e_{f,grid}$) divided by the COP (Equation 7.5). Similarly, the boiler emissions can be calculated from the emissions factor of the reference fuel divided by the efficiency of heat delivery, which is represented by the boiler (η_{boiler}) and distribution ($\eta_{distribution}$) efficiencies. Combining Equations 7.5 and 7.6 gives Equation 7.7 to calculate the breakeven grid emissions factor.

$$e_{f,HP} = \frac{e_{f,grid}}{COP} \tag{7.5}$$

$$e_{f,boiler} = \frac{e_{f,ref\ fuel}}{\eta_{boiler} \cdot \eta_{distribution}} \tag{7.6}$$

$$e_{f,grid\ BE} = e_{f,ref\ fuel} \cdot \eta_{boiler} \cdot \eta_{distribution} \cdot COP \tag{7.7}$$

A range of grid emissions factors ($e_{f,grid}$) for different countries were considered. The reference fuel emissions factors ($e_{f,ref\ fuel}$) and boiler efficiencies (η_{boiler}) are given in Table 28. It was assumed that the distribution efficiency ($\eta_{distribution}$) for both reference fuels was 90 %.

Table 28. Emissions factors for coal and natural gas.

Source	$e_{f,ref\ fuel}$	Unit	η_{boiler}	Reference
Natural gas	0.193	$kgCO_2\text{-}e/kWh_{heating}$	90 %	[151]
Coal emissions (lignite)	1.55	$kgCO_2\text{-}e/kg_{coal}$	80 %	[151]

7.3 Results and discussion

7.3.1 Process applications and temperatures

Sixteen industrial applications have been identified in Table 29 which have the potential to benefit from a large temperature glide HTHP. Possible source and sink conditions for a heat pump have also been included based on the process streams and their supply (T_{supply}) and target (T_{target}) temperatures. As shown, large temperature glide HTHPs are particularly suited to drying processes, such as spray drying and fluidised bed drying. Dryers are utilised across a wide range of industries, including food and beverage, pharmaceuticals, chemical and cosmetic industries. Thus, the development of a large temperature glide HTHP has significant decarbonisation potential.

7.3.2 Estimation of heat potential

Spray drying is a prevalent industrial process which is used for many applications. For example, approximately 60 % of global instant coffee production is produced by spray drying, with coffee being one of the most traded commodities in the world [155]. Spray drying of instant coffee requires process air that is heated from ambient conditions to a target temperature of up to 210 °C. The exhaust air exists at approximately 110 °C from the spray dryer and 35 °C from the belt dryer which are possible source streams for a heat pump. Okada et al. [156] estimated that the thermal energy requirement of spray drying instant coffee was 21.1 MJ/kg, which results in an estimated 33 PJ/year that has the potential to be supplied by a large temperature glide HTHP.

Dairy powders are another significant application for spray drying. Although the focus of the thesis has been centred around milk powder production in New Zealand, China, the EU and Brazil are also large producers of milk powder [157]. Globally, it was estimated that 5.4 million tonnes of whole milk powder and 4.6 million tonnes of skim milk powder was produced in 2021 [157]. With a specific energy consumption of approximately 3000 MJ/t_p for modern milk powder spray dryers [158], an estimated 30 PJ/year is used to spray dry milk powder globally. In the milk powder production process, waste heat can exist in the form of hot water, from the evaporation process, or as exhaust air, from the dryer. The waste hot water (COW water) is produced at approximately 70 °C and the air is exhausted at approximately 60 °C. Both of these streams have the potential to be used for the source stream of a heat pump. Whey powder, also known as cheese whey powder, is another energy intensive dairy powder product. Whey powder constitutes approximately 15 % of the 21.6 million tonnes of cheese whey produced globally per year [159], [160]. As whey has a higher water content than milk, which needs to be evaporated in the drying process, the specific energy of drying whey powder is generally higher than milk powder. Domingues-Nino et al. [159] estimated this value to be 2.049 kWh/kg_p (7376 MJ/t_p), which would result in an estimated 23.8 PJ/year required for drying of whey powder.

Table 29. Processes that require large temperature glides.

Process	Product	ΔT_{glide} (K)	T_{supply} (°C)	T_{target} (°C)	$\dot{m}c_p$ (kW/K)	Ref.
Spray drying	Milk	200	11*	210	57.9	[161]
			73	31	70.1	
			31	11*	237.2	
			52	75	10.2	
	Whey powder	181	9*	220	-	[162]
			81	9*	-	
			75	9*	-	
			69	9*	-	
	Cheese	190	11*	200	54.7	[163]
			80	34.9	71.7	
			34.9	11*	-	
	Coffee	200	11*	210	57.9	[163]
			110	35.7	69	
			35.7	11*	267.2	
	Starch (wheat, corn, potato)	150	13*	160	54.4	[163]
			52	37.8	58.3	
			37.8	13*	240.3	
	Cassava starch	190	10*	200	-	[164]
	Brewing yeast	135	10*	145	1.38	[165]
			60	35.6	1.82	
			35.6	10*	5.57	
	Dried egg powder	150	10*	160	0.51	[166], [167]
			80	35.6	0.64	
			35.6	10*	1.39	
	Fish food	240	30*	280	-	[168]
			90	35	-	
	Soy protein powder	175	15*	190	-	[169]
			70	15*	-	
Drying chamber	Brick	165	15*	180	-	[170]
			50	30	-	
	Automotive serial coating	120	20*	140	-	[171]
			140	165	-	
			165	180	-	
			30	20*	-	
Fluidised-bed drying	Table salt	200	10*	200	1.01	[172]
			110	35	1.15	
			35	10*	6.56	
Belt drying	Colour pigments	240	10*	250	1.12	[173]
			55	53	1.1	
			53	10*	5.41	
	Plastic granulate (polycarbonate)	107	11*	118.4	75.0	[163]
			105	12.6	75.4	
			12.6	11*	188.5	
Cylinder contact drying	Paper drying	100	11	110	42.7	[174]

Drying of wheat, corn and potato starch has a thermal energy requirement of 1.7 GW in the EU alone, which results in an annual thermal energy requirement of approximately 50 PJ/year [162]. While the EU plays a significant role in the global production of starch, particularly wheat and potato starch, it is yet to surpass the total starch production of China and the United States. Globally, between 88.1 million and 97.7 million tonnes of starch was produced in 2020, with 75 % being corn, 14 % being cassava, 7 % wheat and 4 % potato [175]. For starch drying particularly, the specific energy consumption varies widely as there are many types of dryers used in the industry. The most common types include flash drying and rotary drum drying, which generally ranges from 110 °C to 220 °C for the inlet air temperature. Van Giau et al. [176] reported a specific energy requirement for drying cassava starch as 1.898 MJ/kg_p, whereas the average specific energy consumption of producing starch in the EU is 3.792 MJ/kg_p when calculated from the reported thermal energy requirement of 1.7 GW [162] and the mass of starch produced in the EU of 9.7 million tonnes per year [177]. Even when considering a significant portion of cassava starch production is sun dried (~50 %), the energy consumption required to dry starch globally could still be substantial, at up to 310 PJ/year.

While the heat potential of automotive coating can be difficult to quantify, Suresh and Rao [178] stated that approximately 1000 kcal per equivalent passenger vehicle, which equates to approximately 4.18 MJ, is required for air heating to 200 °C in the drying process, with approximately 16 million vehicles manufactured between the financial years of 2012 and 2013 in the Indian automobile industry. Considering 94 million motor vehicles are produced globally every year [179], this is approximately 0.38 PJ/year.

7.3.3 COP calculations

Spray drying generally requires process air to be heated from ambient conditions to 150 °C – 220 °C. Many drying processes occur after an evaporation stage, for increased energy efficiency, and thus, there is an opportunity to utilise waste hot water from the evaporation process to supply the heat source for a heat pump if there is sufficient mass flow. Another potential heat source exists through the spray dryer exhaust in the form of humid air. For applications where this is not an option, it is possible to use air source heat pumping due to the low critical temperature of CO_2, however the performance may be decreased.

Estimated COPs, using cycle TT-4, were calculated for each of the different applications identified in Table 29. To simplify the COP estimations, heating (with the heat pump) was only supplied to a singular air stream, similar to Chapter 4 and Chapter 5. The results of this section have since been published in Kong et al. [180] where it was assumed that the gas cooler heated the air directly with a ΔT_{min} of 5 °C, therefore resulting in higher COPs in comparison to the previous chapters, which assumed ΔT_{min} of 20 °C between the refrigerant and the air stream in the top cycle gas cooler.

Table 30 shows the estimated COPs for the applications using ambient air as the heat source. Two scenarios are considered: the first is at a maximum compressor discharge pressure ($P_{dis,max}$) of 150 bar, and the second at a maximum compressor discharge pressure of 300 bar. The results were grouped by the sink outlet temperature from the heat pump ($T_{sink,out}$), i.e. the process requirement, as some applications had the same process temperature requirement for the air stream. COPs between 2.0 and 3.05 could be achieved for temperatures ranging from 110 °C and 280 °C. The COPs were similar between the 150 bar and 300 bar constraints, however, as the sink temperature increased (>160 °C), it became more beneficial to use a higher discharge pressure. Even so, at the lower pressure constraint, the results present a compelling case for the development of a large temperature glide heat pump as double to triple the performance of an electrode boiler can be achieved.

Table 30. Estimated COPs for TT-4 for a range of large temperature glide applications, using ambient air source, for maximum pressures of 150 bar/300 bar.

$T_{sink,out}$ (°C)	COP	
	$P_{dis,max}$ = 150 bar	$P_{dis,max}$ = 300 bar
110	3.05	3.05
118.4	2.99	2.99
140	2.81	2.81
145	2.77	2.77
160	2.65	2.66
180	2.52	2.53
190	2.45	2.47
200	2.38	2.41
210	2.33	2.35
220	2.27	2.29
250	2.12	2.21
280	2.00	2.10

Exhaust heat recovery was also considered as a potential source to supply the heat pump for select applications. It was assumed that the heat from the dryer exhaust air was used to heat a water loop that transported the heat from the exhaust to the heat pump. The source inlet temperature of the water ($T_{source,in}$) was calculated as per the method in Section 7.2.3 from the exhaust air temperatures in Table 29. The calculated source inlet temperatures and the estimated COPs for the exhaust heat recovery scenarios are shown in Table 31.

Table 31. Estimated COPs for TT-4 for a range of large temperature glide applications for maximum pressures of 150 bar/300 bar using exhaust heat recovery with a water loop.

Application	$T_{sink,out}$ (°C)	$T_{source,in}$ (°C)	$P_{dis,max}$ = 150 bar	$P_{dis,max}$ = 300 bar
Milk powder	210	37.3	2.48	2.60
Cheese	200	41.1	2.56	2.70
Coffee	210	48.8	2.49	2.65
Starch (wheat, corn, potato)	160	36.1	2.99	3.06
Brewing yeast	145	36.5	3.25	3.31
Dried egg powder	160	41.4	3.03	3.12
Table salt	200	48.6	2.59	2.70
Colour pigments	250	48.3	2.21	2.39
Plastic granulate	118.4	43.2	3.71	3.71
Paper drying	110	55.3	3.94	3.94

Using exhaust heat recovery, in comparison to ambient air source, increased the COP by up to 30.4 %. It should be noted that it was possible for the IHX in the top cycle to be bypassed in the optimisation (resulting in cycle TT-2, thermodynamically). This improves the temperature profile match between the supercritical CO_2 and the sink, while simultaneously leveraging the exhaust heat to superheat the CO_2 coming out of the evaporator. The effect was especially prevalent for higher target sink temperatures, for example, superheating the refrigerant out of the evaporator (IHX cold stream inlet temperature) with a source temperature of 55.3 °C would restrict the gas cooler outlet temperature (IHX hot stream inlet temperature) such that it couldn't be cooled past 60 °C. Bypassing the IHX in this case would allow for the CO_2 to be cooled down further in the gas cooler (better temperature profile match), but the superheat of the refrigerant prior to

compression isn't penalised due to the higher source temperature. The top cycle IHX is much more beneficial to the cycle when the source temperature is lower, e.g. ambient air sourcing, to provide the additional superheat required to minimise the compression requirements.

Ambient air sourcing and exhaust heat recovery have differing benefits and disadvantages. For ambient air sourcing, the source is readily available, and the installation is much simpler, however, the fluctuations in temperature due to weather and seasonal changes can result in prohibitively low performance. Exhaust heat recovery has higher COPs and thus a lower operating cost, but the capital expense would be greater and, depending on the system, the installation could be excessively complex.

7.3.4 Emissions reduction potential

The CO_2-abatement potential of a large temperature glide heat pump is dictated by the emissions factor of the reference fuel that is being displaced, generally coal or natural gas, and the electrical grid emissions factor of the location in which the heat pump is to be installed. The emissions factors of different countries are shown in Figure 69. In countries with low grid emissions, such as Brazil, New Zealand, Switzerland and France, heat pump integration is an evident option for decarbonisation. When the grid is carbon-intensive, such as in India, China, Thailand and Australia, a high COP is required to ensure that the emissions per unit of useful heat are lower than those from the displaced fossil fuel boiler. In these countries, the case for heat pumps is weaker in the short term but strengthens as the grid decarbonises.

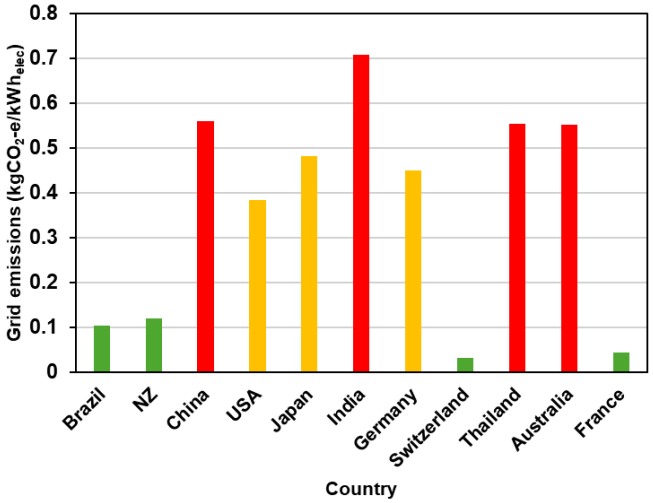

Figure 69. Electricity grid emissions by country, 2024 [181].

The CO_2-abatement potential for the heat pump in comparison to the reference fuel was calculated for different countries for milk powder spray drying (Figure 70), starch drying (Figure 71) and paper drying (Figure 72). Abatement potential was calculated in comparison to natural gas and coal boilers. In the low grid emissions

countries, the CO_2-abatement potential for the heat pump approaches 100 %. For all countries considered, there was significant emissions reduction potential (>40 %) when displacing coal. However, when displacing natural gas heating, the CO_2 abatement was much smaller for countries with high grid emissions factors. The results showed that the emissions would even increase in India if displacing a natural gas boiler in milk powder spray drying with the current grid emissions factor (Figure 70). However, this is an unlikely scenario in comparison to displacing coal as approximately 50 % of India's primary energy consumption is from coal whereas only 6 % is gas [182]. For medium temperature applications (~160 °C), the CO_2 abatement potential increases in comparison, as a result of the higher COPs that can be achieved by the heat pump system (Figure 71). For lower temperature applications such as paper drying, even displacing natural gas heating in a high grid emissions country, like India, could reduce the CO_2 emissions by just over 20 % (Figure 72).

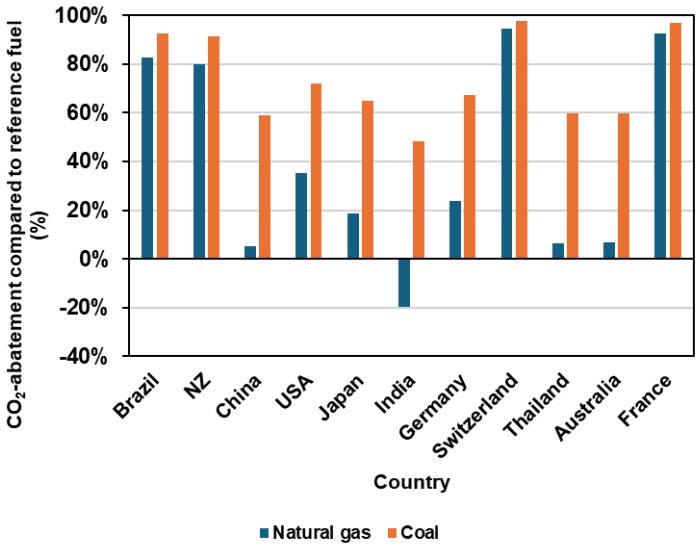

Figure 70. CO_2-abatement compared to reference fuel by country for milk powder drying.

The break-even grid emissions factors for identified applications have been given in Table 32 and Table 33 for ambient air source and exhaust heat recovery, respectively. The break-even emissions factor occurs when the emissions from the electricity consumed by a potential heat pump solution is equal to the emissions from the reference fuel that is to be displaced: coal or natural gas. Therefore, a country with a grid emission factor lower than the break-even grid emissions factor for the heat pump at the target temperature level will result in reduced emissions when displacing the reference fuel with a heat pump. The break-even emissions factors are calculated from the heat pump COP and therefore, the break-even emissions factor is given for the 150 bar maximum pressure constraint and the 300 bar maximum pressure constraint on the heat pump.

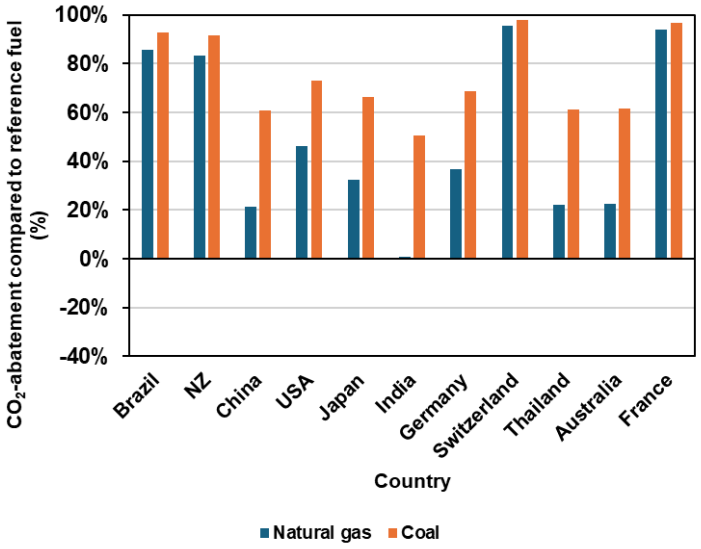

Figure 71. CO_2-abatement compared to reference fuel by country for starch drying.

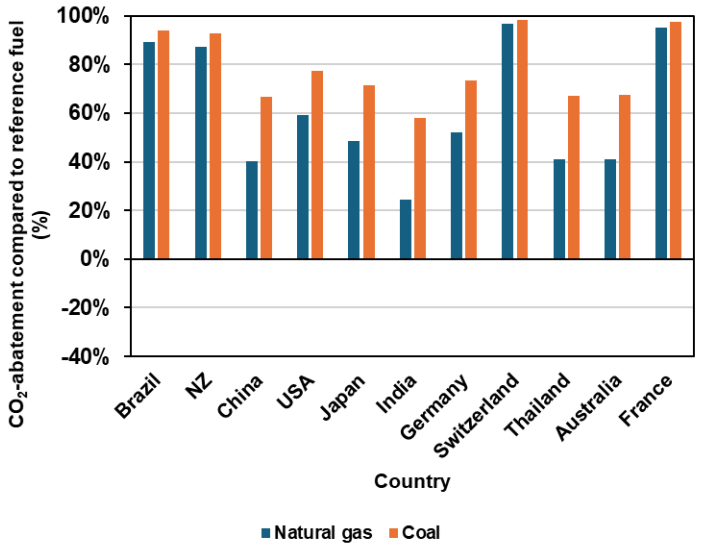

Figure 72. CO_2-abatement compared to reference fuel by country for paper drying.

In nearly all cases, displacing coal through a heat pump will reduce emissions as the break-even grid emissions factor when compared to coal is high (>1.2 $kgCO_2$-e/kWh). Although some countries, such as Turkmenistan, can have emissions factors higher than 1.2 $kgCO_2$-e/kWh, most countries have grid emissions factors below this value, particularly the countries with the highest total emissions, such as China, India and the US [182]. Currently, approximately 75 % of India's electricity mix is supplied by fossil fuels, however, India has committed to 40 % of installed capacity being generated by non-fossil fuel based sources by 2030 [183]. Even with conservative estimates, the projected grid emissions factor in 2030 is 0.55 $kgCO_2$-e/kWh [184], which would increase the temperature that heat could be supplied using a heat pump while abating emissions from approximately 160 °C to 200 °C (Table 32). Simultaneously, lower temperature heat pumping would have greater

CO_2-abatement potential than what would be achieved currently. Zhang et al. [185] predicted that in 2030, the grid emissions for China would also fall to 0.51 $kgCO_2$-e/kWh, which would allow heat up to 250 °C to be supplied with heat pumping while abating emissions (Table 32).

Table 32. Break-even grid emissions factor for each application with ambient air source.

		$e_{f,grid\ (BE)}$ (kgCO₂-e/kWh)			
Application	$T_{sink,out}$ (°C)	$P_{dis,max}$ = 150 bar NG	$P_{dis,max}$ = 150 bar Coal	$P_{dis,max}$ = 300 bar NG	$P_{dis,max}$ = 300 bar Coal
Milk powder	210	0.56	1.30	0.56	1.30
Cheese	200	0.57	1.33	0.57	1.33
Coffee	210	0.56	1.30	0.56	1.30
Starch (wheat, corn, potato)	160	0.63	1.47	0.63	1.47
Brewing yeast	145	0.66	1.53	0.66	1.53
Dried egg powder	160	0.63	1.47	0.63	1.47
Table salt	200	0.54	1.26	0.54	1.26
Colour pigments	250	0.51	1.22	0.51	1.22
Plastic granulate	118.4	0.71	1.65	0.71	1.65
Paper drying	110	0.73	1.68	0.73	1.68

The largest producers of milk powder are New Zealand, China and Brazil [186]. Both New Zealand (0.12 kgCO2-e/kWh) and Brazil (0.103 kgCO2-e/kWh) have grid emissions factors below the break-even for both coal (1.30 kgCO2-e/kWh) and natural gas conversions (0.56 kgCO2-e/kWh). While the grid emissions factor for China (0.56 kgCO2-e/kWh) is approximately equal to the break-even for natural gas conversions, milk powder factories in China that are displacing coal would still benefit from the development of a large temperature glide HTHP. China is also the largest producer of starch, followed by the US and Thailand [175]. At the temperature level of starch drying, all three countries already meet the break-even emissions factor for both natural gas (0.63 kgCO2-e/kWh) and coal (1.47 kgCO2-/kWh). Brazil is also well placed for electrification having a significant share of renewable electricity generation while also being the largest exporter of instant coffee and having significant productions of milk powder and starch (cassava) [187].

Table 33. Break-even grid emissions factor for each application with exhaust heat recovery.

		$e_{f,grid\ (BE)}$ (kgCO₂-e/kWh)			
Application	$T_{sink,out}$ (°C)	$P_{dis,max} =$ 150 bar NG	$P_{dis,max} =$ 150 bar Coal	$P_{dis,max} =$ 300 bar NG	$P_{dis,max} =$ 300 bar Coal
Milk powder	210	0.59	1.44	0.59	1.44
Cheese	200	0.61	1.49	0.61	1.49
Coffee	210	0.59	1.46	0.59	1.46
Starch (wheat, corn, potato)	160	0.71	1.69	0.71	1.69
Brewing yeast	145	0.77	1.83	0.77	1.83
Dried egg powder	160	0.72	1.72	0.72	1.72
Table salt	200	0.62	1.49	0.62	1.49
Colour pigments	250	0.53	1.32	0.53	1.32
Plastic granulate	118.4	0.88	2.05	0.88	2.05
Paper drying	110	0.94	2.17	0.94	2.17

7.3.5 Implementation potential

The integration of HTHPs into industrial processes is inherently complex due to varying process requirements. Not only do variations in process requirements exist across differing industries but many processes which aim to produce even the same product are rarely identical. Variations in operating conditions, plant design, and production strategies all influence how and where heat pumps can be applied. Despite these challenges, opportunities for successful implementation can be realised by considering three key factors:

1) Evaluation and adjustment of "soft" process conditions
2) Centralisation vs. decentralisation
3) Awareness of potential efficiency losses from sources external to the heat pump

"Soft" process conditions refer to operating set points that have generally resulted from design heuristics rather than absolute requirements and can, in some cases, be modified. Modifications to soft process conditions have the potential to improve energy efficiency or facilitate the integration of new technologies. For example, a

dryer with a set point of 220 °C may be able to operate at 200 °C without compromising the product quality. Optimising such set points can significantly reduce the total work consumption of the heat pump [97]. However, these optimisations generally involve trade-offs. In the case of a dryer, lowering the dryer temperature reduces the throughput.

The level of centralisation is another key integration decision. In the case of a steam-generating heat pump, a benefit to centralised heat pumping is that existing steam infrastructure can be reused. Conversely, a decentralised configuration can deliver better performance as the individual heat pumps are optimised for specific processes and temperature levels. Large temperature glide heat pumps offer particular advantages in this context, as they can simultaneously supply multiple process streams across a broad temperature range without efficiency losses. For instance, in milk powder production, the primary drying air must be heated to ~200 °C, while secondary air requires ~100 °C. A CO_2 heat pump can heat all air streams to 100 °C, divert part of the flow for secondary air, and continue heating the remainder to 200 °C, as discussed in Chapter 6. It should be stated that large temperature glide heat pumps are not generally suitable for steam generation due to the high exergy destruction that would occur during heat transfer, unless used to produced pressurised hot water that is flashed to produce steam.

In the integration of high temperature heat pumps, potential efficiency losses that may result from external sources must also be considered. For example, a water or hot oil loop may need to be installed from the heat pump to the heat sink to prevent contamination of the product which would decrease the efficiency of the heat exchange. Additionally, a common process integration method used to integrate heat pumps into a process is Pinch Analysis [30]. However, in the case of large temperature glide HTHPs, the conventional Pinch principles may suggest heat recovery options that degrade the temperature profile match between the refrigerant and the heat sink which could decrease the COP of the heat pump [123].

Sizing is a crucial factor for the development of a large temperature glide HTHP. The MAN CO_2 heat pump is one of the few high temperature CO_2 heat pumps on the market currently and can service very large duties (>10 MW). However, many processes have smaller heating requirements. For example, milk spray dryers generally vary in size from 1 to 30 t/h, which would subsequently require heat pumps that range in size from 500 kW to 15 MW of delivered heating. Despite having an estimated annual thermal energy requirement of 12.8 PJ/year in the EU [162], milk powder spray dryers tend to be smaller (<20 t_p/h), and therefore comprise a suitable market for the smaller capacity heat pumps. Larger capacity heat pump systems would be more suitable for the New Zealand market, where the production capacities of milk powder spray dryers tend to range from 20 – 30 t_p/h. Cassava starch also has a wide variety of production capacities from 1 to 800 t_s/day, with 50 to 800 t_s/day corresponding the size of many factories which operate in Thailand and Brazil [188]. Based on a minimum specific energy requirement of 1361

MJ/t_s [188], an estimation for heat pump sizing would be in the range of 800 kW to 13 MW.

7.3.6 Barriers to implementation and uptake

One of the biggest challenges in the development of CO_2 cycles is the extreme pressures required for transcritical operation for which suitable compressor technology is not yet widely available. The cycle modelled by Sarkar et al. [13] required pressures up to 20 MPa for CO_2. The discharge pressures required in the CO_2 system from Steinberg et al. [189] were up to 27 MPa. Kong et al. [123] performed a numerical evaluation of multiple cascade CO_2 cycles which aimed to lower the discharge pressure requirements required for heating air up to 200 °C. Below 15 MPa, the single-stage cycles were unable to achieve 200 °C heating due to the lack of superheating available prior to compression. MAN Energy Solutions has developed a CO_2 heat pump with an integrated compressor/expander that can achieve a temperature glide of 105 °C for sink heating up to 150 °C and compressor discharge pressure of 13 MPa [190].

Compressor technology for high temperature heat pumps is still in relative infancy. A centrifugal compressor has been developed by Cich et al. [191] which can compress CO_2 at process conditions nearing the conditions required and has been manufactured and tested, however, due to the fluid properties of CO_2, the use of centrifugal compression (such as that used in the MAN heat pump) can be impractical for smaller heat pump systems (at the kW scale) as the rotational speeds required would be extremely high. Smaller CO_2 heat pump systems would likely require piston or (single) screw compression, which introduces the challenge of selecting a suitable lubricant across a large temperature range.

Gas coolers for HTTHPs must be optimised for highly variable heat transfer coefficients along the length of the heat exchanger. In addition to this, supercritical CO_2 heat exchangers must maintain structural integrity under high stress conditions that result from the high temperatures and pressures required. The temperature and pressure requirements for CO_2 HTTHPs can be similar to that required for power cycles. In this application, state of the art heat exchangers include printed circuit heat exchangers, plate fin heat exchangers, micro shell and tube heat exchangers, additive manufacturing heat exchangers and polymer derived ceramic composite heat exchangers [192].

Like other HTHPs, the financial viability of large temperature glide heat pumps is highly dependent on the electricity-to-reference-fuel price ratio [193]. An unfavourable environment for investment in this technology occurs when the electricity-to-reference-fuel price ratios are high, such as is the case in Germany where the electricity to gas price ratio was 4 in 2021 [123]. In the study from Kong et al. [123], electricity-to-reference price ratio of 2.06 or below was required for the heat pump to be economically viable which has already been achieved in some Scandinavian countries.

In terms of emissions, the grid emissions factor of the country which the heat pump is being installed needs to be considered. For highly emissive electrical grids, a very high COP is required to achieve any net emissions reduction. Additionally, policies tied to carbon pricing or emissions reporting may penalise those considering heat pump integration if the upstream grid emissions are high. This could reduce investment incentives or create stranded assets if grids decarbonise slowly. In high grid emissions areas, direct electrification may be less attractive compared to hybrid systems, e.g. heat pump + biomass boiler or electrode boiler + biomass boiler, or measures to first reduce grid emissions, such as investment in renewable generation.

7.4 Conclusions

The wider application potential of a CO_2 HTTHP was evaluated to demonstrate a possible market, in terms of size and location, and the emissions reduction that could be achieved through the development of this new technology. The integration of HTHPs for an industrial process heat user is complex due to many reasons, which includes identification of suitable source and sink temperatures. This chapter collated promising candidate applications for the heat pump concept proposed by this thesis. The proposed heat pump is unique in that it provides both a large temperature glide and large temperature lift, which was found to be particularly suitable for drying processes. Sixteen applications, with possible sink and source streams, were identified, including drying for starch and instant coffee production.

An estimation of the global heat potential demonstrated that large-scale deployment of this type of technology could displace a significant amount of fossil fuel based heating demand, exceeding hundreds of PJ/year. Starch drying alone was estimated to have a global heat demand of up to 310 PJ/year. Dryers span a broad range of capacities, necessitating heat pump systems sized between 500 kW and 15 MW of delivered heating.

The COPs for each of the applications, using cycle TT-4, were calculated. COPs between 2.0 and 3.05 were achieved for sink outlet temperatures from 110 °C to 280 °C. These COPS were used to determine the break-even grid emissions factors, showing that the heat pump will reduce emissions in nearly all countries when compared to coal for all temperature levels considered. When displacing natural gas, either a lower grid emissions factor or a higher COP (or both) is required for emissions reduction to occur. For example, in India, which had a grid emissions factor of 0.708 $kgCO_2$-e, emissions reduction only occurs when the COP is higher than 3 (a temperatures below 160 °C for the TT-4 cycle).

In summary, the results demonstrate that a CO_2 HTTHP with a large temperature glide is technically feasible across a wide range of industrial processes, with the potential to supply tens to hundreds of PJ/year of low-carbon heat globally. Key challenges remain in addressing high operating pressures, ensuring the availability

of suitable componentry, and optimising process integration. The novel contribution of this chapter lies in providing a cross-sectoral assessment of the decarbonisation potential of a large temperature glide CO_2 HTTHP which quantifies efficiency, sizing, and emissions outcomes across multiple industries, demonstrating the broad relevance and emissions abatement potential of the proposed technology.

Chapter 8
Conclusions and future work

8.1 Conclusions

The primary aim of this thesis was to develop, evaluate and contextualise a new high temperature transcritical CO_2 heat pump concept capable of supplying industrial process heat for spray drying and like applications. The research was motivated by the need to provide low emissions heating solutions for existing industrial processes that are significant contributors to the economy, such as milk powder spray drying. Through a combination of thermodynamic modelling of cycle architectures, the integration of a selected architecture into a milk powder spray drying case study, and a wider lens on the global potential, this thesis has collated insight into how CO_2 heat pump technology can be applied to large temperature glide processes and has identified economic and environmental implications for implementation. This chapter amalgamates the key findings from the preceding chapters of this thesis, outlines the original contributions of the research, and presents recommendations for future work to further the deployment of high temperature CO_2 heat pumps for industrial decarbonisation.

8.1.1 Thermodynamic modelling of cycle architectures

Six cycles were investigated in Chapter 4 that combined aspects of internal heat exchange and cascade arrangements. A transcritical-transcritical cascade with internal heat exchangers in both the top and bottom cycles (TT-4) achieved the highest COP of 2.22 for sink outlet temperature of 200 °C and maximum compressor discharge pressure of 150 bar. Both internal heat exchangers and cascade arrangements increased the maximum sink temperature that could be produced by the heat pump through superheating the compressor inlet. Having internal heat exchangers in the bottom cycle of the cascade had a particularly large effect on the maximum sink temperature. Exergy analysis revealed that significant exergy destruction occurred during expansion, especially in two models (TT-1 and TT-2) that had fewer components than TT-4 but similar COPs. This provided the basis for exploring expansion work recovery, which was subsequently investigated in Chapter 5.

8.1.2 Expansion work recovery

Expansion work recovery, using ejectors and expanders, was evaluated as a means of reducing exergy destruction and improving overall system performance. The expander heat pump cycles achieved moderate performance improvements, increasing the COPs by approximately 0.1 to 0.12 compared to the equivalent original cycle concept, while ejectors provided marginal, if any, thermodynamic benefit. A break-even cost was estimated which required expanders to cost less

than 297 NZD/kW of delivered heat (from the heat pump) to be more viable than the equivalent original cycle concept.

While the inclusion of an ejector tended to improve the performance of the respective top or bottom cycle that contained it, it generally caused exergy destruction in other parts of the cycle to increase. This results in barely any benefit to the overall heat pump cycle from the inclusion of an ejector. Additionally, the ejector decreased the maximum sink temperature that could be achieved by the heat pump for the same evaporation temperatures as the pressure ratio decreased. While this is beneficial for increasing performance in refrigeration systems, where ejectors are usually used, it was not beneficial for the high temperature heat pump cycles that were investigated. As a result of these findings, the analysis in the following chapters proceeded with cycle TT-4, which was the highest performing cycle in Chapter 4.

8.1.3 Integration – milk powder spray drying case study

Chapter 6 compared integration options which investigated the chosen heat pump cycle, TT-4, and alternative fuel-switching options, biomass, and electrode boilers. Both standalone and hybrid configurations were assessed to determine the operating cost and emissions reduction potential. The analysis revealed that the non-linear sensible cooling of supercritical CO_2 could be exploited by using multiple gas coolers, i.e., multi-temperature heat pumping. This increased the COP from 2.22 in Chapter 4 to 2.55 as a result of better temperature profile matching between the refrigerant and the sink streams. The lowest operating cost solution depended largely on the electricity-to-biomass price ratio, with heat pumps becoming more favourable below a price ratio of 2.75 while price ratios above 3.75 favoured full biomass conversion. Between these values, a hybrid configuration, where the heat pump is used to heat the air to 102 °C and the biomass boiler was used to provide the remaining heating, had the lowest cost.

The results showed that full heat pump electrification could reduce emissions by approximately 55 to 94 % compared to a reference coal boiler, and by up to 97 % in the hybrid configurations. These findings confirm that high temperature CO_2 heat pumps can be technically and economically competitive within the dairy processing sector under realistic energy pricing conditions, while offering substantial emissions reductions.

8.1.4 Wider decarbonisation potential

Chapter 7 evaluated the broader potential for industrial deployment of high temperature CO_2 heat pumps beyond the dairy industry. By estimating the process heat demand and corresponding sink and source temperature levels across multiple industrial processes, it was shown that high temperature CO_2 heat pumps could supply tens to hundreds of petajoules per year of low emissions heat globally, mainly for drying processes. COPs between 2 and 3 were achievable for sink outlet temperatures between 110 and 280 °C depending on the process conditions. The emissions reduction potential was undeniable when displacing coal-fired boilers,

however, emissions reduction potential can be limited when displacing natural gas boilers in regions with high grid emissions factors. At present, New Zealand, Brazil, and parts of Europe are good candidates for electrification using heat pumps. Many countries are trending towards lower emissions electrical grids, which supports the implementation of high temperature heat pump technology.

8.2 Contributions

The key contributions of this thesis to the field of industrial process heat decarbonisation are:

1. **Novel high temperature CO_2 heat pump concept:** Developed and evaluated a new transcritical-transcritical cascade CO_2 heat pump cycle capable of achieving up to 200 °C sink outlet temperatures with a temperature glide of 185 °C and a temperature lift of approximately 180 °C.
2. **Exergy analysis of ejectors and expanders in high temperature CO_2 heat pump cycles**: Evaluated the effect of ejectors and expanders on the performance of high temperature transcritical CO_2 heat pump cycles.
3. **A comparison of integration options for low-emissions technology into milk powder spray drying:** Quantified the operational cost competitiveness and emissions reduction for various energy price scenarios and calculated the break-even electricity-to-biomass price ratios for the different heating scenarios: full electrification using a heat pump, fuel switching to biomass or electrode boilers, or a hybrid configuration.
4. **Analysis of global potential for a high temperature CO_2 heat pump including process applications and potential source and sink temperatures:** Provided comprehensive estimates of the decarbonisation potential specific to large temperature glide heat pumps across multiple process sectors including estimated COPs and emissions reduction.

8.3 Recommendations for future work

Building on the outcomes of this thesis, future research should focus on addressing the remaining technical, economic, and integration challenges that currently limit large-scale deployment of high temperature CO_2 heat pumps.

8.3.1 Component development and testing

While the research of this thesis aimed to limit the required pressures of CO_2 compressors, operation at elevated temperatures remains a challenge. One way to mitigate this is through the use of oil-free centrifugal compressors; however, centrifugal compressors struggle to operate efficiently at sub-MW capacities. The accuracy of the heat pump modelling is also highly influenced by the accuracy of the efficiency assumptions and at present, the market for CO_2 compressors for high temperature heat pumps is underdeveloped. The field of high temperature CO_2 heat pumps would benefit greatly from the development of a small scale (100 kW to 1 MW) CO_2 compressor, particularly in the aspects of the mechanical design. Developments in expander technologies, such that the capital cost can eventually

reach the economic break-even, would also be a valuable area for future research as it was shown that expanders increase the COPs of the heat pump systems.

8.3.2 Prototype design and experimental validation

Industrial confidence in high temperature CO_2 heat pumps will always waver without a physical system that has been demonstrated. Therefore, future research should include the construction of a pilot-scale heat pump system to experimentally validate the modelling results and identify practical engineering constraints. This would also provide the basis for investigating the transient behaviour, start-up, and part-load characteristics to inform real-world implementation.

8.3.3 Further integration opportunities

Future research should investigate additional opportunities for high temperature CO_2 heat pumps within industrial sites. Chapter 6 investigated the integration of a high temperature CO_2 heat pump in the milk powder spray drying process. The analysis looked at two temperature levels: one at 102 °C for both the static and vibrating fluidised beds and the other at 200 °C for the primary dryer air. Another promising avenue could be to decentralise the vibrating fluidised bed air heating at approximately 70 °C and consider upstream parts of the plant, such as evaporation and pasteurisation. Supplying this heat with a separate, lower temperature heat pump could yield significantly higher COPs in comparison to using a singular large-scale CO_2 heat pump. Not only this, but this lower temperature heat pump could also simultaneously meet other applications on site such as the hot water requirements for clean-in-place (CIP) at around 85 °C.

Current process integration methods are not fully optimised for high temperature heat pump integration. Many process integration methods are focussed on first recovering heat within the process and then using a heat pump to upgrade what is left over. However, with high temperature heat pumps (using any refrigerant), there is a high possibility that conventional process integration methods would suggest a heat pump solution where the temperature glide and temperature lift have been unnecessarily increased. In the case of a CO_2 high temperature heat pump, the temperature glide could also be unnecessarily decreased, degrading the temperature profile match between the refrigerant and the heat sink stream.

Future research could also include a comparison in system efficiency and levelised cost between a decentralised heat pump, such as the one in investigated in this thesis, and a centralised heat pump configuration, such as a steam-generating heat pump. It is expected there would be a trade-off between the heat pump efficiency and invested capital under which each configuration becomes most advantageous for the retrofit of a specified industrial application.

References

[1] Ministry for the Environment, "Climate Change Response (Zero Carbon) Amendment Act 2019," Ministry for the Environment. Accessed: May 18, 2021. [Online]. Available: https://environment.govt.nz/acts-and-regulations/acts/climate-change-response-amendment-act-2019/

[2] TDB Advisory Ltd, "The Dairy Sector in New Zealand: Extending the Boundaries," New Zealand Productivity Commission, Oct. 2020. [Online]. Available: https://www.productivity.govt.nz/assets/Inquiries/frontier-firms/a977484e51/The-dairy-sector-in-NZ-TDB-Advisory.pdf

[3] Energy Efficiency and Conservation Authority and Ministry of Businesss, Innovation & Employment, "Dairy Manufacturing - Process Heat and Greenhouse Gas Emissions," 2018. Accessed: Aug. 29, 2021. [Online]. Available: https://www.mbie.govt.nz/dmsdocument/151-dairy-maufacturing-fact-sheet-pdf

[4] Ministry of Business, Innovation and Employment, "Phasing out fossil fuels in process heat: national direction on industrial greenhouse gas emissions consultation document," Wellington, 2021. [Online]. Available: https://environment.govt.nz/assets/Publications/phasing-out-fossil-fuels-in-process-heat.pdf

[5] "Fonterra's Decarbonisation Journey," Fonterra. Accessed: Oct. 09, 2025. [Online]. Available: https://www.fonterra.com/nz/en/sustainability/planet/climate/decarbonisation-journey.html

[6] Ministry of Business, Innovation and Employment, "Energy in New Zealand 2020." Aug. 2020. Accessed: May 20, 2021. [Online]. Available: https://www.mbie.govt.nz/dmsdocument/11679-energy-in-new-zealand-2020

[7] S. Madeddu *et al.*, "The CO2 reduction potential for the European industry via direct electrification of heat supply (power-to-heat)," *Environ. Res. Lett.*, vol. 15, no. 12, p. 124004, Nov. 2020, doi: 10.1088/1748-9326/abbd02.

[8] K.-M. Adamson *et al.*, "High-temperature and transcritical heat pump cycles and advancements: a review," *Renewable and Sustainable Energy Reviews*, 2022.

[9] Marcos Pelenur, "Response to Official Information Act Request for EECA funded projects," Oct. 04, 2023. [Online]. Available: https://www.eeca.govt.nz/assets/EECA-Resources/OIA-responses/Biomass-Projects.pdf

[10] EECA, "Heat is on to find alternative energy sources," EECA. Accessed: Oct. 09, 2025. [Online]. Available: https://www.eeca.govt.nz/insights/case-studies-and-articles/heat-is-on-to-find-alternative-energy-sources/

[11] E. Klinac, J. K. Carson, D. Hoang, Q. Chen, D. J. Cleland, and T. G. Walmsley, "Multi-Level Process Integration of Heat Pumps in Meat Processing," *Energies*, vol. 16, no. 8, p. 3424, Jan. 2023, doi: 10.3390/en16083424.

[12] T. Trevisan, "European Parliament Approves Bans of HFCs and HFOs in Multiple Applications and HFC Phase Out by 2050," Natural Refrigerants. Accessed: Jan. 06, 2025. [Online]. Available: https://naturalrefrigerants.com/european-parliament-approves-bans-of-hfcs-and-hfos-in-multiple-applications-and-hfc-phase-out-by-2050/

[13] J. Sarkar, S. Bhattacharyya, and M. Ram Gopal, "Natural refrigerant-based subcritical and transcritical cycles for high temperature heating," *International*

Journal of Refrigeration, vol. 30, no. 1, pp. 3–10, Jan. 2007, doi: 10.1016/j.ijrefrig.2006.03.008.
[14] R. U. Rony, H. Yang, S. Krishnan, and J. Song, "Recent Advances in Transcritical CO2 (R744) Heat Pump System: A Review," *Energies*, vol. 12, no. 457, 2019.
[15] M. Tammaro, C. Montagud, J. M. Corberán, A. W. Mauro, and R. Mastrullo, "Seasonal performance assessment of sanitary hot water production systems using propane and CO2 heat pumps," *International Journal of Refrigeration*, vol. 74, pp. 224–239, Feb. 2017, doi: 10.1016/j.ijrefrig.2016.09.026.
[16] B. T. Austin and K. Sumathy, "Transcritical carbon dioxide heat pump systems: A review," *Renewable and Sustainable Energy Reviews*, vol. 15, pp. 4013–4029, 2011.
[17] Cordin Arpagaus, "High-Temperature Heat Pumps: Market Overview, State of the Art, and Application Potential," presented at the EECA HTHP Workshop, Auckland, New Zealand, Feb. 24, 2025.
[18] Piller Blowers and Compressors GmbH, "Piller VapoFan High Speed Blowers for MVR Processes." Jan. 2021. Accessed: Mar. 31, 2022. [Online]. Available: https://www.piller.de/fileadmin/media/pdf-files/product-sheets/VapoFan-high-speed-blowers.pdf
[19] "GEA RedAstrum." Accessed: Sep. 10, 2025. [Online]. Available: https://www.gea.com/en/products/heat-pumps/redastrum-ammonia-heatpump/
[20] N. Kabat, E. Jende, E. Nicke, and P. Stathopoulos, "Investigation on Process Architectures for High-Temperature Heat Pumps Based on a Reversed Brayton Cycle," in *Volume 5: Cycle Innovations*, Boston, Massachusetts, USA: American Society of Mechanical Engineers, Jun. 2023, p. V005T06A015. doi: 10.1115/GT2023-102497.
[21] J. Yoo, C. E. Estrada-Perez, and B.-H. Choi, "Investigation of heat pump technologies for high-temperature applications above 250 °C," *Applied Energy*, vol. 384, p. 125384, Apr. 2025, doi: 10.1016/j.apenergy.2025.125384.
[22] S. Thapa, "Norwegian OEM Enerin Successfully Tests Helium High-Temperature Heat Pump," Natural Refrigerants. Accessed: Feb. 11, 2026. [Online]. Available: https://naturalrefrigerants.com/news/norwegian-oem-enerin-as-successfully-tests-helium-high-temperature-heat-pump-in-biogas-facility/
[23] Annex 58, "Reversed Stirling Cycle | Olvondo Technology AS." 2022. [Online]. Available: https://heatpumpingtechnologies.org/annex58/wp-content/uploads/sites/70/2022/07/olvondo-highlift.pdf
[24] O. Bamigbetan, T. M. Eikevik, P. Nekså, and M. Bantle, "Review of vapour compression heat pumps for high temperature heating using natural working fluids," *International Journal of Refrigeration*, vol. 80, pp. 197–211, Aug. 2017, doi: 10.1016/j.ijrefrig.2017.04.021.
[25] American Society of Heating, Refrigerating and Air-Conditioning Engineers, Inc., *Designation and Safety Classification of Refrigerants*, 34–2007, 2008. [Online]. Available: https://www.ashrae.org/File%20Library/Technical%20Resources/Standards%20and%20Guidelines/Standards%20Addenda/34m_thru_34v_FINAL.pdf
[26] F. Bühler, B. Zühlsdorf, T.-V. Nguyen, and B. Elmegaard, "A comparative assessment of electrification strategies for industrial sites: Case of milk powder production," *Applied Energy*, vol. 250, pp. 1383–1401, Sep. 2019, doi: 10.1016/j.apenergy.2019.05.071.
[27] "Ammonia Refrigeration - Overview | Occupational Safety and Health Administration." Accessed: Aug. 14, 2025. [Online]. Available: https://www.osha.gov/ammonia-refrigeration

[28] A. S. Gaur, D. Z. Fitiwi, and J. Curtis, “Heat pumps and our low-carbon future: A comprehensive review,” *Energy Research & Social Science*, vol. 71, p. 101764, Jan. 2021, doi: 10.1016/j.erss.2020.101764.
[29] J. J. Aguilera *et al.*, “A review of common faults in large-scale heat pumps,” *Renewable and Sustainable Energy Reviews*, vol. 168, p. 112826, Oct. 2022, doi: 10.1016/j.rser.2022.112826.
[30] F. Schlosser, M. Jesper, J. Vogelslang, T. G. Walmsley, C. Arpagaus, and J. Hesselbach, “Large-scale heat pumps: Applications, performance, economic feasibility and industrial integration,” *Renewable and Sustainable Energy Reviews*, vol. 133, 2020.
[31] B. J. Lincoln, L. Kong, A. M. Pineda, and T. G. Walmsley, “Process integration and electrification for efficient milk evaporation systems,” *Energy*, vol. 258, p. 124885, Nov. 2022, doi: 10.1016/j.energy.2022.124885.
[32] EECA, “About the Government Investment in Decarbonising Industry Fund,” EECA. Accessed: Oct. 17, 2022. [Online]. Available: https://www.eeca.govt.nz/co-funding/industry-decarbonisation/about-the-government-investment-in-decarbonising-industry-fund/
[33] R. Yokoyama, T. Shimizu, K. Ito, and K. Takemura, “Influence of ambient temperatures on performance of a CO2 heat pump water heating system,” *Energy*, vol. 32, no. 4, pp. 388–398, Apr. 2007, doi: 10.1016/j.energy.2006.06.020.
[34] Annex 58, “Task 1 - Technologies,” Annex 58. Accessed: Jan. 23, 2023. [Online]. Available: https://heatpumpingtechnologies.org/annex58/task1/
[35] Annex 58, “Task 1 - Technologies,” Annex 58. Accessed: Jun. 14, 2024. [Online]. Available: https://heatpumpingtechnologies.org/annex58/task1/
[36] Annex 58, “High Temperature Heat Pump for Steam Production at AstraZeneca.” 2022. [Online]. Available: https://heatpumpingtechnologies.org/annex58/wp-content/uploads/sites/70/2022/07/caseastrazenecaolvondo.pdf
[37] Annex 58, “Large Heat Pumps Turboden S.p.A.” Dec. 2023. [Online]. Available: https://heatpumpingtechnologies.org/annex58/wp-content/uploads/sites/70/2024/01/20231222hthpannex58templatesuppliertechnologyrev3.pdf
[38] Annex 58, “Steam Grow Heat Pump / SGH165,” 2022. [Online]. Available: https://heatpumpingtechnologies.org/annex58/wp-content/uploads/sites/70/2022/07/technologykobelcosgh165.pdf
[39] Annex 58, “Boiler 2.0 | AtmosZero,” Aug. 2024. [Online]. Available: https://heatpumpingtechnologies.org/annex58/wp-content/uploads/sites/70/2024/09/annex58azboiler20.pdf
[40] Annex 58, “Rotation Heat Pump | ecop Technologies GmbH.” 2022. [Online]. Available: https://heatpumpingtechnologies.org/annex58/wp-content/uploads/sites/70/2022/07/hthpannex58ecopv2.pdf
[41] Annex 58, “Screw compressor high-temperature heat pump | Rank.” 2022. [Online]. Available: https://heatpumpingtechnologies.org/annex58/wp-content/uploads/sites/70/2022/07/hthpannex58templatesuppliertechnologyrankfinal.pdf
[42] Annex 58, “Screw compressor for water vapor heat pump technology | Svenska Rotor Maskiner International AB.” 2022. [Online]. Available: https://heatpumpingtechnologies.org/annex58/wp-content/uploads/sites/70/2022/07/srmhthpannex58final.pdf

[43] Annex 58, “ThermBooster | SPH Sustainable Process Heat GmbH.” 2022. [Online]. Available: https://heatpumpingtechnologies.org/annex58/wp-content/uploads/sites/70/2022/07/sph-thermbooster.pdf
[44] Annex 58, “HeatBooster | Heaten.” 2023. [Online]. Available: https://heatpumpingtechnologies.org/annex58/wp-content/uploads/sites/70/2023/12/hthpannex58templatesuppliertechnologyrev4-v3.pdf
[45] Annex 58, “HoegTemp UHT Heat Pump | Enerin AS.” 2023. [Online]. Available: https://heatpumpingtechnologies.org/annex58/wp-content/uploads/sites/70/2023/11/enerin-hoegtemp-v2.pdf
[46] Annex 58, “ETES CO2 Heat Pump - MAN Energy Solutions.” 2022. [Online]. Available: https://heatpumpingtechnologies.org/annex58/wp-content/uploads/sites/70/2022/07/man-es-etes-co2-hthp-system.pdf
[47] Annex 58, “Industrial Heat Pump | Siemens Energy.” 2022. [Online]. Available: https://heatpumpingtechnologies.org/annex58/wp-content/uploads/sites/70/2022/07/siemens-energy-hthp-technology.pdf
[48] Annex 58, “Steam compressor for steam recycling at pulp drying with pressurized superheated steam dryer (PSSD).” 2022. [Online]. Available: https://heatpumpingtechnologies.org/annex58/wp-content/uploads/sites/70/2022/07/spillinghthpannex58democaseifinal-1.pdf
[49] F. Cao, Z. Ye, and Y. Wang, “Experimental investigation on the influence of internal heat exchanger in a transcritical CO2 heat pump water heater,” *Applied Thermal Engineering*, vol. 168, 2019.
[50] F. Cao, Y. Wang, and Z. Ye, “Theoretical analysis of internal heat exchanger in transcritical CO2 heat pump systems and its experimental verification,” *International Journal of Refrigeration*, vol. 106, pp. 506–516, Oct. 2019, doi: 10.1016/j.ijrefrig.2019.05.022.
[51] N. Fernandez, Y. Hwang, and R. Radermacher, “Comparison of CO2 heat pump water heater performance with baseline cycle and two high COP cycles,” *International Journal of Refrigeration*, vol. 33, no. 3, pp. 635–644, May 2010, doi: 10.1016/j.ijrefrig.2009.12.008.
[52] L. Cecchinato *et al.*, “Thermodynamic analysis of different two-stage transcritical carbon dioxide cycles,” *International Journal of Refrigeration*, vol. 32, no. 5, pp. 1058–1067, Aug. 2009, doi: 10.1016/j.ijrefrig.2008.10.001.
[53] N. Agrawal, S. Bhattacharyya, and J. Sarkar, “Optimization of two-stage transcritical carbon dioxide heat pump cycles,” *International Journal of Thermal Sciences*, vol. 46, no. 2, pp. 180–187, Feb. 2007, doi: 10.1016/j.ijthermalsci.2006.04.011.
[54] S. Lecompte *et al.*, “Review of Experimental Research on Supercritical and Transcritical Thermodynamic Cycles Designed for Heat Recovery Application,” *Applied Sciences*, vol. 9, no. 12, Art. no. 12, Jan. 2019, doi: 10.3390/app9122571.
[55] D. Wu, B. Hu, and R. Z. Wang, “Performance simulation and exergy analysis of a hybrid source heat pump system with low GWP refrigerants,” *Renewable Energy*, vol. 116, pp. 775–785, Feb. 2018, doi: 10.1016/j.renene.2017.10.024.
[56] W. Yang, X. Cao, Y. He, and F. Yan, “Theoretical study of a high-temperature heat pump system composed of a CO2 transcritical heat pump cycle and a R152a subcritical heat pump cycle,” *Applied Thermal Engineering*, vol. 120, pp. 228–238, Jun. 2017, doi: 10.1016/j.applthermaleng.2017.03.098.
[57] L. Yao, M. Li, Y. Hu, Q. Wang, and X. Liu, “Comparative study of upgraded CO2 transcritical air source heat pump systems with different heat sinks,” *Applied*

Thermal Engineering, vol. 184, p. 116289, Feb. 2021, doi: 10.1016/j.applthermaleng.2020.116289.
[58] C. Arpagaus, F. Bless, J. Schiffmann, and S. S. Bertsch, "Multi-temperature heat pumps: A literature review," *International Journal of Refrigeration*, vol. 69, pp. 437–465, Sep. 2016, doi: 10.1016/j.ijrefrig.2016.05.014.
[59] Y. T. Jiang, "Research on CO2 transcritical water-water heat pump and two-rolling piston expander," Tianjin University, China, 2009.
[60] J. Sarkar, S. Bhattacharyya, and M. R. Gopal, "Transcritical CO2 heat pump systems: exergy analysis including heat transfer and fluid flow effect," *Energy Conversion and Management*, vol. 46, pp. 2053–2067, 2005, doi: 10.1016/j.enconman.2004.10.022.
[61] Z. Ye, Y. Wang, Y. Song, X. Yin, and F. Cao, "Optimal discharge pressure in transcritical CO2 heat pump water heater with internal heat exchanger based on pinch point analysis," *International Journal of Refrigeration*, vol. 118, pp. 12–20, Oct. 2020, doi: 10.1016/j.ijrefrig.2020.06.003.
[62] S. Singh and M. Dasgupta, "Evaluation of research on CO2 trans-critical work recovery expander using multi attribute decision making methods," *Renewable and Sustainable Energy Reviews*, vol. 59, pp. 119–129, Jun. 2016, doi: 10.1016/j.rser.2016.01.013.
[63] Y. Ma, Z. Liu, and H. Tian, "A review of transcritical carbon dioxide heat pump and refrigeration cycles," *Energy*, vol. 55, pp. 156–172, Jun. 2013, doi: 10.1016/j.energy.2013.03.030.
[64] J. Sarkar, "Ejector enhanced vapor compression refrigeration and heat pump systems—A review," *Renewable and Sustainable Energy Reviews*, vol. 16, no. 9, pp. 6647–6659, Dec. 2012, doi: 10.1016/j.rser.2012.08.007.
[65] Y. Zhu, Y. Huang, C. Li, F. Zhang, and P.-X. Jiang, "Experimental investigation on the performance of transcritical CO2 ejector–expansion heat pump water heater system," *Energy Conversion and Management*, vol. 167, pp. 147–155, Jul. 2018, doi: 10.1016/j.enconman.2018.04.081.
[66] X. X. Xu, G. M. Chen, L. M. Tang, and Z. J. Zhu, "Experimental investigation on performance of transcritical CO2 heat pump system with ejector under optimum high-side pressure," *Energy*, vol. 44, no. 1, pp. 870–877, Aug. 2012, doi: 10.1016/j.energy.2012.04.062.
[67] M. Nakagawa, A. R. Marasigan, and T. Matsukawa, "Experimental analysis on the effect of internal heat exchanger in transcritical CO2 refrigeration cycle with two-phase ejector," *International Journal of Refrigeration*, vol. 34, no. 7, pp. 1577–1586, Nov. 2011, doi: 10.1016/j.ijrefrig.2010.03.007.
[68] L. Hays and J. J. Brasz, "A transcritical CO2 turbine-compressor," *International Compressor Engineering Conference*, 2004.
[69] Y. Zhang, X. Wei, and X. Qin, "Experimental study on energy, exergy, and exergoeconomic analyses of a novel compression/ejector transcritical CO2 heat pump system with dual heat sources," *Energy Conversion and Management*, vol. 271, p. 116343, Nov. 2022, doi: 10.1016/j.enconman.2022.116343.
[70] GEA Refrigeration Netherlands, "GEA CO2 Heat Pump." Annex 58, 2022. [Online]. Available: https://heatpumpingtechnologies.org/annex58/wp-content/uploads/sites/70/2022/07/hthpannex58suppliertechnologygea.pdf
[71] Dürr thermea GmbH, "CO2 Refrigeration Machines and High Temperature Heat Pumps." 2016. [Online]. Available: https://d3pcsg2wjq9izr.cloudfront.net/files/616/download/704734/2.pdf
[72] Mayekawa Mfg, "CO2 Air Heat Heat Pump/Eco Sirocco," 2022, *Annex 58*. Accessed: Nov. 22, 2022. [Online]. Available:

https://heatpumpingtechnologies.org/annex58/wp-content/uploads/sites/70/2022/07/technologymayekawaecosirocco-1.pdf
[73] Mayekawa Mfg, "Unimo AW." 2013. [Online]. Available: https://mayekawa.com.au/494/wp-content/uploads/2013/07/unimoAW_Flyer100713.pdf
[74] Mitsubishi Heavy Industries, "High efficiency CO2 hot water solution - Q-ton: Air to water," New Zealand, 2020. [Online]. Available: https://mhiheatpumps.co.nz/document/q-ton-brochure/
[75] Atlas Copco AB, "Eight-stage 200-bar CO2 compressor." 2016. [Online]. Available: https://www.atlascopco.com/content/dam/atlas-copco/compressor-technique/gas-and-process/documents/Atlas%20Copco%20GAP%208%20Stage%20200%20bar%20CO2%20compressor.pdf
[76] P. Neksa, H. Rekstad, G. Zakeri, P. Schiefloe, and M. Svensson, "Commercial heat pumps for water heating and heat recovery," presented at the Workshop on CO2 Technology in Refrigeration, Heat Pump and Air Conditioning Systems, Mainz, Germany, 1999.
[77] M. Chamoun, R. Rulliere, P. Haberschill, and J. F. Berail, "Dynamic model of an industrial heat pump using water as refrigerant," *International Journal of Refrigeration*, vol. 35, no. 4, pp. 1080–1091, Jun. 2012, doi: 10.1016/j.ijrefrig.2011.12.007.
[78] GEA Bock GmbH, "GEA Bock CO2 Compressors." 2015. [Online]. Available: https://vap.bock.de/Documentation/Data/DocumentationFiles/96219_CO2%20Compressor_Gb.pdf
[79] Emerson Climate Technologies, Inc., "Copeland™ compressors for transcritical CO2 refrigeration." 2021. [Online]. Available: https://climate.emerson.com/documents/copeland-compressors-for-transcritical-co2-refrigeration-en-us-2884908.pdf
[80] "BITZER Software." Accessed: Jan. 07, 2023. [Online]. Available: https://www.bitzer.de/websoftware/Calculate.aspx?cid=1673056103175&mod=HHK
[81] "CO2 - carbon dioxide," Mehrer Compression GmbH. Accessed: Jan. 07, 2023. [Online]. Available: https://www.mehrer.de/en/applications/carbon-dioxide
[82] Dorin Innovation, "CD Series." 2023. [Online]. Available: https://www.dorin.com/documents/Download/18/1LTZ016_CD_02.22_rev.pdf
[83] R. C. Decovert and E. Jacquemoud, "Industrial heat pumps," 2021, *MAN Energy Solutions*.
[84] C. You, B. Michel, and R. Revellin, "Transcritical carbon dioxide heat pump cycle: Validation and comparison of one-dimensional models of ejector with independent data sets," *Applied Thermal Engineering*, vol. 213, p. 118668, Aug. 2022, doi: 10.1016/j.applthermaleng.2022.118668.
[85] Z. Zhang, X. Feng, D. Tian, J. Yang, and L. Chang, "Progress in ejector-expansion vapor compression refrigeration and heat pump systems," *Energy Conversion and Management*, vol. 207, p. 112529, Mar. 2020, doi: 10.1016/j.enconman.2020.112529.
[86] S. Elbel and N. Lawrence, "Review of recent developments in advanced ejector technology," *International Journal of Refrigeration*, vol. 62, pp. 1–18, Feb. 2016, doi: 10.1016/j.ijrefrig.2015.10.031.
[87] J. Sarkar, "Optimization of ejector-expansion transcritical CO2 heat pump cycle," *Energy*, vol. 33, no. 9, pp. 1399–1406, Sep. 2008, doi: 10.1016/j.energy.2008.04.007.

[88] X. Qin, Y. Zhang, D. Wang, and J. Chen, “System development and simulation investigation on a novel compression/ejection transcritical CO2 heat pump system for simultaneous cooling and heating,” *Energy Conversion and Management*, vol. 259, p. 115579, May 2022, doi: 10.1016/j.enconman.2022.115579.
[89] K. Sumeru, H. Nasution, and F. N. Ani, “A review on two-phase ejector as an expansion device in vapor compression refrigeration cycle,” *Renewable and Sustainable Energy Reviews*, vol. 16, no. 7, pp. 4927–4937, Sep. 2012, doi: 10.1016/j.rser.2012.04.058.
[90] M. J. Bergander, “Refrigeration cycle with two-phase condensing ejector,” *International Refrigeration and Air Conditioning Conference*, 2006, [Online]. Available: https://docs.lib.purdue.edu/cgi/viewcontent.cgi?article=1747&context=iracc
[91] X. Chen, Y. Zhou, and J. Yu, “A theoretical study of an innovative ejector enhanced vapor compression heat pump cycle for water heating application,” *Energy and Buildings*, vol. 43, no. 12, pp. 3331–3336, Dec. 2011, doi: 10.1016/j.enbuild.2011.08.037.
[92] K. E. Ringstad, Y. Allouche, P. Gullo, Å. Ervik, K. Banasiak, and A. Hafner, “A detailed review on CO2 two-phase ejector flow modeling,” *Thermal Science and Engineering Progress*, vol. 20, p. 100647, Dec. 2020, doi: 10.1016/j.tsep.2020.100647.
[93] S. Elbel and P. Hrnjak, “Experimental validation of a prototype ejector designed to reduce throttling losses encountered in transcritical R744 system operation,” *International Journal of Refrigeration*, vol. 31, no. 3, pp. 411–422, May 2008, doi: 10.1016/j.ijrefrig.2007.07.013.
[94] Y. Song, Y. Ma, H. Wang, X. Yin, and F. Cao, “Review on the simulation models of the two-phase-ejector used in the transcritical carbon dioxide systems,” *International Journal of Refrigeration*, vol. 119, pp. 434–447, Nov. 2020, doi: 10.1016/j.ijrefrig.2020.04.029.
[95] C. Arpagaus, F. Bless, M. Uhlmann, J. Schiffmann, and S. S. Bertsch, “High temperature heat pumps: Market overview, state of the art, research status, refrigerants, and application potentials,” *Energy*, vol. 152, pp. 985–1010, Jun. 2018, doi: 10.1016/j.energy.2018.03.166.
[96] Bodo Linnhoff and John R. Flower, “Synthesis of heat exchanger networks: I. Systematic generation of energy optimal networks,” *AIChE Journal*, vol. 4, no. 24, Jul. 1978, doi: https://doi.org/10.1002/aic.690240411.
[97] B. J. Lincoln, L. Kong, A. M. Pineda, and T. G. Walmsley, “Process integration and electrification for efficient milk evaporation systems,” *Energy*, vol. 258, p. 124885, Nov. 2022, doi: 10.1016/j.energy.2022.124885.
[98] Timothy G. Walmsley, Martin J. Atkins, Michael R. W. Walmsley, and James R. Neale, “Appropriate placement of vapour recompression in ultra-low energy industrial milk evaporation systems using Pinch Analysis,” *Energy*, vol. 116, pp. 1269–1281, Mar. 2016.
[99] F. Schlosser, H. Wiebe, T. G. Walmsley, M. J. Atkins, M. R. W. Walmsley, and J. Hesselbach, “Heat Pump Bridge Analysis Using the Modified Energy Transfer Diagram,” *Energies*, vol. 14, no. 1, Art. no. 1, Jan. 2021, doi: 10.3390/en14010137.
[100] M. Yang, T. Li, X. Feng, and Y. Wang, “A simulation-based targeting method for heat pump placements in heat exchanger networks,” *Energy*, vol. 203, p. 117907, Jul. 2020, doi: 10.1016/j.energy.2020.117907.
[101] J. A. Stampfli, M. J. Atkins, D. G. Olsen, M. R. W. Walmsley, and B. Wellig, “Practical heat pump and storage integration into non-continuous processes: A

hybrid approach utilizing insight based and nonlinear programming techniques," *Energy*, vol. 182, pp. 236–253, Sep. 2019, doi: 10.1016/j.energy.2019.05.218.
[102] A. S. Wallerand, M. Kermani, I. Kantor, and F. Maréchal, "Optimal heat pump integration in industrial processes," *Applied Energy*, vol. 219, pp. 68–92, Jun. 2018, doi: 10.1016/j.apenergy.2018.02.114.
[103] J. K. Jensen, T. Ommen, L. Reinholdt, W. B. Markussen, and B. Elmegaard, "Heat pump COP, part 2: Generalized COP estimation of heat pump processes," *Proceedings of the13th IIR-Gustav Lorentzen Conference on Natural Refrigerants*, 2018, doi: 10.18462/iir.gl.2018.1386.
[104] A. M. Elias, R. de C. Giordano, A. R. Secchi, and F. F. Furlan, "Integrating pinch analysis and process simulation within equation-oriented simulators," *Computers & Chemical Engineering*, vol. 130, p. 106555, Nov. 2019, doi: 10.1016/j.compchemeng.2019.106555.
[105] D. Cleland, "Matching Heat Pumps to Heating & Cooling Profiles in the NZ Food Processing Sector," presented at the The Role of Heat Pumps in Decarbonisation (Online Conference), 2021. [Online]. Available: https://www.eeca.govt.nz/assets/Heat-Pump-Slides/Don-Cleland-Slides.pdf?fbclid=IwAR0O-EFFKgd_tWR68cGfMGqahrS_PoUJK5Q9SU5SM7K2FrRVP4-tmG5qP2A
[106] L. Reinholdt *et al.*, "Heat pump COP, part 1: Generalised method for screening of system integration potentials," *13th IIR Gustav Lorentzen Conference, Valencia*, 2018, doi: 10.18462/iir.gl.2018.1380.
[107] H. Pieper, I. Krupenski, W. Brix Markussen, T. Ommen, A. Siirde, and A. Volkova, "Method of linear approximation of COP for heat pumps and chillers based on thermodynamic modelling and off-design operation," *Energy*, vol. 230, p. 120743, Sep. 2021, doi: 10.1016/j.energy.2021.120743.
[108] I. S. Ertesvåg, "Uncertainties in heat-pump coefficient of performance (COP) and exergy efficiency based on standardized testing," *Energy and Buildings*, vol. 43, no. 8, pp. 1937–1946, Aug. 2011, doi: 10.1016/j.enbuild.2011.03.039.
[109] L. Bellemo and R. Bergamini, "Integration of high temperature CO2 heat pumps and conventional heaters for spray dryers," *High-Temperature Heat Pump Symposium*, 2022.
[110] M. Zehnder, "Efficient air-water heat pumps for high temperature lift residential heating, including oil migration aspects," Jan. 2004, doi: 10.5075/epfl-thesis-2998.
[111] BMWK, "Facts and figures: Energy data: National and international development." [Online]. Available: https://www.bmwk.de/Redaktion/DE/Artikel/Energie/energiedaten-gesamtausgabe.html
[112] Eurostat, "Electricity prices and gas prices for non-household consumer. Second half-year 2019." Accessed: Jul. 12, 2020. [Online]. Available: https://ec.europa.eu/eurostat/web/energy/data/database
[113] EEA, "Greenhouse gas emission intensity of electricity generation." [Online]. Available: https://www.eea.europa.eu/ims/greenhouse-gas-emission-intensity-of-1
[114] prognos, "Energy economic projections and impact assessments 2030/2050," Bundesministerium für Wirtschaft und Energie, 2020.
[115] EC, "EU Reference Scenario 2020: Energy, transport and GHG emissions - Trends to 2050," 2021.
[116] M. Woods, D. Parker, and J. Shaw, "Government delivers next phase of climate action," The Beehive. Accessed: Aug. 15, 2021. [Online]. Available:

http://www.beehive.govt.nz/release/government-delivers-next-phase-climate-action
[117]"Exhaust Air Heat Recovery," Marriott Walker Corporation. Accessed: Aug. 10, 2023. [Online]. Available: https://www.marriottwalker.com/equipment-solutions/exhaust-air-heat-recovery-sytems/
[118] M. J. Atkins, M. R. W. Walmsley, and J. R. Neale, "Integrating heat recovery from milk powder spray dryer exhausts in the dairy industry," *Applied Thermal Engineering*, vol. 31, no. 13, pp. 2101–2106, Sep. 2011, doi: 10.1016/j.applthermaleng.2011.03.006.
[119] Timothy G. Walmsley, "Heat Integrated Milk Powder Production," University of Waikato, 2014. [Online]. Available: https://researchcommons.waikato.ac.nz/bitstream/handle/10289/8767/thesis.pdf?sequence=3&isAllowed=y
[120] B. Zuhlsforf, F. Buhler, R. Mancini, S. Cignitti, and B. Elmegaard, "High temperature heat pump integration using zeotropic working fluids for spray drying facilities," *12th IEA Heat Pump Conference*, 2017, [Online]. Available: https://backend.orbit.dtu.dk/ws/portalfiles/portal/132571251/O.3.9.3_High_Temperature_Heat_Pump_Integration_using_Zeotropic_Working_F....pdf
[121] T. G. Walmsley, B. J. Lincoln, R. Padullés, and D. J. Cleland, "Advancing Industrial Process Electrification and Heat Pump Integration with New Exergy Pinch Analysis Targeting Techniques," *Energies*, vol. 17, no. 12, p. 2838, Jan. 2024, doi: 10.3390/en17122838.
[122] J. Sarkar, S. Bhattacharyya, and M. Ram Gopal, "Natural refrigerant-based subcritical and transcritical cycles for high temperature heating," *International Journal of Refrigeration*, vol. 30, no. 1, pp. 3–10, Jan. 2007, doi: 10.1016/j.ijrefrig.2006.03.008.
[123] L. Kong *et al.*, "Transcritical-transcritical cascade CO2 heat pump cycles for high-temperature heating: A numerical evaluation," *Applied Thermal Engineering*, vol. 238, p. 122005, Feb. 2024, doi: 10.1016/j.applthermaleng.2023.122005.
[124] E. W. Lemmon, I. H. Bell, M. L. Huber, and M. O. McLinden, "NIST Standard Reference Database 23: Reference Fluid Thermodynamic and Transport Properties-REFPROP, Version 10.0, National Institute of Standards and Technology," 2018, doi: https://doi.org/10.18434/T4/1502528.
[125] D. Wu, H. Yan, B. Hu, and R. Z. Wang, "Modeling and simulation on a water vapor high temperature heat pump system," *Energy*, vol. 168, pp. 1063–1072, Feb. 2019, doi: 10.1016/j.energy.2018.11.113.
[126] W. Yang, X. Cao, Y. He, and F. Yan, "Theoretical study of a high-temperature heat pump system composed of a CO2 transcritical heat pump cycle and a R152a subcritical heat pump cycle," *Applied Thermal Engineering*, vol. 120, pp. 228–238, Jun. 2017, doi: 10.1016/j.applthermaleng.2017.03.098.
[127] W. Li, B. Yue, H. Zhang, C. Zheng, P. Jiang, and Y. Zhu, "Optimization of trans-critical CO2 high-temperature heat pump cycle and study of maximum heating temperature," *International Journal of Refrigeration*, vol. 177, pp. 99–110, Sep. 2025, doi: 10.1016/j.ijrefrig.2025.05.023.
[128] B. Linnhoff *et al.*, *User Guide on Process Integration for the Efficient Use of Energy*, 1st ed. Rugby, UK: IChemE, 1982.
[129] F. Cao, Y. Wang, and Z. Ye, "Theoretical analysis of internal heat exchanger in transcritical CO2 heat pump systems and its experimental verification," *International Journal of Refrigeration*, vol. 106, pp. 506–516, Oct. 2019, doi: 10.1016/j.ijrefrig.2019.05.022.

[130] X. Qin, F. Zhang, D. Zhang, Z. Gao, and S. Tang, “Experimental and theoretical analysis of the optimal high pressure and peak performance coefficient in transcritical CO2 heat pump,” *Applied Thermal Engineering*, vol. 210, p. 118372, Jun. 2022, doi: 10.1016/j.applthermaleng.2022.118372.
[131] J. Sarkar, S. Bhattacharyya, and M. Ramgopal, “Pressure drop for in-tube supercritical CO2 cooling: Comparison of correlations and validation,” presented at the Proceedings of the 19th National & 8th ISHMT-ASME Heat and Mass Transfer Conference, Hyderabad, India: JNTU Hyderabad, Jan. 2008, p. 2008/01/05.
[132] Y. Zhu, C. Li, F. Zhang, and P.-X. Jiang, “Comprehensive experimental study on a transcritical CO2 ejector-expansion refrigeration system,” *Energy Conversion and Management*, vol. 151, pp. 98–106, Nov. 2017, doi: 10.1016/j.enconman.2017.08.061.
[133] D. Li and E. A. Groll, “Transcritical CO2 refrigeration cycle with ejector-expansion device,” *International Journal of Refrigeration*, vol. 28, no. 5, pp. 766–773, Aug. 2005, doi: 10.1016/j.ijrefrig.2004.10.008.
[134] L. Wolscht, K. Knobloch, E. Jacquemoud, and P. Jenny, “Dynamic simulation and experimental validation of a 35 MW heat pump based on a transcritical CO2 cycle,” *Energy*, vol. 294, p. 130897, May 2024, doi: 10.1016/j.energy.2024.130897.
[135] S. Paul, P. Kumar, and S. M. Rao, “Thermodynamic analysis on the effect of supercritical CO2 ejector in cogeneration cycle for dairy application,” *Thermal Science and Engineering Progress*, vol. 39, p. 101729, Mar. 2023, doi: 10.1016/j.tsep.2023.101729.
[136] M. Palacz, M. Haida, J. Smolka, M. Plis, A. J. Nowak, and K. Banasiak, “A gas ejector for CO2 supercritical cycles,” *Energy*, vol. 163, pp. 1207–1216, Nov. 2018, doi: 10.1016/j.energy.2018.09.030.
[137] “Government ban on new coal boilers in place | Beehive.govt.nz.” Accessed: Dec. 14, 2023. [Online]. Available: https://www.beehive.govt.nz/release/government-ban-new-coal-boilers-place
[138] J. Brown, *Improving nutrient management for dairy factory wastewater land treatment systems. In: Integrated nutrient and water management for sustainable farming. (Eds L.D. Currie and R. Singh). http://flrc.massey.ac.nz/publications.html. Occasional Report No. 29. Fertilizer and Lime Research Centre, Massey University, Palmerston North, New Zealand. 6 pages.* 2016. doi: 10.13140/RG.2.1.2690.3449.
[139] “Open Country Dairy Products Company, New Zealand Locations.” Accessed: Aug. 26, 2025. [Online]. Available: https://www.opencountry.co.nz/en-nz/about-us/locations/
[140] “SUSTAINABLE MILK COMPANY | MIRAKA | NEW ZEALAND,” Miraka. Accessed: Dec. 14, 2023. [Online]. Available: https://www.miraka.co.nz
[141] Tetra Pak, *Dairy Processing Handbook*. 2021. [Online]. Available: https://dairyprocessinghandbook.tetrapak.com/chapter/evaporators
[142] I. H. Bell, J. Wronski, S. Quoilin, and V. Lemort, “Pure and Pseudo-pure Fluid Thermophysical Property Evaluation and the Open-Source Thermophysical Property Library CoolProp,” *Ind. Eng. Chem. Res.*, vol. 53, no. 6, pp. 2498–2508, Feb. 2014, doi: 10.1021/ie4033999.
[143] B. Zühlsdorf, J. K. Jensen, S. Cignitti, C. Madsen, and B. Elmegaard, “Analysis of temperature glide matching of heat pumps with zeotropic working fluid mixtures for different temperature glides,” *Energy*, vol. 153, pp. 650–660, Jun. 2018, doi: 10.1016/j.energy.2018.04.048.
[144] Ministry of Business, Innovation & Employment, “Energy prices.” Accessed: Apr. 15, 2024. [Online]. Available: https://www.mbie.govt.nz/building-and-

energy/energy-and-natural-resources/energy-statistics-and-modelling/energy-statistics/energy-prices/
[145] EECA, “Biomass boilers for industrial process heat,” EECA. Accessed: Apr. 15, 2024. [Online]. Available: https://www.eeca.govt.nz/insights/eeca-insights/biomass-boilers-for-industrial-process-heat/
[146] Ministry of Business, Innovation & Employment, “Energy in New Zealand 2023 shows renewable electricity generation increased to 87% | Ministry of Business, Innovation & Employment.” Accessed: Apr. 15, 2024. [Online]. Available: https://www.mbie.govt.nz/about/news/energy-in-new-zealand-2023-shows-renewable-electricity-generation-increased-to-87-percent/
[147]International Energy Agency, “Germany - Countries & Regions,” IEA. Accessed: Apr. 15, 2024. [Online]. Available: https://www.iea.org/countries/germany
[148] EECA, “Biomass,” EECA. Accessed: Apr. 15, 2024. [Online]. Available: https://www.eeca.govt.nz/insights/energys-role-in-climate-change/renewable-energy/biomass/
[149] R. Syivarulli, N. Pambudi, M. Syamsiro, and L. Saw, “Upgrading the Quality of Solid Fuel Made from Nyamplung (Calophyllum inophyllum) Wastes Using Hydrothermal Carbonization Treatment,” *Energy Engineering*, vol. 118, pp. 189–197, Jan. 2021, doi: 10.32604/EE.2020.010493.
[150] Forest Research, “Typical calorific values of fuels.” Accessed: Apr. 15, 2024. [Online]. Available: https://www.forestresearch.gov.uk/tools-and-resources/fthr/biomass-energy-resources/reference-biomass/facts-figures/typical-calorific-values-of-fuels/
[151] Ministry for the Environment, “Measuring emissions: A guide for organisations.” Jul. 2023. [Online]. Available: https://environment.govt.nz/assets/publications/Measuring-Emissions-Guidance_DetailedGuide_2023_ME1764.pdf
[152] M. Stöckl, J. Idda, V. Selleneit, and U. Holzhammer, “Flexible Operation to Reduce Greenhouse Gas Emissions along the Cold Chain for Chilling, Storage, and Transportation-A Case Study for Dairy Products,” *Sustainability*, vol. 15, p. 15555, Nov. 2023, doi: 10.3390/su152115555.
[153] C. Arpagaus *et al.*, “Transcritical-Transcritical CO_2 High-Temperature Heat Pump Cycle for Dairy Spray Dryers,” *High Temperature Heat Pump Symposium*, Sep. 2025.
[154] EECA, “Biomass boilers for industrial process heat,” EECA. Accessed: Oct. 06, 2025. [Online]. Available: https://www.eeca.govt.nz/insights/eeca-insights/biomass-boilers-for-industrial-process-heat/
[155] Exactitude Consultancy, “Instant Coffee Market by Type (Freeze-dried, Spray-dried), Flavouring (Flavoured Coffee, Unflavoured Coffee), and Region, Global Trends and forecast from 2023 to 2030,” Dec. 2023. [Online]. Available: https://exactitudeconsultancy.com/reports/33932/instant-coffee-market/#faq-report
[156] M. Okada, M. A. Rao, J. E. Lima, and M. Torloni, “Energy Consumption and the Potential for Conservation in a Spray-Dried Coffee Plant,” *Journal of Food Science*, vol. 45, no. 3, pp. 685–688, 1980, doi: 10.1111/j.1365-2621.1980.tb04132.x.
[157] USDA Foreign Agricultural Service, “Whole Milk Powder.” Accessed: Sep. 19, 2024. [Online]. Available: https://fas.usda.gov/data/production/commodity/0224400
[158] T. G. Walmsley, M. J. Atkins, M. R. W. Walmsley, M. Philipp, and R.-H. Peesel, “Process and utility systems integration and optimisation for ultra-low energy milk

powder production," *Energy*, vol. 146, pp. 67–81, Mar. 2018, doi: 10.1016/j.energy.2017.04.142.
[159] A. Domínguez-Niño, D. Cantú-Lozano, J. Ragazzo-Sanchez, I. Andrade, and G. Luna-Solano, "Energy Requirements and Production Cost of the Spray Drying Process of Cheese Whey," *Drying Technology*, vol. 36, Jul. 2017, doi: 10.1080/07373937.2017.1350863.
[160] A. C. A. Lopes, S. H. Eda, R. P. Andrade, J. C. Amorim, and W. F. Duarte, "14 - New Alcoholic Fermented Beverages—Potentials and Challenges," in *Fermented Beverages*, A. M. Grumezescu and A. M. Holban, Eds., Woodhead Publishing, 2019, pp. 577–603. doi: 10.1016/B978-0-12-815271-3.00014-2.
[161] F. Schlosser, S. Zysk, T. Walmsley, L. Kong, B. Zühlsdorf, and H. Meschede, "Break-even of High-Temperature Heat Pump Integration for Milk Spray Drying," *Energy Conversion and Management*, 2023, doi: 10.1016/j.enconman.2023.117304.
[162] A. Marina, S. Spoelstra, H. Zondag, and A. Wemmers, "Industrial process and waste heat data for EU28," *Mendeley Data*, Nov. 2020, doi: 10.17632/gyxjmvzbx8.1.
[163] F. Schlosser, "Integration of Heat Pumps for Decarbonisation of Industrial Process Heat Supply.," Kassel University Press GmbH, 2020.
[164] K. Assawamartbunlue and W. Luknongbu, "Specific energy consumption of native starch industry in Thailand," *Energy Reports*, vol. 6, pp. 299–303, Feb. 2020, doi: 10.1016/j.egyr.2019.11.078.
[165] G. Luna-Solano, M. A. Salgado-Cervantes, G. C. Rodríguez-Jimenes, and M. A. García-Alvarado, "Optimization of brewer's yeast spray drying process," *Journal of Food Engineering*, vol. 68, no. 1, pp. 9–18, May 2005, doi: 10.1016/j.jfoodeng.2004.05.019.
[166] K. Franke and M. Kießling, "Influence of spray drying conditions on functionality of dried whole egg," *Journal of the Science of Food and Agriculture*, vol. 82, no. 15, pp. 1837–1841, 2002, doi: 10.1002/jsfa.1269.
[167] S. Ma, S. Zhao, Y. Zhang, Y. Yu, J. Liu, and M. Xu, "Quality characteristic of spray-drying egg white powders," *Mol Biol Rep*, vol. 40, no. 10, pp. 5677–5683, Oct. 2013, doi: 10.1007/s11033-013-2669-1.
[168] M. P. Andersen, J. L. Poulsen, B. Elmegaard, and B. Zühlsdorf, "Developing a high-temperature heat pump technology concept using natural refrigerants." HPT Magazine, 2023. [Online]. Available: https://backend.orbit.dtu.dk/ws/portalfiles/portal/331682585/Mag_01_23_Topical_Article_Pihl_Andersen.pdf
[169] S. Ai, B. Wang, X. Li, and W. Shi, "Analysis of a heat recovery system of the spray-drying process in a soy protein powder plant," *Applied Thermal Engineering*, vol. 103, pp. 1022–1030, Jun. 2016, doi: 10.1016/j.applthermaleng.2016.04.108.
[170] V. Wilk, F. Helminger, M. Lauermann, A. Sporr, and B. Windholz, "High temperature heat pumps for drying - first results of operation in industrial environment," in *Proceedings for the 13th IEA Heat Pump Conference*, 2021.
[171] J. Geldermann, M. Treitz, and O. Rentz, "Integrated technique assessment based on the pinch analysis approach for the design of production networks," *European Journal of Operational Research*, vol. 171, no. 3, pp. 1020–1032, Jun. 2006, doi: 10.1016/j.ejor.2005.01.015.
[172] A. Williams-Gardner, *Industrial Drying*. London: Godwin, 1976.
[173] E. Tittmann, "Trocknung thixotroper Produkte auf dem Bandtrockner." ELA, 2012. [Online]. Available: Trocknung thixotroper Produkte auf dem Bandtrockner
[174] Konrad Treppe *et al.*, "Energetische Optimierung der Trockenpartie," Technische Universität Dresden, Jun. 2012. [Online]. Available: https://tu-

dresden.de/ing/maschinenwesen/ifvu/ressourcen/dateien/tvu/forschungsprojekte/forschung_alt/INFOR117/Bericht_INFOR117.pdf?lang=en
[175] O. F. Vilpoux and J. F. Santos Silveira Junior, “Chapter 3 - Global production and use of starch,” in *Starchy Crops Morphology, Extraction, Properties and Applications*, M. Pascoli Cereda and O. François Vilpoux, Eds., Academic Press, 2023, pp. 43–66. doi: 10.1016/B978-0-323-90058-4.00014-1.
[176] V. Van Giau *et al.*, “The role of specific energy consumption in a heat recovery system for cassava starch production using an integrated agro-industrial system,” *Energy, Sustainability and Society*, vol. 14, no. 1, p. 43, Jul. 2024, doi: 10.1186/s13705-024-00473-0.
[177] admin, “The European starch industry - Starch Europe.” Accessed: Mar. 05, 2025. [Online]. Available: https://starch.eu/the-european-starch-industry/
[178] N. S. Suresh and B. S. Rao, “Solar energy for process heating: A case study of select Indian industries,” *Journal of Cleaner Production*, vol. 151, pp. 439–451, May 2017, doi: 10.1016/j.jclepro.2017.02.190.
[179] “Motor vehicle production, by world region,” ACEA - European Automobile Manufacturers’ Association. Accessed: Sep. 18, 2025. [Online]. Available: https://www.acea.auto/figure/motor-vehicle-production-by-world-region/
[180] L. Kong, S. Kloeppel, F. Schlosser, N. Kabat, J. K. Carson, and T. G. Walmsley, “Advances in High-Temperature Heat Pump Technologies for Industrial Process Applications with Large Temperature Glides: Assessing the Potential for CO2 as a Refrigerant”, doi: 10.2139/ssrn.5396884.
[181]“Carbon intensity of electricity generation,” Our World in Data. Accessed: Sep. 11, 2025. [Online]. Available: https://ourworldindata.org/grapher/carbon-intensity-electricity
[182] H. Ritchie, M. Roser, and P. Rosado, “Energy,” *Our World in Data*, Oct. 2022, Accessed: Sep. 22, 2025. [Online]. Available: https://ourworldindata.org/energy/country/india
[183] A. Shankar, A. K. Saxena, and T. Idnani, “Roadmap to India’s 2030 Decarbonization Target,” The Energy and Resources Institute, New Delhi, 2022.
[184] N. Rodrigues, A. K. Saxena, S. Thakare, R. Pachouri, and G. Renjith, “India’s Electricity Transition Pathways to 2050: Scenarios and Insights,” The Energy and Resources Institute, New Delhi, 2023.
[185] Q. Zhang *et al.*, “Study on life-cycle carbon emission factors of electricity in China,” *Int J Low-Carbon Tech*, vol. 19, pp. 2287–2298, Jan. 2024, doi: 10.1093/ijlct/ctae181.
[186] “Top countries for Dry Whole Milk Powder Production,” NationMaster. Accessed: Sep. 22, 2025. [Online]. Available: https://www.nationmaster.com/nmx/ranking/dry-whole-milk-powder-production
[187] “Instant coffee from Brazil: A brewing success,” DatamarNews. Accessed: Sep. 22, 2025. [Online]. Available: https://datamarnews.com/noticias/instant-coffee-from-brazil-a-brewing-success/
[188] T. Tran *et al.*, “A comparison of energy use, water use and carbon footprint of cassava starch production in Thailand, Vietnam and Colombia,” *Resources, Conservation and Recycling*, vol. 100, pp. 31–40, Jul. 2015, doi: 10.1016/j.resconrec.2015.04.007.
[189] L. Steinberg, S. Glos, T. Korte, V. Bertsch, and R. Span, “Carbon-neutral steam supply for a chemical plant: Simulation of the integration of a high-temperature heat pump using CO2,” in *Proceedings of the 16th IIR-Gustav Lorentzen Conference on Natural Refrigerants*, Maryland, USA, Aug. 2024.

[190] L. Wolscht, M. Podeur, M. Adams, and E. Jacquemoud, “Off-design heat exchanger modelling for transcritical CO2 heat pump cycles,” in *Proceedings of ASME Turbo Expo 2024*, London, United Kingdom, Jun. 2024.
[191] S. D. Cich, J. J. Moore, C. Kulhanek, M. D. Towler, and J. Mortzheim, “Mechanical Design and Testing of a 2.5 MW sCO2 Compressor Loop,” in *GT2021*, Volume 10: Supercritical CO2, Jun. 2021. doi: 10.1115/GT2021-04155.
[192] J. S. Kwon, S. Son, J. Y. Heo, and J. I. Lee, “Compact heat exchangers for supercritical CO2 power cycle application,” *Energy Conversion and Management*, vol. 209, p. 112666, Apr. 2020, doi: 10.1016/j.enconman.2020.112666.
[193] J. V. M. Walden and R. Padullés, “An analytical solution to optimal heat pump integration,” *Energy Conversion and Management*, vol. 320, p. 118983, Nov. 2024, doi: 10.1016/j.enconman.2024.118983.
[194] S. Taslimi Taleghani, M. Sorin, S. Poncet, and H. Nesreddine, “Performance investigation of a two-phase transcritical CO2 ejector heat pump system,” *Energy Conversion and Management*, vol. 185, pp. 442–454, Apr. 2019, doi: 10.1016/j.enconman.2019.02.004.
[195] C. Aprea and A. Maiorino, “An experimental evaluation of the transcritical CO2 refrigerator performances using an internal heat exchanger,” *International Journal of Refrigeration*, vol. 31, no. 6, pp. 1006–1011, Sep. 2008, doi: 10.1016/j.ijrefrig.2007.12.016.
[196] Fenagy, “CO2 Heat Pump System for Hot Water Production Fenagy A/S.” Annex 58, 2022. [Online]. Available: https://heatpumpingtechnologies.org/annex58/wp-content/uploads/sites/70/2022/07/hthpannex58fenagy.pdf
[197] S. Wang, H. Tuo, F. Cao, and Z. Xing, “Experimental investigation on air-source transcritical CO2 heat pump water heater system at a fixed water inlet temperature,” *International Journal of Refrigeration*, vol. 36, no. 3, pp. 701–716, May 2013, doi: 10.1016/j.ijrefrig.2012.10.011.
[198] Y. Liu, E. A. Groll, K. Yazawa, and O. Kurtulus, “Theoretical analysis of energy-saving performance and economics of CO2 and NH3 heat pumps with simultaneous cooling and heating applications in food processing,” *International Journal of Refrigeration*, vol. 65, pp. 129–141, May 2016, doi: 10.1016/j.ijrefrig.2016.01.020.
[199] L. Bellemo, J. Gerritsen, and K. Hoffmann, “High temperature CO2 heat pump integration into the spray drying process,” *2nd Conference on High Temperature Heat Pumps*, 2019.
[200] A. Cavallini, L. Cecchinato, M. Corradi, E. Fornasieri, and C. Zilio, “Two-stage transcritical carbon dioxide cycle optimisation: A theoretical and experimental analysis,” *International Journal of Refrigeration*, vol. 28, no. 8, pp. 1274–1283, Dec. 2005, doi: 10.1016/j.ijrefrig.2005.09.004.
[201] S. Sawalha, “Theoretical evaluation of trans-critical CO2 systems in supermarket refrigeration. Part I: Modeling, simulation and optimization of two system solutions,” *International Journal of Refrigeration*, vol. 31, no. 3, pp. 516–524, May 2008, doi: 10.1016/j.ijrefrig.2007.05.017.
[202] S. Fangtian and M. Yitai, “Thermodynamic analysis of transcritical CO2 refrigeration cycle with an ejector,” *Applied Thermal Engineering*, vol. 31, no. 6, pp. 1184–1189, May 2011, doi: 10.1016/j.applthermaleng.2010.12.018.
[203] G. Boccardi, F. Botticella, G. Lillo, R. Mastrullo, A. W. Mauro, and R. Trinchieri, “Experimental investigation on the performance of a transcritical CO2 heat pump with multi-ejector expansion system,” *International Journal of Refrigeration*, vol. 82, pp. 389–400, Oct. 2017, doi: 10.1016/j.ijrefrig.2017.06.013.

[204] T. Bai, G. Yan, and J. Yu, “Thermodynamic analyses on an ejector enhanced CO2 transcritical heat pump cycle with vapor-injection,” *International Journal of Refrigeration*, vol. 58, pp. 22–34, Oct. 2015, doi: 10.1016/j.ijrefrig.2015.04.010.
[205] J. Sarkar and N. Agrawal, “Performance optimization of transcritical CO2 cycle with parallel compression economization,” *International Journal of Thermal Sciences*, vol. 49, no. 5, pp. 838–843, May 2010, doi: 10.1016/j.ijthermalsci.2009.12.001.
[206] C. Arpagaus, F. Bless, and S. S. Bertsch, “Theoretical Analysis of Transcritical HTHP Cycles with low GWP HFO Refrigerants and Hydrocarbons for Process Heat up to 200 °C,” *IIR International Rankine 2020 Conference*, 2020.
[207] V. Pérez-García, J. M. Belman-Flores, J. Navarro-Esbrí, and C. Rubio-Maya, “Comparative study of transcritical vapor compression configurations using CO2 as refrigeration mode base on simulation,” *Applied Thermal Engineering*, vol. 51, no. 1, pp. 1038–1046, Mar. 2013, doi: 10.1016/j.applthermaleng.2012.10.018.
[208] S. D. White, M. G. Yarrall, D. J. Cleland, and R. A. Hedley, “Modelling the performance of a transcritical CO2 heat pump for high temperature heating,” *International Journal of Refrigeration*, vol. 25, no. 4, pp. 479–486, Jun. 2002, doi: 10.1016/S0140-7007(01)00021-4.
[209] J. Wang, M. Belusko, M. Evans, M. Liu, C. Zhao, and F. Bruno, “A comprehensive review and analysis on CO2 heat pump water heaters,” *Energy Conversion and Management: X*, vol. 15, p. 100277, Aug. 2022, doi: 10.1016/j.ecmx.2022.100277.
[210] F. Cao, Y. Song, and M. Li, “Review on development of air source transcritical CO2 heat pump systems using direct-heated type and recirculating-heated type,” *International Journal of Refrigeration*, vol. 104, pp. 455–475, Aug. 2019, doi: 10.1016/j.ijrefrig.2018.12.023.
[211] Y. Song, C. Cui, X. Yin, and F. Cao, “Advanced development and application of transcritical CO2 refrigeration and heat pump technology—A review,” *Energy Reports*, vol. 8, pp. 7840–7869, Nov. 2022, doi: 10.1016/j.egyr.2022.05.233.
[212] K. Banasiak, A. Hafner, and T. Andresen, “Experimental and numerical investigation of the influence of the two-phase ejector geometry on the performance of the R744 heat pump,” *International Journal of Refrigeration*, vol. 35, no. 6, pp. 1617–1625, Sep. 2012, doi: 10.1016/j.ijrefrig.2012.04.012.
[213] M. J. Bergander, D. Butrymowicz, K. Smierciew, and J. Karwacki, “Refrigeration Cycle With Ejector for Second Step Compression,” *International Refrigeration and Air Conditioning Conference*, 2010, [Online]. Available: https://docs.lib.purdue.edu/cgi/viewcontent.cgi?article=2052&context=iracc
[214] F. Schlosser, C. Arpagaus, and T. G. Walmsley, “Heat Pump Integration by Pinch Analysis for Industrial Applications: A Review,” *Chemical Engineering Transactions*, vol. 76, pp. 7–12, Oct. 2019.
[215] T. G. Walmsley, J. J. Klemes, M. R. W. Walmsley, M. J. Atkins, and P. Varbanov, “Innovative hybrid heat pump for dryer process integration,” *Chemical Engineering Transactions*, vol. 57, 2017, doi: 10.3303/CET1757174.
[216] MAN Energy Solutions, “Industrial heat pumps and ems,” MAN Energy Solutions. [Online]. Available: https://www.man-es.com/process-industry/campaigns/industrial-heat-pumps-and-ems?7d50521b-a524-41af-9ad2-c5a5f3170117%5B%5D=0
[217] “On the path to climate neutrality with thermeco2 | ENGIE Refrigeration.” Accessed: Nov. 22, 2022. [Online]. Available: https://www.engie-refrigeration.de/en/heating/thermeco2-heat-pump

[218] ENGIE Refrigeration GmbH, “Pump it up!” Publik. Agentur fur Kommunikation GmbH, 2022. [Online]. Available: engie-refrigeration.de/sites/engie-refrigeration.de/files/2022-10/2022-10-06_engie_broschuere-thermeco2_en.pdf
[219] Tetra Pak, “Tetra Pak HighLift Heat Pump PD Leaflet,” Tetra Pak, 2024. Accessed: Mar. 09, 2026. [Online]. Available: https://www.tetrapak.com/content/dam/tetrapak/media-box/global/en/documents/tetra-pak-highlift-heat-pump-pd-leaflet.pdf

Appendix

8.4 Literature review tables

8.4.1 Cycle summary

Table 34. Summary of cycles identified in literature.

* - structure not identified in Adamson et al. [8]

Code	Cycle schematic and description	$T_{sink\ (in)}$ / $T_{sink\ (out)}$ (°C)	$T_{gc\ (in)}$/ $T_{gc\ (out)}$ (°C)	$T_{source\ (in)}$/ T_{amb} (°C)	T_{evap}/ $T_{suction}$ (°C)	P_{gc} (MPa)	COP	E, S or M[1]	Compressor type	Ref.	Year
T1-1	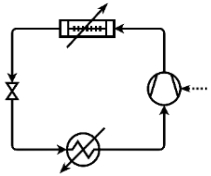 Transcritical, single-stage	-/-	12 – 24/ 20 – 50	-/-	12 – 27/-	9 – 12	3.4 – 3.8	E	SH reciprocating	[194]	2019
		13 – 17/55 – 70	-/-	-/10 – 30	-/-	10	2.0 – 3.9	E	Two-stage rotary/piston	[51]	2010
		-/60 – 90									
		20 – 40/-	-/-	-/-25 – 43	-/-	8 – 14	2.8 – 4.3	M	Rotary scroll	[74]	2020
			120/30	-/-	5/-	5.5 – 12	1.1 – 1.9	E	SH unspecified	[195]	2008

[1] E – Experimental, S – Simulation or thermodynamic model, M – Market available

T1-2	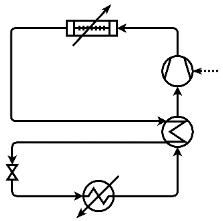 Transcritical, single-stage with IHX	10/- 20 – 40/73 17 – 40/- 10 – 40/70 – 90 20/60 – 120 -/80 – 110 30/110 – 120 -/- 30 – 100/100 – 200 20 – 40/- -/55 – 80 2 – 28/25 – 100	-/- -/- 68 – 140/40 – 68 -/- -/- -/- -/160 -/70 – 130 109 – 213/-120/30 -/12 – 36 -/160	30/- -/30 -/2 – 7 -/2 – 16 30/- 8 – 40/- -5 – 0/- -/-17 -/- -/- -/20 -/-	-/- 4/- -/- -/- -/- -/- -/- -12/-7 – 8 20 – 60/- 5/- -/14.5 – 19.5 0/15	8.5 - 7.5 – 9.5 9 – 12.5 15 - 12.5 8 – 12 11 – 20 5.5 – 12 8 – 13 5 – 14	4.1 2.9 – 5 2.8 2.2 – 3.8 2.8 – 4.3 3.9 – 4.3 2.5 – 2.9 1.6 – 2.4 1.5 – 3.3 1.2 – 2.1 1.8 – 4.2 0 – 0.8	E S S E M M M S S E E S	- - - SH reciprocating Rotary screw SH reciprocating Reciprocating - - SH unspecified SH reciprocating -	[88] [60] [50] [49] [72] [71] [196] [57] [13] [195] [197] [198]	2022 2005 2019 2020 2022 2022 2022 2021 2007 2008 2013 2016
T1-3	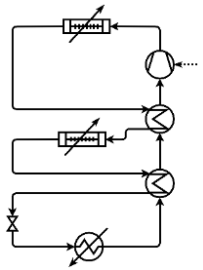 Transcritical, single-stage with mid-gas cooler IHX and normal IHX	-/75 & 135 2 – 28/100 – 160	-/145 -/-	-/- -/-	-/- 0/70	36 & 13 5 – 14	3.5 1.2 – 1.8	E S	SH reciprocating -	[199] [198]	2019 2016

TI-3	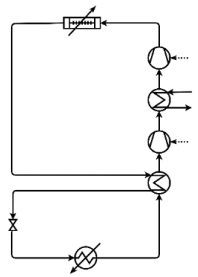 Transcritical, two compression stages with IHX and external intercooling	30/- -/- -/- 13 – 17/55 – 70 -/-	33/- -/- 130 – 240 /- -/- -/-	-/- -/- -/- -/10 – 30 -/-	2.7/- -30 – 4/- -50 – -30/- -/- -30 – 4/-	11.0 9 8 – 17 10 8 – 11.5	1.8 – 3.0 1.8 – 2.3 2.0 – 3.5 1.9 – 3.7 1.8 – 3.3	E S S E S	SH reciprocating - - Two-stage rotary piston -	[200] [52] [53] [51] [52]	2005 2009 2007 2010 2009
TI-4*	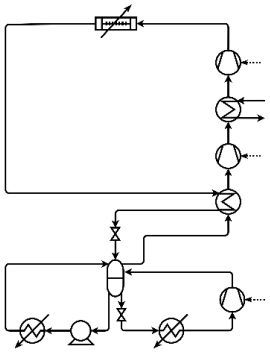 Transcritical, two evaporator stages with open economiser, IHX, and external intercooling	-/-	-/-	-/10 – 40	-37 – -8/-	8 – 12	5.5 – 1.8	S	-	[201]	2007

T1e-1	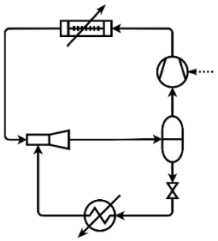 Transcritical, single-stage with ejector and separator	-/- 25/- 30/60 – 93 -/-	-/40 -/32 – 27 -/30 – 60 -/20 – 50	-/30 25/- -/- -/-	-5 – 17/- -/- -45 – 5/- 12 – 27/-	9 8.4 – 9.1 7.3 – 18 9 – 12	2.1 – 4.0 2.8 – 2.9 2.2 – 11.2 3.7 – 4.1	S E S E	- SH reciprocating - SH reciprocating	[202] [66] [87] [194]	2011 2012 2008 2019
T1e-1a*	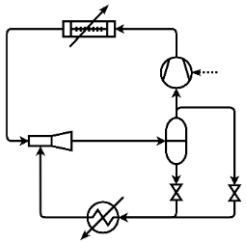 Transcritical, single-stage with ejector, separator and double expansion	30/61 – 103	-/30 – 60	-/-	-45 – 5/-	7.3 - 18	2.2 – 11.2	S	-	[23]	2008
T1e-2	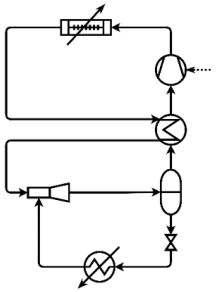	40/60 45/- -/- 20/50 – 90 10/40 – 110	-/- 150/- -/42 -/35 – 55 -/-	-15 – 12/- 27/- -/- -/20 30/-	-3/- -/- 0/- -/- -/-	8.4 10.5 10.5 8 – 12 8.5	1.5 – 2.9 1.15 1.75 6 – 3.4 4.6	E E E E S	SH unspecified SH unspecified - Rotary swing -	[203] [93] [67] [65] [88]	2017 2008 2011 2018 2022

	Transcritical, single-stage with IHX, ejector and separator										
T1e-3*	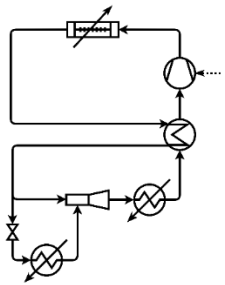 Transcritical, single-stage with IHX, ejector and two evaporators	10/40 – 110	-/-	30/-	-/-	8.5	4.3	S	-	[88]	2022
T1e-4	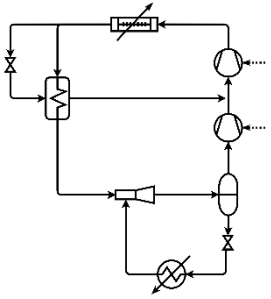 Transcritical, two compression stages with closed economiser, ejector and separator	25/35 – 50	-/-	-5/-	-25 – 5/-	7.5 – 11	2 – 4.1	S	-	[204]	2015

TE-2	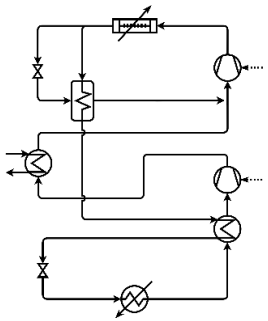 Transcritical, two compression stages with closed economiser, IHX and external intercooling	-/-	-/-	-/-	4 – 30/-	8 – 11.5	2.5 – 3.7	S	-	[52]	2009
TE-3	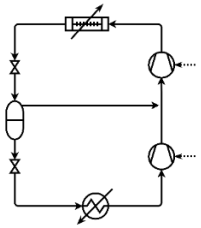 Transcritical, two compression stages with open economiser	-/- -/-	100 – 160/- -/30 – 60	-/- -/-	-30 – -50/- -45 – 5/-	8 – 15 7 – 17	2.3 – 3.8 -	S S	- -	[53] [205]	2007 2010

TE-4	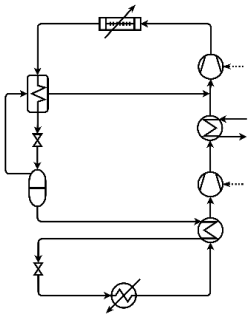 Transcritical, two compression stages with closed and flash economisers, IHX and external intercooling	-/-	-/-	-/-	4 – 30/-	8 – 11.5	2.3 – 3.7	S	-	[52]	2009
TE-5*	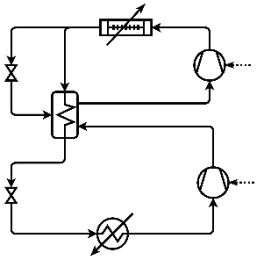 Transcritical, two compression stages with closed economiser between stages	-/-	70 – 130/35 – 45	-/-17	-12/-7 – 8	8 – 12	2.3 – 2.7	S	-	[57]	2021

TI-1*	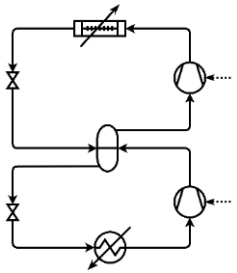 Transcritical, two compression stages with open economiser/ intercooler	-/-	50 – 130/-	-/-	-30 – -50/-	8 – 16	2.7 – 3.8	S	-	[53]	2007
TP-1	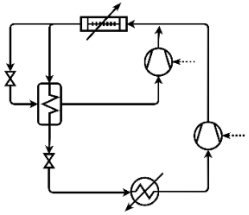 Transcritical, single-stage with closed economiser and parallel compression	-/-	-/-	-/-	4 – 30/-	8 – 11.5	2.3 – 3.6	S	-	[52]	2009
TP-2	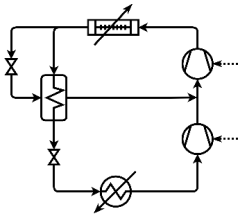	25/- 13 – 17/55 – 70	-/35 – 50 -/-	5/- -/10 – 30	-25 – 5/- -/-	8.6 10	2.5 – 3.7 2.0 – 3.6	S E	- Two-stage rotary/ piston	[204] [51]	2015 2010

	Transcritical, two compression stages with closed economiser										
TP-3[2]	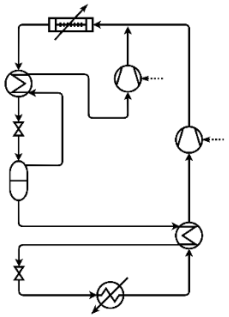 Transcritical, single-stage with flash economiser with superheating, parallel compression and IHX	30 – 100/200	206/105	80/30	-/-	6.8	2.7 – 3.5 (R514a)	S	-	[206]	2020
TS-1	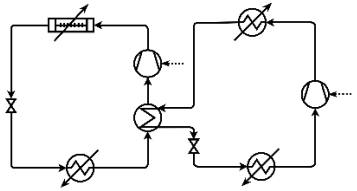	20/90 – 100 20/92 – 102	-/30 -/35	10/- 50/-	10/- 0/-	8 – 10 7.5 – 11	4.3 – 4.6[3] 2.3 – 6.3[4]	S S	- -	[55] [56]	2018 2017

[2]Cycle is not CO_2 but sink temperatures of 200 °C were investigated.

[3]CO_2 is used for the transcritical cycle, R1234ze(Z) is used for the subcritical cycle.

[4] CO_2 is used for the transcritical cycle, R152a is used for the subcritical cycle.

	Cascade with transcritical, single-stage (left cycle) and subcritical, single-stage (right cycle) with subcooler										
TS-2	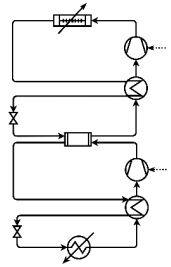 Cascade with transcritical, single-stage with IHX (top) and subcritical, single-stage with IHX (bottom)	-/-	70 – 130/35 – 45	-/-17	-22/-12	8 – 12	2.2 – 2.6	S	-	[57]	2021
TT-1	Cascade with transcritical, single-stage (top) and single-stage (bottom) with two evaporators										2022
TT-2	Cascade with transcritical, single-stage (top) and single-stage (bottom) with two evaporators and two IHXs										2022

TT-3	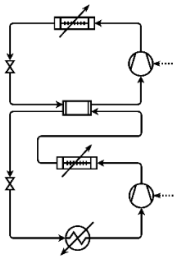 Cascade with transcritical, single-stage (top) and transcritical, single-stage (bottom) with gas cooler and cascade in series	-/30	-/-	-/-	-10/-0	-	2.4	S	-	Cited in [8]	2009
TM-6	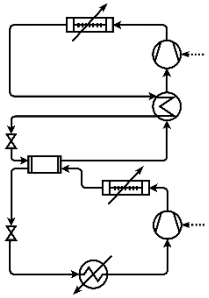 Cascade with transcritical, single-stage with IHX (top) and transcritical, single-stage (bottom) with gas cooler and cascade exchanger in series	-/-	70 – 130/35 – 45	-/-17	-12/-7 – 8	8 – 12	2.3 – 2.8	S	-	[57]	2021

TX-1	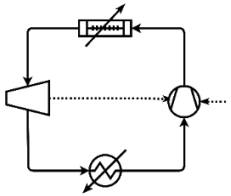 Transcritical, single-stage with expander	30 – 50/95 – 150 -/- -/15 – 55	-/- -/20 -/-	2 – 20/- -/- -/-	-/- 0.2/10.2 -20 – 0/-	>15 10 7.3 – 15	2.9 – 3.3 4.4 1.3 – 2.6	M S S	Hermetic centrifugal - -	[83] [63] [207]	2022 2013 2013
TX-2	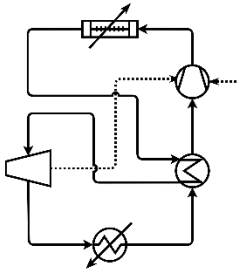 Transcritical, single-stage with expander and IHX	-/15 – 55	-/-	-/-	-20 – 0/-	7.3 – 15	1.5 – 2.3	S	-	[207]	2013
TX-3*	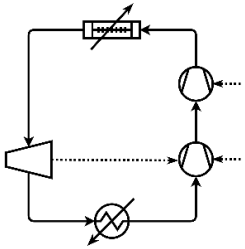 Transcritical, two-stage compression with expander on the low stage	-/-	-/20	-/-	0.2/10.2	10	4.3	S	-	[63]	2013

TX-4*	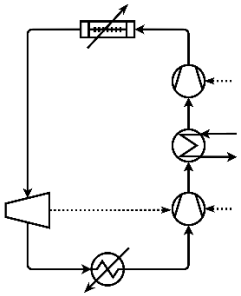 Transcritical, two-stage compression with expander on the low stage and external intercooling	-/-	-/20	-/-	0.2/10.2	10	5.0	S	-	[63]	2013
TX-5	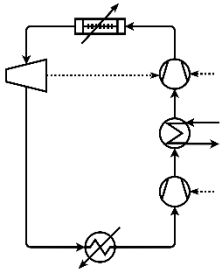 Transcritical, two-stage compression with expander on the high stage and external intercooling	-/-	-/20	-/-	0.2/10.2	10	5.0	S	-	[63]	2013

8.4.2 *Review papers*

Table 35. Review papers including transcritical CO_2 heat pumps.

Author	Paper title	Contribution	Year	Reference
Adamson et al.	High-temperature and transcritical heat pump cycles and advancements: a review	Identifies 49 unique HTHP cycle configurations both subcritical and transcritical. The paper also identifies six key challenges in the development of HTHPs (Table 2).	2022	[8]
Austin and Sumathy	Transcritical carbon dioxide heat pump systems: A review	Identifies that existing correlations to represent the fluid properties of CO_2 are inaccurate, affecting the ability to accurately predict the heat transfer coefficient and pressure drop and is especially true near the critical point. 5 heat pump cycle configurations discussed – T1-1, T1-2, TI-3a, TE-3, and TE-2. The highest sink temperature identified in the literature was 200 °C (simulation), modelled by Sarkar et al. [13] and the highest experimental sink temperature was 90 °C [208]. Promising modifications to heat exchanger design that can significantly impact the CO_2 heat pump performance were also discussed.	2011	[16]
Ma, Liu and Tian	A review of transcritical carbon dioxide heat pump and refrigeration cycles	An overview of transcritical carbon dioxide heat pump and refrigeration systems. The paper includes an analysis of supercritical CO_2 and polyalkylene glycol (PAG) lubricant properties. Provides a comparison of thermophysical properties among common refrigerants and a	2013	[63]

		comparison of the specific heat of CO_2 at varying temperatures and pressures. Performs a comparative analysis on expander cycles with discharge temperatures of approximately 100 °C. The analysis also includes isentropic efficiency estimations of different types of expanders. Cycles discussed – T1-1, T1-2, TX-1, TX-3, TX-4, TX-5		
Arpagaus et al.	High-temperature heat pumps: Market overview, state of the art, research status, refrigerants, and applications potentials	Reviews 20 market available HTHPs (between 90 °C and 160 °C) from 13 manufacturers and state of the air for high-temperature heat pump development. Heating capacities range from 20 kW to 20 MW. Identifies barriers for high-temperature heat pumps, including lack of awareness of technical and economic possibilities related to the application of HTHPs for users, consultants, investors, plant designers, producers and installers, lack of knowledge around HTHP integration, long payback periods (> 3 years), competing technologies, lack of available refrigerants in HTHP range with low GWP, lack of pilot and demonstration systems, and lack of training. Identifies research projects on HTHPs but there were no HTTHP CO2 projects. In depth comparison of refrigerants and refrigerant selection criteria for HTHPs. Cycles discussed – TX-2.	2018	[95]

Wang et al.	A comprehensive review and analysis on CO_2 heat pump water heaters	Reviews CO_2 heat pump water heaters for industrial and residential applications. The mass flow ratio of water to CO_2, the sink inlet temperature and refrigerant pressure have significant impact on the heat exchange performance. Wang et al. also identified limitations related to pinch points in the gas cooler and proposed possible solutions: optimising operational parameters, using zeotropic refrigerant mixture and optimising the cycle configuration. Bitzer was identified as a CO_2 compressor (reciprocating) manufacturer for heat pumps. Oil decomposes at approximately 245 °C, limiting the discharge temperature. A possible solution of oil-free compressors (turbo and scroll) was suggested. Cycles discussed – T1-1, T1-2, T1-2 with flash gas bypass, T1e-1	[209]	2022
Sarkar	Ejector enhanced vapor compression refrigeration and heat pump systems – A review	Reviews two-phase ejectors and ejector heat pump/refrigeration systems. The study identifies ejectors as an expansion device that significantly improves cycle performance. The gas cooler pressure in a transcritical cycle can be optimised by adjusting the ejector geometry. Cycles discussed – T1e-1, T1e-1a, T1e-2	[64]	2012
Arpagaus et al.	Multi-temperature heat pumps: A literature review	Reviews heat pumps with multi-temperature applications	[58]	2016

		Simulation revealed that multi-stage compression cycles had the highest COP when compared to cascade, ejector and expansion valve cycles. Identified ejectors as a promising modification to improve cycle performance.		
Cao et al.	Review on development of air source transcritical CO_2 heat pump systems using direct-heated type and recirculating-heated type	Discussed transcritical CO_2 cycle developments: IHX, multi-stage compression, economisers, ejectors, parallel compression and combined cycles. Studies with sink temperatures up to 75 °C are discussed in the review.	[210]	2019
Lecompte et al.	Review of experimental research on supercritical and transcritical thermodynamic cycles design for heat recovery application	Reviews experimental research for heat-to-upgraded heat (heat pumps) and heat-to-power systems that operate in the supercritical range. Identifies the following barriers for supercritical heat pumps: Heat pump components are not optimised for supercritical operation. HFOs and HFCs give much higher temperature lifts than CO_2. The source temperatures for CO_2 cycles needs to be low and so is generally only suitable for ambient air source as opposed to industrial heat recovery.	[54]	2019
Schlosser et al.	Large-scale heat pumps: Applications, performance, economic feasibility and industrial integration	Reviews 155 case studies of large-scale industrial heat pumps to identify promising attributes and avenues for heat pump uptake. Introduces the price ratio as a secondary metric from COP.	[30]	2020
Song et al.	Advanced development and application of transcritical CO_2 refrigeration and heat	Transcritical CO_2 cycles used for various applications – air conditioning, hot water production, industrial, commercial cold chain.	[211]	2022

	pump technology – a review	Recommends the use of IHX, parallel compression optimisation of discharge pressure, reverse cycle defrosting and subcooler based modifications. For heat pump dryers, the increasing dehumidification needs to be considered, COP is no longer an appropriate metric to quantify performance of the CO_2 cycle for this application.		

Table 36. Reviews on ejector technologies found in the literature

Author	Paper title	Contribution	Year	Reference
Elbel and Lawrence	Review of recent developments in advanced ejector technology	Review on the use of ejectors to recover expansion work in vapor compression cycles. Fluids with high irreversibility or throttling loss are better suited for ejectors. CO_2 has high throttling losses compared to other refrigerants.	2016	[86]
Sarkar	Ejector enhanced vapour compression refrigeration and heat pump systems – A review	Discusses geometry, operation, and modelling of ejectors in vapour compression cycles. Conservations of mass, energy, momentum equations, equations of stage, phase change principles and isentropic relations need to be considered when modelling ejectors. Concludes that a lot more research still needs to be done for large scale applications in industry.	2012	[64]
Sumeru, Naution and Ani	A review on two-phase ejector as an expansion device in vapour compression refrigeration cycle	The review focusses on the ejector as an expansion device and how two-phase flow in the ejector, geometric parameters and working fluid selection affects the cycle performance. The author recommends that future research should be directed towards improving the design of the ejector to generate pressure rise in the diffuser section to decrease compression work.	2012	[89]
Zhang et al.	Progress in ejector-expansion vapour compression	Reviews experimental and thermodynamic studies on transcritical and subcritical ejector heat pump systems. The study also discusses the geometric optimisation of ejectors and cascade ejector systems.	2020	[85]

	refrigeration and heat pump systems			
Ringstad et al.	A detailed review on CO_2 two-phase ejector flow modelling	Reviews two-phase CO_2 ejector modelling for use in vapour compression cycles.	2020	[92]
Song et al.	Review on the simulation models of the two-phase ejector used in the transcritical carbon dioxide systems	Key barrier to the use of transcritical CO_2 ejectors is the lack of understanding around the thermodynamic interactions of the ejector. Reviews 1D and 3D models.	2020	[94]

Table 37. Review of high-temperature ejector CO_2 heat pumps and ejector modelling

Author	Paper title	Contribution	Year	Reference
Zhu et al.	Experimental investigation on the performance of transcritical CO_2 ejector-expansion heat pump water system	Experimental. Investigated a transcritical CO_2 system (T1e-2) that produced water at 90 °C, achieving a COP of 3.3. The COP of the cycle was improved by 10.3% compared to the equivalent cycle with no ejector. Investigated the effect of sink outlet temperature, compressor discharge pressure compressor rotation speed on the ejector efficiency.	2018	[65]
Sarkar	Optimization of ejector-expansion transcritical CO_2 heat pump cycle	Simulation. Compared two transcritical CO_2 ejector heat pump cycles with sink temperatures up to 103 °C. The proposed	2008	[87]

		modifications (double expansion for evaporator quality control) increased the sink temperature by 10 °C. The COPs in the modified system were lower than the conventional ejector heat pump system due to a lower optimum discharge pressure. Second law efficiency of the heat pump can be improved by up to 9% compared to the equivalent cycle with no ejector.		
Qin et al.	System development and simulation investigation on a novel compression/ejection transcritical CO_2 heat pump system for simultaneous heating and cooling	Experimental and simulation. Proposes a novel ejector-expansion CO_2 heat pump (T1e-3) that can produce sink temperatures up to 110 °C.	2022	[88]
Banasiak, Hafner and Andresen	Experimental and numerical investigation of the influence of the two-phase ejector geometry on the performance of the R744 heat pump	One dimensional ejector modelling to optimise geometry of the ejector. The study found that the mixer length, mixer diameter and the diffuser divergence angle have the most significant effect on the ejector efficiency. The COP increase between T1-1 and T1e-1 was up to 8%. Operating parameters of the heat pump were not specified.	2012	[212]
Elbel and Hrnjak	Experimental validation of a prototype ejector designed to reduce throttling losses encountered in transcritical R744 system operation	Proposed measure ejector performance through a single metric rather than two (entrainment ratio and suction pressure ratio), called ejector work recovery efficiency.	2008	[93]

Table 38. Review of ejectors - other papers of interest

Author	Paper title	Contribution	Year	Reference
Bergander	Refrigeration cycle with two-phase condensing ejector	Simulation and experimental. Novel cycle with ejector after compression. Analysis was performed on a subcritical cycle (Figure 14c) that used R22 as the refrigerant. Validated experimentally. The proposed cycle was shown to increase the COP by up to 38 %. The experimental results proved energy savings of 16 % could be achieved.	2006	[90]
Bergander et al.	Refrigeration cycle with ejector for second step compression	Experimental. Analysis was performed on a subcritical cycle (Figure 14c) that used R507 as the refrigerant.	2010	[213]
Chen et al.	A theoretical study of an innovative ejector enhanced vapor compression heat pump cycle for water heating application	Simulation. Novel cycle with ejector after the compressor and closed economiser. Improvements in volumetric heating capacity were estimated to be up to 7 % and COP improvements between 15 and 37 % compared to a conventional cycle.	2011	[91]
Taslimi Taleghani et al.	Performance investigation of a two-phase transcritical CO_2 ejector heat pump system	Experimental. The integration of ejector expansion work recovery in a single-stage transcritical heat pump (T1-1, T1e-1) was investigated.	2019	[194]

		For the ejector model, constant polytropic efficiencies are assumed in each section to account for frictional losses. The study found that an increase in heat transfer area ratio improves the system performance but the ejector efficiency is decreased. The primary nozzle throat diameter and effective area ratio are important design considerations which affect the system performance. A COP increase between 9 and 12 % was observed in the T1e-1 compared to the T1-1.		

Table 39. Review of high-temperature heat pump integration

Author	Paper title	Contribution	Year	Reference
Bellemo and Bergamini	Integration of high temperature CO_2 heat pumps and conventional heaters for spray dryers	Integrates the AddCool (Market available, standardised CO2 HTTHPs. Table 41) into the spray drying process. The heat pump heats the air from ambient to 120 °C indirectly. The air is then heated to 200 °C using a steam heater supplied by an NG boiler. An economiser is used for the boiler. Chilled water can be produced on the low side. Six integration cases were considered: Steam heater with condensate recovery (85 °C). Steam heater with condensate recovery (30 °C). Produce chilled water at 2 °C with no parallel condensate heat recovery. Produce chilled water at 2 °C with parallel condensate heat recovery. Produce chilled water at 12 °C, no parallel condensate heat recovery. Produce chilled water at 12 °C with parallel condensate heat recovery. Process simulation was used as the method to integrate the heat pump into the system. The results showed that parallel condensate recovery increased the overall COP of the system and reduced the load and therefore the size required for the heat pump. The highest heat pump COP did not necessarily correlate to the highest overall heating COP. The highest overall COP (COP = 1.3) resulted from Case 4.	2022	[109]

Schlosser et al.	Large-scale heat pumps: Applications, performance, economic feasibility and industrial integration	Reviews 155 heat pump implementations in an industrial context. Combines existing process integration methods with accurate heat pump performance models. COPs of 3 to 6 favour HP implementations.	2020	[30]
Jensen et al.	Heat pump COP, part 2: Generalised COP estimation of heat pump processes	Generalised method for the estimation of COP for industrial heat pump integration. Extended method is provided to eliminate combinations of working fluids, compressors and heat exchangers that are unviable.	2018	[103]
Yang et al.	A simulation-based targeting method for heat pump placements in heat exchanger networks	Hybrid Pinch Analysis and process simulation method that supplies accurate heat pump models for the process integration method.	2020	[100]
Lincoln et al.	Process integration and electrification for efficient milk evaporation systems	Integrates transcritical CO_2 heat pumps into the milk evaporation process. Proposes a method that targets full electrification efficiency over minimised heat demand.	2022	[31]
Stampfli et al.	Practical heat pump and storage integration into non-continuous processes: A hybrid approach	Hybrid pinch analysis and mathematical programming method for heat pump and storage integration in non-continuous processes.	2019	[101]
Elias et al.	Integrating pinch analysis and process simulation within equation-oriented simulators	Proposed a tool to estimate the minimum energy demand and total annual cost heat exchanger networks that can solve simultaneously with the convergence loop of the process simulator. The new method provides the capability to support dynamic changes in input data and avoids the simulation of heat exchanger units, improving the performance of the solver.	2019	[104]

Wallerand et al.	Optimal heat pump integration in industrial processes	Hybrid mathematical programming and Pinch Analysis based method for design heat pump superstructures that are integrated within the process.	2018	[102]
Zuhlsdorf et al.	High temperature heat pump integration using zeotropic working fluids for spray drying facilities	Considers the integration of a high-temperature subcritical heat pump with an IHX that uses zeotropic mixtures. No integration method presented, the study focusses on the optimum concentrations of the components in the mixture.	2017	[120]
Schlosser et al.	Heat pump integration by Pinch Analysis for Industrial Applications: A Review	Derivation of pinch temperature, temperature lift, COP and savings potential using the GCC. The results found that 23 to 100% of heating demands could be supplied by a heat pump for six industrial cases.	2019	[214]
Walmsley et al.	Innovative hybrid heat pump for dryer process integration	Integration of an ammonia-water hybrid heat pump into the spray drying process using Pinch Analysis. Heat pump heats the air up to 80 °C.	2017	[215]
Schlosser et al.	Heat pump bridge analysis using the modified energy transfer diagram	Targeting technical and economic heat pump potential by applying COP curves into the modified energy transfer diagram.	2020	[99]

8.4.3 *Transcritical CO_2 cycles with T_{sink} or T_{GC} >80 °C*

Table 40. Review of high temperature transcritical CO_2 heat pump cycle configurations (T_{sink} or T_{GC} > 80 °C).

Author	Component category	Paper title	Contribution	E or S[5]	T_{sink} (°C)	Cycle code	Year	Ref.
Agrawal et al.	Multi-stage compression with intercooling	Optimization of two-stage transcritical carbon dioxide heat pump cycles	Compares the performance of three transcritical CO_2 cycles with two-stage compression. Simulated a single-stage system which could achieve a discharge temperature of 290 °C (T_{evap} = -50 °C) with a discharge pressure > 20 MPa, but components of the single-stage system were not specified. The COP of the single-stage system at these conditions was 1.8. A two-stage compression system with compression intercooling from an external source was able to achieve a discharge temperature of 240 °C (T_{sink} ≈ 200 – 220 °C) with a COP of approximately 2.	S	<130 <160 <240	TI-1 TE-3 TI-3	2007	[53]

[5] Experimental or simulation.

Sarkar et al.	Standard cycle	Natural refrigerant based subcritical and transcritical cycles for high-temperature heating	Compares the performance of T1-1 with subcritical cycles using natural refrigerants, identifying the high-pressure requirements as a barrier to uptake for transcritical CO_2 heat pumps.	S	200	T1-1	2007	[13]
Cao et al.	Internal heat exchanger	Theoretical analysis of internal heat exchanger in transcritical CO_2 heat pump systems and its experimental verification	Investigates the effectiveness of IHX in a transcritical CO_2 heat pump. The simulation was validated for sink temperatures up to 70 °C. The length of the IHX was also considered as part of the study. The results indicated that the discharge temperature is the limiting factor for IHX length.	S, E	<140	T1-1, T1-2	2019	[50]
Cao et al.	Internal heat exchanger	Experimental investigation on the influence of internal heat exchanger in a transcritical CO_2 heat pump water heater	Exergy analysis was carried out on the experimental data. The highest COP of 3.81 was achieved when heating water from 10 °C to 70 °C. The COP decreased when the sink inlet temperature was increased to 40 °C. The addition of an IHX increased the COP by up to 7 %.	E	70 – 90	T1-1, T1-2	2020	[49]
Liu et al.	Internal heat exchanger	Theoretical analysis of energy-saving performance and economics of CO_2 and	Analyses the T1-2 and T1-3 systems with two gas coolers for hot water (72 – 100 °C) and warm water (25 – 71 °C) generation.	S	70 – 100	T1-2, T1-3	2016	[198]

		NH_3 heat pumps with simultaneous cooling and heating applications in food processing	Having two gas coolers allows for better temperature profile matching for heat exchange. Interpretation of the COPs is unclear as there is co-generation of hot water and warm water, and cooling.					
Aprea and Maiorino	Internal heat exchanger	An experimental evaluation of the transcritical CO_2 refrigerator performances using an internal heat exchanger	Experimental comparison between the T1-1 and T1-2 system. COP improvement of up to 10.5 % was achieved with T1-2. The cycle was used for refrigeration applications but the discharge temperature of 120 °C had been recorded. A semi-hermetic (unspecified) compressor had been used for the experiment, reaching a maximum pressure of 12 MPa.	E	120	T1-1, T1-2	2008	[195]
Wang et al.	Internal heat exchanger	Experimental investigation on air-source CO_2 heat pump water system at a fixed water inlet temperature	Investigates the performance and optimal discharge pressures of the T1-2 cycle at varying ambient temperatures (15 – 35 °C) and sink temperatures (55 – 80 °C). Concludes that the optimal discharge pressure is difficult to characterise as it is dependent on multiple factors – ambient temperature, sink temperature, componentry.	E	55 – 80	T1-2	2013	[197]

			COPs range between 2.8 and 4.1 for sink temperature of 60 °C (T_{amb} = 25 °C). COPs for the system were higher when the tube length in the heat exchangers was longer (19 m).					
Bellemo, Gerritsen and Hoffman	Internal heat exchanger	High temperature CO_2 heat pump integration into the spray drying process	Analysis of the GEA AddCool system (Market available, standardised CO2 HTTHPs. Table 41). Spray dryers consume typically, 1.2 kWh of air heating per kg of powder for temperatures above 200 °C. Two semi-hermetic 4-cylinder GEA Bock HGX 34/110-4 SH compressors are used in the system.	E	75 & 135	T1-3	2019	[199]
Sarkar	Ejector	Optimisation of ejector-expansion transcritical CO_2 heat pump cycle	Energetic and exergetic analysis of the T1e-1 and T1e-1a. The T1e-1a cycle includes a separator at the outlet of the evaporator that feeds back to the inlet of the evaporator to regulate the quality. The COP improvement between the two cycles was negligible.	S	61 – 103	T1e-1	2008	[87]
Elbel and Hrnjak	Ejector with internal heat exchanger	Experimental validation of a prototype ejector designed to reduce throttling losses encountered in transcritical R744 system operation	Comparative analysis between T1-1 and T1e-2. The cycle was intended for refrigeration applications but the discharge temperature of 150 °C was recorded. A COP improvement of 7% was found for T1e-2 when compared to T1-1. The COP improvement was greater at high	E	150	T1-1, T1-e2	2008	[93]

			discharge pressures due to the greater potential for work recovery.					
Zhu et al.	Ejector with internal heat exchanger	Experimental investigation on the performance of transcritical CO_2 ejector-expansion heat pump water heater system	A prototype ejector-expansion transcritical CO_2 heat pump system was investigated for hot water heating. The T1e-2 cycle performance was compared to the T1e-1 cycle performance. A COP improvement of 10.3% was found for a sink temperature of 70 °C. A COP of 3.3 was achieved for a sink temperature of 90 °C ($T_{sink,in}$ = 20 °C). A rotary swing compressor was used for the experimental prototype. The designed capacity was 5 kW from the gas cooler.	E	50 – 90	T1e-1, T1e-2	2018	[65]
Yao et al.	Internal heat exchanger, closed economiser, open economiser, two-stage compression	Comparative study of upgraded CO_2 transcritical air source heat pump systems with different heat sinks	Investigated three cycles as possible performance improvements compared to T1-2. All of the cycles feature two-stage compression with intercooling, where the method of intercooling varies between internal and external heat exchange. The COP improvement ranged between 10 and 50 % compared to T1-2. The optimal cycle was dependent on the operating conditions of the heat pump.	S	70 – 130	T1-2, TE-5, TS-2, TM-6	2021	[57]
Wu, Hu and Wang	Cascade	Performance simulation and exergy analysis of hybrid	Analysis of a cascade heat pump system with a subcritical top cycle using R1234ze(Z) and a transcritical bottom cycle	S	90 – 100	TS-1	2018	[55]

		source heat pump system with low GWP refrigerants	using CO_2 as the refrigerant. The outlet of the condenser is used to superheat the suction inlet of the transcritical cycle, subcooling the R1234ze(Z) prior to expansion. The COP improvement of the system was 25% compared to a single-stage subcritical R1234ze(Z) system. COPs were above 4 for a condensing temperature of 100 °C.					
Yang et al.	Cascade	Theoretical study of a high-temperature heat pump system composed of a CO_2 transcritical heat pump cycle and a R152a subcritical heat pump cycle	Analysis of a cascade heat pump system with a subcritical top cycle using R152a and a transcritical bottom cycle using CO_2 as the refrigerant. The outlet of the condenser is used to superheat the suction inlet of the transcritical cycle, subcooling the R152a prior to expansion. The COPs range between 2.3 and 6.3 for sink temperatures between 92 and 102 °C.	S	92 – 102	TS-1	2017	[56]

8.4.4 Market available, standardised CO_2 HTTHPs.

Table 41. Market available standardised high temperature transcritical CO_2 heat pumps.

Manufacturer	**Model name**	**T_{sink} (°C)**	**T_{evap} or T_{amb} (°C)**	**Heating capacity (kW)**	**COP**	**Compressor type**	**Cycle code**	**Year**	**Reference**
GEA	AddCool	90 – 130	4 – 20	100 – 200	2.5 – 4.1	Semi-hermetic reciprocating compressors (BLUE)	T1-3	2020	[70]
MAN Energy Solutions (Everllence)	MAN CO_2 Heat Pump	< 150	-20 – 40	5000 – 80,000	2.9 – 3.3	Centrifugal turbocompressor (hermetic) with integrated expander	TX-1	2022	[216], [83]
Mitsubishi	Q-ton	60 – 90	-25 – 43	30	2.8 – 4.3	Rotary scroll (hermetic inverter compressor)	T1-1	2020	[74]
Mayekawa	Eco Sirocco	120	-10 – 43	65 -90	2.9 – 5.5	Screw	T1-2	2022	Cited in [95], [72]
Mayekawa	Eco Cute Unimo	90	7 – 25	45 – 110	1.5 – 4.4	Screw	-	2013	Cited in [95], [73]

Dürr thermea	thermeco2	80 – 110	8 – 40 (source)	51 – 2,200	3.9 – 4.3 (80 °C sink)	Semi-hermetic reciprocating	T1-2	2022	Cited in [95], [217], [218], [71]
Fenagy	Fenagy Heat Pump	110 – 120	-5 – 5	300 – 1800	2.5 – 2.9	Reciprocating	T1-2	2022	[196]

8.5 Comparison of natural refrigerants

Table 42. Comparison of natural refrigerants

Refrigerant	Cycle	Phase	COP	VHC (kJ/m^3)	P_{max} (bar)
Air	Brayton*	Supercritical	1.60	12561	180
Air	Brayton*	Gas	1.53	216	3.5
Helium	Brayton*	Supercritical	1.52	450	5.5
Helium [219]	Stirling	-	~1.4	-	-
Nitrogen	Brayton*	Supercritical	1.58	12473	180
Nitrogen	Brayton*	Gas	1.53	215	3.5
Argon	Brayton*	Supercritical	1.65	13560	180
Argon	Brayton*	Gas	1.53	154	2.5
CO_2	Brayton with IHX	Supercritical	1.98	17864	180
CO_2	Brayton with IHX	Supercritical/gas	1.67	5499	30

*Modelled as a Brayton with an IHX but the IHX provided no thermodynamic benefit.

8.6 Co-authorship forms

THE UNIVERSITY OF WAIKATO
Te Whare Wānanga o Waikato

Co-Authorship Form

School of Graduate Research
The University of Waikato
Private Bag 3105
Hamilton 3240, New Zealand
Phone +64 7 838 5096
Email: SGR@waikato.ac.nz
Website: http://www.waikato.ac.nz/students/research-degre

This form is to accompany the submission of any PhD that contains research reported in published or unpublished co-authored work. **Please include one copy of this form for each co-authored work.** Completed forms should be included in your appendices for all the copies of your thesis submitted for examination and library deposit (including digital deposit).

Chapter 4 - Thermodynamic modelling for the proposed cycle includes modelling and results from "Transcritical-transcritical cascade CO2 heat pump cycles for high-temperature heating: A numerical evaluation."The modelling and results included were modelled entirely by the PhD candidate except for the break-even price ratio stated in Section 4.4.3. **Other results modelled by other co-authors were not included in the thesis.** The co-authors were material in contributing to the conceptualisation, methodology, supervision and review of the publication.

Nature of contribution by PhD candidate	Methodology, Investigation, Writing – original draft.
Extent of contribution by PhD candidate (%)	85 %

CO-AUTHORS

Name	Nature of Contribution
Timothy Gordon Walmsley	Conceptualisation, Methodology, Writing – review & editing, Supervision, Funding acquisition
Duy Khanh Hoang	Supervision, Methodology, Writing – review & editing
Florian Schlosser	Methodology, Investigation, Writing – original draft
Qun Chen	Supervision, Writing – review & editing
James K. Carson	Supervision, Writing – review & editing, Funding acquisition
Donald John Cleland	Writing – review & editing, Funding acquisition

Certification by Co-Authors

The undersigned hereby certify that:

- the above statement correctly reflects the nature and extent of the PhD candidate's contribution to this work, and the nature of the contribution of each of the co-authors; and
- that the candidate wrote all or the majority of the text.

Name	Signature	Date
James Carson		26/9/25
Duy Hoang	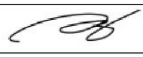	26/09/2025
Florian Schlosser		29/09/2025
Tim Walmsley	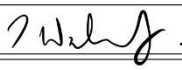	20/10/2025

July 2015

THE UNIVERSITY OF WAIKATO
Te Whare Wānanga o Waikato

Co-Authorship Form

School of Graduate Research
The University of Waikato
Private Bag 3105
Hamilton 3240, New Zealand
Phone +64 7 838 5096
Email: SGR@waikato.ac.nz
Website: http://www.waikato.ac.nz/students/research-degre

This form is to accompany the submission of any PhD that contains research reported in published or unpublished co-authored work. **Please include one copy of this form for each co-authored work.** Completed forms should be included in your appendices for all the copies of your thesis submitted for examination and library deposit (including digital deposit).

Chapter 5 – Expansion work recovery includes modelling and results from "Energy and exergy analysis of high temperature transcritical CO2 heat pump cycles with ejectors." The modelling and results included were modelled entirely by the PhD candidate. **Other results modelled by other co-authors were not included in the thesis.** The co-authors were material in contributing to the conceptualisation, methodology, supervision and review of the publication.

Nature of contribution by PhD candidate	Methodology, Investigation, Writing – original draft.
Extent of contribution by PhD candidate (%)	85 %

CO-AUTHORS

Name	Nature of Contribution
Timothy Gordon Walmsley	Conceptualisation, Methodology, Writing – review & editing, Supervision, Funding acquisition
Omar Abu Khass	Methodology, Writing – review & editing
Florian Schlosser	Methodology, Writing – review & editing
Donald John Cleland	Conceptualisation, Writing – review & editing, Funding acquisition
James K. Carson	Supervision, Methodology, Writing – review & editing
Qun Chen	Supervision, Methodology, Writing – review & editing
Duy Khanh Hoang	Supervision, Methodology, Writing – review & editing

Certification by Co-Authors

The undersigned hereby certify that:

- the above statement correctly reflects the nature and extent of the PhD candidate's contribution to this work, and the nature of the contribution of each of the co-authors; and
- that the candidate wrote all or the majority of the text.

Name	Signature	Date
James Carson		26/9/25
Duy Hoang		26/09/2025
Florian Schlosser		29/09/2025
Tim Walmsley	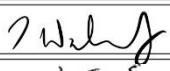	20/10/2025
Omar Abu Khass		24.10.2025

July 2015

THE UNIVERSITY OF WAIKATO
Te Whare Wānanga o Waikato

Co-Authorship Form

School of Graduate Research
The University of Waikato
Private Bag 3105
Hamilton 3240, New Zealand
Phone +64 7 838 5096
Email: SGR@waikato.ac.nz
Website: http://www.waikato.ac.nz/students/research-degre

This form is to accompany the submission of any PhD that contains research reported in published or unpublished co-authored work. **Please include one copy of this form for each co-authored work.** Completed forms should be included in your appendices for all the copies of your thesis submitted for examination and library deposit (including digital deposit).

Chapter 6 – Integration case study for milk powder spray drying includes modelling and results from " High-temperature CO_2 heat pump integration for milk powder spray drying." The modelling and results included were modelled entirely by the PhD candidate. **Other results modelled by other co-authors were not included in the thesis.** The co-authors were material in contributing to the conceptualisation, methodology, supervision and review of the publication.

Nature of contribution by PhD candidate	Methodology, Investigation, Writing – original draft.
Extent of contribution by PhD candidate (%)	85 %

CO-AUTHORS

Name	Nature of Contribution
Timothy Gordon Walmsley	Conceptualisation, Methodology, Writing – review & editing, Supervision, Funding acquisition
James K. Carson	Supervision, Methodology, Writing – review & editing
Steffen Kloeppel	Supervision, Writing – review & editing
Florian Schlosser	Methodology, Writing – review & editing
Donald John Cleland	Writing – review & editing, Funding acquisition

Certification by Co-Authors

The undersigned hereby certify that:

- the above statement correctly reflects the nature and extent of the PhD candidate's contribution to this work, and the nature of the contribution of each of the co-authors; and
- that the candidate wrote all or the majority of the text.

Name	Signature	Date
Florian Schlosser	F. Schlosser	29/09/2025
Tim Walmsley	T Walmsley.	20/10/2025

July 2015

THE UNIVERSITY OF WAIKATO
Te Whare Wānanga o Waikato

Co-Authorship Form

School of Graduate Research
The University of Waikato
Private Bag 3105
Hamilton 3240, New Zealand
Phone +64 7 838 5096
Email: SGR@waikato.ac.nz
Website: http://www.waikato.ac.nz/students/research-degre

This form is to accompany the submission of any PhD that contains research reported in published or unpublished co-authored work. **Please include one copy of this form for each co-authored work.** Completed forms should be included in your appendices for all the copies of your thesis submitted for examination and library deposit (including digital deposit).

Chapter 7 – The wider potential for uptake globally includes modelling and results from "Advances in high-temperature heat pump technologies for industrial process applications with large temperature glides." The modelling results included were modelled entirely by the PhD candidate. **Other results modelled by other co-authors were not included in the thesis. However, data collated by the co-authors has been included in Section 7.3.2.** The co-authors were material in contributing to the conceptualisation, methodology, data collation, supervision and review of the publication.

Nature of contribution by PhD candidate	Methodology, Investigation, Writing – original draft.
Extent of contribution by PhD candidate (%)	75 %

CO-AUTHORS

Name	Nature of Contribution
Steffen Kloeppel	Conceptualisation, Investigation, Methodology, Writing – original draft, Supervision
Florian Schlosser	Methodology, Investigation, Data curation, Writing – original draft
Nancy Kabat	Data curation, Writing – review & editing
James K. Carson	Supervision, Writing – review & editing
Timothy Gordon Walmsley	Supervision, Writing – review & editing, Funding acquisition

Certification by Co-Authors

The undersigned hereby certify that:

- the above statement correctly reflects the nature and extent of the PhD candidate's contribution to this work, and the nature of the contribution of each of the co-authors; and
- that the candidate wrote all or the majority of the text.

Name	Signature	Date
James Carson		26/9/25
Florian Schlosser	F. Schlosser	29/09/2025
Nancy Kabat	N. Kabat	14/10/2025
Tim Walmsley	T Walmsley	20/10/2025

July 2015